BLEED AIR OIL CONTAMINATION PARTICULATE CHARACTERIZATION

by

JAKE ROTH

B.S., Kansas State University, 2011

A THESIS

submitted in partial fulfillment of the requirements for the degree

MASTER OF SCIENCE

Department of Mechanical and Nuclear Engineering
College of Engineering

KANSAS STATE UNIVERSITY
Manhattan, Kansas

2015

Approved by:

Co-Major Professor
Dr. Mohammad H. Hosni

Approved by:

Co-Major Professor
Dr. Byron W. Jones

Copyright

Abstract

Gas turbine engine oil is contaminating the bleed air of an aircraft with enough frequency and intensity that health concerns are of public interest. While previous work measured micro particles and used only a simulator, this work mainly consists of measurements in the nanoparticle and ultrafine range using both the simulator and two different gas turbine engines. No previous research has been conducted using working jet engines to simulate a bleed air system and characterize the oil particulate contamination. Oil was injected into a bleed air simulator and an Allison 250 CC18 turbine engine in order to observe the particle size distributions resulting from thermal degradation and was measured with three particle sizing counters and an FTIR. The aerosol size distributions are given for various temperature and pressure ranges consistent with the process conditions associated with the bleed air in a commercial aircraft. Particle sizes of approximately 80nm to 100nm were observed at temperatures over 200°C while particles similar to injection distributions and smaller than measureable size were observed at lower power settings. Temperature is thought to be the controlling factor affecting particle size above 200°C while blade shear is likely the dominant factor for lower temperatures. The bleed air simulator produced results similar to the gas turbine engine results at higher temperatures, but did not replicate the size characteristics at lower temperatures. The observed particles are ultrafine and situated in the size range that may impact health safety more than larger particles.

Table of Contents

List of Figures vii
List of Tables xii
Acknowledgements xiii
Dedication xiv
Chapter 1: Introduction 1
1.1 Background 1
1.2 Defining air quality incidents on aircraft 2
1.3 Literature Review 3
1.3.1 Typical Aircraft Bleed Air System 3
1.3.2 Contamination Events 7
1.3.3 Thermal Degradation 9
1.3.4 TOCS & VOCs 12
1.3.5 Small particles health effects 13
1.3.6 Particulate Studies 14
1.4 Particulate Analysis Review and Presentation 18
1.5 Particle Counters and Gas Measuring Equipment 22
1.5.1 APS (TSI Model 3321) 23
1.5.2 APS Diluter (TSI Model 3302A) 24
1.5.3 Electrostatic Classifier (TSI Model 3080L) 25
1.5.4 CPC (TSI Model 3775) 28
1.5.5 SMPS 29
1.5.6 OPC (Climet Spectro 0.3) 30
1.5.7 FTIR 31
Chapter 2: Bleed Air Simulator (BAS) 32
2.1 Note of Health Effects 32
2.2 Experimental Setup 32
2.2.1 Test Procedure and Testing Matrix 36
2.2.2 Laskin Nozzle Aerosol Generator 38

2.2.2.1 Expected Mass Input 39
2.2.2.2 Measured Mobile Jet II Aerosol Output 41
2.2.2.2.1 Note On Test Legends 42
2.3 Results and discussion 53
2.3.1 Testing Data (30 Minutes) 53
2.3.2 Testing Data (10 Minutes) 64
2.4 Conclusions 69
Chapter 3: Allison T63-A-700 (C18) Engine 71
3.1 Experimental Setup 73
3.1.1 Design Modeled after real aircraft 74
3.1.2 Engine Safety 76
3.1.3 Oil Injection 77
3.1.4 Bleed Air Extraction Line 81
3.1.5 Process Control and Monitoring 86
3.1.5.1.1 Data Extraction 86
3.2 Data Analysis 87
3.2.1 Design and Error Estimations 87
3.2.1.1 Losses due to non-isokinetic 87
3.3 Results and Discussion 91
3.3.1 Notes on data naming 91
3.3.2 Notes on FTIR Data 91
3.3.3 Ambient Separation 92
3.3.4 Steady State Decay 98
3.3.4.1 Nozzle Injection Variation of Particle Concentrations 98
3.3.4.2 Decay of Oil Film 102
3.3.5 Results & Trends 107
3.3.6 Discussion 118
Chapter 4: Comparison Results & Discussion 120
Chapter 5: Conclusions 124
5.1 Future Work 125
References 128

Appendix A: Bleed Air Simulator Data 132
Appendix B: C18 Engine Data 1
Appendix C: C28B Engine Information & Data 1
Appendix D: Bleed Air C17 Data Information 3
Appendix E: Fractional Concentrations Calculation Routine 7
Appendix F: Additional Photos of Project 12

List of Figures

Figure 1-1. Typical Bleed Air System 3
Figure 1-2. Bleed Air Ports, Pratt & Whitney F117-PW-100 4
Figure 1-3 Filtration Efficiency 6
Figure 1-4 Histogram of Frequency Verse Particle Size Example 20
Figure 1-5. Aerodynamic Particle Sizer Diagram 24
Figure 1-6 APS Diluter Diagram 25
Figure 1-7 Cross Sectional View of an Inertial Impactor 26
Figure 1-8. Electrostatic Classifier Flow 28
Figure 1-9. Condensation Particle Counter Diagram 29
Figure 2-1 Aerosol Generator Portion of BAS 34
Figure 2-2 Compressor and Heater Portion of BAS 35
Figure 2-3 Main Ducting Portion BAS 36
Figure 2-4 Laskin Nozzle Injection Comparison of Multiple Charge Correction 43
Figure 2-5 Laskin Nozzle Multiple Charge Correction – Larger Bounds 44
Figure 2-6 Laskin Nozzle Comparison (Fractional) 45
Figure 2-7 Laskin Nozzle Mass Injection Distribution 46
Figure 2-8 Laskin Nozzle Injection Fractional Mass 47
Figure 2-9 Comparison of Soft X-Ray Laskin Nozzle 48
Figure 2-10 Laskin Nozzle Ambient Concentrations Comparison 49
Figure 2-11 Laskin Nozzles Ambient Cumulative Run 50
Figure 2-12 Laskin Nozzle SMPS & APS Comparison 51
Figure 2-13 Laskin Nozzle SMPS & APS Comparison Narrowed 52
Figure 2-14 BAS Constant Pressure 200kPa (30psi) 55
Figure 2-15 APS Total Concentration vs. Time 56
Figure 2-16 BAS Constant Pressure 345kPa 57
Figure 2-17 BAS Constant Pressure 480kPa 57
Figure 2-18 SMPS Geometric Mean at Constant Pressure 58
Figure 2-19 BAS Constant Temperature 230 & 250°C 58
Figure 2-20 BAS Constant Temperature 250 & 280°C 59

Figure 2-21 Gibbs free energy for BAS testing conditions 61
Figure 2-22 Enthalpy for BAS testing conditions 61
Figure 2-23 BAS Gibbs 3D Plot 62
Figure 2-24 BAS Enthalpy 3D Plot 62
Figure 2-25 BAS Gibbs Contour Plot 63
Figure 2-26 BAS Enthalpy Contour Plot 63
Figure 2-27 BAS Constant Temperature (185°C) 65
Figure 2-28 BAS Constant Temperature (220°C) 66
Figure 2-29 BAS Constant Temperature (250°C) 66
Figure 2-30 BAS Constant Temperature (280°C) 67
Figure 2-31 BAS Constant Temperature (310°C) 67
Figure 2-32 BAS Sample Geometric Mean_SMPS 68
Figure 2-33 Stability of Concentrations at 310°C 69
Figure 3-1 Allison C18 Test Engine 72
Figure 3-2 C18 Air Inlet System 78
Figure 3-3 C18 Oil Injection and Sample Ports 80
Figure 3-4 C18 Ambient Air Pickoff Inside Plenum Box 81
Figure 3-5 C18 Bleed Air Extraction System 84
Figure 3-6 C18 System Setup 84
Figure 3-7 C18 Engine Accessory Systems 85
Figure 3-8 Aspiration Efficiency 88
Figure 3-9 Aspiration Efficiency using Rader 1988 formulation 89
Figure 3-10 Diffusional Losses in General 90
Figure 3-11 Diffusional Losses Plotted 90
Figure 3-12 C18 Background Measurements 93
Figure 3-13 C18 No Injection 94
Figure 3-14 C18 Initial Injection 95
Figure 3-15 Air Plenum Comparison 96
Figure 3-16 C18 Bleed Air Line Measurements 97
Figure 3-17 C18 Initial Mass Decay 97
Figure 3-18 C18 Nozzle Concentration Variation 99

Figure 3-19 C18 Nozzle Geometric Mean Variation 100
Figure 3-20 Nozzle Variation – Mass 101
Figure 3-21 Nozzle Variation Total Mass 102
Figure A-22 T02 Oil Decay Total % 103
Figure 3-23 T02 Oil Decay Total Mass 104
Figure 3-24 T02 Oil Decay Concentration 11min averages 105
Figure 3-25 T03 Oil Decay Concentration 11min averages 105
Figure 3-26 Oil Decay T03 Total % 106
Figure 3-27 C18 100°C Compiled Concentration Data 108
Figure 3-28 C18 115°C Compiled Concentration Data 108
Figure 3-29 C18 125°C Compiled Concentration Data 109
Figure 3-30 C18 135°C Compiled Concentration Data 109
Figure 3-31 C18 140°C Compiled Concentration Data 110
Figure 3-32 C18 140°C & 143°C Compiled Concentration Data 110
Figure 3-33 C18 143°C & 145°C Compiled Concentration Data 111
Figure 3-34 C18 150°C Compiled Concentration Data 111
Figure 3-35 C18 155°C Compiled Concentration Data 112
Figure 3-36 C18 160°C Compiled Concentration Data 112
Figure 3-37 C18 165°C Compiled Concentration Data 113
Figure 3-38 C18 180°C Compiled Concentration Data 113
Figure 3-39 C18 200°C Compiled Concentration Data 114
Figure 3-40 C18 210°C Compiled Concentration Data 114
Figure 3-41 C18 210°C & 213°C Compiled Concentration Data 115
Figure 3-42 C18 213°C & 215°C Compiled Concentration Data 115
Figure 3-43 C18 220°C Compiled Concentration Data 116
Figure 3-44 C18 230°C Compiled Concentration Data 116
Figure 3-45 C18 235°C Compiled Concentration Data 117
Figure 3-46 C18 240°C Compiled Concentration Data 117
Figure 4-1 C18 & BAS Comparison 121
Figure 4-2 C18 & BAS Comparison Percent 121
Figure 4-3 C18 & BAS Low Run Comparison 122

Figure 4-4 High Temperature Test Comparison 123
Figure A-1 BAS 30Min Mass - 200kPa (30psi) 1
Figure A-2 BAS 30Min Mass - 345kPa (50psi) 2
Figure A-3 BAS 30Min Mass - 480kPa (70psi) 3
Figure A-4 BAS 30Min Mass - 230°C & 250°C 4
Figure A-5 BAS 30Min Mass - 250°C to 300°C 5
Figure A-6 BAS 10Min Mass - 200kPa (30psi) 1
Figure A-7 BAS 10Min Mass - 345kPa (50psi) 2
Figure A-8 BAS 10Min Mass - 480kPa (70psi) 3
Figure A-9 BAS 10Min Mass - 690kPa (100psi) 4
Figure A-10 BAS 10Min Mass - 185°C 5
Figure A-11 BAS 10Min Mass - 220°C 6
Figure A-12 BAS 10Min Mass - 250°C 7
Figure A-13 BAS 10Min Mass - 280°C 8
Figure A-14 BAS 10Min Mass - 310°C 9
Figure A-15 BAS 30Min Cumulative - 200kPa (30psi) 10
Figure A-16 BAS 30Min Cumulative - 345kPa (50psi) 11
Figure A-17 BAS 30Min Cumulative - 480kPa (70psi) 12
Figure A-18 BAS 30Min Cumulative - 230°C to 250°C 13
Figure A-19 BAS 30Min Cumulative - 250°C to 300°C 14
Figure A-20 BAS 10Min Cumulative - 200kPa (30psi) 15
Figure A-21 BAS 10Min Cumulative - 345kPa (50psi) 16
Figure A-22 BAS 10Min Cumulative - 480kPa (70psi) 17
Figure A-23 BAS 10Min Cumulative - 690kPa (100psi) 18
Figure A-24 BAS 10Min Cumulative - 185°C 19
Figure A-25 BAS 10Min Cumulative - 220°C 20
Figure A-26 BAS 10Min Cumulative - 250°C 21
Figure A-27 BAS 10Min Cumulative - 280°C 22
Figure A-28 BAS 10Min Cumulative - 310°C 23
Figure B-1 C18 Cumulative - 100°C 1
Figure B-2 C18 Cumulative - 115°C 2

Figure B-3 C18 Cumulative - 125°C 3
Figure B-4 C18 Cumulative - 135°C 4
Figure B-5 C18 Cumulative - 140°C 5
Figure B-6 C18 Cumulative - 140°C to 143°C 6
Figure B-7 C18 Cumulative - 143°C to 145°C 7
Figure B-8 C18 Cumulative - 150°C 8
Figure B-9 C18 Cumulative - 155°C 9
Figure B-10 C18 Cumulative - 160°C 10
Figure B-11 C18 Cumulative - 165°C 11
Figure B-12 C18 Cumulative - 180°C 12
Figure B-13 C18 Cumulative - 200°C 13
Figure B-14 C18 Cumulative - 210°C 14
Figure B-15 C18 Cumulative - 210°C to 213°C 15
Figure B-16 C18 Cumulative - 213°C to 215°C 16
Figure B-17 C18 Cumulative - 220°C 17
Figure B-18 C18 Cumulative - 230°C 18
Figure B-19 C18 Cumulative - 235°C 19
Figure B-20 C18 Cumulative - 240°C 20
Figure C-1 C28B Test Engine 1
Figure F-1 Driveshaft required to run engine 12
Figure F-2 C8 Driveshaft 2 12
Figure F-3 Engine Inspection after Hot Start 13
Figure F-4 Close-up of Engine Turbines during Inspection 14
Figure F-5 C18 Bleed Ports Illustrated 15
Figure F-6 C18 Setup 2 15
Figure F-7 C18 During test run 16
Figure F-8 C28B Engine Setup 16
Figure F-9 C28B Engine Setup_2 17
Figure F-10 C28B Engine Setup_3 17

List of Tables

Table 1-1 Summary of Potential Bleed Air Contaminants 11
Table 2-1. Bleed Air Typical Operating Conditions (National Research Council. Committee on Air Quality in Passenger Cabins of Commercial Aircraft, 2002) 37
Table 2-2 Test Matix Table 37
Table 2-3 Mass Flow Injection of Oil @ 20psi 40
Table 2-4 Ambient and Blower Concentrations (dN/cc) 49
Table 2-5 BAS Data Summary (30 Min) 54
Table 4-1 230°C 70psia Test Conditions 120
Table A-1 30 Minute Data Summary 132
Table A-2 10 Minute Data Summary 2
Table B-1 C18 Data Summary 2

Acknowledgements

I would like to acknowledge my advisor Dr. Byron Jones for his support and guidance throughout this project and his dedication to me as a student during the preparation of this thesis and during my course studies. I would also like to thank my committee members Dr. Donald Fenton and Dr. Mohammad Hosni for providing me assistance during my graduate career with advice and technical feedback.

Additionally, I would like to thank Eric Figge for all of his guidance and teaching lessons during the design and construction of the test stand and his efforts to help maintain the schedule of the project. I am grateful for the National Gas Machinery Laboratory (NGML) personnel in assistance with the construction of the test rig and running the engine.

I want to acknowledge the Federal Aviation Administration (FAA) of USA for their financial support of this project. Their funding has allowed me as a student to pursue my dreams of getting M.S. degree and without it this work would not be possible.

Finally, I wish to thank all my friends and family and their support to me while I purse my dreams and education.

Dedication

To my wife Kate, may I always provide you the best I am able to.

Chapter 1: Introduction

1.1 Background

Modern airplanes and jetliners are an impressive feat of technology. They utilize many inventions and readily adapt new technology to increase passenger safety and security. One important aspect of safety for any airline traveler is the air quality inside the aircraft cabin. This air is supplied by the bleed air from the engine compressor. The air is 'bleed off' of the compressor at a designated stage in the engine compressor suitable to provide the pressure and temperature needed to be properly utilized. The outside ambient conditions during a flight at 10,000m (32,808 ft) are typically at a pressure of 26.5 kPa (3.84psi) and temperature of -50°C (-58°F) (ASHRAE, 2013). According to (Hunt, Reid, Space, & Tilton, 1995), the aircraft can cruise as high as 12,000m (39,000ft) in which the pressure and temperature continue to lower according to standard atmospheric tables. This heated and pressurized outside air is then conditioned to a suitable pressure and temperature for introduction into the aircraft cabin. The air quality is subject to contamination from outside sources and the engine itself, most notably in the event of an oil leak due to worn or leaky seals. In recent years, it has become an increasingly higher priority for scientist and safety activists to monitor bleed air quality as two studies highlighted this possibility of air quality contamination. The frequency of an air quality contamination event was estimated at 1 in 22,000 flights (Winder & Balouet, 2000) to 1 in 1000 flights(Hood, Environmental, Perspectives, & Apr, 2001). With the U.S. air fleet containing a vast amount of planes transporting over fifty million people each year, the incident rate could be as high as 2 to 3 occurrences each day (Shehadi, Hosni, & Jones, n.d.). This potential frequency has prompted several studies into the effects of bleed air contamination to understand the potential health risks considering that each occupant will be on the aircraft from 1 to 20 hours in

an enclosed environment. Contaminants that are of the greatest concern to passenger safety are microscopic airborne bacteria and viruses, volatile organic compounds, and carbon monoxide (CO). Large volumes of air are provided to the aircraft to reduce the buildup of any one of these contaminates and provide relatively fresh air for occupants. Additionally, several guidelines and regulations are also in place to assure passenger safety. However, most of these guidelines do not address aircraft air quality incidents (Magoha, 2012).

1.2 Defining air quality incidents on aircraft

In this report, an aircraft quality incident, or cabin air contamination, will be generally defined as a problem that can arise with the air quality introduced into the aircraft cabin. While not a solid technical definition, many different variations exist to define an air quality incident. More specifically, the air quality incidents of concern in this study are those relating to a fume or smoke incident. This fume or smoke incident is a complex phenomenon that can arise from many causes of which, the primary one is examined in the study addressed in this thesis. The more informal way of characterizing this serious issue is the reports of burnt oil smell, or some other unpleasant smoky, greasy, dirty smell that some report as being similar to a wet dog. ASHREA standards refer to the smoke/fume incident as an episodic event or incident-occurrence. (Shehadi et al., n.d.) narrowed the definition of an air quality incident to an event that caused illness related to smoke/fire and fumes/odor on the aircraft flight deck or cabin and identified events by utilizing the Federal Aviation Administration (FAA) online database Aviation Safety Reporting System (ASRS) and several other databases.

1.3 Literature Review

1.3.1 Typical Aircraft Bleed Air System

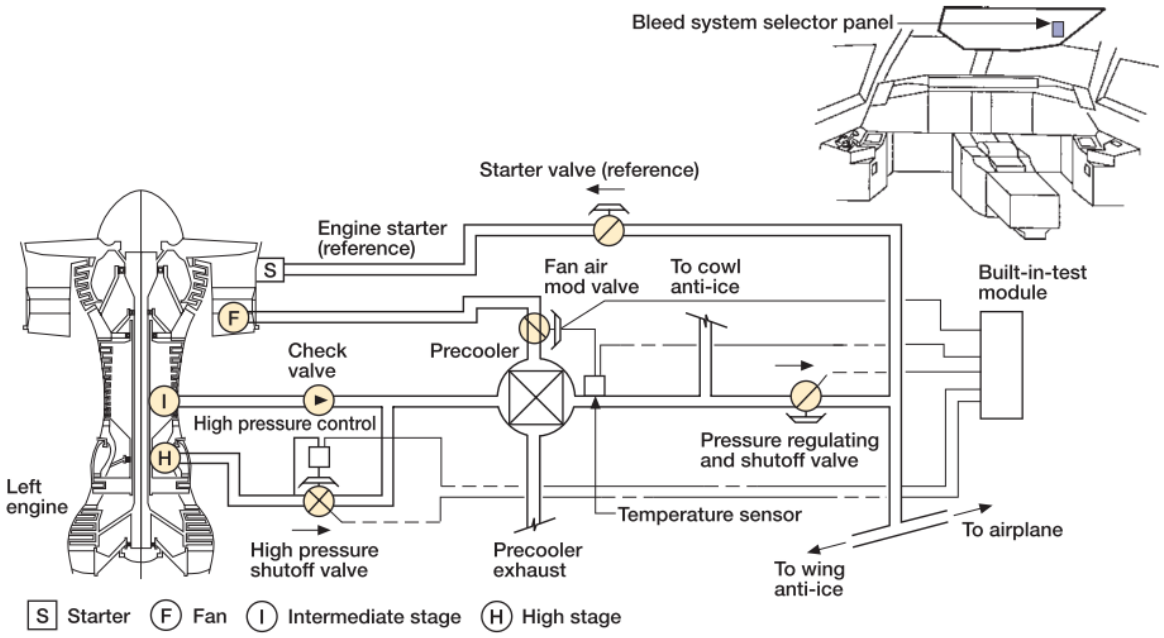

Figure 1-1. Typical Bleed Air System
Reproduced from (Hunt et al., 1995) with permission.

Anyone who has flown has probably been informed by an aircrew member that the aircraft is pressurized for your comfort and safety. The flight attendant's statement actually means the aircraft is pressurized so passengers do not suffocate. The ambient temperatures and pressures are well below that of living conditions for a human being at cruise altitudes. As such, the aircraft needs to provide heated pressurized air, and the most effective way this pressurization has been achieved so far is through the bleed air system on an aircraft. The typical arrangement of a commercial engine bleed air system is shown in Figure 1-1. The bleed air system on an aircraft extracts the air from the engine compressor section. While the bleed air system varies between engine models, the modern commercial jet liner will pull the air from two

different stages for use at different points in the flight. Modern engines such as the C-17 Pratt & Whitney PW2000 have over 20 stages of compression and compression ratios up to 30 thus allowing the option of multiple bleed air taps. Engines used on smaller aircraft may have many less stages, and will only have one available bleed air extraction stage as the pressure ratio will be between 5 and 10. The compressors on a jet engine are generally axial on a large aircraft with a single centrifugal stage showing up on smaller engines utilized on small helicopters, such as the very popular Allison T63-A-700. A C-17 engine currently has a 10^{th} and 17^{th} stage bleed air extraction (Matthews, 2013) and is shown in Figure 1-2.

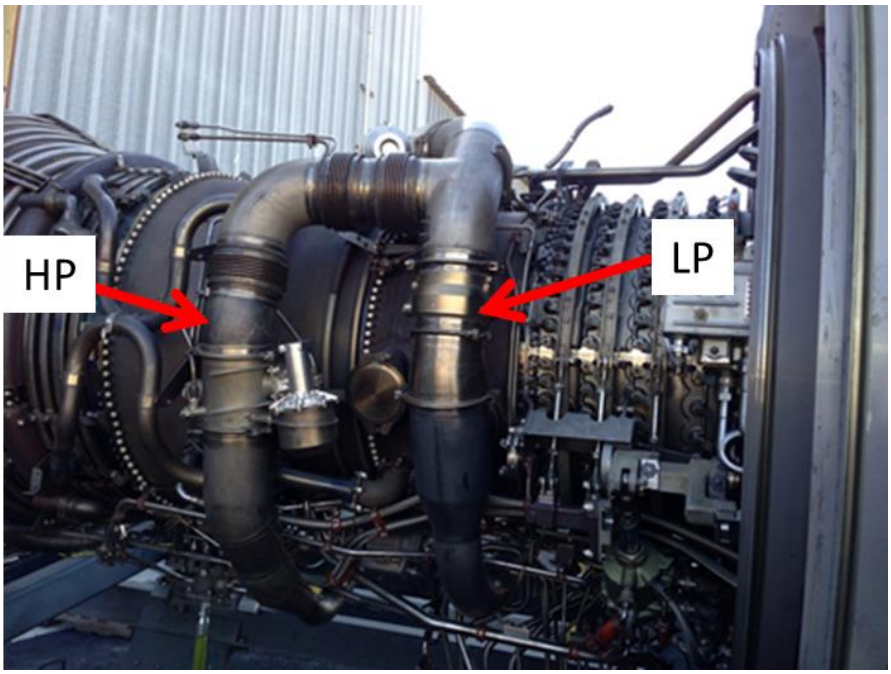

Figure 1-2. Bleed Air Ports, Pratt & Whitney F117-PW-100

The low pressure (LP) stage bleed air port is used during high power operations such as cruising power, while the high pressure (HP) stage is used for extraction during lower power operations. The low pressure stage is used during take-off when the engine is operating at high power and high pressure stage is used during landing when the engine is operating at low power.

During cruise flight the power level is in between these extremes but generally the low pressure stage is able to provide the necessary bleed air flow. The rate of air exchange for the entire cabin is on the order of 20 cfm per person or about 25 air changes per hour (Hunt et al., 1995). The air is passed through a precooler, pressure regulating valve, ozone converter, air condition pack system and some sort of mixing air plenum before being introduced into the aircraft. An oil leak in the compressor would introduce the lubricating fluid to a high temperature environment via the heated compressed air. With bleed air temperatures reaching up to 320°C (608°F) it is possible for the oil to experience thermal decomposition. At these elevated temperatures the oil will release CO, CO2, and other toxic compounds. The term "toxic" in this context refers to any substance harmful to a human being.

While outside air is supplied by the bleed air line, to reduce costs of fuel some air is recirculated within the aircraft. Air recirculation rates can vary between models of aircraft and engine requirements. Typical ratios for air recirculation to outside air are about 50-50. However, certain aircraft will go lower with the ratio of outside air. The recirculated cabin air is filtered using high efficiency particulate air (HEPA) filters that will generally filter out 99.99% of particulate contaminations. It is further understood that the efficiency of filtering is lowest at approximately 0.3μm (300nm) due to the various effects of particle dynamics and can be observed in Figure 1-3 (Hinds, 1999). Thus the recirculation filters will remove most of the aerosols, but HEPA filters don't trap all the particles at the filter surface. The particles penetrate into the filter and thus the smaller particles are removed by diffusion within the filter media while the larger are removed by impaction. It is common thinking that the efficiency will increase as a filter is loaded with more particles. While this may be true for solid particles and dust that accumulates on the face of a filter; research by (Payet, Boulaud, Madelaine, & Renoux,

1992) suggests otherwise. The authors experimentally measured that as the filter becomes more clogged, the pressure differential across the filter must increase. This increase in pressure and subsequent reduction in porosity will increase the velocity of the air and thus increase the penetration of the particles. The smaller particles, at approximately 0.12μm, were shown to have a ten times increased penetration for a relative pressure increase of five. The particles that penetrate through the filter are then recirculated into the aircraft. However, it should be understood that, even with a ten-fold increase in penetration, the vast majority of these particles are captured by the filter.

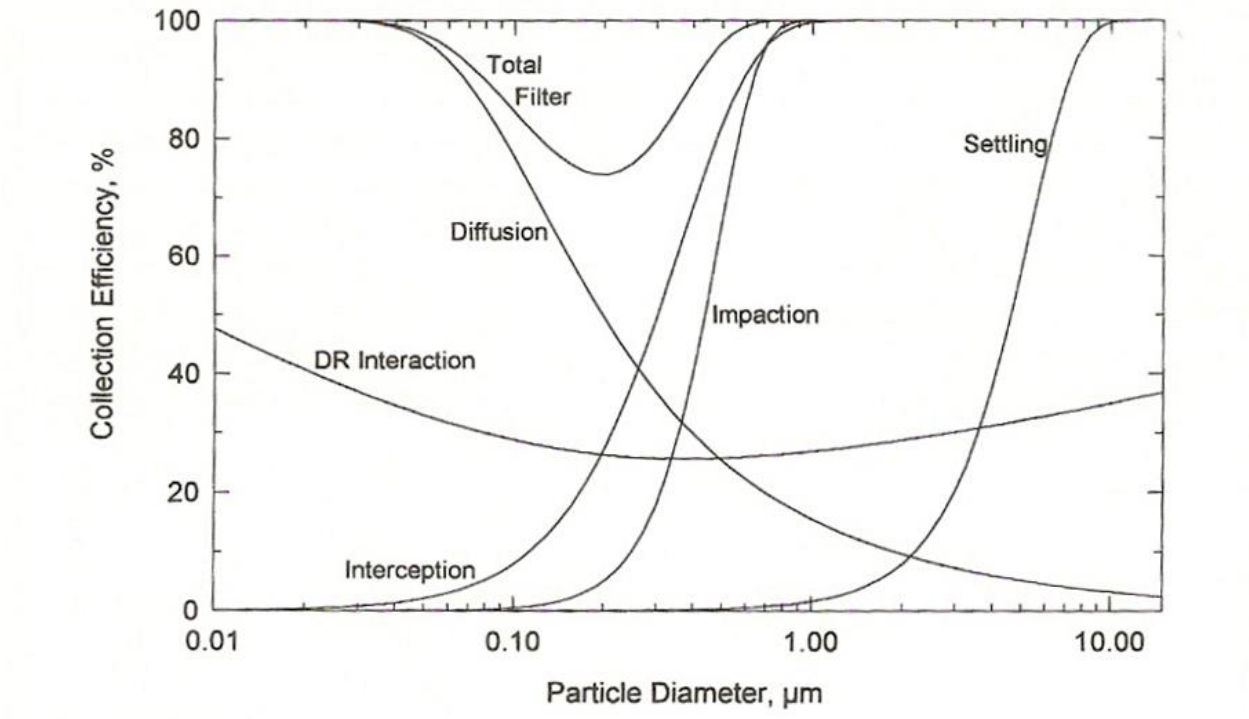

Filter efficiency for individual single-fiber mechanisms and total efficiency; t = 1 mm, α = 0.05, d_f = 2 μm, and U_0 = 0.10 m/s. [10 cm/s].

Figure 1-3 Filtration Efficiency
Reproduced from (Hinds, 1999) with permission

The bleed air isn't used only for air supply to the cabin. The anti-ice, anti-surge protection, and on some engines the fuel control systems also use the bleed air. Surge in an aircraft engine is a potentially very violent and dangerous event that can occur during acceleration or deceleration. When the aircraft changes speeds, if the pressure downstream of the compressor does not fall quickly enough, the air flow will temporarily stop or reverse direction, thus eliminating the power output of the engine. This event can lead to engine stall, which results in loss of flight power and is a very serious event. Modern aircraft have been able to design around and almost completely eliminate surge (Saravanamuttoo, Rogers, Cohen, & Straznicky, 2009), but the problem still exists due to the varied conditions that an engine encounters in flight. All of these air systems just mentioned use the bleed air. Pulling more bleed flow from the compressor increases the temperature the turbines experience as less air is then available for the same required power output, requiring the temperature of the combustion gases to rise. The bleed air flow extraction rate is limited on an engine during operation due to the turbine temperature limit thus; an engine larger than required for flight power is needed to maintain the required air change rates in the aircraft. Powering a larger engine leads directly to cost increases to the airlines via fuel consumption (Hunt et al., 1995).

1.3.2 Contamination Events

Several studies have investigated the contamination of the bleed air system which can arise due to worn or leaky oil seals. The introduction of oil may also arise when the compressor fails to maintain a vacuum pressure on the lubricating oil reservoir. While these events are rare, current estimates suggest one of these events may occur in the aircraft fleet every day on the average. (Shehadi et al., n.d.) presented data breaking down the bleed air contamination events by engine model and plane airframe. The data have also shown that the axillary power units

(APU) that are used to power an aircraft while it is on the ramp may also produce a bleed air contamination event. Using data made available by the Federal Aviation Administration's Aviation Safety Reporting System, United States Department of Transportation (USDoT) website, Bureau of Transportation Statistics, and Research and Innovative Technology Administration, it was concluded that no one model or manufacturer is responsible for a large portion of the bleed air contamination events. While there are engines or aircraft models whose incident frequencies are larger than the rest of the fleet, they are higher by only a factor of five at the most. It is of further interest that, in order to detect such an event, it is not the best solution to use the highest number of aircraft incidents. The B757-200 had close to the most reported incidents, but was among the lowest reported in terms of incident per aircraft, whereas the DC-9 reported incidents were large for the number of departures made but were relatively low on the number of reported incidents. Further breakdown of the FAA data indicated that 33% of incidents were due to fuel leaks, 23% were due to engine oil leaks, 18% were due to APU oil leaks and 13% were due to hydraulic fluid leaks, with the rest being attributed to air cycle machine oil leaks (Overfelt, Jones, Loo, Haney, & Neer, 2012; Shehadi et al., n.d.). Additionally, one must consider that the fleet is constantly changing and thus new engine and airframe combinations are being introduced while older aircraft are continually retired. The new commercial aircraft commissioned make the data not entirely representative of what the future may hold or what is currently present. Nevertheless, the information presented by (Shehadi et al., n.d.) illustrates the difficulties of trying to capture a bleed air contamination event during flight on a commercial plane.

However, there is one case where the issue appeared so frequently that the Australian Senate launched an investigation into the causes of the events (Rural, Affairs, & Committee,

2000). It was stated in the report that the BAe-146 started having issues in the mid-1980's and they persisted into the early 1990's, in which passengers reported the smell of unpleasant odors, even though the air flow was approximately 60 percent fresh and 40 percent recirculated. The air recirculated in the cabin amounts to about 16 air changes each hour, which is smaller than the recommendation by (Hunt et al., 1995). The report also stated that a pilot had become incapacitated due to the fumes while flying the aircraft, with data suggesting that 1 out of 66 flights experienced an air quality incident. Further studies of the BAe-146 were also undertaken as concerns about health conditions rose (Currie, 1995; Vasak, 1992). (Shehadi et al., n.d.) provided information that both studies indicated above normal concentration of oil mist levels in the cabin.

1.3.3 Thermal Degradation

Thermal degradation of oil in the bleed air is of some concern and is considered an important factor in bleed air contamination evens. When oil thermally decomposes, the process is similar to that of burning oil however, there is no open flame during thermal decomposition. When this process is undertaken, carbon dioxide and carbon monoxide are released as a result along with other gaseous chemicals and smoke particles. While work has been done regarding the combustion of aerosols and the byproducts (Lighty, Veranth, & Sarofim, 2000), only a few publications regarding the thermal degradation of oil, specifically jet engine oil, have been published. One study examined the thermal decomposition of two popular commercial jet engine oils and the conditions present in which decomposition took place (Van Netten & Leung, 2000). During this study, Van Netten looked for CO, CO2, NO2, HCN, and volatile compounds such as neurotoxins tri-cresyl phosphates (TCP) and trimethly propane phosphate (TMPP) while the oils were heated up to 525°C (977°F) under laboratory conditions. Generation of TMPP was

not detected, even though its appearance would be expected at 350-650°C (660°F-1200°F) and is produced from TCP and trimethylolpropane esters (TMPE). Both TCP and TMPE are common constituents in jet engine oils. TCP is commonly used as an anti wear additive and can drastically reduce wear under loading (Ghose, Ferrante, & Honecy, 1987). It is present in oils by up to 3%, with the most neurotoxic isomer occurring up to 1%. During the thermal degradation, the confirmation of TCP and other volatiles was found along with the increase in generation of CO2 & CO between 208°C and 306°C. Two different oils were evaluated and both oils were reported to have almost identical results, suggesting that regardless of jet engine oil used, neurotoxins and volatiles are likely to be found in the case of oil thermal degradation.

The introduction of TCP and other contaminates such as CO into the aircraft can have very serious results. Other contaminates can also cause serious air quality events. One such event occurred in December 2008 when de-icer fumes entered the cabin of an Alaskan Airlines plane. The resulting effects were evident when 18 passengers and seven crewmen were sent to the hospital and treated for eye irritation, dizziness, and nausea. The CO2 generation and mass loss from a heated sample of Mobile Jet II were analyzed by (Overfelt et al., 2011) in order to determine the characteristics of thermal degradation during the transition period from room temperature to approximately 250°C (480°F). The results indicate that as the temperature increases, the generation of CO & CO2 similarly increases, and supports the idea that a sensor based on CO & CO2 may possibly detect a bleed air contamination event. The temperature of 250°C was used as a representative temperature of a bleed air system on a typical commercial aircraft as indicated by (Hunt et al., 1995; Matthews, 2013).

(Van Netten & Leung, 2001) evaluated the thermal degradation of one jet engine oil along with two hydraulic fluids at temperatures up to 525°C. The fluids were put into a 250L

stainless steel chamber with the top lid open to air at atmospheric pressure. A multi-gas TMX-412 monitor was used to measure gaseous constituents such as NO2, O2 and CO. The observed results show that CO concentrations reached 100 ppm for Mobile Jet II and up to 180 ppm for the hydraulic fluids. Likewise an increase in CO2 concentrations was observed from the control case, showing increases in the range of 40ppm up from the 390 ppm baseline. In addition to thermal degradation of the oil and hydraulic fluid chemical makeup, visible smoke and change of color can be seen. This smoke also indicates that the fluid is undergoing some type of chemical reaction.

In addition, the ACER report provides a breakdown of the potential bleed air contaminates reproduced here as Table 1-1 (Overfelt et al., 2012).

Table 1-1 Summary of Potential Bleed Air Contaminants
Reproduced from (Overfelt et al., 2012).

Potential Bleed Air Contamination Event	*Probable Contaminant*
Engine oil leak producing aerosolized droplets of oil in the engine compressor	• Very fine mist of engine oil aerosols • Small amounts of carbon monoxide (CO) and carbon dioxide (CO_2)
Partially pyrolized jet engine oil	• Very fine mist of engine oil aerosols • Carbon monoxide (CO) • Carbon dioxide (CO_2) • Misc. unburned hydrocarbons • Ultrafine smoke particles
Fully pyrolized jet engine oil	• Carbon monoxide (CO) • Carbon dioxide (CO_2) • Ultrafine smoke particles

1.3.4 TOCS & VOCs

Much work has already been undertaken to characterize the chemicals involved in a bleed air contamination event. Studies include (Bartl, Völkl, & Kaiser, 2008; Eckels, Jones, Mann, Mohan, & Weisel, 2014; Guan et al., 2014; Nagda & Rector, 2003; Van Netten & Leung, 2001; Van Netten, 1999, 2005; Winder & Balouet, 2000, 2001, 2002). Additionally many of these papers present the detrimental effects of volatile organic compounds (VOC) and semi-volatile organic compounds (SVOC). Adverse health effects range wildly, from eye and throat irritation blurred vision to disorientation, nausea and vomiting. In rare or serious cases, loss of consciousness is possible. The rate at which bleed air contamination events have occurred is worrisome, as unlike passengers, the pilots and flight crew spend much more time in aircrafts and the potential for repeated exposure is much greater. While the long term health effects are being studied, it is obvious that acute effects can be deadly if the pilots are exposed to sufficiently high concentrations.

One of the notable and recent publications is (Guan et al., 2014) in which a large study that was conducted on 107 commercial flights from August 2010 to August 2012. GC/MS analysis on air samples gave an average number of 59 VOCs detected in each flight within a total of 346 VOCs detected in all flights combined. The VOC breakdown is as follows: 41% for alkanes and alkenes, 15% for ester and alcohols, 11% for ketones and aldehydes, 6% for halides, 20% for aromatics and 6% for nitrogen containing VOCs. It was concluded that the detection rate of all VOCs was actually the lowest during the landing phase as compared to the cruise and takeoff phase of the flight plan. In a second publication from this study, (Guan et al., 2014) found 29 compounds that were identified as target VOCs in cabin air. These target VOCs had concentration levels that were statistically different ($p < 0.05$) compared to the other VOCs

detected. They also concluded that the effect of bleed air dilution on the cabin is present as the concentration levels of some target VOCs were significantly lower than in recirculated air.

(Eckels et al., 2014) investigated the use of recirculation filters to capturing air quality incidents by conducting chemical analysis of filters removed from aircraft. They used a laboratory bleed air simulator to artificially generate oil contaminated air at conditions representative of bleed air conditions in a commercial aircraft. This air was passed through recirculation filters, which were analyzed using GC/MS procedures outlined in the document. The data obtained using the bleed air simulator were used to identify robust markers of oil contamination as a base reference for comparing to analysis results for filters pulled from aircraft. They then tested 184 filters, 107 from non-incident aircraft (standard) and 77 pulled from aircraft that have experienced some type of air quality air issue (non-standard). It was observed that 90% of the filters had some sort of detectable level of TCP, with the nonstandard filters showing larger amount of oil present than the standard filters. This study has shown it is possible to identify incident occurrence with filter analysis but one cannot determine when the incident occurred based on that information.

1.3.5 Small particles health effects

It should come as no surprise that ultrafine particles can be damaging to the human body. The *ASHRAE Handbook Fundementals* (ASHRAE, 2013) provides information on some important health effects, indicating that health professionals are concerned mainly with particles smaller than 2 μm as those above this size range will be separated out in the upper respiratory system by impaction. Sub-micron particles may actually penetrate deeper into the lungs with about 50% settling into the lungs. It is possible however, that nanoparticles less than 100 nm can enter the blood stream. Once in the blood stream they have the ability to be transported to the

brain or other organs. According to the *ASHRAE Handbook of Fundamentals*, the U.S. EPA states that fine particulate matter less than 2.5 μm in diameter is associated with lung disease, asthma, and other respiratory problems. Short term exposure conditions are similar to those experienced by the VOCs and volatile compounds, including light-headedness, shortness of breath, and eye and lung irritation. (Lighty et al., 2000) touched on the issue regarding respiration in the human body and particles on the order of 2.5 μm (termed $PM_{2.5}$). Generally the health standards are set not on concentration, but rather the amount of mass potentially deposited into the lungs. It is the mass amount that causes the issues of exposure and is thus the generally accepted way to represent threats to health. While there is no single standard, according to (ASHRAE, 2013) the EPA National Ambient Air Quality standard (NAASQS) is 150μg/m^3 for particles less than 10μm and about 35μg/m^3 for particles less than 2.5μm in diameter for an annual mean averaged over three year time period.

1.3.6 Particulate Studies

While there have been studies of particles emanating from exhaust gases on engines and gas turbines, there have been virtually no articles on the bleed air contamination events that may occur. Many of the studies that have examined the particles and compounds of exhaust gases from gas turbines have focused on other factors, such as sulfur content in the fuel (Wilson, Petzold, Nyeki, Schumann, & Zellner, 2004) and ion cluster formation in aircraft plumes (Starik, Savel'ev, Titova, Loukhovitskaya, & Schumann, 2004). While these studies do highlight needed information to improve the gaseous and particulate emissions put into the atmosphere, they are not highly relevant to the bleed air contamination discussion. Although it is possible for these particles to be intercepted in flight, it is unlikely that the exhaust gas trail would be followed so closely by another plane and the time of contamination would be very short. These trails will

dissipate over time as can be observed by the naked eye near an active air field or airport location.

Others have focused on the measurement of oil mist droplets and their generation (Jian-Wen & Jin-chun, 2009), where it was found that pressure is the governing factor of particle generation from a liquid. The experimental variables covered testing air pressure ranges of 100kPa (14.5psi) to 650kPa (94.3psi) and both oil and air temperatures of 10°C (50°F) to 65°C (149°F). It is noted that the measurement equipment during these studies had a range of 0.5μm to 1000μm, and was unable to detect sub-micron particles. Their results do not cover the temperatures approached in heat of compression in turbine engines, but approximate the pressures reached by the air bled off of the compressor.

(Magoha, 2012) investigated many aspects of the bleed air contamination from chemicals and compounds to the particulate analysis of oil being introduced into the system. His study used a TDA-4B lite Laskin nozzle generator to introduce oil particles into an air stream to create a simulated bleed air event. The results indicate that the particles are primarily located between approximately 0.3μm and 20μm. This study also laid the groundwork for monitoring an aircraft air quality incident event and highlighted the health risks of such incidents. It was found that TCP isomers were present on filters after oil underwent the simulated jet engine compressor conditions, thus suggesting that it would be possible for occupants to be exposed to such compounds during a fume/smoke event. However, it could not be concluded that sub-micron particles would or would not present during such an incident.

(Mann, Eckels, & W. Jones, 2014) investigated simulated bleed air contamination events using the same bleed air simulator as (Magoha, 2012). They characterized the particle concentration and size range from 13nm to 20μm using particle counters. These same particle

counters are mentioned later in this study and used for the instrumentation to characterize bleed air contamination events. Their results and findings are that pressure has a negligible effect on the particulate size and concentration and the primary controlling factor is temperature. Additionally, at higher temperatures and pressures, the particulate size mean diameter was sub-micron. The study additionally pointed out that the majority of the particles are under 0.5μm (500 nm) at elevated temperatures, which would be expected during the majority of bleed air operation, and thus are not picked up by instrumentation using laser refraction and time of flight technology. This study also provided evidence that a water based condensation particle counter will not accurately gage or measure oil particles presumably due to the inability of water to condense onto oil droplets. It was recommended that a butanol condensation particle counter would provide better accuracy for measurements involving oil droplets.

Thus, an aspect of current literature is that no study exists yet characterizing the oil particulate sizes and composition obtained from a gas turbine engine via the bleed air line. While (Mann et al., 2014) started work in this area, sub-micron measurements were could not be collected at that time. It is then of importance to characterize the particle size distribution and concentration of a bleed air contamination event that is defined by an oil leak from a compressor. Several important reasons dictate why such a study should be done. First, in order to understand the impacts upon a person's health, it is important to know the particle sizes that are involved and how it may be introduced into the aircraft cabin. The main absorption method of contaminates of this size is respiration, due to the small size of particles reported so far. Another reason to do this study is to properly develop a real time sensor that is able to detect when an incident occurs. The issue is stated earlier, that testing a monitor on a real aircraft, while the most representative in terms of data, would be impractical as contamination could not be

introduced to create a simulated event and actual events occur on a very small fraction of flights. There is also the issue of ensuring that the incident is directly related to the bleed air. Additionally, much of the current equipment utilized to detect particles in the sub-micron and micron range, and analyze gas compositions are very expensive and delicate and not easily adapted to in-flight measurements. There is one instance where oil was directly injected into an aircraft engine and the effects observed. (Crane, Sanders, Endecott, & Abbott, 1983) injected oil into an Auxiliary Power Unit (APU) in order to simulate a bleed air contamination event, such as a malfunctioning seal in the gear-reduction box of a turboprop engine. However, their findings were that none of the gases analyzed were present in toxic concentrations, and no particulate data were taken.

The present study is a continuation of the studies done by (Magoha, 2012) and (Mann et al., 2014) in which oil particulate concentrations and size distributions are measured under conditions intended to simulate oil thermal decomposition in the bleed airline. As stated earlier, information regarding the size distribution from a typical bleed air system from both a bleed air simulator test stand and an operating gas turbine test stand would provide valuable data. Previous information gathered has indicated sub-micron particle sizes are important to observe and detect as they have more serious health effects. These smaller particles also allow and easier path for a gaseous substance to be generated. This study will present information regarding the bleed air simulator used in (Magoha, 2012; Mann et al., 2014) with the focus on smaller particle sizes. Additionally, gas spectrometry was included in the analysis in order to provide more data about the thermal degradation effects that could be taking place. This study also will present data of sub-micron particle sizes from a gas turbine system designed to represent a typical aircraft

bleed air system. Oil was artificially introduced into the gas turbine to simulate an oil leak from a compressor.

1.4 Particulate Analysis Review and Presentation

The data presented will be presented in multiple ways. It is important for the reader to understand how these data are presented and why the author chose to present the data in this format. The intent of this section of the thesis is not to be a complete review of particle data or analysis, but rather to explain the reasons for presenting the data in the matter shown in the paper and appendices.

Particle distributions typically have a skewed particle size distribution with a long tail appearing at the larger particle sizes. This skewed nature of particle distributions may be attributed to many factors such as the gravitational settling and other factors. Equations describing particle generation and dissipation mechanics tend to have exponential or power terms. Furthermore the governing equations for particles may change with particle size as the particle sizes span orders of magnitude. Indeed, in this study, the particle size range covers 10nm to 20μm. These particles are so small that they start to approach the wavelengths of visible light, and thus light itself will interact differently around these particles than a human-scale object. Corrections to the distributions have been formulated for these very small particles and the general accepted correction is the Cunningham correction factor. Many equations include empirical or theoretical fits for the Cunningham correction factor for a particular size distribution. This author uses the following empirical equation specified for oil droplets by Rader, 1990 (Baron & Willeke, 2001):

$$C_{c\_oil}(d_p) := 1 + Kn(d_p) \cdot \left(\alpha + \beta \cdot e^{\left(\frac{-\gamma}{Kn(d_p)}\right)}\right)$$

- $\alpha = 1.207$
- $\beta = 0.440$
- $\gamma = 0.596$
- d_p = particle diameter (concentration)
- Kn = Knudsen number (as a function of particle diameter)

It is common then to represent the particle size value in a semi log plot with the concentrations shown in a linear fashion. Several references have given arguments into why not to use a logarithmic distribution density function to represent the data (Incorporated, 2014; Kostic, 2003; Sommer, 2001). More information about these plotting features and graphing aerosol data may be found in textbooks such as (Baron & Willeke, 2001; Friedlander, 2000; Hinds, 1999).

The information presented by the TSI equipment used in these experiments shows the channels or bins which are spaced geometrically or logarithmically. The channels are arranged in this manner to obtain a higher resolution in the areas where the aerosol is generally to be found in greater concentrations. However, this information will skew the data. The information stored in the lower particle midpoint diameter bin will have a smaller width as compared to a higher particle midpoint diameter bin. This non-uniformity in channel spacing will result in the larger diameter bins showing more particles as compared to the smaller diameter bins for the same concentration. Thus, the representation, while not inaccurate, is misleading and should be presented in a mathematically different form. One drawback is that an important parameter, concentration amounts, are now shown by this approach. The fractional distribution may be multiplied by the total concentration to achieve the best overall result. This problem may be seen in Figure 1-4.

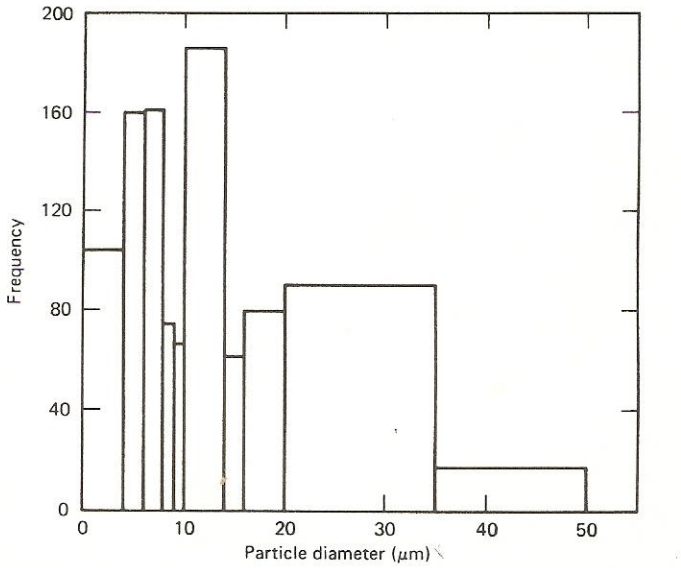

Figure 1-4 Histogram of Frequency Verse Particle Size Example
Reproduced from (Hinds, 1999) with permission.

To get around this misrepresentation, we may use the fractional concentration to represent the data. The cumulative distribution is given by the integral of the frequency function as a function of the particle diameter:

$$\int_0^\infty f(d_p)dd_p = 1.0$$

where f is the frequency function in units of fraction/μm and d_p is the particle diameter. The information provided in terms of diameter midpoint however does not show the lower and upper bounds of the channel data. Additionally since the information is either spaced geometrically or logarithmically without the absolute lower or upper bounds being known, the channel lower and upper bounds cannot be determined very easily. The information from the diameter midpoint though does provide the details to determine the cumulative percent of concentration. However, to properly average the data over multiple tests, the concentrations must be summed. From this information we may determine the percent of concentration of the bin by the following relations:

$$N_{i\_percent} = \frac{N_i}{N_{tot}} \quad where, \quad N_{tot} = \sum_{i=\,Bin\,Lowest}^{Bin\,Highest} N_i$$

- N_i = Particles in bin 'i'

From the percent of concentration ($N_{i\_percent}$) we may get the cumulative concentration percent, where the summation will be equal to 1 or 100%. Thus, to get the proper value for $f(d_p)$ we take the derivative. A packaged software program was used to determine the proper frequency function and ensure continuous lines. A basis spline (B-spline) fit was used instead of a cubic spline fit or some other type of data fit. This B-spline produced the most accurate data representation when taking the derivative. More information on how this derivative is determined may be found in "Appendix E: Fractional Concentrations Calculation Routine" of this report.

If the distribution of a monomodal aerosol is typical of a long tail at the upper sizes with the larger concentrations appearing at the small sizes, then the geometric mean is the best way to represent the data. An arithmetic mean works as well, but doesn't properly weight the data for the large range at hand and this normalization is then lost. It is in this nature then that the geometric deviation is also used in order to quantify how 'grouped' the data of the aerosol is about the geometric mean. However, if the aerosol is polydisperese or polymodal, in any form, then mathematically the singular representation of the geometric mean (or any other mean) falls out of favor. While there are complex methods used in order to quantify these multimodal aerosols, this author has chosen to not use the multimodal geometric mean as the peaks should be presented in the size distribution graphs.

As a note, all the data collected from the tests for the SMPS system were processed through a calculation routine in MathCad using VBA code. This calculation routine allows the

operator to add extra graphs, or information to be calculated very easily after the program was properly set up in said manner. The information was verified for calculated variables and data against the Aerosol Instrument Manager (AIM) software provided by TSI. The custom routine allows the output of only concentration data to be imported, but the entire data-set may be determined from the imported information. Code created in the current study also allows the rapid comparison of data to easily determine the differences between tests. This 'software' will be made available to the public or interested parties via Kansas State University.

1.5 Particle Counters and Gas Measuring Equipment

The equipment used to measure particles is often very expensive and very delicate. In order to properly measure particles, it is necessary to not only detect they are present, but also determine the size of the particle. While it sounds very simple in nature, in practice obtaining accurate measurements for particles is relatively difficult. In addition, there is the problem of classifying particles in a manner that is both clearly understood and interpreted. Almost all particle measuring equipment will 'bin' the particles that are counted into discrete size ranges, just like a histogram. While not all of the particles measured will be properly binned due to equipment resolution and accuracy, statistics may be used to characterize the error probability and corrections may then be applied.

The equipment listed below is the same measurement equipment that was used in the study done by (Mann et al., 2014). Additionally, between each one of the experimental setups that were tested (Bleed Air Simulator, C18, C28B) the equipment was not changed or altered in any way other than the regular maintenance practices prescribed by the technical documentation provided with the equipment.

1.5.1 APS (TSI Model 3321)

The TSI Aerodynamic Particle Sizer (APS) is an apparatus that will count particles from the size range of approximately 0.5μm to 20μm using reflected light. The manufacturer specified uncertainty is ±10% of the reading for concentration and ±0.03μm. The equipment works on the principle of time-of-flight spectrometry that measures the velocity of particles in an accelerating airflow through a nozzle. The particle stream is kept centered by a sheath flow as they pass through focused laser beams. The larger particles lag more in the air stream than smaller ones and thus the flight time between the particles is altered. Light is scattered as the particles pass though the two beams and exit the equipment. From this scattered light the equipment is able to pick up the time of flight information and convert it into a calibrated aerodynamic particle size. These particles are then binned into 52 channels on a logarithmic scale. Particles between 0.3 and 0.5 μm are able to be detected, but the statistical chance that the detection is false rises rapidly with decreasing particle size as the extinction coefficient rises exponentially. Thus the particles between 0.3 and 0.5 μm are grouped into one bin, even though there should be multiple bins for this range based on the logarithmic scale used for the rest of the bins. From experimental data taken, experience has suggested that the number of particles in this bin is usually much higher than the rest due to this binning procedure. This equipment also provides a real time assessment of the aerosol stream that gains accuracy the longer it runs. More information on the APS theory and operation may be found in (Baron & Willeke, 2001).

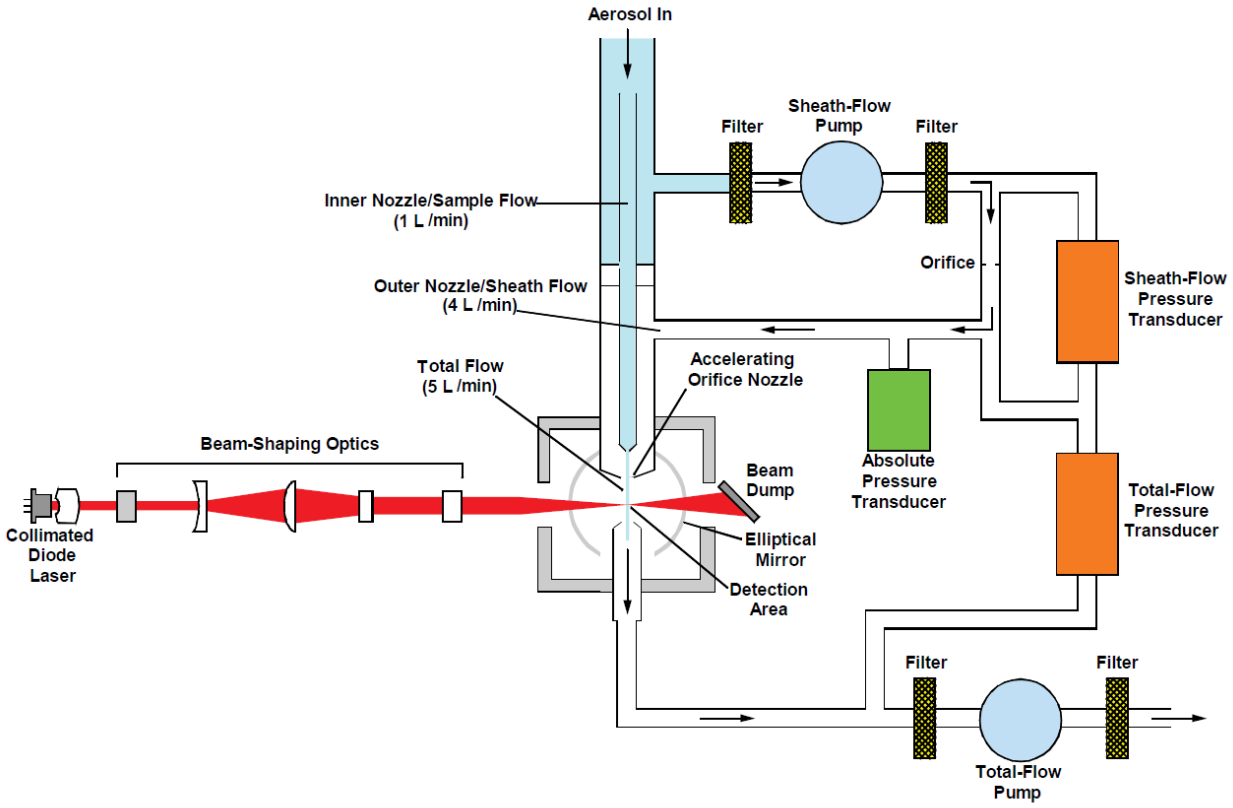

Figure 1-5. Aerodynamic Particle Sizer Diagram
Courtesy of TSI Incorporated, Copyright 2014 TSI Incorporated, Used with permission

1.5.2 APS Diluter (TSI Model 3302A)

The TSI APS was used during portions of testing where the concentrations where in general too high for the equipment to handle. In these cases, the APS Diluter is required. The diluter works on a very simple principle, laminar flow separation and area proportions as shown in Figure 1-6. The bypass flow ratio is controlled by the clean air bypass valve, whose effects may be seen on the pressure gages. Each diluter comes with a capillary tube required to separate the flow with typical ratios of 1:20 and 1:100. Calibration efficiency curves are stored in the AIM software and are selected when setting up the equipment for data collection.

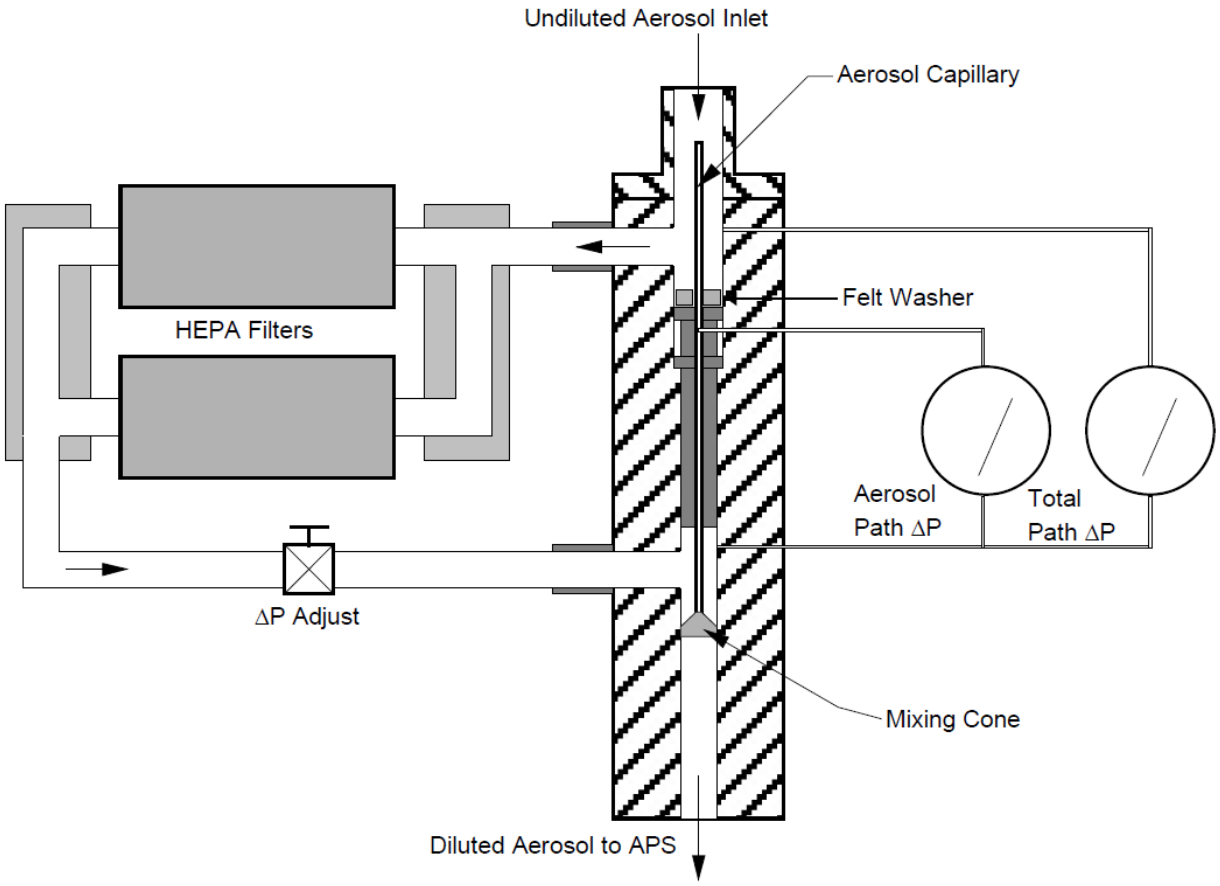

Figure 1-6 APS Diluter Diagram
Courtesy of TSI Incorporated, Copyright 2014 TSI Incorporated, Used with permission

1.5.3 Electrostatic Classifier (TSI Model 3080L)

The TSI Electrostatic Classifier (EC) is a particle separator, or band-pass filter, that works in conjunction with a condensation particle counter. The purpose of the EC is to separate a known size fraction of submicron/nanometer particles from the incoming polydisperse aerosol. The separation is performed in a series of steps and ultimately leads to a nearly monodisperse aerosol that is routed to a particle counter. The flow, shown in Figure 1-7, enters the EC where the larger particles are separated out by impaction in what is appropriately called the impactor. The impactor consists of a plate and 90° bend of the flow. Larger particles are separated out due

to a higher inertia and are thus unable to follow the streamlines around this bend. A figure indicating this event is illustrated in Figure 1-7.

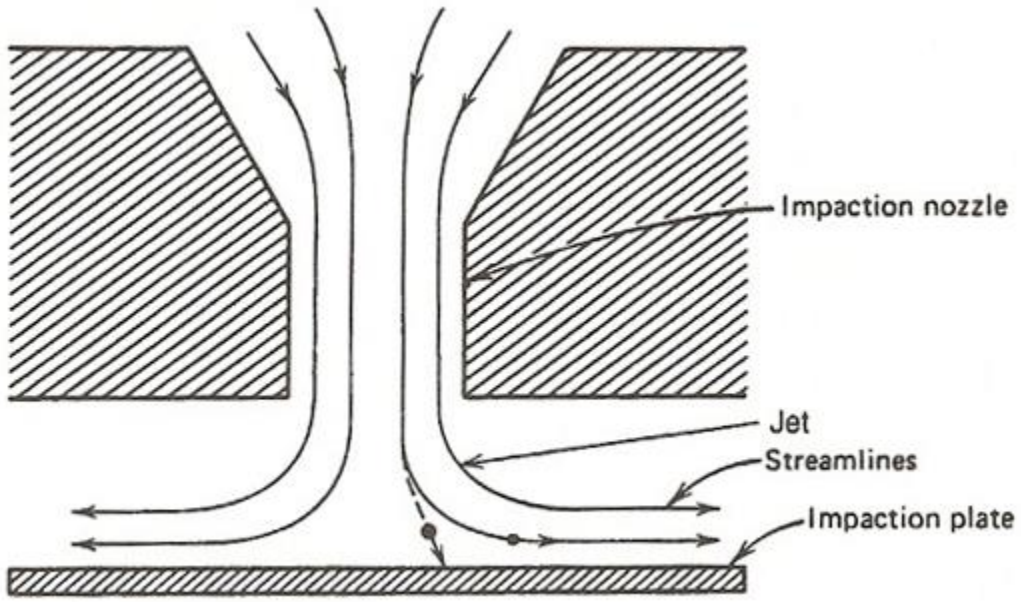

Figure 1-7 Cross Sectional View of an Inertial Impactor
Reproduced from Hinds, Used with permission

After the impactor has separated out the unwanted particles the aerosol is charged by a radiation source as shown in Figure 1-8. A soft xray is used as the radiation source for the equipment in this study. This process is known as neutralizing the aerosol and the purpose of this operation is to ensure a fixed percentage of particles carrying one unit of electrical charge. As a result of the bipolar ion bombardment, an electrical equilibrium state is obtained with a known fraction of particles carrying no charge, a single charge, or multiple charges either positive or negative in polarity. The aerosol then enters the high voltage rod area of the equipment along with a sheath flow of clean air. The now charged airborne particles drift to the electrified voltage rod according to electric field particle mobility and are separated out at the bottom of the charging area. By knowing the sheath flow rate, aerosol flow rate, and expected

particle mobility, the equipment is able to separate the particles and thus provide a first principle measurement due to the electric fields. A charge of +1 is assumed to be on the particles during separation and thus particles carrying different charges may continue with the exit aerosol. The software provided by TSI is then able to determine statistically the amount of particles that were not associated with the exiting aerosol flow, due to different charges, and quantify automatically the proper size and concentration of the aerosol. It should be noted that, for this correction to be applied appropriately, the entire polydisperse aerosol needs to be in the range of the electro static classifier (EC). If it is not, then errors are associated as the statistical corrections cannot be applied to the measured aerosol as the needed values/variables are out of measurement range. This situation would occur if a large portion of the aerosol is at the diameter breakpoint 1000nm, the upper measurement range of the EC. This can be avoided by turning off the multiple charge correction inside the AIM software, but is not recommended.

The EC is able to classify particles as small as 10nm and as large as of 1000 nm in aerodynamic diameter. It will give accurate separation of particles for concentrations reaching up to 10^8 particles/cm^3. The manufacture specified uncertainties are 3 – 3.5% for the size separation. The EC is not limited by any type of binning. However in the control program, AIM, the data feedback is displayed in a binning pattern. Selections of 4, 8, 16, 32, 64 channels are allowed with channel space being at uniform geometric width per decade of particle size. Thus the highest resolution of displayed data and data output will contain 64 channels or bins, however, the bounds of this system are set by the sheath to aerosol flow rate ratio and particle diffusion.

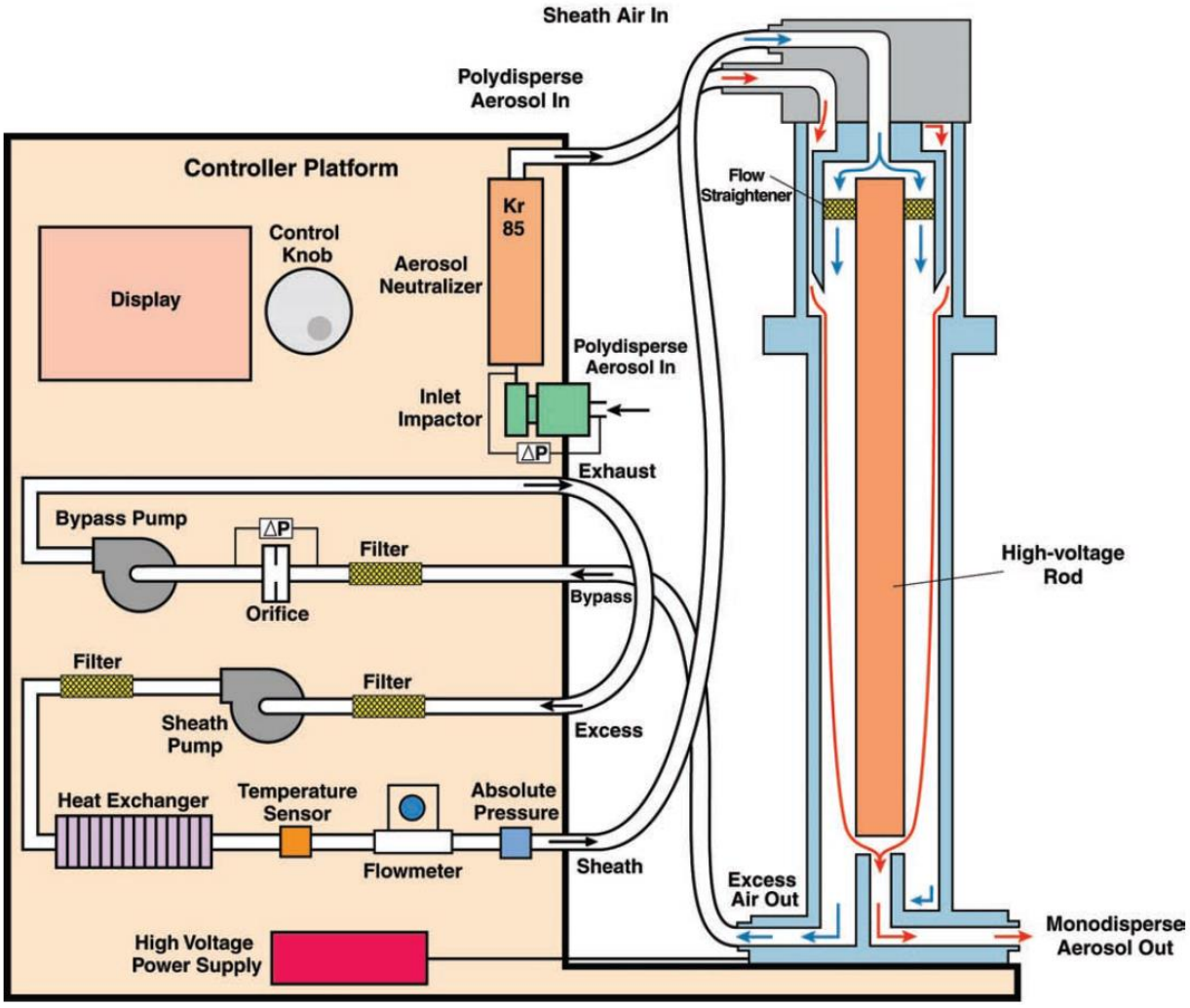

Figure 1-8. Electrostatic Classifier Flow
Courtesy of TSI Incorporated, Copyright 2014 TSI Incorporated, Used with permission

1.5.4 CPC (TSI Model 3775)

The TSI condensation particle counter (CPC) is a device that will count the particles entering it very much like an optical particle counter. However, the difference is that the aerosol first encounters a saturated vapor, which is controlled in this model at 39°C. The air is then cooled which causes the vapor to condense on the particles and increases the size of the particles allowing them to be counted by optical techniques. The particle sizes will grow from nanometer sizes up to 10 to 12 micrometers, and allows a particle detection efficiency of 50% for particles

as small as 10nm. These particles are then measured using reflected light as shown in Figure 1-9.

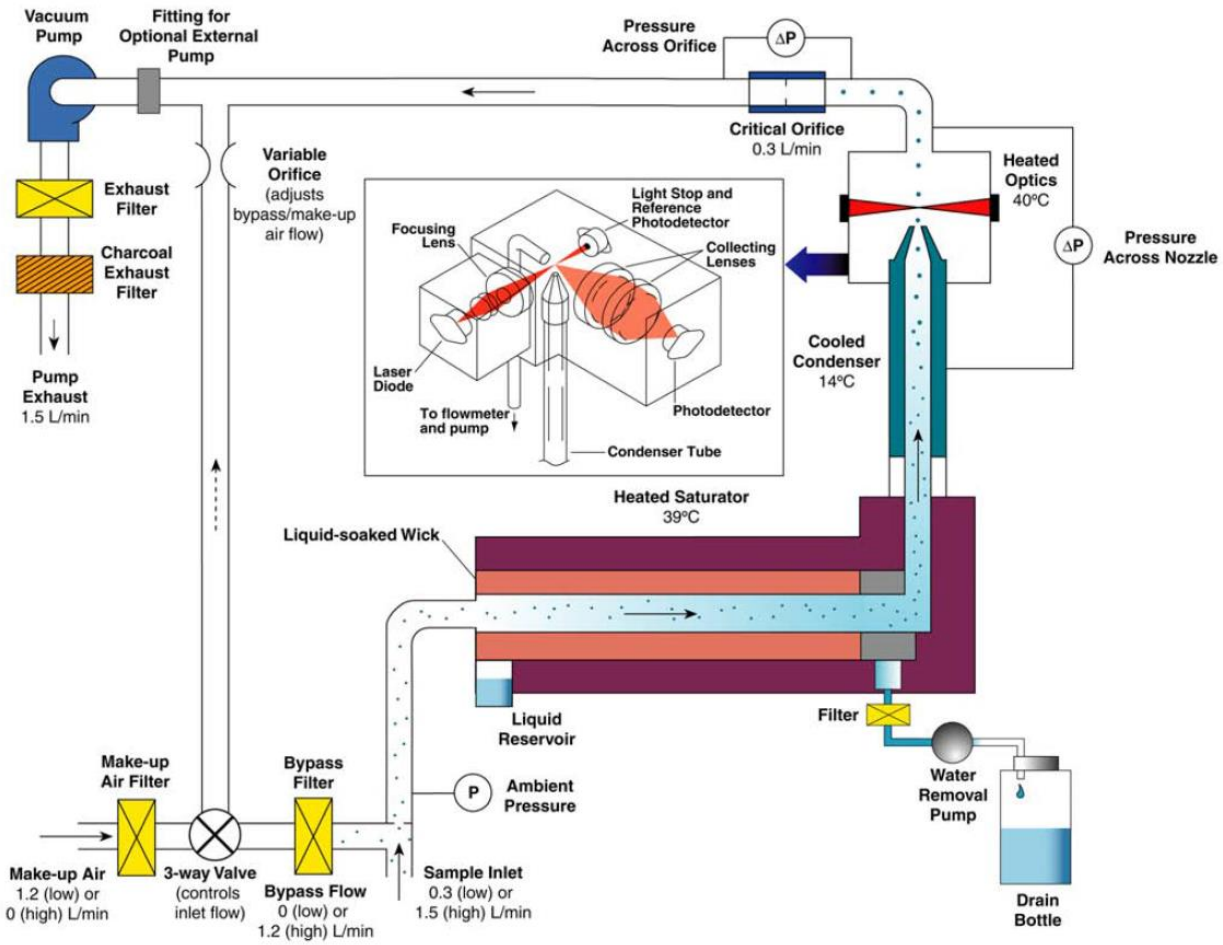

Figure 1-9. Condensation Particle Counter Diagram
Courtesy of TSI Incorporated, Copyright 2014 TSI Incorporated, Used with permission

The manufacture specified uncertainty of the CPC is ±10% at < 5x 10^4 particles/cm^3 and ±20% at < 5x 10^7 particles/cm^3. The particle counter is able to measure over a wide range of concentration and particle size. These limits are about 10^7 particles/cm^3 and 4nm to 3µm.

1.5.5 SMPS

The EC and CPC together make up what is referred to as the scanning mobility particle sizer (SMPS). The SMPS system therefore has the uncertainties of the above EC and CPC.

Together the SMPS system and the APS cover a wide range of particle sizes spanning from 10nm to 20μm. It was observed that this particle range covers the majority of aerosols that were sampled with the general upper limits of the aerosol measured across all three test platforms at approximately 1.5μm. An important feature of the SMPS is that the EC separates the particles by size by creating a continually change particle size window by applying a exponential ramped charge to the voltage rod. At a given time, only allow a narrow range of sizes pass to the CPC but this range changes continuously. This moving size window is synchronized with the CPC measurements to dynamically create a particle size distribution. It is possible that sudden changes particulate concentrations can be missed when the equipment is performing the scan. An example would be the voltage corresponds to a mobility size of 500nm and the event happened at the 70nm range. These 70nm particles would have been filtered out from the sample being sent to the CPC, and thus the event could in theory be missed. The test systems were only operated at approximately steady state conditions for this reason.

1.5.6 OPC (Climet Spectro 0.3)

The optical particle counter (OPC) uses the intensity of scattered light to determine the size of the particle. The aerosol flows through a focused light or laser beam surrounded by sheath air similar to that of the APS. However, the concentration limits of the OPC are much less as the system is meant to count only one particle at a time. The particles counted are binned into 16 channels of different sizes. The particle size range for the OPC is 0.3μm to 10μm with an uncertainty of ±3.5% for size. The OPC was used to monitor the bleed air simulator in real time. Once again, a more references exist that go into greater detail regarding optical particle counter theory of operation and use, including (Baron & Willeke, 2001; Hinds, 1999).

1.5.7 FTIR

In this study, a Nicolet 6700 Fourier transform infrared spectroscopy (FTIR) was used to identify and quantify the chemicals in the bleed air during the testing. The data were pulled from the same bleed air extraction line that the particulate samples were drawn from. An FTIR works on a simple principle interaction between sampled gas stream and light. Each gas will absorb infrared radiation at a specific wavelength(s) or frequencies, producing what can essentially be called a fingerprint of absorption. The concentration of the gas may be determined by the intensity of light absorbed. Once a library database is built of known gas signatures, the detection of the gases may be performed perform.

Chapter 2: Bleed Air Simulator (BAS)

2.1 Note of Health Effects

The literature review presented in this paper gave references about the health effects due to volatile organic compounds and other toxins that can result from the thermal decomposition of oil. The current author and several colleagues have had firsthand experience of these health effects during the initial running of the bleed air simulator. During the majority of testing, gas masks utilizing carbon filters were used to minimize the effects of breathing any contaminates that might occur. However, during the early stages of testing a fellow Ph.D. student at Kansas State University neglected to wear the gas mask citing that expected concentrations at the temperature level planned for testing on this particular day would not cause any harm. However, later in the evening and the next day, this individual experienced a severe headache, difficulty breathing, and burning pains in the upper left chest area near the heart. This event repeated itself when a visiting academic also ignored the safety protocol and proceeded to perform testing without respiratory protection. This visiting researcher also experienced the same conditions and vomiting. This illness postponed the testing by a few days until the conditions experienced alleviated allowing the individual to proceed with his schedule and tasks. These accounts demonstrate the potentially serious consequences of a bleed air contamination event during a commercial aircraft flight.

2.2 Experimental Setup

Properly modeling a bleed air system contamination event requires separate processes to be undertaken using components that are not part of a gas turbine engine, such as an axial or centrifugal compressor, combustor, and turbine. A bleed air simulator must emulate the effects of the compressor section of a running gas turbine engine and the ducting following the bleed air

extraction ports. For the bleed air simulator (BAS), this process is achieved in the following steps:

1. Oil particle generation
2. Pressure increase
3. Temperature increase
    a. Increase due to compression as well as additional heating
4. Dilution of sample into main duct for cooling and velocity reduction

Figure 2-1 shows the general arrangement of the aerosol generation portion of the bleed air simulator. The aerosol generator is a TDA-4Blite packaged component off the shelf from Air Techniques International (ATI). It has two on and off valves on the front which allow for adjustment of particulate injection rates. The incoming air from a compressor is regulated and sent through a dryer for dehumidification and a filter to eliminate particulates in the compressed air. A variable area flow meter allows for the measurement of the flow rate to the generator, while solenoid valve 2 allows the aerosol generator to be bypassed if no oil injection is desired, such as during shut down or start up. Although the valves on the front face could stop the aerosol generation, the aerosol generator is far away from the controller station posing an issue of safety.

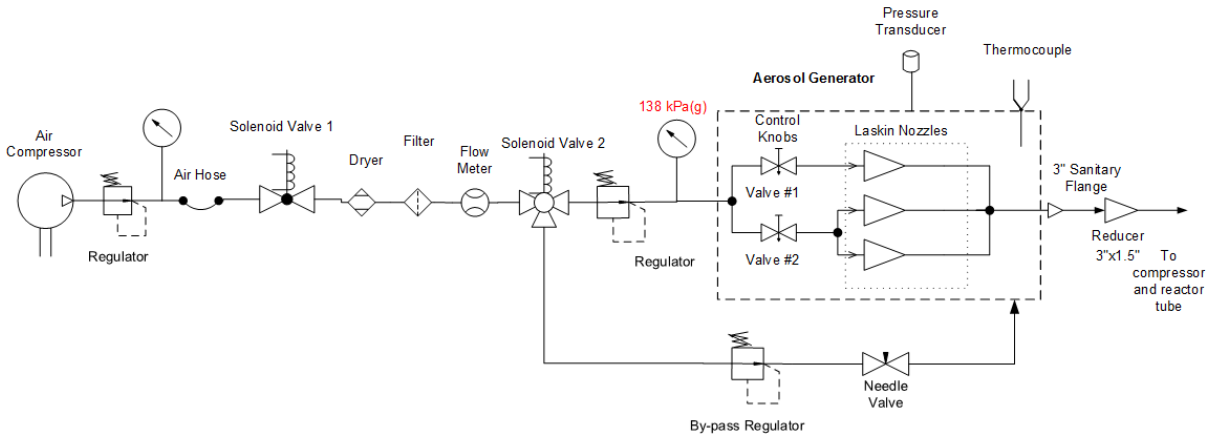

Figure 2-1 Aerosol Generator Portion of BAS
Reproduced from (Mann et al., 2014) with permission.

The compressor and heater sections follow the aerosol generation and are shown below in Figure 2-2. Two check valves keep the incoming air to the reciprocating compressor between 20kPa (2.9psi) and 34kPa (4.9psi) gage air pressure. If the reciprocating air compressor pulls more air flow than required by the aerosol generator, a vacuum will be created and the differential pressure will rise thus creating more particles from the Mobile Jet II oil. The opposite will occur in the reverse case. This makeup air will allow the aerosol generator to maintain a constant differential pressure. A HEPA filter is installed to eliminate contamination of this makeup air. The discharge air pressure from the compressor is controlled via a back pressure regulator that the operators can manually alter. The sub-micron polydisperse aerosol then enters the heater tube section. The heater tube is of stainless steel construction and is designed to provide a constant heat flux by electric heaters to the gas contained within. The inlet temperature will change depending on the pressure settings of the compressor. Temperature of the pressurized fluid is controlled by changing the voltage on a variable transformer. The length of the stainless steel tube was designed to approximate the residence time between the bleed air connection port and the precooler on a typical aircraft engine. This time was reported as

approximately 70ms according to (Magoha, 2012).

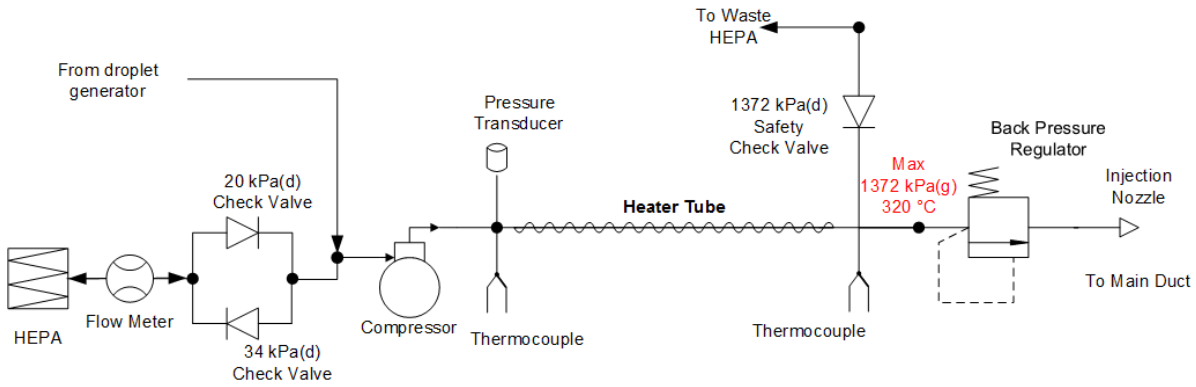

Figure 2-2 Compressor and Heater Portion of BAS
Reproduced from (Mann et al., 2014) with permission.

Finally the main ducting is represented in Figure 2-3. The aerosol is injected into the main duct and cooled by the dilution air from a high pressure blower. The duct itself is a converted ASHRAE 52.2 test rig which was originally designed to test aircraft air recirculation filters. The high pressure blower provides approximately $0.47 m^3/s$ (1000cfm) of air flow though a 610mm x 610mm (2ft x 2ft) cross sectional area. The resulting velocities inside the ducting are about 1.26 m/s (4.13 ft/s). Immediately after the blower is a HEPA filter which is again used to eliminate any particulates from the dilution air. This dilution air provides the necessary aerosol cooling so the measuring equipment can safely sample the aerosol flow stream. It also lowers the concentrations so that the equipment is not overwhelmed by the high particulate counts. A mixing plate after the injection nozzle helps to assure the concentrations are uniformly distributed. The APS and SMPS systems are sampled off of the main duct, while the OPC is sampled off a bypass duct as it was discovered more dilution was necessary for the OPC to accurately measure the aerosol flow. The flow then passes through a last HEPA filter before exhausting into the lab. The sample pickoff ports were sized to be isokinetic for the

system flow. Further details of design and construction of this apparatus may be found in (Magoha, 2012).

The instrumentation for the reactor tube includes a high temperature K-type thermocouple with an uncertainty of ±1°C. The pressure was monitored with a pressure transducer providing a 0-500psia range and ±0.11% full scale accuracy.

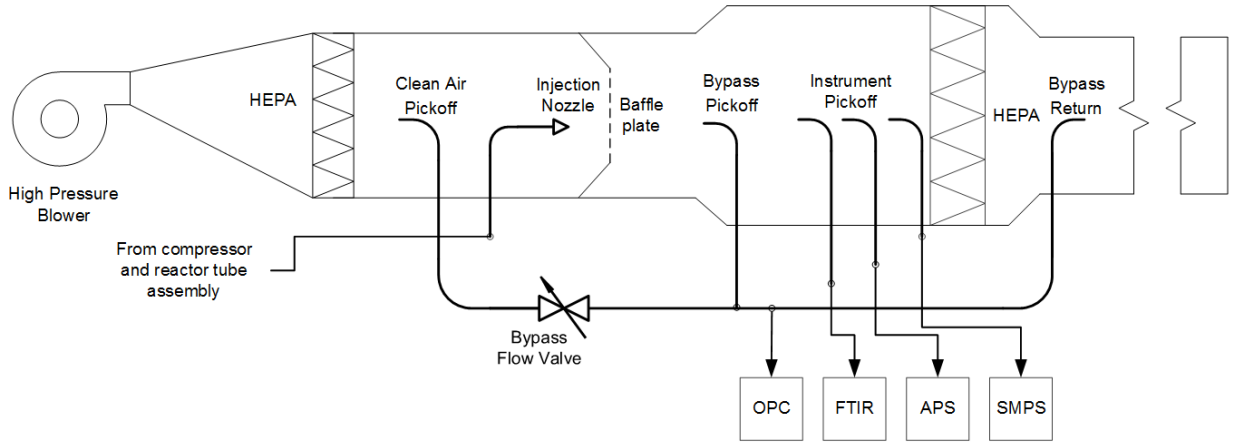

Figure 2-3 Main Ducting Portion BAS
Reproduced from (Mann et al., 2014) with permission.

2.2.1 Test Procedure and Testing Matrix

The testing matrix consisted of reproducing the various flow processes that would most likely be experienced by a bleed air system. These conditions are highlighted in Table 2-1and show the extraction port they are associated with as compiled by the National Research Council (National Research Council. Committee on Air Quality in Passenger Cabins of Commercial Aircraft, 2002). This data also correlates with the information presented by (Hunt et al., 1995) and various gas turbine engineering texts.

Table 2-1. Bleed Air Typical Operating Conditions (National Research Council. Committee on Air Quality in Passenger Cabins of Commercial Aircraft, 2002)

Mode of Operation	Temperature °C (°F)	Absolut Pressure kPa (psi)	Extraction Stage
Top of Climb	310 (590)	690 (100)	Low Pressure
Cruise	250 (482)	340 (50)	Low Pressure
Initial descent from cruise	185 (365)	200 (29)	High Pressure
End of descent (ground level)	230 (446)	460 (67)	High Pressure
High Pressure to low pressure switch-over	280 (536)	480 (70)	High Pressure

The test matrix for the simulation data is shown below in Table 2-2. It should be noted that some of these conditions could be outside the actual operating conditions of the engine compressor but where included to further explore the effect of temperature and pressure. It was determined that testing with these parameters would lead to a better understanding of the aerosol and provide valuable feedback information. This larger test matrix was also utilized to confirm results presented by (Mann et al., 2014) and to measure the particulate data with the SMPS system.

Table 2-2 Test Matix Table

	Temperatre °C (°F)				
Pressure kPa (psi)	185 (365)	220 (428)	250 (482)	280 (536)	310 (590)
200 (29)	x	x	x	x	x
340 (50)	x	x	x	x	x
480 (70)	x	x	x	x	x
690 (100)	x	x	x	x	x

There were two testing procedures followed which produced two data sets. While the conditions of operation and pressure temperature points were the same, the manner in how long they were tested and prior system running differed. The first set of data was taken under the assumption that the oil could be accumulating on the heater tube. There are obvious drawbacks if this is the case, as during the higher testing or even lower testing points the data may be skewed one way or another by the previous test condition. It was also thought that this oil

accumulation could be charring on the heater wall as the heater walls are hotter than the actual gas, thus producing particulate data that would not represent the testing conditions. In order to minimize this effect, the system was run for at least one to two hours with no oil injection at the maximum permissible temperature. The maximum temperature before alarm settings would activate is limited to 350°C. According to various studies mentioned in the literature review, Mobile Jet II will start to smoke at approximately 280°C and starts to char and darken from 300-350°C. The OPC provided a real time measurement of the particles in the system and an exponential decay was observed during this 'burnoff' process. When this decay line was at approximately zero the system was brought to the specified testing conditions. This process was repeated after every oil injection in addition to another one hour 'burnoff' at the end of the testing day. These tests were run for 30 minutes. The SMPS and APS took several measurements during this time period and the data for these will be presented. A total concentration indicates the overall 30 minute measurement, while a graph with time as the independent variable will show the information for each individual test.

The second set of data was generated in 10 minute segments where the 'burnoff' was not performed. The data were once again collected in the same manner as that in the 30 minute tests.

2.2.2 Laskin Nozzle Aerosol Generator

The aerosol generator used for production of the polydisperse particulate flow is a TDA-4B lite. Information for this generator may be found in the user's manual (Air Techniques International, 2014). An example of poly-alpha-olefin (PAO) oil aerosol generation shows that the geometric mean diameter is approximately 230 nm. PAO oil is synthetic base stock oil that is used in various applications and it similar to mineral oil. From data testing experience, this diameter fits very close to the particle sizes generated by Mobile Jet II. Additional information

for the Laskin nozzles is presented in (Andrews, McDiarmid, Vijayakumar, & Mills, 2003). At 20 psi, PAO oil produces a geometric mean of 267nm while the di-octyl phthalate (DOP) oil is at 253 nm. These differences can be attributed to many causes in a system, including viscosity differences due to temperature, and using different generators. Additionally it is important to understand that while the particles generated are about the same size every time, they do vary. This variation is due to small changes in how the particles are generated and more importantly how they are measured.

The pressure of the aerosol generator was kept at 20psi for all portions of the testing across all of the systems. This constant input pressure was to insure that the aerosol output would not change due to a pressure effect, and this pressure is controlled by a pressure regulator on the air input of the TDA-4B lite aerosol generator unit.

2.2.2.1 Expected Mass Input

The amount of oil injected into the engine flow streams should be measured for calculations and to determine if there are significant oil losses occurring in the system. The aerosol generator was first weighed and then turned on for a period of time at the prescribed pressure setting of 20 psi. After the allotted time of test was completed (in general 60 minutes or 100minutes) the system was weighed again. This procedure was repeated several times for each nozzle setting. The scale used to measure the mass loss was an Ohaus Ranger scale. The readability is ±0.0002lbm with a full scale measurement of 30lbm. Equation 1 is used to estimate the amount of air injected into the dilution flow stream and the amount has been normalized to the standard flow rate settings. This equation allows the results of multiple tests to be added up with the proper weighting of flow rates for the time measured for the same number of nozzles open for injection. A Dwyer RMC-104-SSV variable area flow meter capable of reading up to

400 scfh was used to measure the flow rate through the aerosol generator. No information about the uncertainty could be found for this model, but is estimated to be ±2scfh. An upstream pressure regulator was used to prevent the flowmeter from bursting/exploding and was set between 30 to 40 psi.

Equation 1

$$Q(j,k) := \frac{\sum_{i=j}^{k} \left(\Delta T_i \cdot Q_{read_i} \cdot \sqrt{\frac{\left(P_{wall_i} + P_{amb_i}\right) \cdot (70\ °F)}{14.7\ psi \cdot \left(T_{amb_i}\right)}} \right)}{\sum_{i=j}^{k} \Delta T_i}$$

Table 2-3 Mass Flow Injection of Oil @ 20psi

	Mass/Nozzle	Flow Rate	%Error Flow Rate
# of Nozzles	gm/hr (lbm/hr)	L/min (cfm)	%
1	20.5 (0.045)	90.4 (3.2)	20.6
2	22.0 (0.048)	64.0 (2.3)	14.6
3	19.6 (0.043)	66.6 (2.4)	11.1

As shown in Table 2-3 the amount of oil that is deposited into the dilution air stream is nominally about the same amount per nozzle. The slight variations are most likely due to the nozzles operating slightly differently. The flow rate error in Table 2-3 is the deviation from the nominal value and is not the accuracy of the measurement. However, the large errors from the nominal 75 L/min (2.65 cfm) may be due to the meter. These errors are likely due to the higher pressures of air flowing through the meter and the correction formula not accurately predicting the frictional losses of the air hose via a basic mass flow rate balance. There will be a pressure loss associated with the flow through the line that was not able to be measured upstream of the flow meter. At a pressure of 30 psig and 80°F the density of air is 1.145kg/m^3, which amounts to a 210% change. Additionally, the temperature range during testing was 69°F to 84°F. It is not possible to put a flow meter in the line after the oil injection where the pressure would be close

to atmospheric. Any meter used after the injection of oil would result in deposition of particles on the innards of the parts contained within the meter. This deposition would defeat the purpose of injecting an aerosol into the flow stream and thus give inaccurate values. However, the errors introduced with the flow through the aerosol generator are very minor. The nominal flow for the bleed air simulator is approximately 1000 cfm while the highest flow rate into the dilution stream is at most 7 cfm. This flow amounts to an added flow rate of 0.7%, well within the uncertainty of the flow measuring equipment on main bleed air ducting in the simulator. This will be even lower on the gas turbine engines as the flow rates at STP at higher power settings will exceed 2300cfm and 3500cfm for the C18 and C28B respectively.

2.2.2.2 Measured Mobile Jet II Aerosol Output

The oil aerosol output size distribution was also measured prior to the engine run tests and subsequent to the BAS testing. The size distribution should be known prior to the engine or simulation injection, so as to identify changes to the particulate distribution at low temperature settings. These changes would indicate if the manner in which the aerosol is compressed or how it is heated would have an effect on the final aerosol size distribution. Earlier work by (Mann et al., 2014) indicated that the pressure did not have a large effect on the aerosol output, but the SMPS was not available during testing for the confirmation of such conclusions for sub-micron sizes. The aerosol output could indeed vary in the ultrafine range if the methods of compression vary. In the bleed air simulator, the simulated bleed air pressure is generated by a reciprocating compressor. In the Allison T63-A-700 (C18) the bleed air pressure is generated by five stages of axial and one centrifugal stage for an overall pressure ratio of approximately 6.2:1. The Allison C28B engine has only one centrifugal stage and a ratio of about 7:1.

The graphs below show the aerosol outputs of the Laskin nozzle injection system. It is interesting to note that the diameter maximum points do change throughout the different tests done. This change in diameter highlights the problem with continually generating an aerosol that is of a constant nature each and every time. Part of these issues may be attributed to temperature as shown in (Jian-Wen & Jin-chun, 2009). As the temperature of the oil increases, the average droplet size will decrease. The same outcome is also found if the air temperature increases as well. Conditions in Kansas varied during some parts of testing, and the temperature fluctuations were greater than °35F in a three hour time period in some cases. The current facility setup at the National Gas Machinery Laboratory (NGML) does not have the ability to run a gas turbine in a controlled environment, and thus the ambient temperatures are influenced by the ambient weather conditions.

2.2.2.2.1 Note On Test Legends

In the data presented, a unique naming convention was used for the graphs to provide a unique name for each plot. This naming convention also prevents confusion about the conditions for the graphs presented in this report.

The test during which the data were taken is labeled as TXX, with 01 being the initial collection. A test is referred to an entire run without shutting down, while the SXX refers to a sample within that test. If multiple samples were taken, such as five continuously back to back, and displayed, they have the added suffix of RXX, which refers to the runs within a sample. The runs will always start one after the other; otherwise they will be categorized as a sample. That is, if there is any time delay between data sets, it will be labeled as a sample. If 'LN' is added on the data set the information was recorded with only the aerosol generator. Additionally, the suffix of Inj X indicates how many nozzles were active during the injection of oil. The entire set

of data points for the engine conditions may be found in Appendix B: . The ambient conditions were not found to influence the aerosol generator output and thus no data table for it is presented.

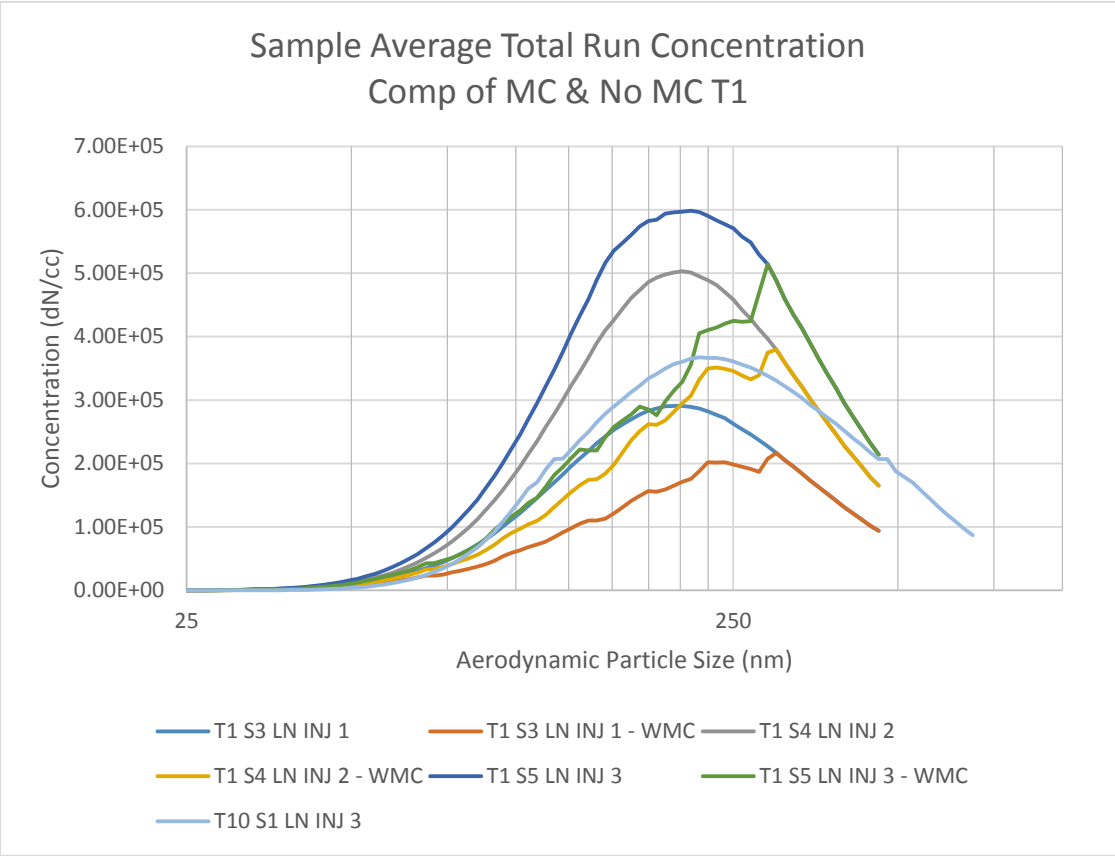

Figure 2-4 Laskin Nozzle Injection Comparison of Multiple Charge Correction

Figure 2-4 shows the effects of the multiple charge correction applied to an aerosol. The multiple charge correction should be applied at all times, but as mentioned earlier, there are issues when aerosol encounters the bounds of the equipment when the D50 isn't set close to this bound. The tail end of the aerosol is above the set bounds on the equipment, and thus the charge correction isn't able to be applied appropriately. For better results the entire peak or size distribution data should be inside the bounds measured.

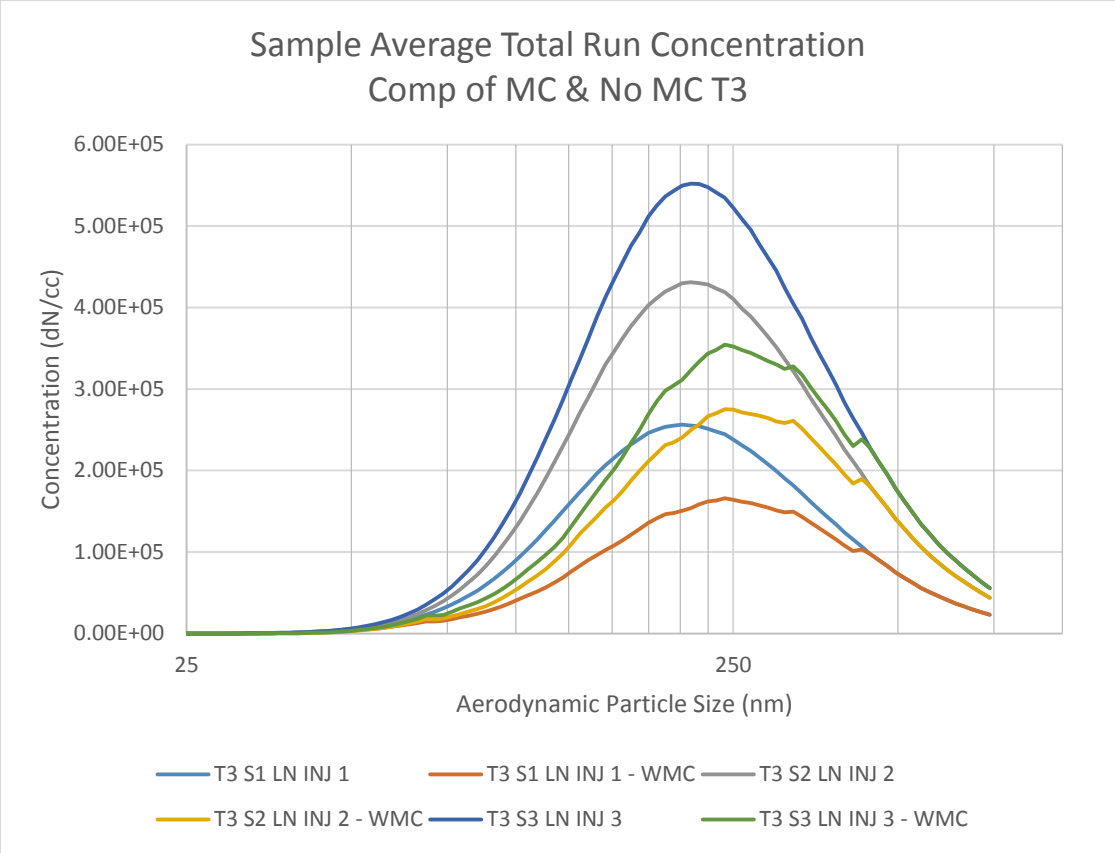

Figure 2-5 Laskin Nozzle Multiple Charge Correction – Larger Bounds

As can be seen in Figure 2-4 and Figure 2-5, the corrections are being statistically applied to the previous particle sizes as the particles move though the measurement system. The distributions in Figure 2-5 were generated under the same test conditions with the SMPS time of scan and flow altered to increase the size bounds. From this increase in measureable range, the data with the multiple charge correction is more accurately represented than in Figure 2-4, but there are still errors. Due to this effect the particle data will be represented without a multiple charge correction for the Laskin nozzles. The effect becomes larger as the particle size increases, but for the majority of aerosols measured on the simulator and the two engines, this effect will have a minor impact on the final results. The aerosol measured at test conditions is in a range below 300nm for the size peak distributions. It is, however, important to note these

corrections are applied to the system in order to represent the data as accurately as possible. Diffusional corrections have no such issues being applied and are based on the stream flow information, such as mass flow rate, temperature, and pressures. No adjacent bins are needed to apply these corrections.

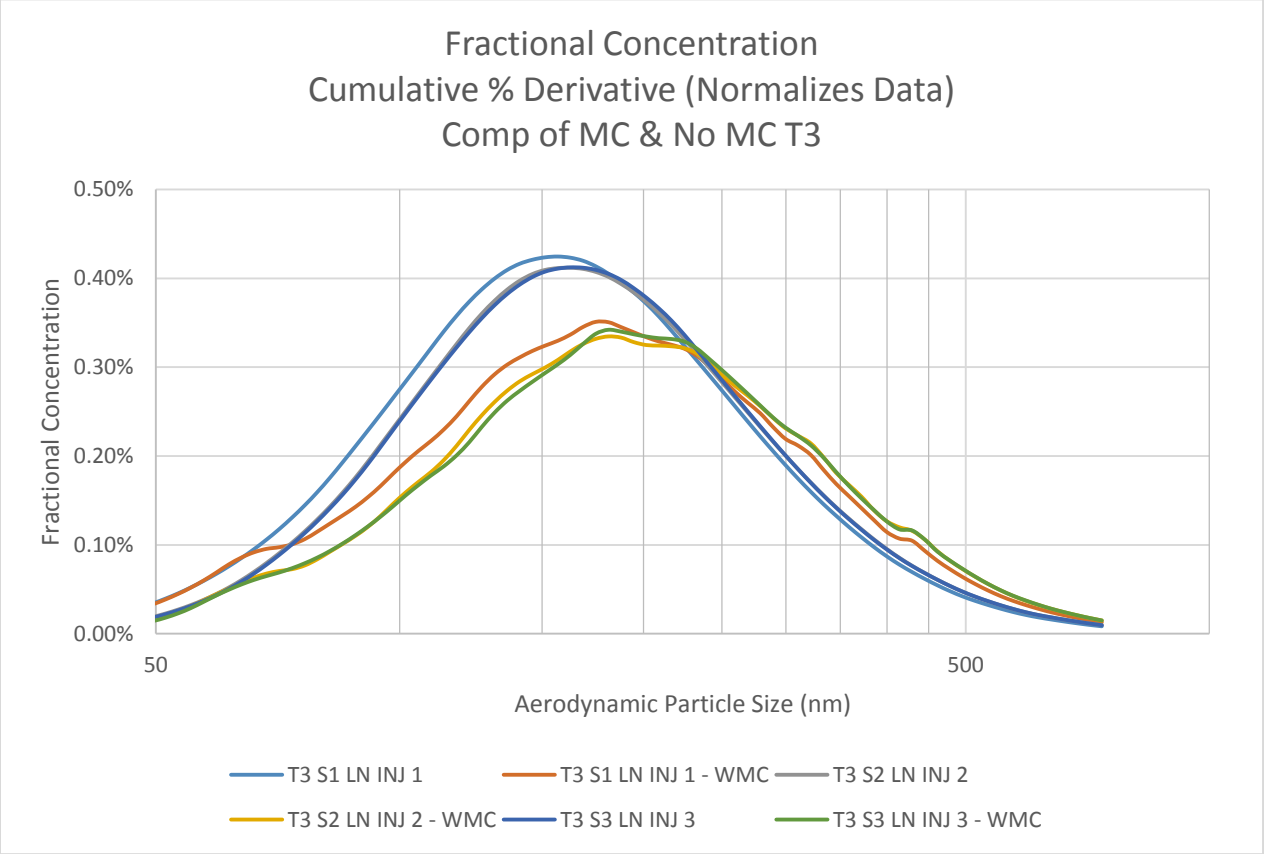

Figure 2-6 Laskin Nozzle Comparison (Fractional)

Figure 2-6 is the same figure as Figure 2-4 with regards to the data presented. However, the key difference between the two figures is the following. The information presented in Figure 2-4 shows the sample average concentration, whose points on the graph are the diameter midpoint. The information shown in Figure 2-6 is the cumulative summation derivative. These data were discussed earlier and shows the information in a normalized manner. It can be seen

from this image that the injection size distributions of all three nozzles appear to match fairly well.

Figure 2-7 shows the mass injections between two different days and how the results line up in regards to different ambient conditions. The fractional mass amount, Figure 2-8, shows where the mass is located and once again all three of the Laskin nozzles line up on the size distributions. These two graphs indicate the Laskin nozzles have reproducible aerosol outputs within reason.

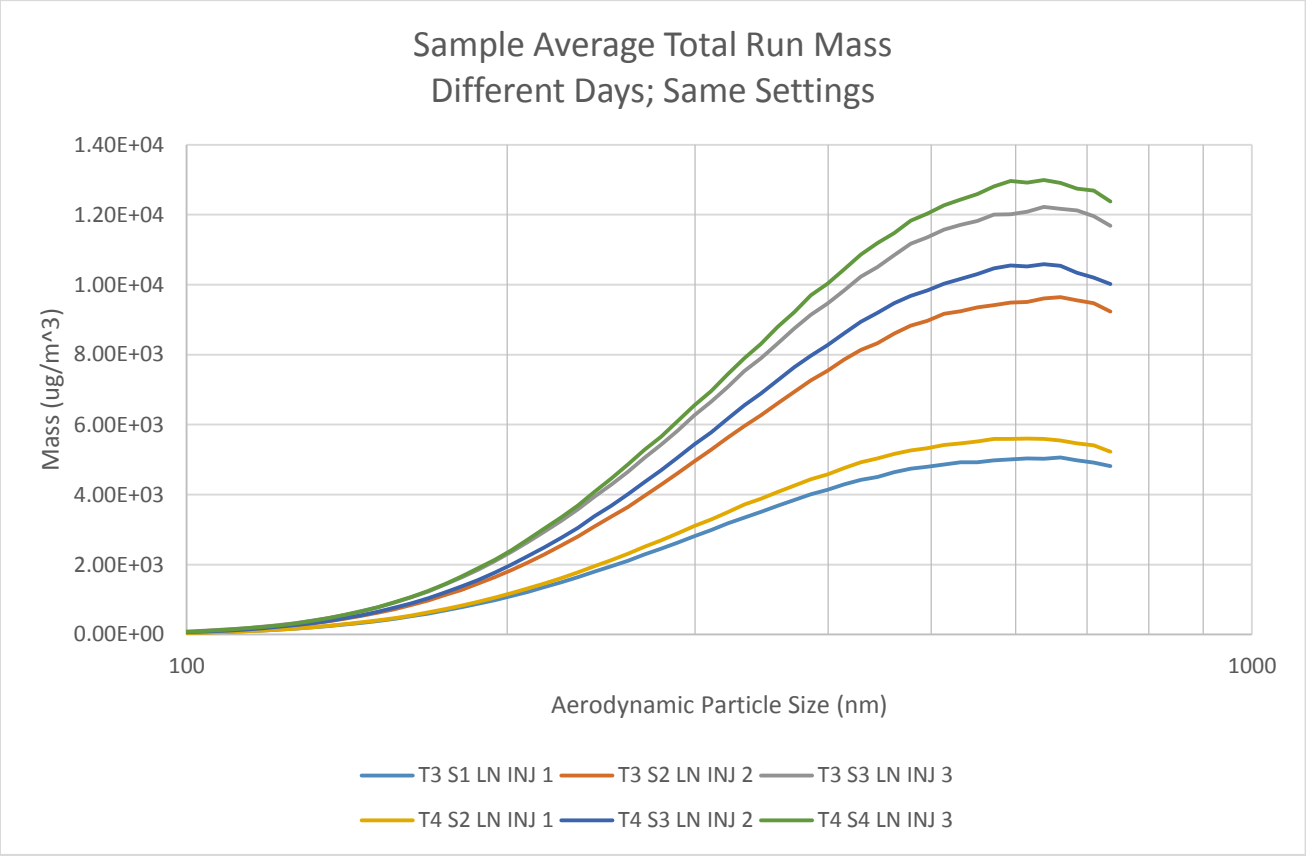

Figure 2-7 Laskin Nozzle Mass Injection Distribution

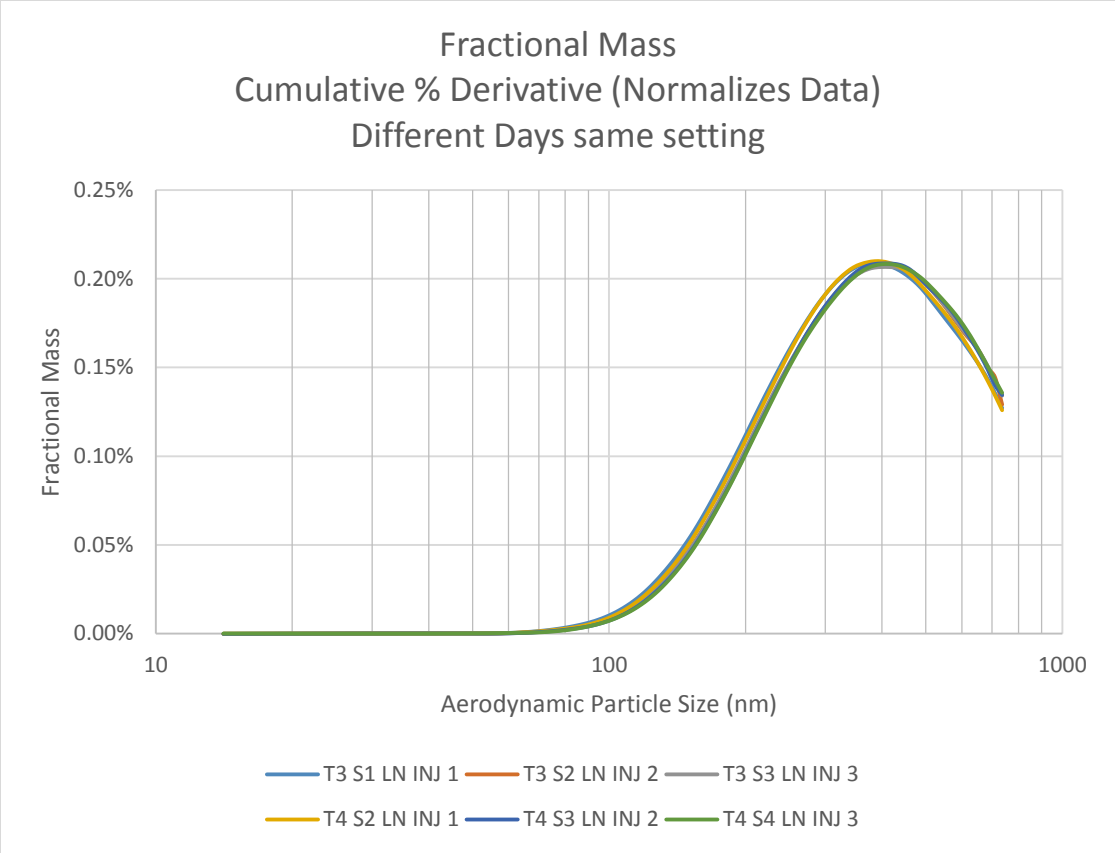

Figure 2-8 Laskin Nozzle Injection Fractional Mass

The neutralizer also makes a very large impact on the data that is collected. The job of the neutralizer is to put a known charge distribution onto the particles so that accurate sizing occurs. There is not a software correction for this item, but rather the physical information is relayed to the output data based on the principles of physics. It makes the largest difference on small particles not being able to be picked up. If these particles are not registered by the equipment, then there is the issue of an artificial peak shift. This effect is readily seen in Figure 2-9.

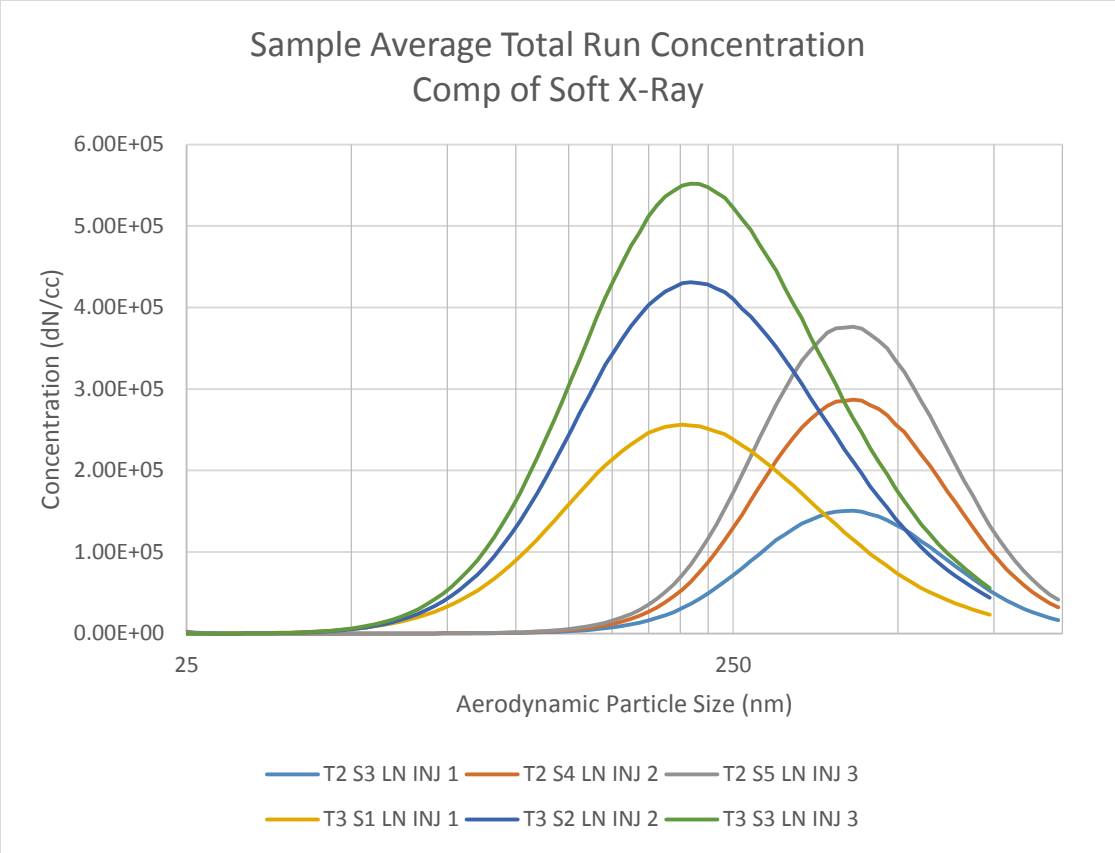

Figure 2-9 Comparison of Soft X-Ray Laskin Nozzle

The final information piece about the testing is the determination of ambient air and how much the Laskin nozzle injection will outweigh the ambient air concentrations. This information is important for the two jet engines because a HEPA filter is not able to be installed on the air inlet for the engines due to pressure drop limitations. Figure 2-10 and Figure 2-11 show the comparison of an ambient measurement to the injection measurement with one nozzle. The VAC is the measurement with no particulate injection as pushed by the blower/vacuum through the system. This measurement was used to determine if the blower had any effect on the system particles generated, and the results indicate that negligible, if any, impact was made. If particles are detected, they are above the readable size on the SMPS system but particles of this size are highly unlikely. The particle concentrations are continually lowering as the aerodynamic

particle sizes increase. The concentrations of the ambient air were so much lower they are at least three orders of magnitude below the concentrations with injection. More dilution air will not lower the concentrations by more than a magnitude which will be shown on the ambient air data for the two gas turbine engines.

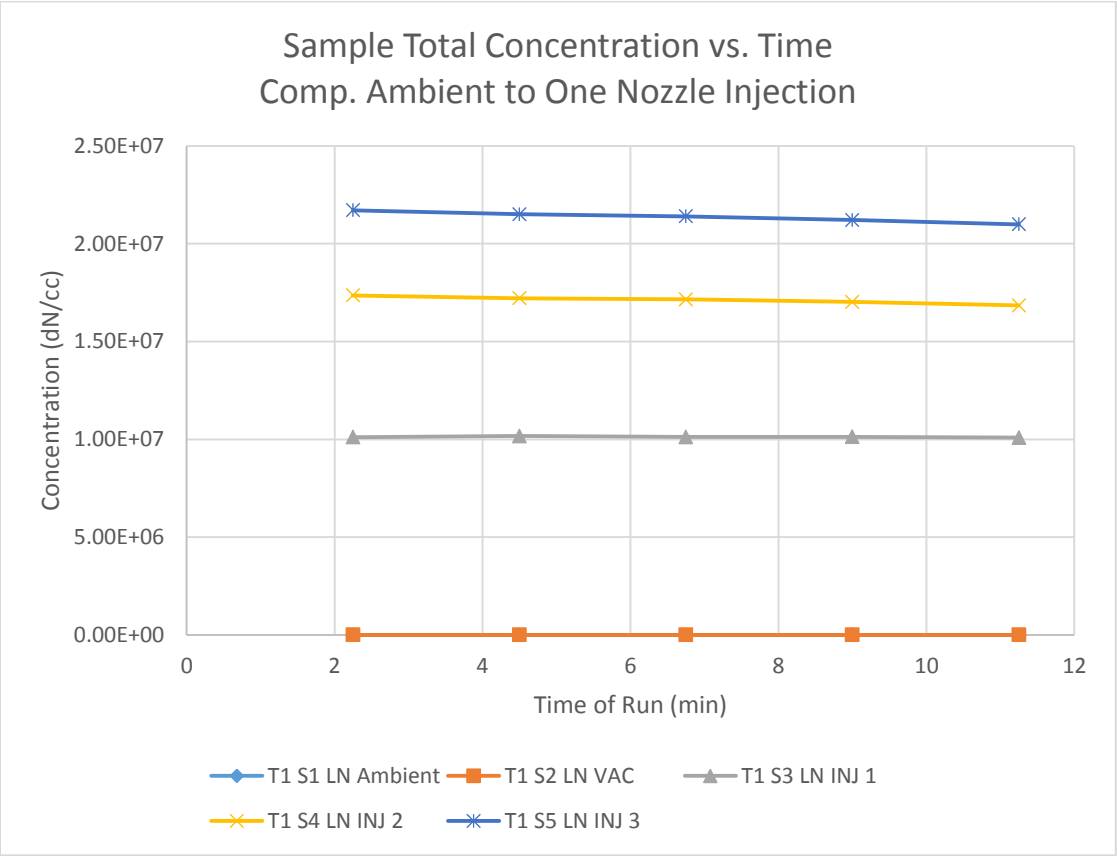

Figure 2-10 Laskin Nozzle Ambient Concentrations Comparison

Table 2-4 Ambient and Blower Concentrations (dN/cc)

	Run 1	Run 2	Run 3	Run 4	Run 5
Ambient	3.96E+03	4.34E+03	3.70E+03	4.46E+03	4.05E+03
Blower	5.04E+03	4.41E+03	3.85E+03	3.61E+03	3.82E+03
1 Nozzles	1.01E+07	1.02E+07	1.01E+07	1.01E+07	1.01E+07

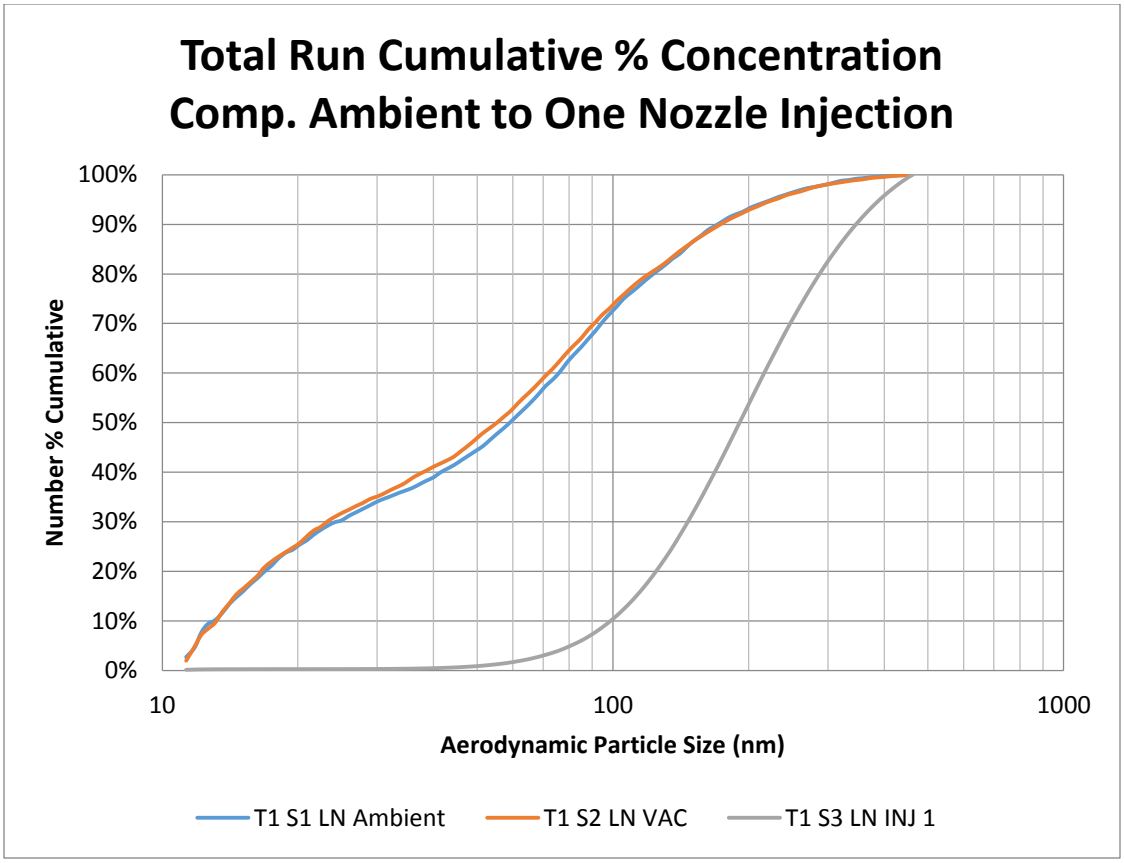

Figure 2-11 Laskin Nozzles Ambient Cumulative Run

It is also readily seen that even if the concentrations are closer in amount, graphs such as Figure 2-11 would help to distinguish the ambient data from the generated particulate data.

Observations also indicate that the ambient concentrations change from time to time. Indeed information was picked up during the burning of local fields around the Manhattan, Kansas area. Even when visible smoke was observed in the air, the ambient concentrations did not increase above 1.E3 dN/cc/min in concentration. With this information at hand, the injection concentrations stayed roughly a factor of 100 above the ambient conditions, which includes the contributions of the blowers or air flow generators. Thus, any contamination from the ambient air will have very little impact on the data taken for testing.

The Aerodynamic Particle Sizer picked up the tail end of the particle size distribution. A repeat set of tests were run to determine the repeatability of the equipment and how well they agreed with the SMPS on the overlapped sample particle size ranges. During this test, the APS utilized the diluter in order to accurately measure the particulate counts. The dilution ratio was 100:1.

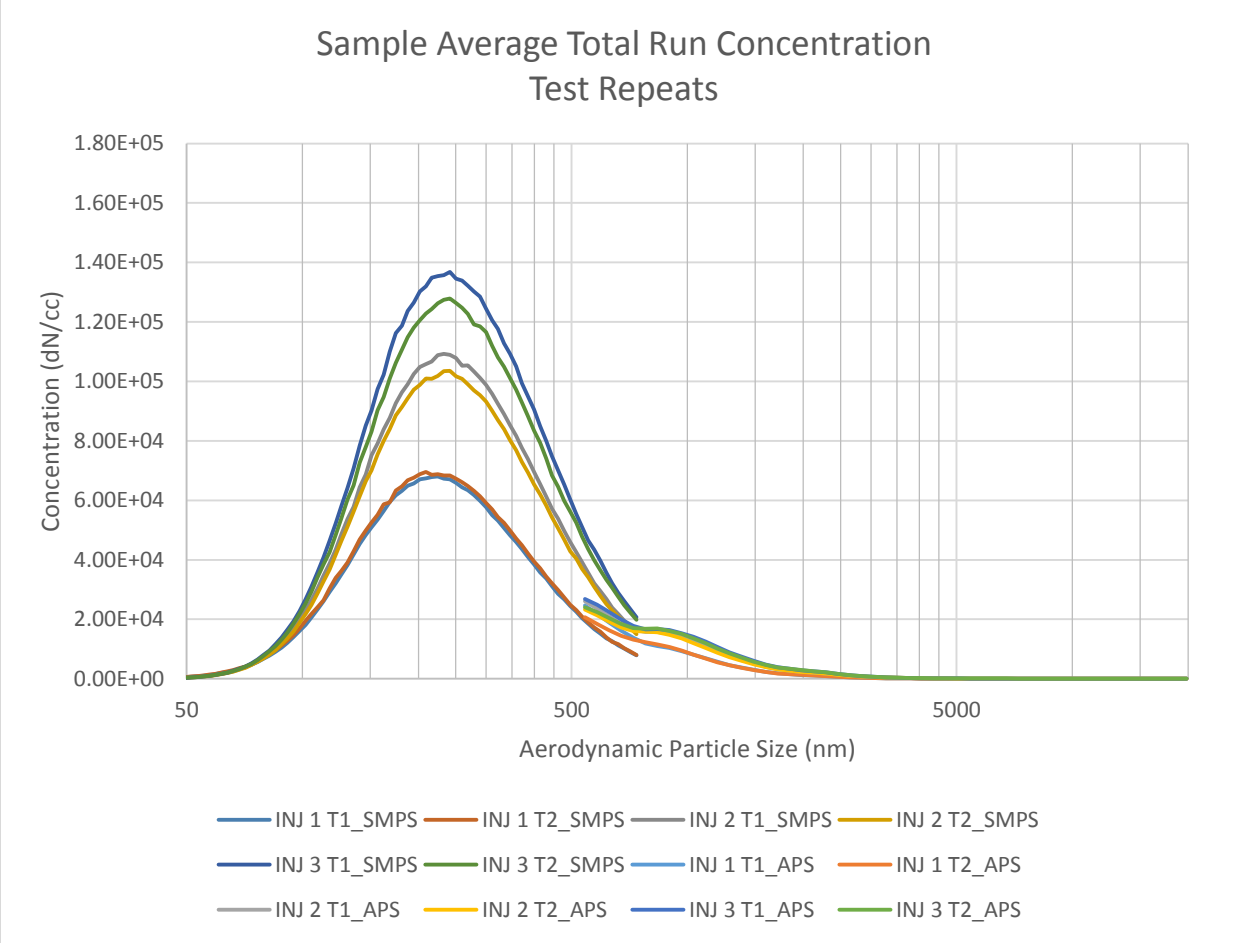

Figure 2-12 Laskin Nozzle SMPS & APS Comparison

Figure 2-12 shows the SMPS and APS data for the repeated test runs. The APS data is clustered tighter than the SMPS data, but they appear to correlate very well, considering that not all corrections are being applied to the SMPS data and that they size participles by completely different physical processes.

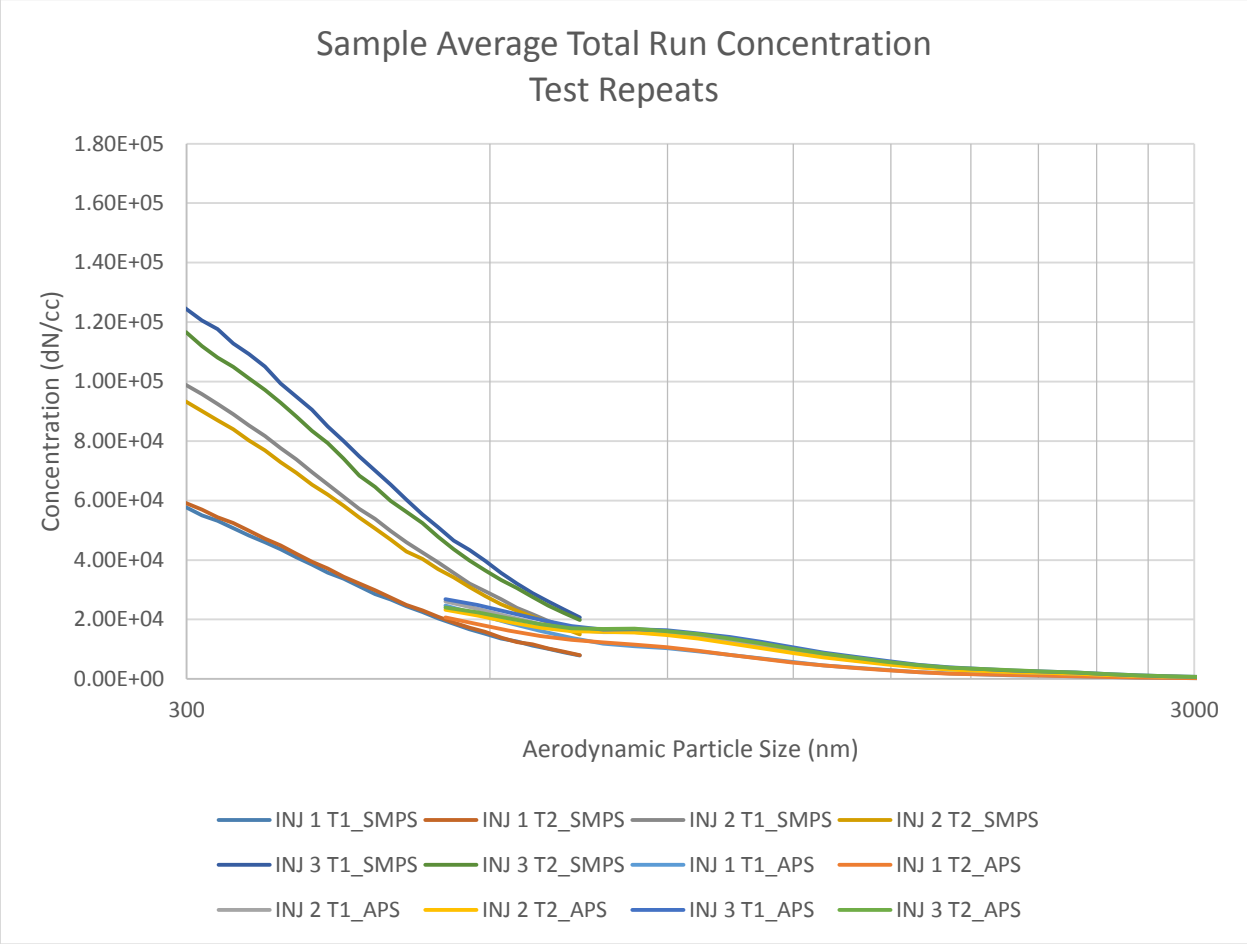

Figure 2-13 Laskin Nozzle SMPS & APS Comparison Narrowed

Figure 2-13 highlights the overlap of the data even better and tends to show that the information matches well. It should be noted that the APS data at sizes <0.523µm were neglected in the graphed data. The APS performs the calculations for mean, mode, geometric mean diameters for the various number, surface, volume, and mass properties ignoring the <0.523µm information. While the APS is able to detect that particles exist at sizes <0.523µm, it is not able to properly define their size and thus they are clumped in a single group below 0. 523µm. The APS also has channels that are spaced logarithmically and thus the particles detected

below <0.523μm would be sorted into multiple bins. The equipment is informing the operator that particles below this size exist, but it is not able to provide any more detailed information about the particle sizes with the proper accuracy as compared to the other channels of data.

2.3 Results and discussion

2.3.1 Testing Data (30 Minutes)

The data taken for the 30 minute tests were taken over multiple samples on the SMPS and APS systems. The SMPS system was set to the standard 120s scan time with 15s retrace. At times this testing scan uptime may vary, which will reduce the uncertainty errors in the data provided by the SMPS. The testing concentrations may then be divided by the testing time to allow direct comparison between the two sets of data. The APS test time was increased to 135s to match the SMPS scan time. This time period results in 15 SMPS data sets and 15 APS data sets for each test conditions.

Table 2-5 shows the data summary of test conditions regarding the bleed air simulator. The designated names will be used on the information in the graphs and, as stated in the name, those conditions are the target conditions. Test conditions were limited to within ±4°C (±7.2°F) and ±14kPa (±2psi) of the specified values. The table also lists the average temperature and pressure values of the heater tube along with the average surface temperatures. Additionally the standard deviation values are given for the temperature measurements in order to help quantify the variation from the average temperatures measured. It is interesting to note that some of the heater tube temperatures are much higher than the aerosol test conditions. It could very well be this issue is what causes the observed variations in the data when comparing multiple test runs.

Table 2-5 BAS Data Summary (30 Min)

	Actual		Std. Deviation		Reactor Tube Temp				
	C	psi	C	psi	C	C	C	C	C
Designated Name	Temp	Pressure	Temp	Pressure	TS1	TS2	TS3	TS4	TS5
115C 30psia	115	29	0.72	0.46	106	113	116	116	115
185C 30psia	187	28	2.96	0.41	157	192	208	215	225
230C 30psia	230	29	2.95	0.46	186	232	255	281	291
230C 50psia	230	54	0.51	1.01	181	217	239	262	271
230C 50psia T2	N/A	N/A	N/A	N/A	N/A	N/A	N/A	N/A	N/A
230C 50psia T3	N/A	N/A	N/A	N/A	N/A	N/A	N/A	N/A	N/A
230C 70psia	236	69	1.43	1.77	185	219	241	263	273
250C 30psia	248	30	3.14	0.50	195	247	272	301	313
280C 30psia	281	31	4.00	0.53	217	279	309	344	357
280C 50psia	285	51	1.74	1.01	210	263	295	331	344
280C 50psia T2	274	50	1.16	0.78	233	282	307	331	340
280C 70psia	281	69	1.69	1.33	202	250	282	317	332
305C 67psia	305	66	2.89	1.78	220	274	312	352	368

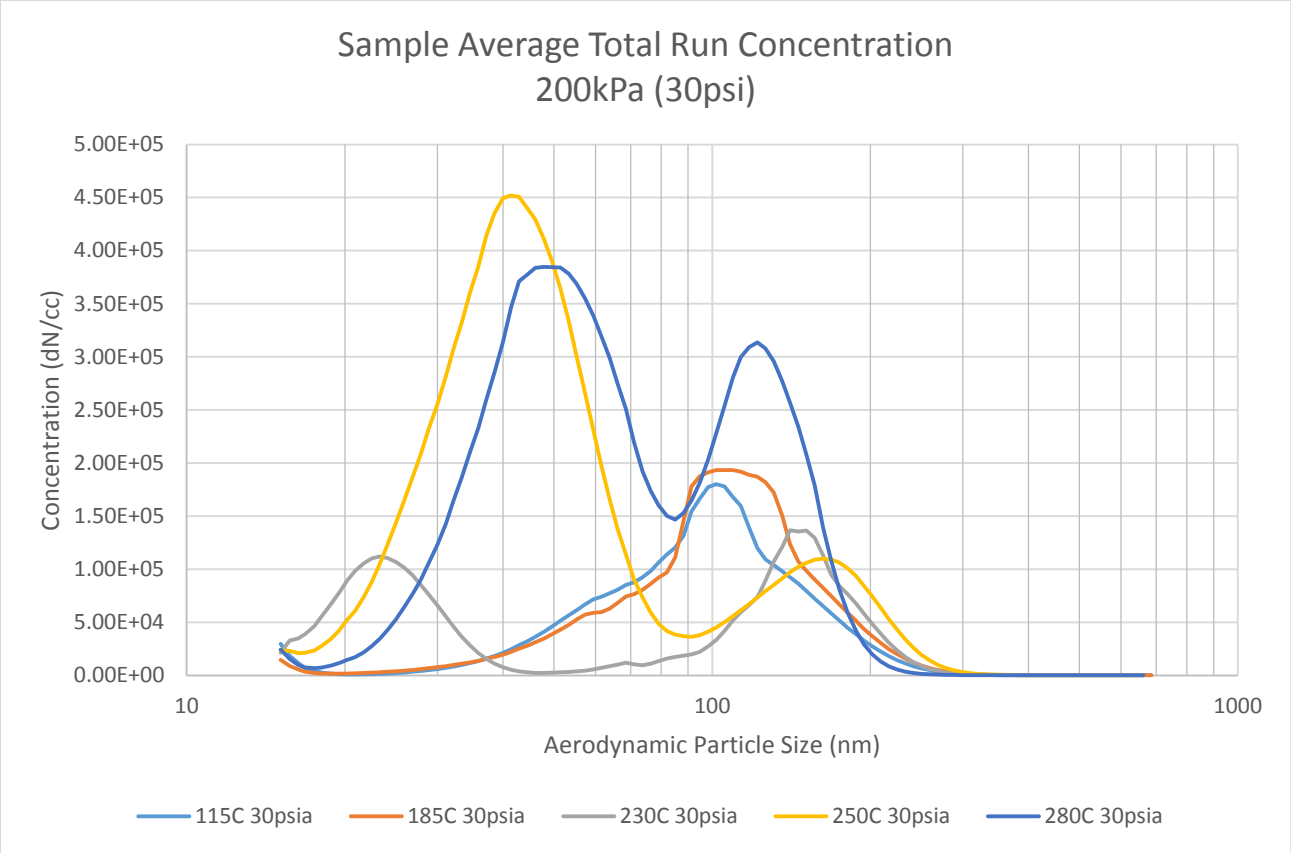

Figure 2-14 BAS Constant Pressure 200kPa (30psi)

As was evident in the data presented by (Mann et al., 2014), the concentrations seen in the data in Figure 2-14 clearly show that the majority of the concentrations and particle sizes are submicron and situated in the ultrafine and nanoparticle regions. The concentrations are seen to increase in the ultra-fine range when the temperature is increased. A second peak starts to appear at 230°C while simultaneously shifting the 100nm peak to the right closer to 110nm. The concentrations measured by the APS are minimal for all of the tests. Figure 2-15 illustrates the amount of particles the equipment was able to detect. Nearly all of these particles were under 1500nm. This information corresponds very well with the information present by (Mann et al., 2014) and indicates that the aerosol size distribution with oil degradation is nearly all submicron in nature. The particle counts observed during some of the runs were five to size orders of

magnitudes in difference between the SPS and the SMPS. Thus, with the APS presenting so little data the results from it are not included in most of the data analysis. For all practical purposes, the APS data compared to the SMPS data gathered during the thermal degradation of the oil was of little value.

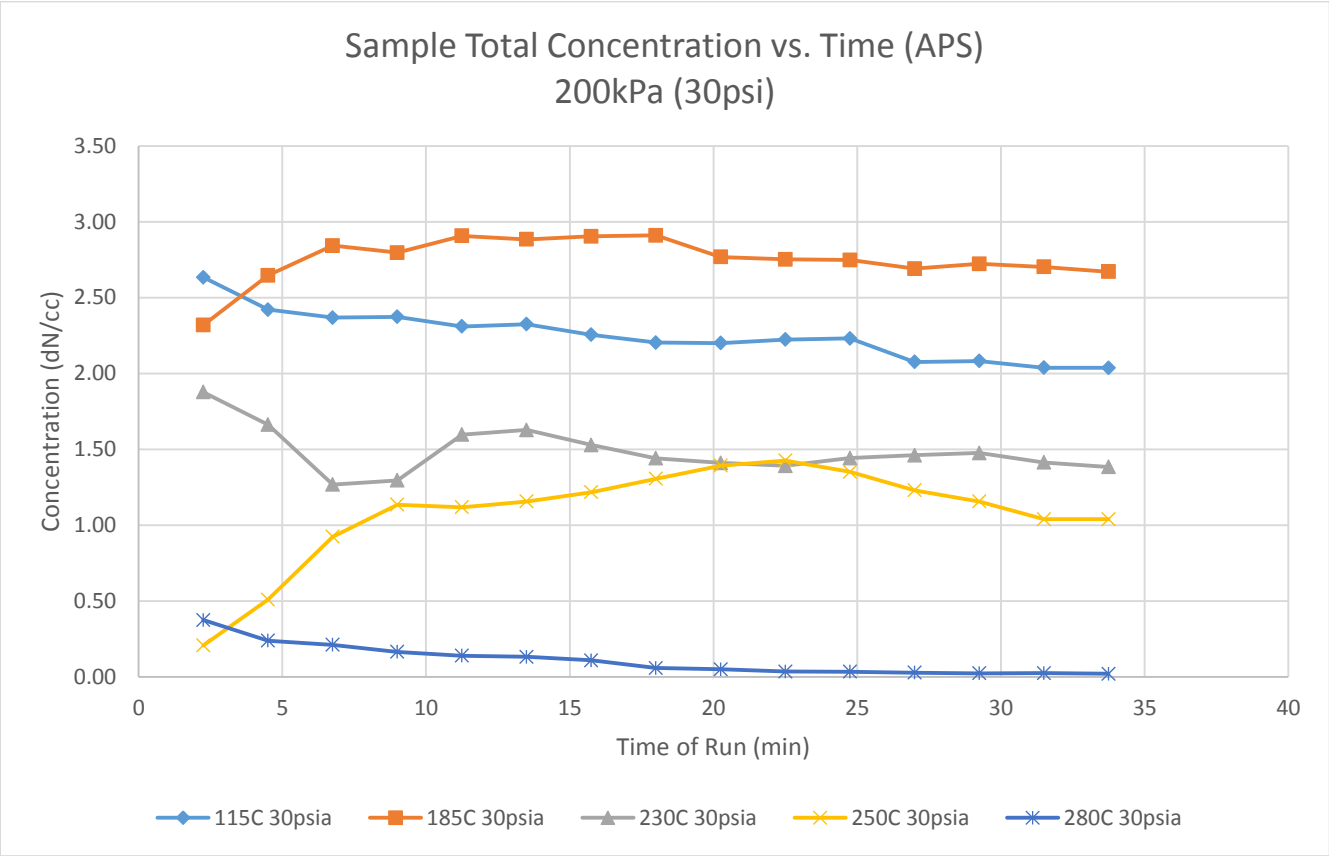

Figure 2-15 APS Total Concentration vs. Time

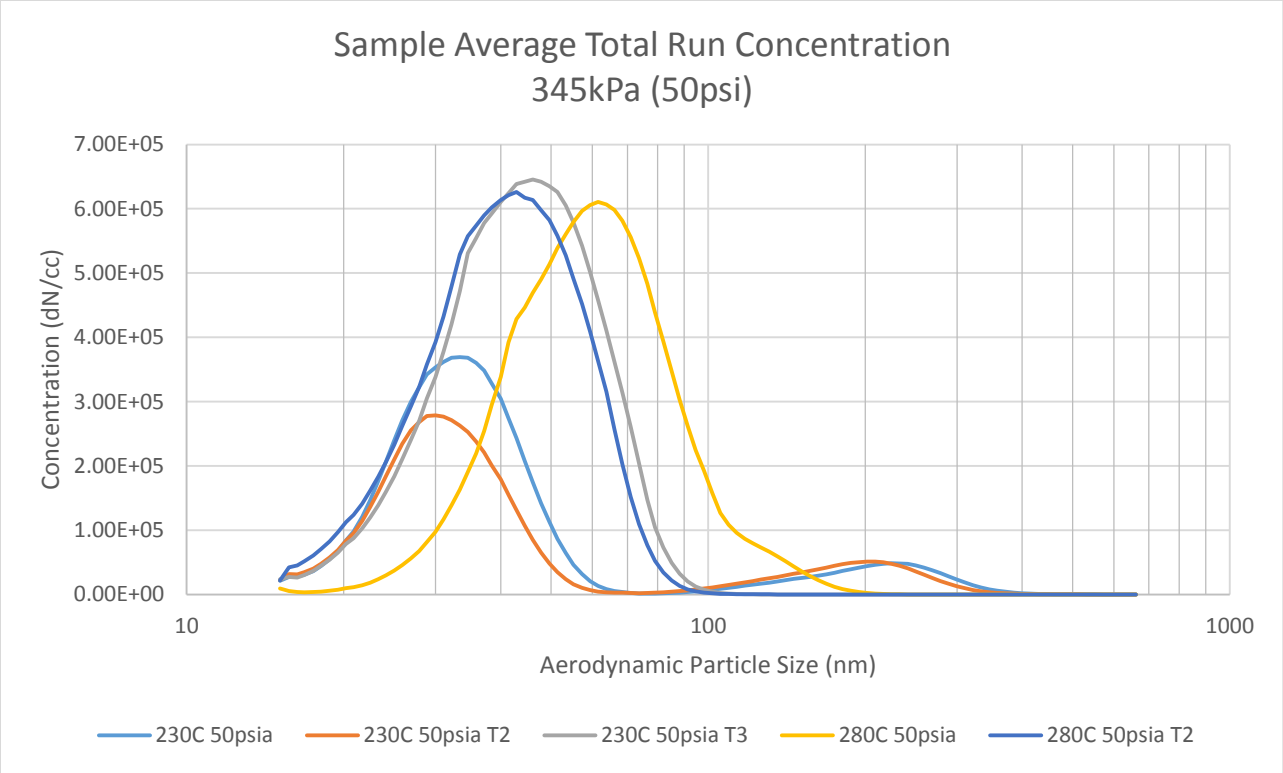

Figure 2-16 BAS Constant Pressure 345kPa

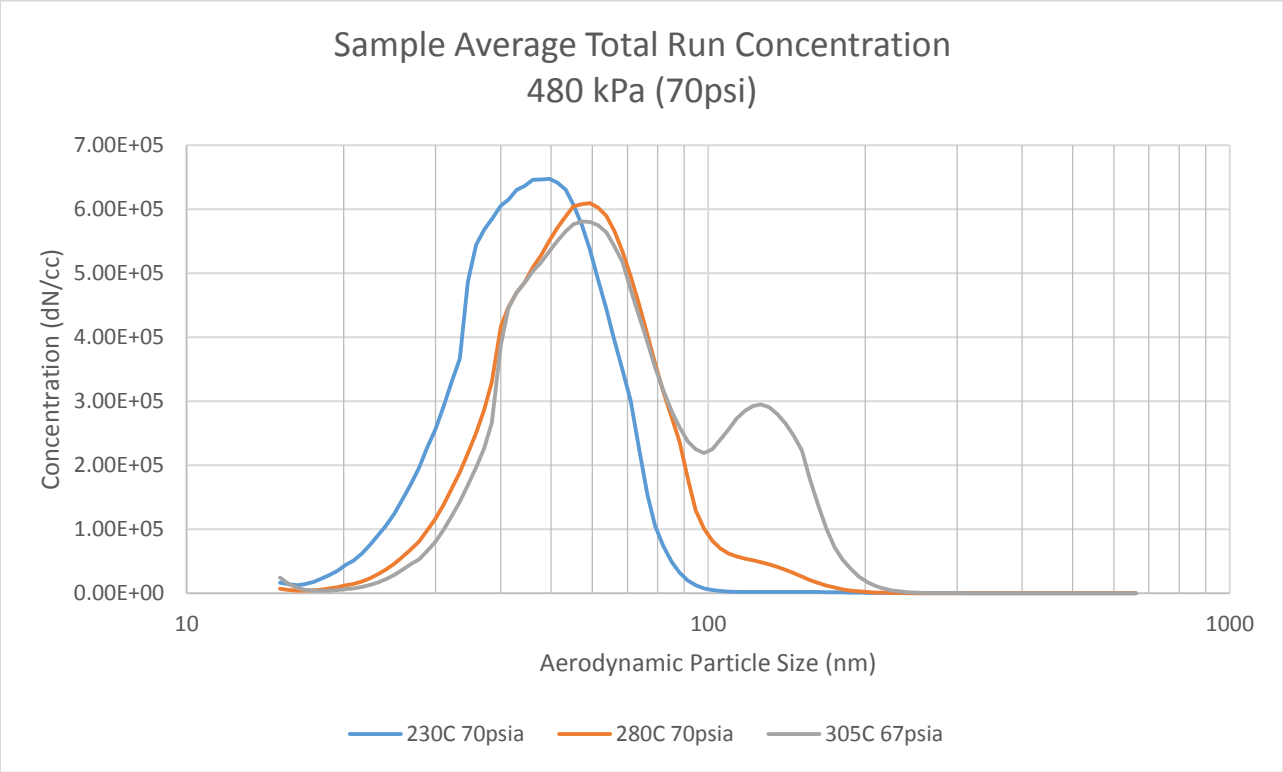

Figure 2-17 BAS Constant Pressure 480kPa

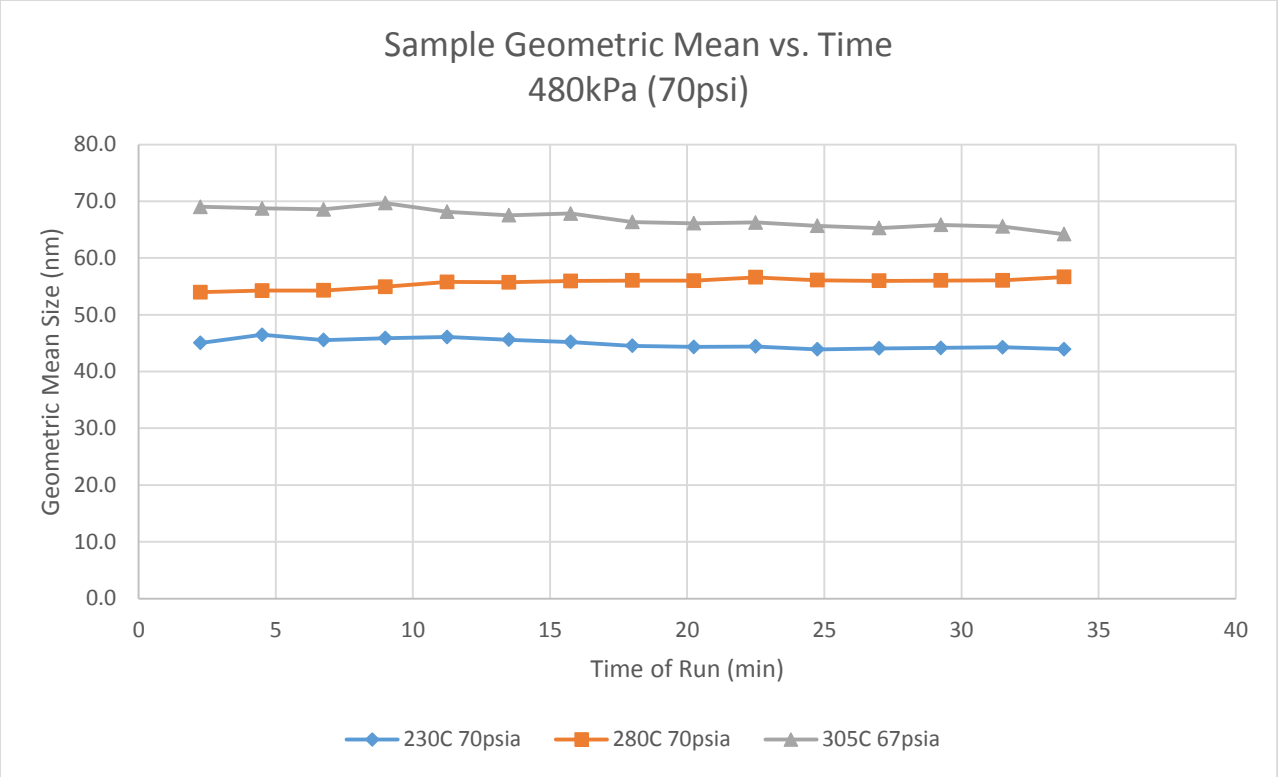

Figure 2-18 SMPS Geometric Mean at Constant Pressure

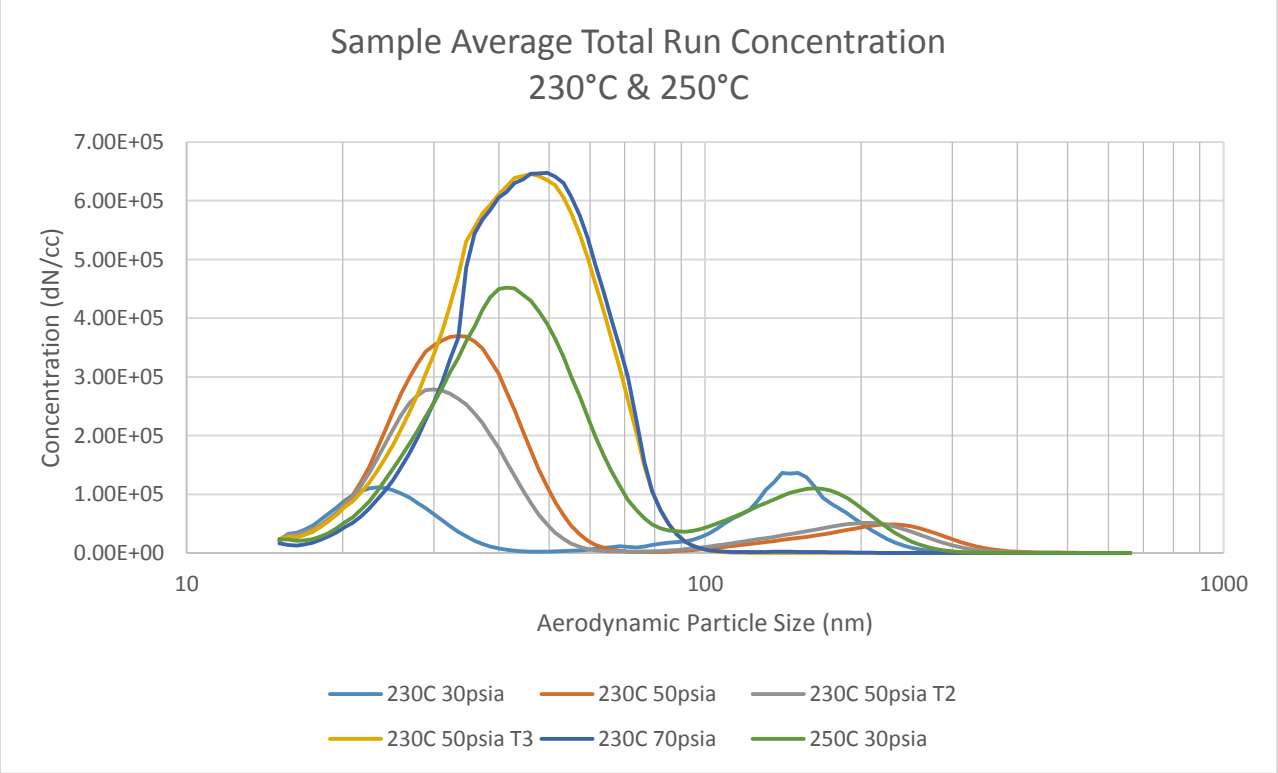

Figure 2-19 BAS Constant Temperature 230 & 250°C

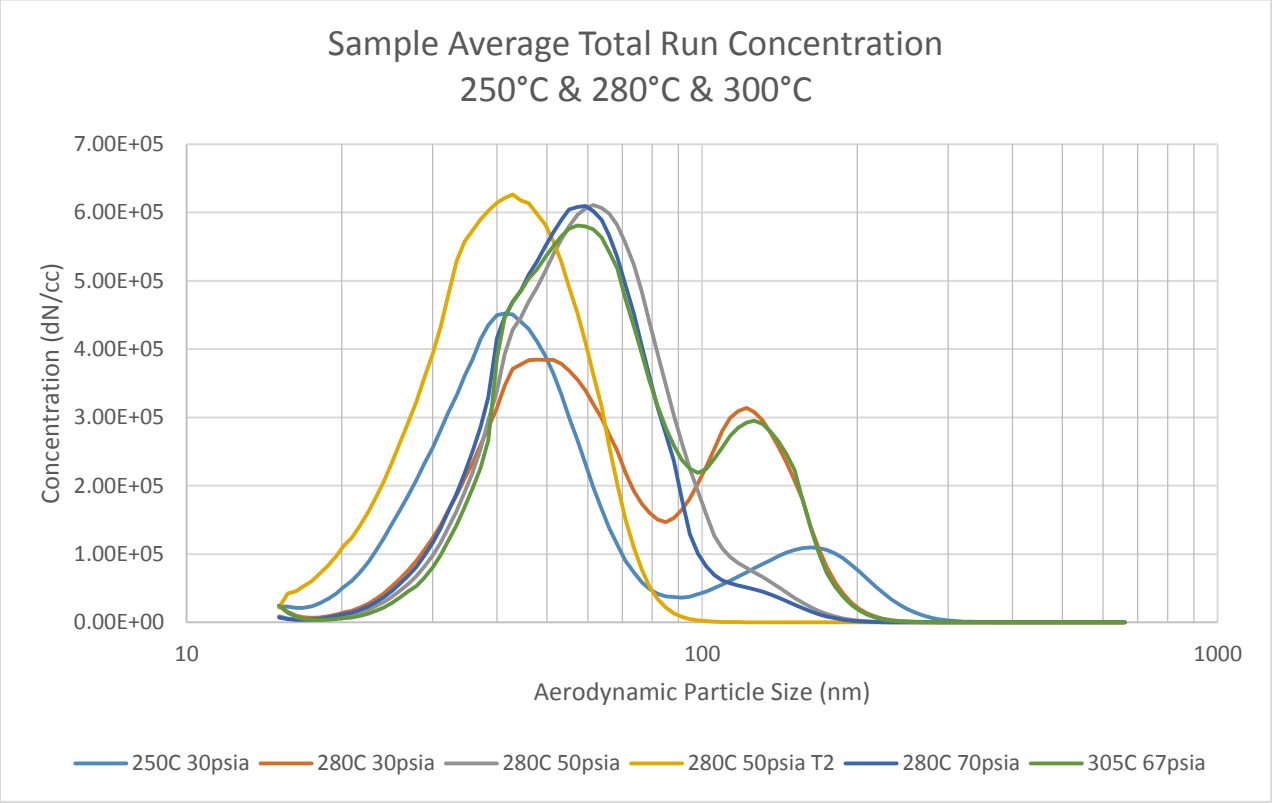

Figure 2-20 BAS Constant Temperature 250 & 280°C

It can be observed that in each case of increasing temperature at a constant pressure, the particle concentrations will increase at the lower size range of approximately 40nm to 65nm. However, the concentration increases do not correspond with certainty to any one temperature. Indeed one case is the three tests at 230°C and 50psia in which two of the curves approximately overlap while the third shows a trend closer to that of 280°C. There also seems to be a bimodal tendency when the temperature is high and the pressure is comparatively low.

Information about the geometric means for the pressure setting of 480kPa (70psi) indicate that the size distribution increases with increasing temperature, suggesting that there are many factors at play that influence the particle sizes measured. Indeed, increasing the pressure has some viewable effect as well, and there is a smaller secondary peak that does not correspond to

the aerosol injection peak. These smaller peaks are situated closer to 105 to 115nm, well below the 230nm of the aerosol injection peaks as seen in the presentation of the Laskin nozzle data. The mass graphs may be found in the Appendix.

What appears to be taking place is that as the pressure increases at a constant temperature the particle size shifts slightly to a larger size. As the pressure increases, it prevents the particles from becoming smaller as the air pressure will put a greater force on the surface of the small particle, thus reducing the chance for it to disintegrate or tend to give off molecules. The molecules will want to react or vaporize as the temperature increases. If we look at the data in terms of the Gibbs free energy, there appears to be some correlation. The concentration data are plotted as a function of Gibbs functions in Figure 2-21. As can be seen from the figure, the lower pressures give rise to more energy available for reactions to take place. Additionally over the ranges plotted there are points at 280°C that are equivalent to points at 310°C for different pressures. The Gibbs energy functions are based on the real gas equations as provided by (Lemmon, Jacobsen, Penoncello, & Firend, 2000) and presented by NIST.

It could also very well be that the heater tube is having an effect causing the particles generated to not be consistent over the course of multiple tests. The particles will adhere to the walls of the tubes and then be exposed to increased reactions. Since the compressor adds heat, the conditions of low pressure and high temperature, which may very well be out of range of a real gas turbine engine, can produce particles that are associated with larger temperatures. If a large amount of particles deposit onto the heater tube, the system will artificially inflate the temperature. In a real gas turbine, the largest bleed temperature possible (neglecting conduction effects) is the stagnation temperature exiting the compressor.

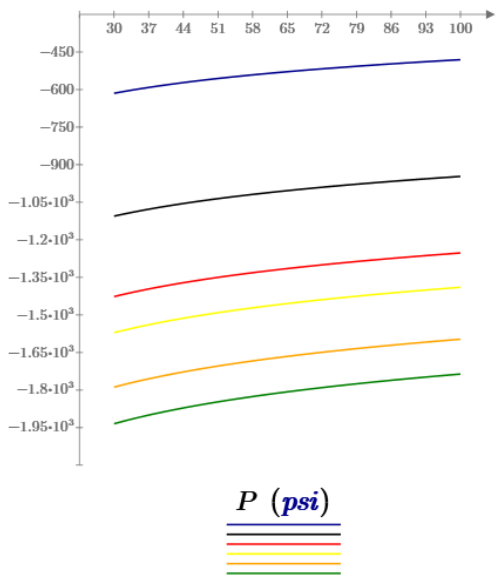

$g_{air}(115\ °C, P) - g_{air}(T_{std}, P_{std})$ $\left(\frac{kJ}{kg}\right)$

$g_{air}(185\ °C, P) - g_{air}(T_{std}, P_{std})$ $\left(\frac{kJ}{kg}\right)$

$g_{air}(230\ °C, P) - g_{air}(T_{std}, P_{std})$ $\left(\frac{kJ}{kg}\right)$

$g_{air}(250\ °C, P) - g_{air}(T_{std}, P_{std})$ $\left(\frac{kJ}{kg}\right)$

$g_{air}(280\ °C, P) - g_{air}(T_{std}, P_{std})$ $\left(\frac{kJ}{kg}\right)$

$g_{air}(300\ °C, P) - g_{air}(T_{std}, P_{std})$ $\left(\frac{kJ}{kg}\right)$

Figure 2-21 Gibbs free energy for BAS testing conditions

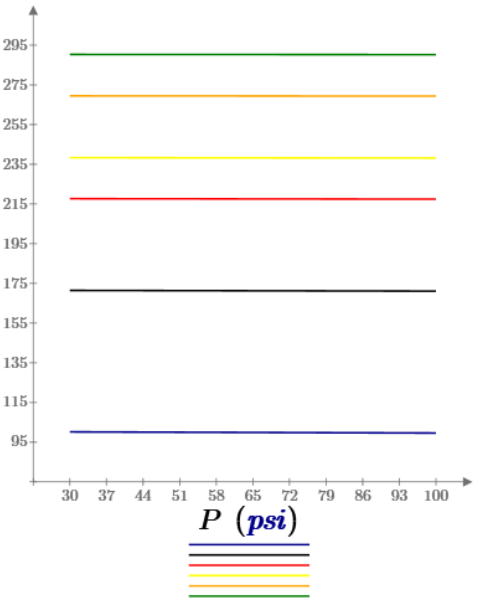

$h_{air}(115\ °C, P) - h_{air}(T_{std}, P_{std})$ $\left(\frac{kJ}{kg}\right)$

$h_{air}(185\ °C, P) - h_{air}(T_{std}, P_{std})$ $\left(\frac{kJ}{kg}\right)$

$h_{air}(230\ °C, P) - h_{air}(T_{std}, P_{std})$ $\left(\frac{kJ}{kg}\right)$

$h_{air}(250\ °C, P) - h_{air}(T_{std}, P_{std})$ $\left(\frac{kJ}{kg}\right)$

$h_{air}(280\ °C, P) - h_{air}(T_{std}, P_{std})$ $\left(\frac{kJ}{kg}\right)$

$h_{air}(300\ °C, P) - h_{air}(T_{std}, P_{std})$ $\left(\frac{kJ}{kg}\right)$

Figure 2-22 Enthalpy for BAS testing conditions

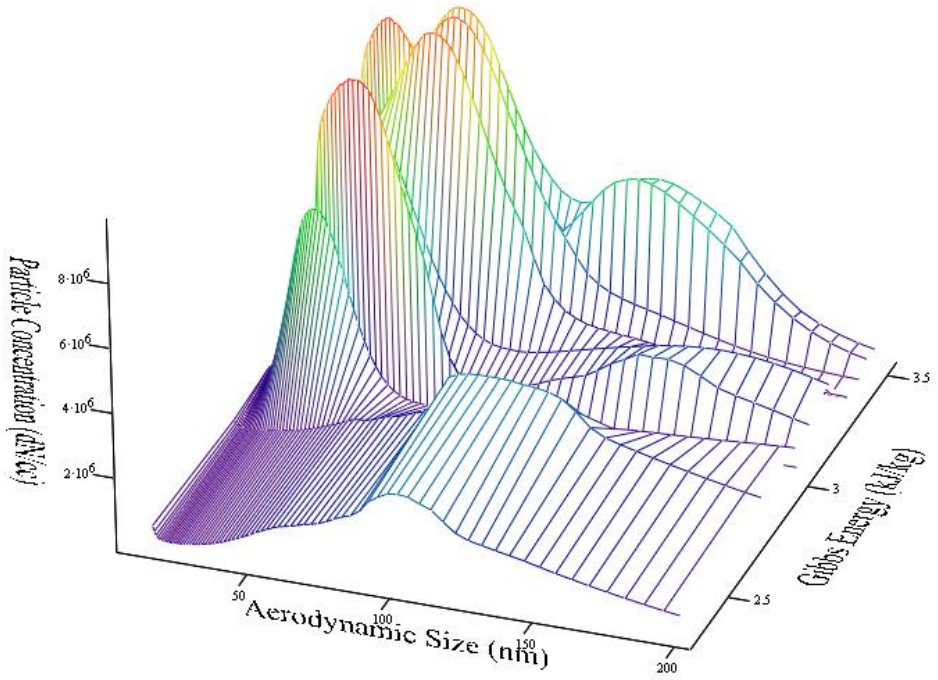

Figure 2-23 BAS Gibbs 3D Plot

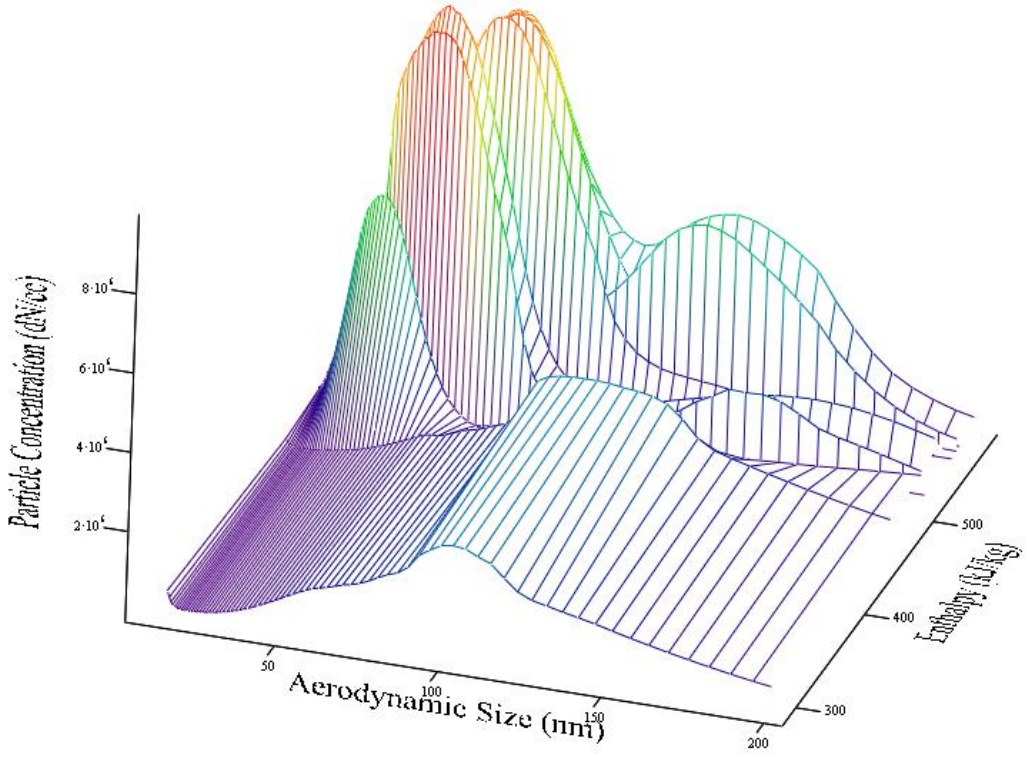

Figure 2-24 BAS Enthalpy 3D Plot

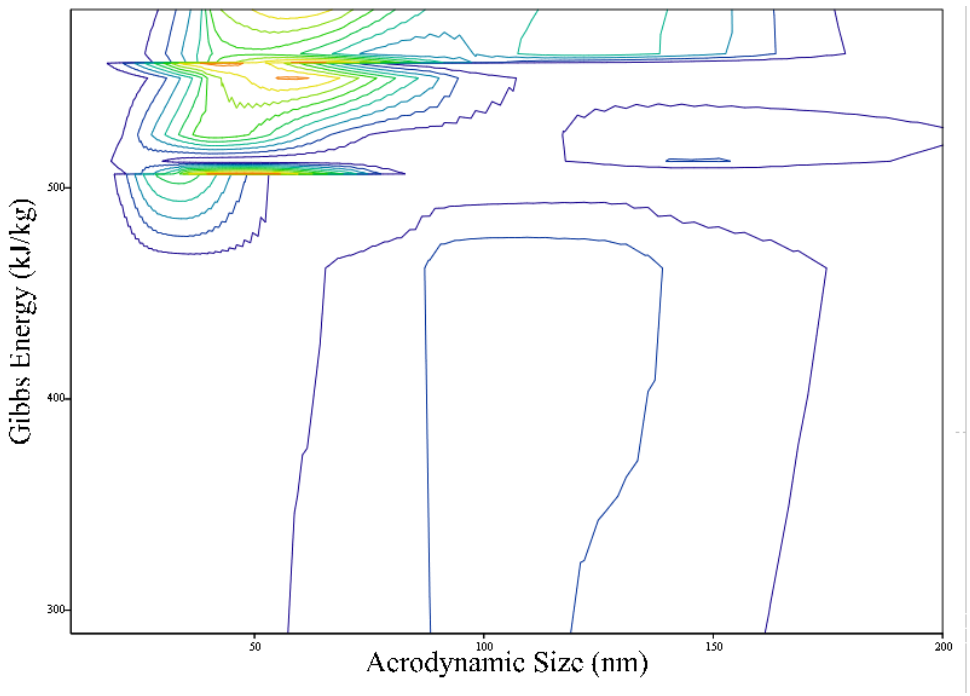

Figure 2-25 BAS Gibbs Contour Plot

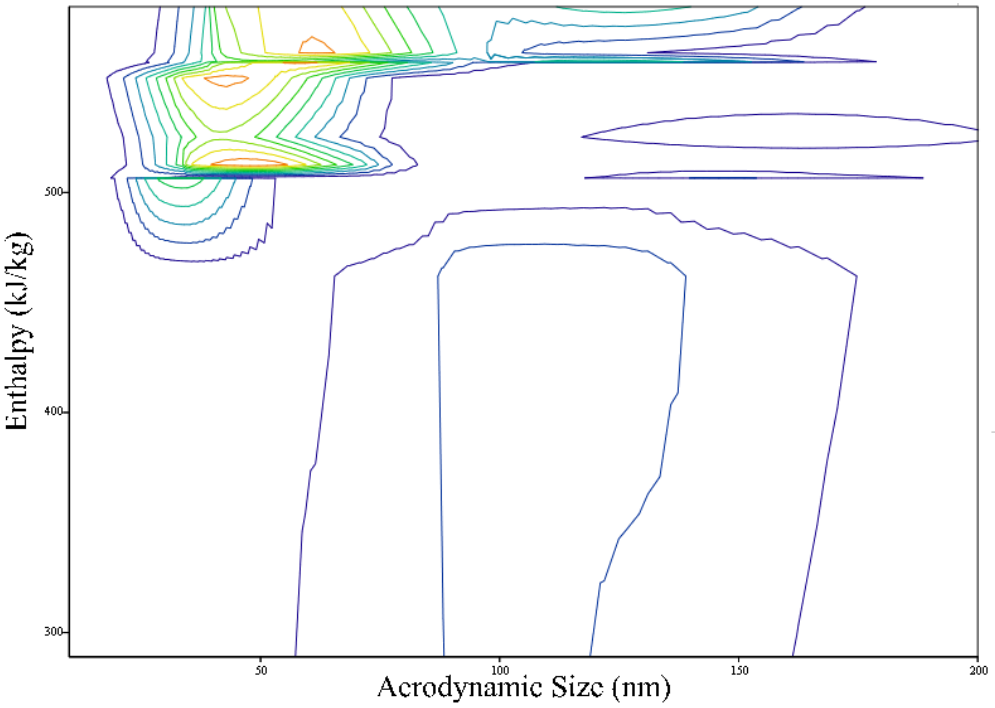

Figure 2-26 BAS Enthalpy Contour Plot

While the Gibbs free energy plots are not definitive in terms of the particle sizes produced, the plots show some valuable trends. It is seen that, as the energy available for reactions continues to increase, the more nanoparticles are produced. It is evident however, that the production of nanoparticles is influenced by both temperature and pressure effects.

The enthalpy plots provide information that is almost analogous directly to temperature. It is well understood that air at the pressures and temperatures involved behaves like an ideal gas. Under this consideration enthalpy is a function of temperature only, which is why the enthalpy plots vs. pressure are straight lines. When air is compressed in a gas turbine there will always be the heat of compression and frictional heat generated. The compressibility factor will remain close to one indicating an ideal gas approximation is valid. Evident in Figure 2-22, the enthalpy lines are almost completely horizontal in nature and any variation is extremely minor and is by far less than the uncertainty of measurements. Figure 2-26 shows the contour lines of the 3D plot for enthalpy, aerodynamic size and particle concentrations. There are fewer discontinuities than with the Gibbs energy indicating that the pressure has a smaller effect on the particle sizes than does the temperature. This author however, cannot provide a complete theory for the particle size variations as a function of temperature and pressure, but only conjecture as to what may be the cause for the differences in results.

2.3.2 Testing Data (10 Minutes)

Unlike the data taken during 30 minute runs, the data taken during the 10 minute tests were collected one right after the other. The measurements were performed with no 'burn off' of the system during this time. As such, the nature of the measurements is subject to change as the oil that may have deposited onto the heater tube will accumulate until a reaction temperature is

met. However, the data had the same trends as the 30 minute data. The trends are illustrated though the following figures.

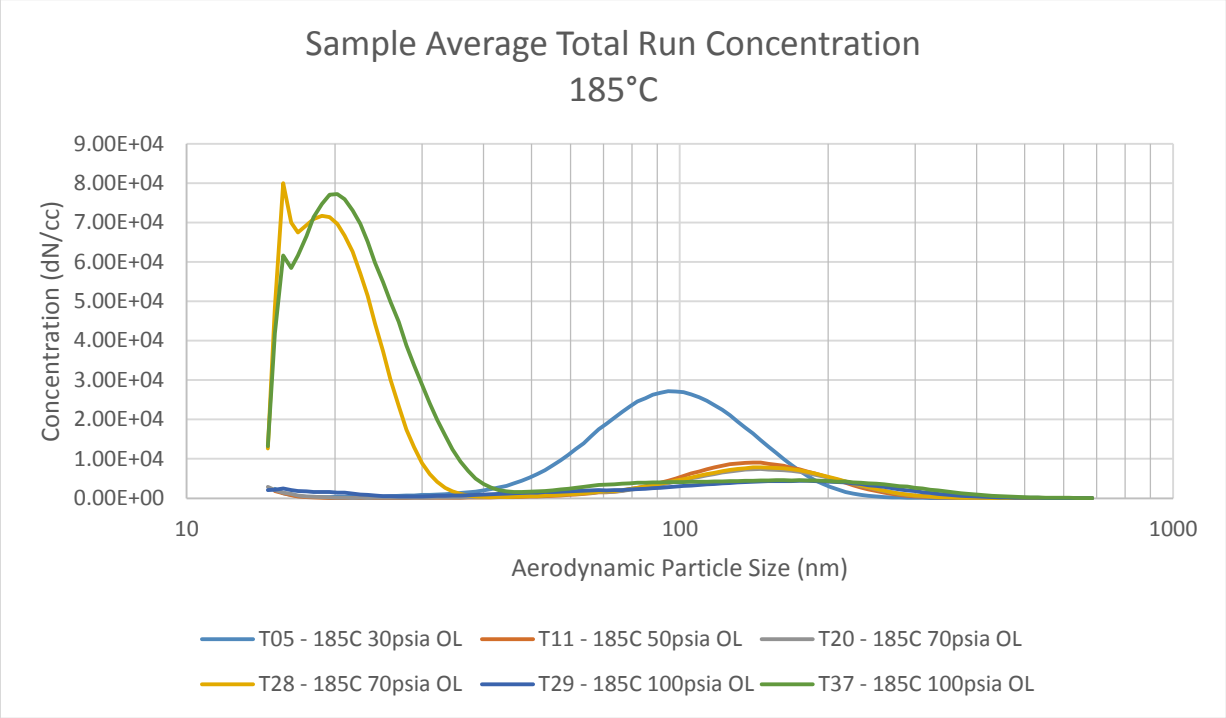

Figure 2-27 BAS Constant Temperature (185°C)

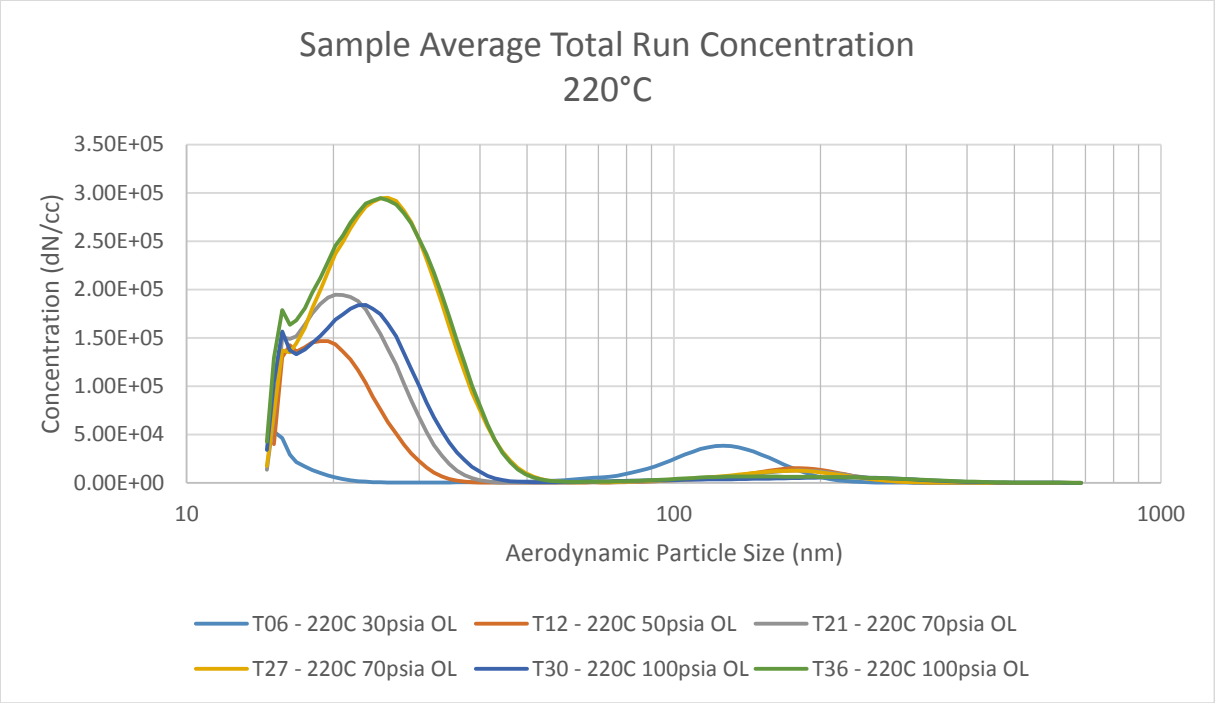

Figure 2-28 BAS Constant Temperature (220°C)

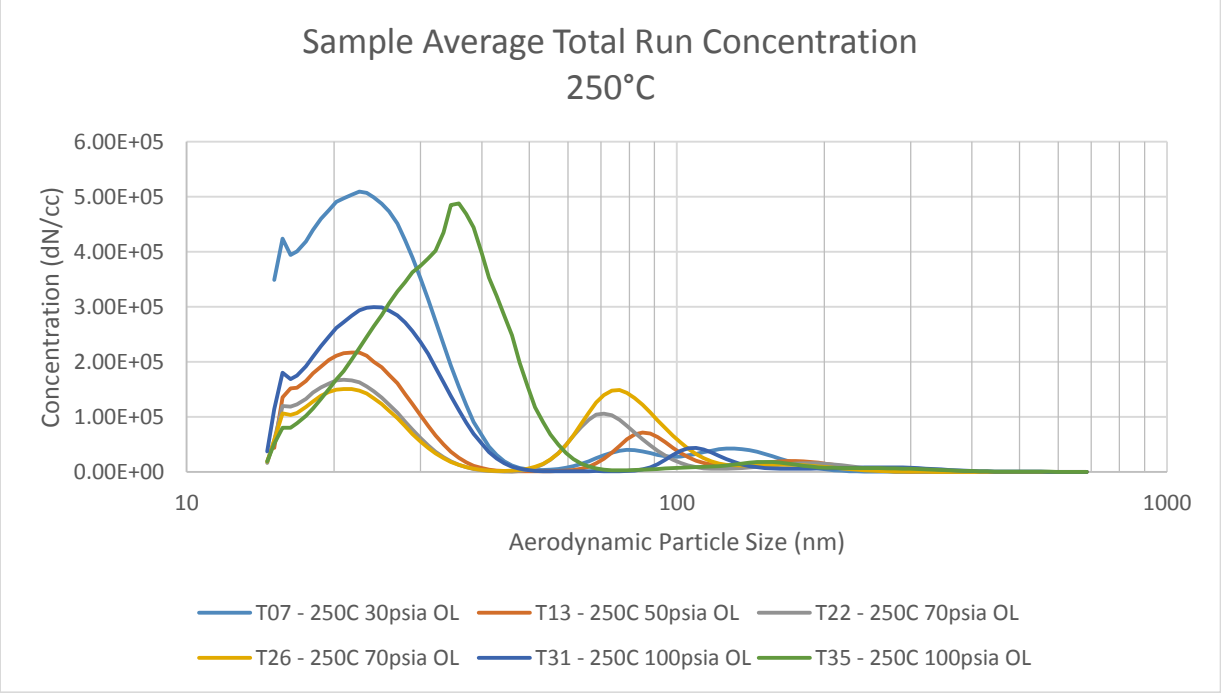

Figure 2-29 BAS Constant Temperature (250°C)

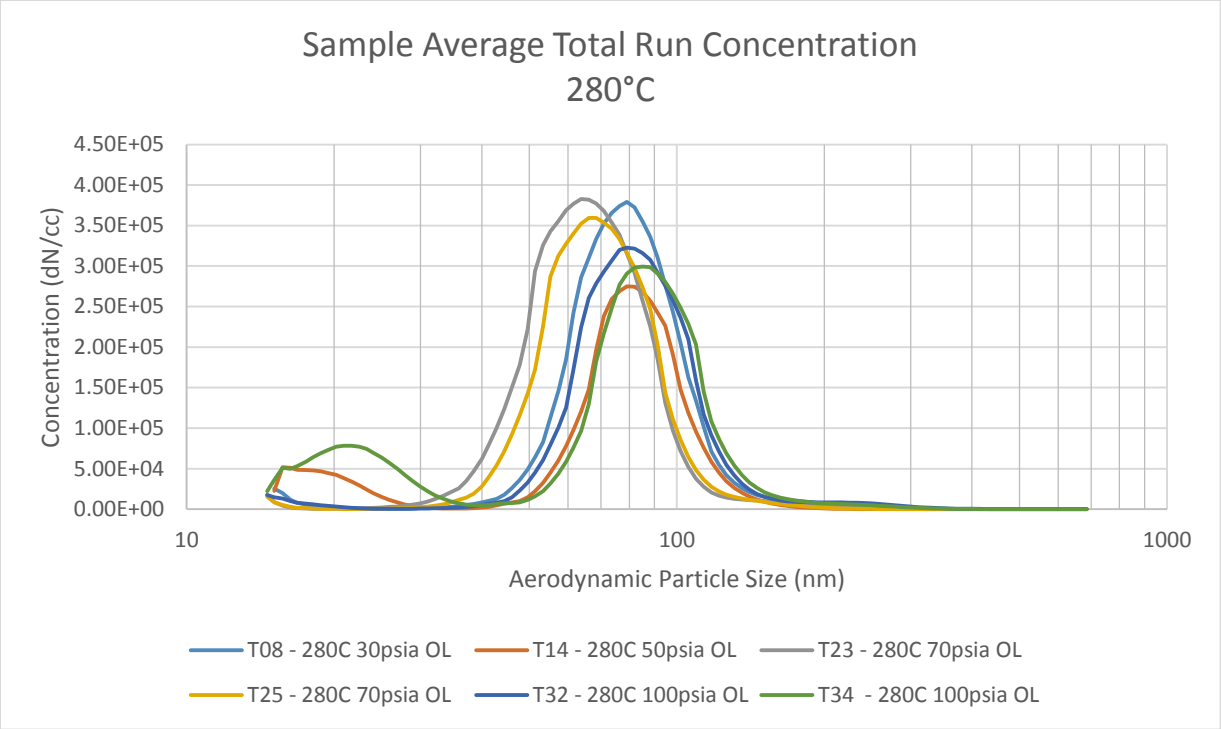

Figure 2-30 BAS Constant Temperature (280°C)

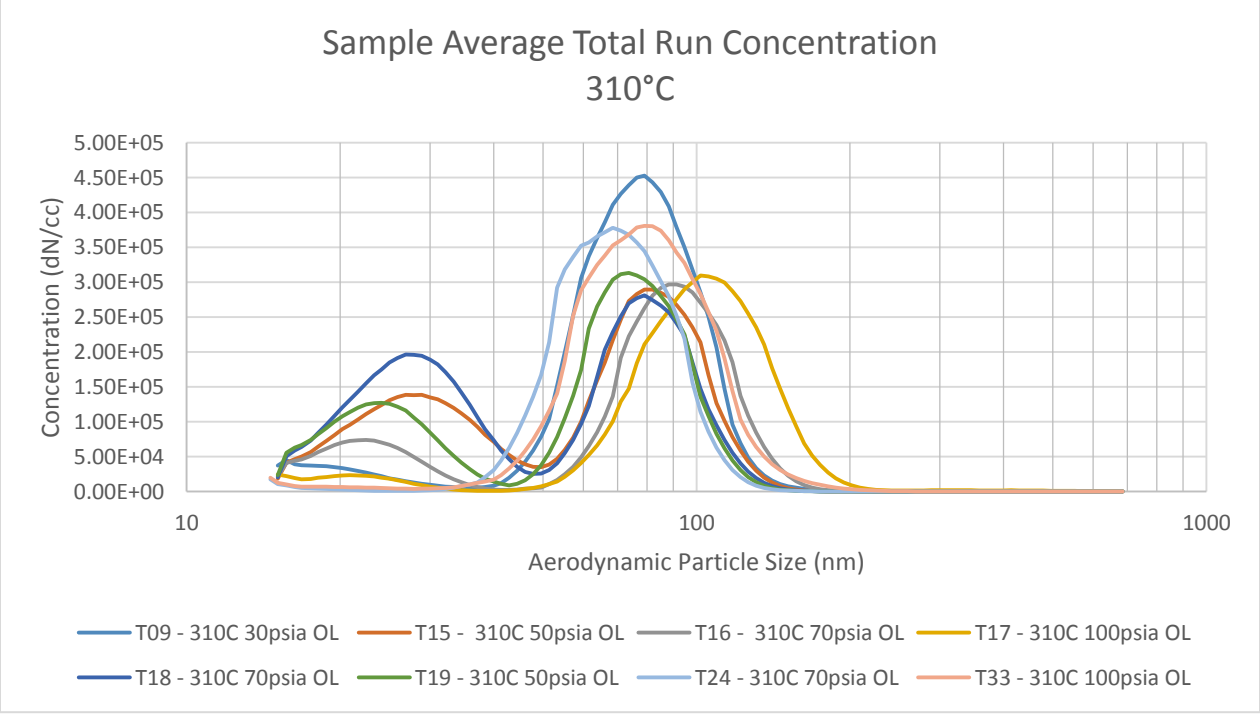

Figure 2-31 BAS Constant Temperature (310°C)

It can be seen that the pressure has a smaller effect on the particle sizes than the temperature by the similarity of the graphs for the 10 minute data. Since the Mobile Jet II will start to smoke at approximately 280°C, Figure 2-30 and Figure 2-31 have very similar size distributions. The particles situated at 280°C have such a tight clumping of particle sizes that the geometric means are within 20nm of each other, and may be observed in Figure 2-32. It is stated again that, since multiple peaks occur in the aforementioned graphs, the geometric and arithmetic means are not a very accurate representation of the data. Instead the concentration or mass graphs provide more information into how the particles are sized and how the mass is distributed.

It is further seen that the particles being generated are at a steady condition as evident in Figure 2-33. It was observed that in the course of a two hour measurement that the bleed air simulator produced the same particle concentrations.

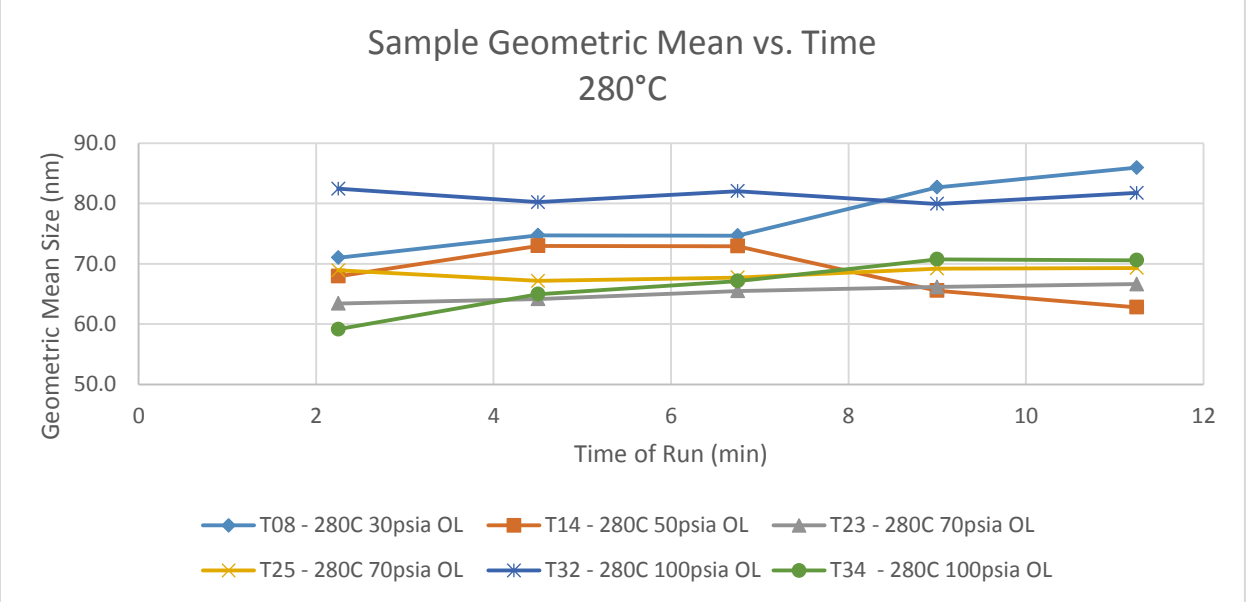

Figure 2-32 BAS Sample Geometric Mean_SMPS

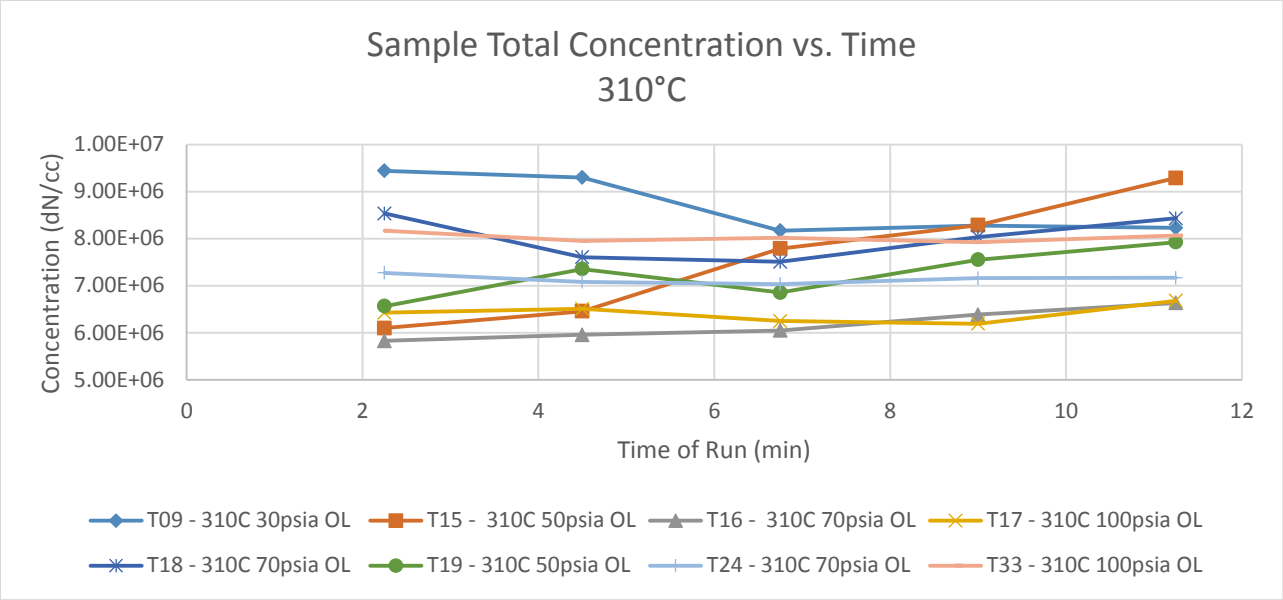

Figure 2-33 Stability of Concentrations at 310°C

2.4 Conclusions

The bleed air simulator provides the information necessary to investigate the requirements for the simulated engine runs. The simulator gave insight into how the particles are distributed across the various pressures and temperature ranges that an aircraft bleed air might operate at. It was observed that the particles are mainly submicron around the 100nm and 20nm sizes with various peaks during these simulated conditions. The smaller particles are generally associated with a higher Gibbs free energy, or for the most part a higher temperature. There is the question about the way in which the processes are simulated by a reciprocal compressor and a heater tube and whether or not the BAS actually simulates the conditions to which a contamination aerosol may be subjected in an aircraft engine. The compressor blades on an aircraft will spin up to 50,000 rpm and this influence is still unknown.

However, it was observed that the main influencing factor on the particle sizes was indeed the temperature. Increased pressure appears to produce the smaller particle sizes. These

conclusions coincide with those given by (Mann et al., 2014). The bleed air simulator was able to produce consistent data for the particle sizes as shown by the data presented in the 10 minute measurement section with a greater correlation at the higher temperatures of 280°C and 310°C.

The Laskin nozzles also have been shown to produce repeatable aerosols with the particle detection equipment able to measure the concentrations accurately over multiple tests. This information helps to secure the knowledge that the particles are being influenced by the pressure and temperatures experienced by the flow stream.

Chapter 3: Allison T63-A-700 (C18) Engine

The second phase of the project for the measurement of particle distributions from thermal degradation utilizes a turboprop engine. For experiments to reach the temperatures required the engine will need a pressure ratio of approximately six to nine. Based on an ambient temperature of 21°C (70°F), to reach a temperature of 280°C, the pressure ratio must be 9.4. This is a large ratio for any non-modern small engine under 1000 hp. However, the gas will never be compressed isentropically and thus the temperatures leaving the compressor will be larger than for an isentropic compression. With an engine compressor isentropic efficiency of 75%, a pressure ratio of 6.0 will produce the required 280°C. Lower efficiencies are found in older engines and with this information in hand it was decided to utilize an Allison T63-A-700, also known as the Allison 250 C18 for the civilian application use. The fact that such an engine was already available was also a factor in its selection. This engine has five stages of axial and one centrifugal stage for compression and is rated at an approximate pressure ratio of 6.2. The engine has a maximum power rating of 238kW (319hp) shaft output at sea level while only weighing approximately 670N (150 lbf). This engine has an approximate air flow rate at 90% cruise power of 1.36 kg/s (3 lbm/s).

Figure 3-1 Allison C18 Test Engine

3.1 Experimental Setup

Unfortunately it is impossible to separate bleed air pressure and temperature from engine power. The nature in which a gas turbine engine works does not allow for these variables to be quantified independently of each other. Additionally, the problem is compounded by the ambient conditions. The engine will run at higher power settings to meet the same compressor bleed air temperature on a colder day than is required on a hotter day. Thus, the output pressure and engine speed are fixed for any one given temperature, which is a unique function of the atmospheric conditions. Earlier testing on the bleed air simulator indicates that the temperature is the main controlling factor in regards to the particle sizes generated. The choice was made to utilize the temperature as the independent variable for testing on the C18 engine. Unfortunately fuel costs prohibited additional testing of pressure as the independent variable and was not valued enough to test based on the bleed air simulator results. The influence of the engine speed is unknown and thus was not included as an independent variable for testing. It was assumed that any engine would be running at cruise power settings or close to it and the difference in blade shear impact between the two settings would not be enough to contribute any meaningful effect. The C18 engine idles at 60% N1, which is the gas producer turbine, and produces a bleed air temperature of about 100°C at this speed. To bring the temperature up to 200°C, which is below the point of thermal decomposition, the engine needed to run at about 80% power.

The experimental setup consists of several components for the engine but may be grouped as.

1. Oil Injection & Air Intake Plenum
2. Bleed Air Extraction Line
3. Engine Accessories
    a. Dyno; Coolant Loops; Oil Coolers; Fuel Pumps;

3.1.1 Design Modeled after real aircraft

The system for the bleed air take-off was designed to be modeled after a real aircraft. According to data provided by (Matthews, 2013), the time until the bleed air reaches the precooler after exiting the engine compressor is between 60 to 130ms or 30 to 60ms depending on the associated temperatures and pressures. The bleed air simulator was designed with an approximate 70ms residual time. This transient time is an important parameter in the design of the bleed air extraction line as this is the time until the chemical reactions are quenched by the heat exchanger.

Another critical factor in the bleed air design is the amount of bleed air extracted. According to the design manual, no more than 4.5% of the total flow for the engine should be extracted. It should be noted that the more bleed flow extracted, the higher the exhaust gas temperature (EGT) or also known as the turbine out temperature (TOT). The total flow for the engine will vary greatly from 0.68kg/s (1.5 lbm/s) up to 1.5kg/s (3.3 lbm/s) to power the engine. These flow rates will also change depending on the outside ambient temperature and pressure conditions of the day. No more flow should be extracted than is necessary to prevent a high EGT. This requirement is counter to the transit time constraint as more mass flow would reduce the travel time from the bleed air extraction port to the heat exchanger. A 0.25in diameter orifice plate is used to restrict the bleed air flow and at 220°C and 61 psia provides about 47ms for the residence time and gives a mass flow of bleed air of 2.5lbm/min. A 0.15in diameter orficie plate can also be used and, at 160°C and 54 psi, provides a mass flow of 0.97lbm/min and a residual time of 140ms. From testing data available after running the gas turbine, calculations of mass flow compared to measurements were within 1% to 7% error from the measurement giving credence to the design calculations. Thus, the two orifice plate sizes yield transit times that are approximately representative of the bleed air system as given by Boeing and research into the

topic. As stated, the engine power and test settings will influence the time to cooling of the bleed air and it will not be the same between different runs or even during a period of testing as the atmospheric conditions can vary.

Finally the particle dynamics should be considered in the design of the system. The flows in the bleed air extraction system will be turbulent throughout the entire flow regime in order to meet the transit time constraint. Laminar flow coefficients and losses have been well established for particle dynamics, with references including the famous article by (Gormley & Kennedy, 1949) characterizing the diffusion losses from a stream flowing through a cylindrical tube. The losses for a turbulent system however are less well understood due to the random nature of the flow within the tube and the probability that a particle will penetrate the boundary layer and stick to the wall. There are also thermomephoric losses to be considered, which will be very high through the precooler. However, in light of these difficulties, it should be understood that this system is intended to simulate a system on a real aircraft. Any common airliner bleed air system will have the pressure regulator and precoolers integrated into the system. The associated particle losses will occur regardless of the airframe or engine due to the nature of how the bleed air system is conditioned for aircraft use. The losses that may occur are also outweighed by the reaction times and safety of the operators. It is then assumed that these losses, even though may be great, will not be considered. It is possible to characterize these losses by the equations and formulas presented in literature by various authors, but the uncertainty would be substantial and the tested formulas do not account for the increased pressure of the flow stream either.

The ultimate goal of this paper is to provide insight and data on the particles that result from oil thermal degradation that could be measured on a typical aircraft and used for

development of a bleed air system sensor. It should be understood that the bleed air sensors will also be situated after the precooler and pressure regulator systems. While there are a few ways to use sensitive equipment in a high temperature and pressure environment, most sensors are not suited for such conditions. The air temperature may easily rise up to 300°C, but the surrounding casing in the engine may be much hotter due to radiation and conduction effects. This temperature will severely limit any electronic measuring devices that are between the precooler and the bleed air taps. Additionally there is the issue of safety again in regards to the engine. It is not wise to put a sensor meant to monitor the bleed air in a high temperature environment close to the operational parts of the engine. Any failure that may result could have potentially devastating consequences.

3.1.2 Engine Safety

It is important to note that the bleed air system set up in this experiment was not on a simulator but rather was on an operating gas turbine engine. It is then of importance to note that safety was taken at all steps during this testing and also illustrates that some temperature settings could not be reached as the engine was shut down by control systems to prevent any serious malfunction. The compressor turbine and power turbine sections are spinning over 50,000rpm and 35,000rpm respectively along with a GE 1G335 dyno capable rotating at close to 8000rpm and capable of handling 600hp. It was decided to put in safety systems such as the safety ball valve on the bleed air extraction and the fuel control solenoid along with other redundant systems. These systems were integrated in order to ensure the engine may be shut down quickly and remotely in an emergency. Additionally, these safety priorities and spacing issues will also limit the design of the bleed air extraction system.

3.1.3 Oil Injection

The oil injection for this experiment used the same model TDA-4B lite Laskin nozzle unit from Air Techniques as used with the bleed air simulator and which has shown to be reliable for injecting the oil at consistent aerosol size distributions. Figure 3-2 shows the oil injection portion of the operational system. Shop air is supplied to the aerosol generator. This air is dried in order to remove any moisture that may be in the atmospheric air. From the building air tap, the air passes through a pressure regulator and a solenoid valve. The pressure regulator prevents the flow meter from bursting due to the high (100psi) supplied air. The solenoid valve is the backup valve to shut off any air supplied to the aerosol generator as a safety system. It may also be used to turn the aerosol generator on and off without being next to the operating engine, assuming that the Laskin nozzles are in an open position. The Laskin nozzle air inlet pressure was limited to 20psi as the default and was not changed. This constant inlet pressure was controlled by an air pressure regulator on the aerosol generator unit. The oil was injected into the air plenum box through a 1" swaglok tube bent to a smooth curve. This tube inserted oil parallel to the ambient air flow stream leading into the engine. This arrangement may be seen in Figure 3-3 along with the oil sample line. The oil sample line was later removed from the system as the velocity in the air inlet produced pressures to great for the particle measuring equipment. After this problem was identified, a pump was considered for use in the oil extraction line, however it was ultimately disregarded as the aerosol sample would be altered while passing through a pumping device.

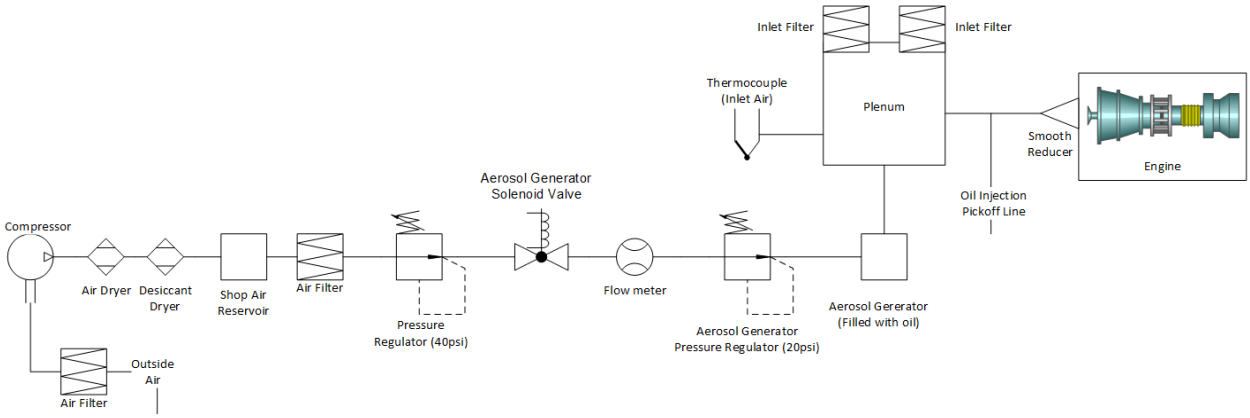

Figure 3-2 C18 Air Inlet System

The air entering the engine from the atmosphere passed through an air plenum box, as was specified in the design manual. Two K&N filters were used on the top of the system to provide air filtering for a flow rate of 2460scfm at 1.5inH2O pressure drop. These filters are not HEPA filters and are intended to limit debris that may cause malfunction to the engine. They are not effective at removing the submicron particles of interest in the bleed air. Additionally, since the engine is not on a moving platform, there is no inlet velocity assistance to the compressor for pressure generation. Thus, any pressure drop leading to the compressor section of the engine should be minimized in order for the system to run properly and prevent potential overheating. An ambient air pickoff line is situated under a filter on the air plenum box and is arranged parallel to the flow direction. This pickoff line is shown in Figure 3-4. No flow meter was established on the inlet of the engine as the length of straight inlet duct required upstream of the flow meter was not available and thus any measurement of the inlet flow would have been inaccurate. Prices for short measurement venturi nozzles were investigated but costs became prohibitive for procurement. Additionally, the pressure drops for available flow meters were not acceptable.

All of the thermocouples on the engine system are high temperature K-type with an uncertainty of ±1°C. One thermocouple was placed next to one of the air filters in order to provide an incoming air temperature measurement. It was stationed on the side closest to the exhaust gases in case the wind redirected any of the combusted gas back into the air inlet. The convection over the temperature probe is much larger than any radiation or conduction effects and thus gives the accurate temperature of the incoming air. It was found during testing that the incoming air did indeed fluctuate by up to 10°F due to the exhaust gases but no particles were detected relative to the ambient conditions from this contamination. If particles did intermittently enter the engine from the combustion gases, the SMPS system may have completely missed them as the size set by the classifier at that point in time may not have matched the particles entrained. The temperature of this incoming air could also vary from the lab ambient temperature measurements by up to 4°F depending on the time of day.

Figure 3-3 C18 Oil Injection and Sample Ports

Figure 3-4 C18 Ambient Air Pickoff Inside Plenum Box

3.1.4 Bleed Air Extraction Line

Figure 3-5 illustrates the bleed air system extraction line. All of the bleed air extraction line was constructed of stainless steel Swagelok tubing indicated for gaseous transport. The grounded metallic tubing ensures that minimal electrostatic losses will occur inside the lines, though other particle losses still exist. The C18 engine has two bleed air ports on the compressor scroll and it was decided to pull flow from both ports in order to minimize any effect or chance

of unbalancing flows. An American Sensor Technologies #A 4000A00100P4B100 analog pressure transducer with ±0.5%BFSL accuracy and ±0.25% FS stability was used to measure pressure on one bleed air tap. It was situated vertically in order to minimize the chance of water condensing inside the tubing and causing inaccurate readings. A thermocouple was placed on the other bleed air port. The two bleed air lines were connected by flexible stainless steel hoses in order to minimize the vibrational effects of the engine. The two lines were combined into a single line and sent through a 3-PC high performance metal seat ball valve. This ¾" valve was designed for a fail closed position via a spring and a metal seat and had a design temperature of 370°C (700°F). After the valve, the flow will encounter the orifice plate. Several orifice plates were made but only the 3.8mm (0.15in) and 6.35mm (0.25in) orifice plates were used for the C18 engine testing. It was determined that the 6.35mm (0.25in) orifice plate provided flow at approximately 1.13 kg/min (2.5 lbm/min) or velocities after the orifice plate of 69 m/s (225 ft/s). The 6.35mm (0.15in) orifice plate provided approximately 0.45 kg/min (1 lbm/min) to 0.54 kg/min (1.2 lbm/min) or about 30.5 m/s (100 ft/s) after the orifice plate. These velocity calculations include pressure and heat losses of the lines using known factors for friction and heat transfer. After the orifice plate the 1" flow line transitions into a 1.5" line after 15". The precooler is from a King Air 200 aircraft which has a larger working engine than the C18. Thus the precooler would have enough cooling capacity to lower the bleed line temperatures to suitable sampling conditions. The sampling conditions should nominally be below 40°C (104°F) for the SMPS and APS to measure properly. The working pressure of the precooler is approximately 241kPag (35psig) and thus the orifice plate is required to lower the pressure of the system and control the flow. It was originally intended that the orifice plate would be a control valve, however the decision to use a precooler forced the design to incorporate an orifice plate as

the precooler working pressure was discovered to be below the bleed air pressures. Additionally any high temperature control valve would have been too costly for the project.

After the precooler the flow rate is measured by an orifice flow meter plate procured from Lambda Squared. The flow measurement orifice plate is an ORIPAC Model 5300 which features the pressure taps on the side of the plate thus reducing the piping lengths required. The orifice plate complies with the ASME MFC-3M-2004 standard and meets or exceeds the AGA and ISO standards as well. A thermocouple is situated on this 3in line and an Omega Px725-100WCGI pressure transducer measures the static flow pressure with an accuracy of ±0.15% of calibrated span with ±0.05% repeatability. An Omega Px771A-100WCDI pressure transducer measures the differential pressure across the ORIPAC orifice plate with an accuracy of ±0.1% of URL with the upper limit set to 20" of H_2O.

Following the measurement devices, the sampling pickoff line is located inside the 3in pipe, which transitions to PVC after approximately 10 more inches of metallic tubing. As stated earlier the metal piping ensures that the electrostatic losses are minimized. The FTIR pulls its measurement off the PVC piping since gas compositions are not influenced by the PVC piping. The pickoff lines run through two solenoid valves used to control measurements during testing and allow rapid response. The bleed line and oil injection line run to the first solenoid valve with the ambient air measurement line connected to the second solenoid valve. During testing where only one parameter will be measured, the equipment was hooked directly to the bleed air pickoff line to minimize any losses.

The 3in bleed air line was also insulated from radiant energy produced from the exhaust gasses and may be seen in Figure 3-6. This figure shows the overall system setup as implemented for testing.

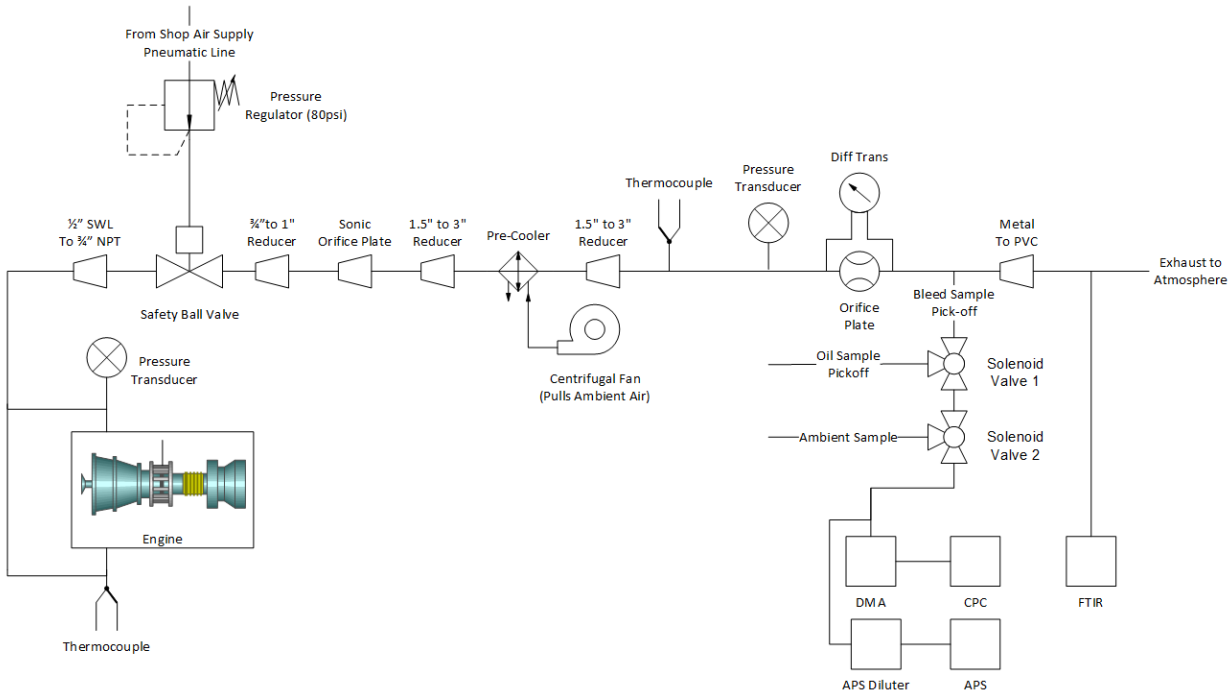

Figure 3-5 C18 Bleed Air Extraction System

Figure 3-6 C18 System Setup

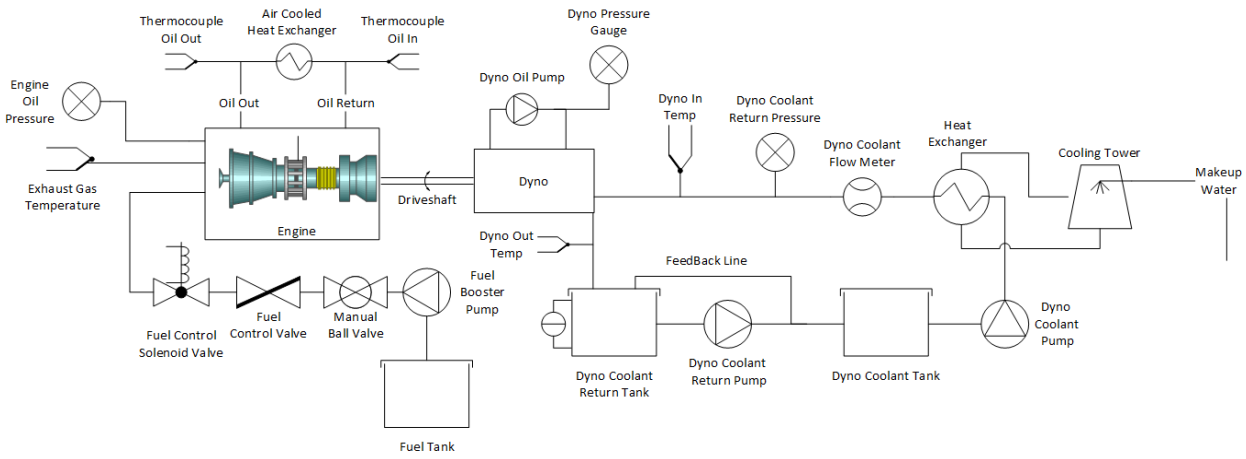

Figure 3-7 C18 Engine Accessory Systems

The accessories for the engine are shown in Figure 3-7. This information is displayed to show the reader the required systems needed to enable the engine to run. During testing all the this information was monitored by OPTO 22 and warnings were set to ensure that the fuel system would be shut off as soon as any limit was exceeded. As shown in Figure 3-7, the control valve was used as an on an off valve for the fuel. Another solenoid valve was inserted at the combustion chamber inlet fuel line to prevent hot starts of the engine, while a manual ball valve ensured that if all electronics failed this valve would cut the fuel from the engine. Gas turbines are self-sustaining power generators that will continue to run as long as fuel is provided. Thus the only sure way to stop a gas turbine engine is to eliminate any fuel source. Figure 3-7 also shows the coolant loop system for the dynamometer. The cooling capacity required for the dynamometer was meet with a JE205 GS cooling tower. Pressures and temperatures of this system were also monitored during the system run as any overheating or pressure irregularities would also cease the engine testing for the day.

3.1.5 Process Control and Monitoring

OPTO 22 was used for the entire system monitoring and is the National Gas Machinery Laboratory (NGML) default control utility. It is an entire system package of controllers, I/O, solid-state relays and software. It uses a brain design where the control information is loaded into the brain and allows the process control and monitoring to take place independent of edits to the system. OPTO monitored the readings from all control components and was set up to display any warnings in a manner to grab the operator's attention. In case limits were exceeded and a shutdown was implemented, the fuel control valves were closed. All of the fuel control systems were established in series and thus if any one of the fuel controls lost power or was ordered off no fuel would be provided to the engine. A manual switch controlling power to the system was also next to the operators' station for ease of access. During start the fuel was allowed to enter the engine only when the compressor speeds had reached approximately 20%. The fuel control governors on the gas turbine were set to idle flow during the prestart check of the system. This procedure was done to minimize the probability of a hot start where the combustion gasses exceed the EGT. When a hot start occurs the engine must be inspected for damage and if necessary sent back for repair. The fuel control system was implemented in this way after a hot start was encountered but luckily the OPTO controls prevented any damage.

3.1.5.1.1 Data Extraction

The data were extracted from the brain using VBA code to access the information over the network. An Excel spreadsheet connected to the controller and then pulled the information stored for output from the controller memory. This information was then processed by more VBA code and put into the spreadsheet itself. When recording was initiated, the data would be recorded every 3 seconds during the testing until the time allotted expired. A black box coding

section was also created in order to capture the data in case of power outages or other connection errors. Whenever the code was connected to the controller brain, the information stored for output was recorded at intervals of 10s. These data were not only recorded in the excel spreadsheet but also written and appended to a text file every 10s in case an error on windows or with excel occurred. This black box implementation allowed the data to be captured and was implemented after a short on the system blew the main breakers during the initial trial starts of the engine.

3.2 Data Analysis

3.2.1 Design and Error Estimations

3.2.1.1 Losses due to non-isokinetic

The variations in the flow rate in the bleed air extraction line do not allow for isokinetic sampling. The flow rates mentioned earlier from the orifice plate used may vary between 450LP (15.9cfm) to 1250LPM (44.1fm) depending on the engine power setting and the conditions of the day. The bleed air extraction line sizes do not change meaning that the velocities encountered on the bleed air sample port will change and be non-isokinetic. These variations however are able to be quantified. From testing data available the maximum particle size generated that is significant in concentration is about 1000nm or 1.0μm. The Stokes number of a 1000nm particle in the flow stream at 7.6m/s (25ft/s) for oil particles in the sampling tube is 0.003. The Stokes number for most testing will be lower than this worst case scenario and closer to a value of 2E-4. Figure 3-8 provides the aspiration efficiency based on the well-known relation by Belyaev and Levin (1974). We can see that even for our system the aspiration efficiency will be very close to 1. (Baron & Willeke, 2001) gives a reference for Rader and Marple (1988) that provides the aspiration efficiency for a larger Stokes range and is graphed in Figure 3-9. This image shows

that the aspiration for the majority of the particles concerning our testing will have aspiration efficiency close to 1. The aspiration efficiencies will only deviate at higher flow rates but currently the flow rates produced by the 0.25in orifice will provide the needed residence time and thus more flow is not needed. More flow will also raise the EGT and restrict the ability of the engine to achieve higher operating conditions.

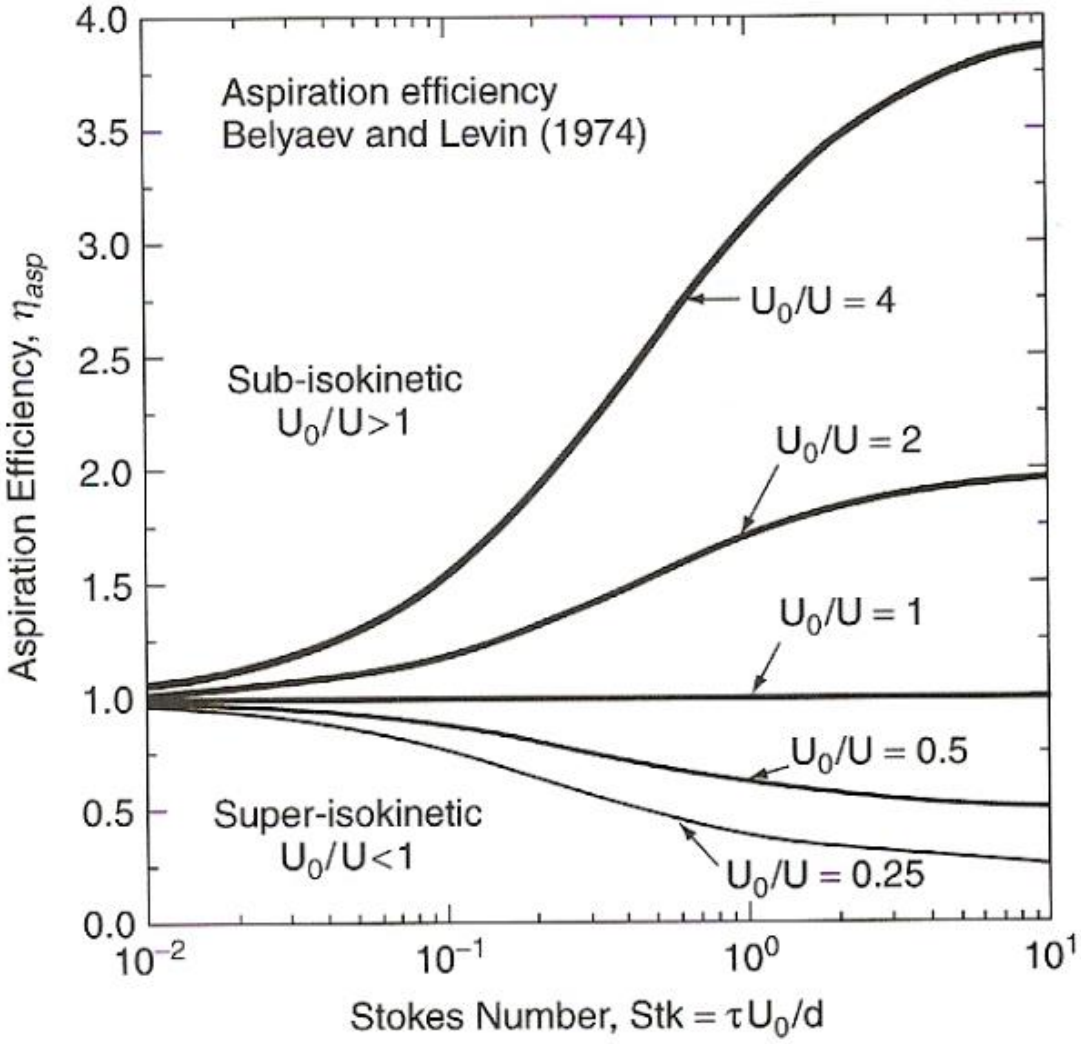

Figure 3-8 Aspiration Efficiency
Reproduced from (Baron & Willeke, 2001) with permission.

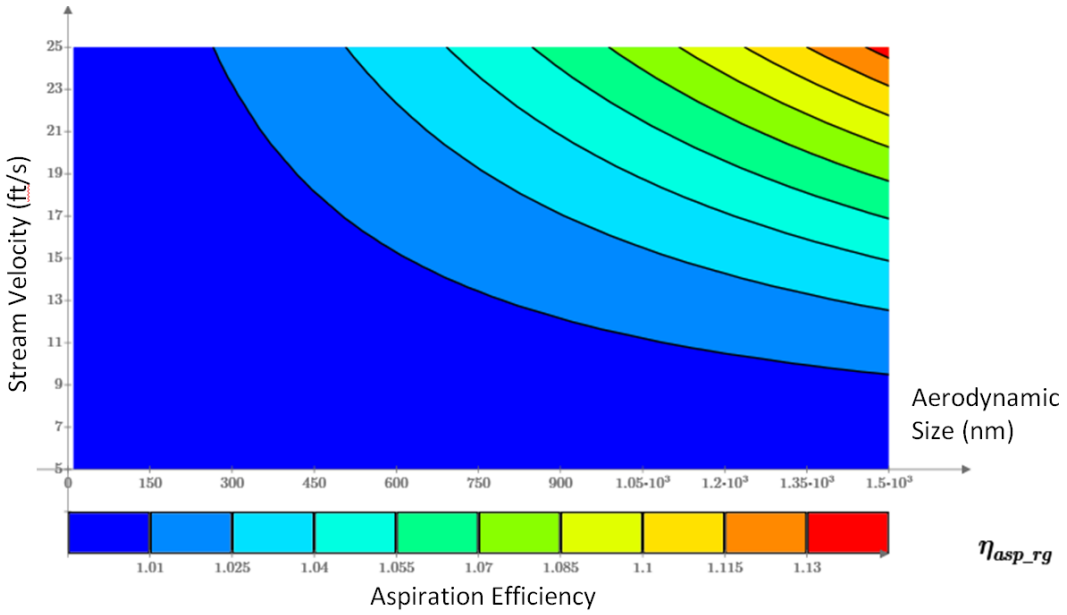

Figure 3-9 Aspiration Efficiency using Rader 1988 formulation

The diffusional losses, while large for small particles, will not be more than 2.5% at the low range end for our particle size ranges. In fact the SMPS system is limited as to how small of particles it may measure purely by the fact of diffusion. Figure 3-10 shows the information regarding diffusional losses. 10nm is the smallest particle size our system is able to measure with the typical lower range being set at 14 nm. From this image, it is clear that the losses will not be great in the sampling tube as the Reynolds number is approximately 900 to 1000. Figure 3-11 also shows the diffusional losses for the sampling tubes going from the SMPS and APS to the bleed air pickoff line. These estimates indicate a loss of approximately 10% at most and only for the smallest particle sizes measureable by the SMPS. The flow velocities using a 0.25in diameter orifice plate are no more than 15ft/s at the most.

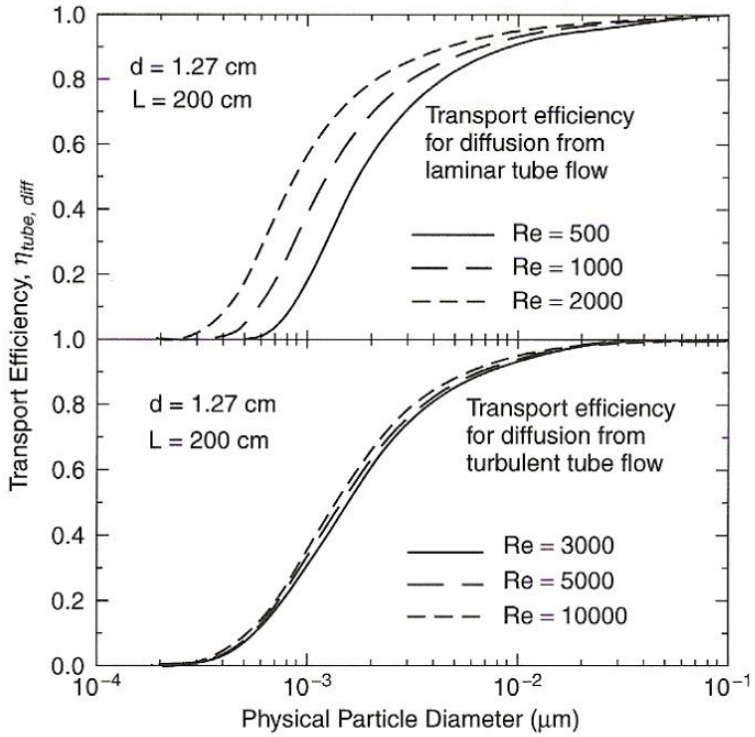

Figure 3-10 Diffusional Losses in General
Reproduced from (Baron & Willeke, 2001)

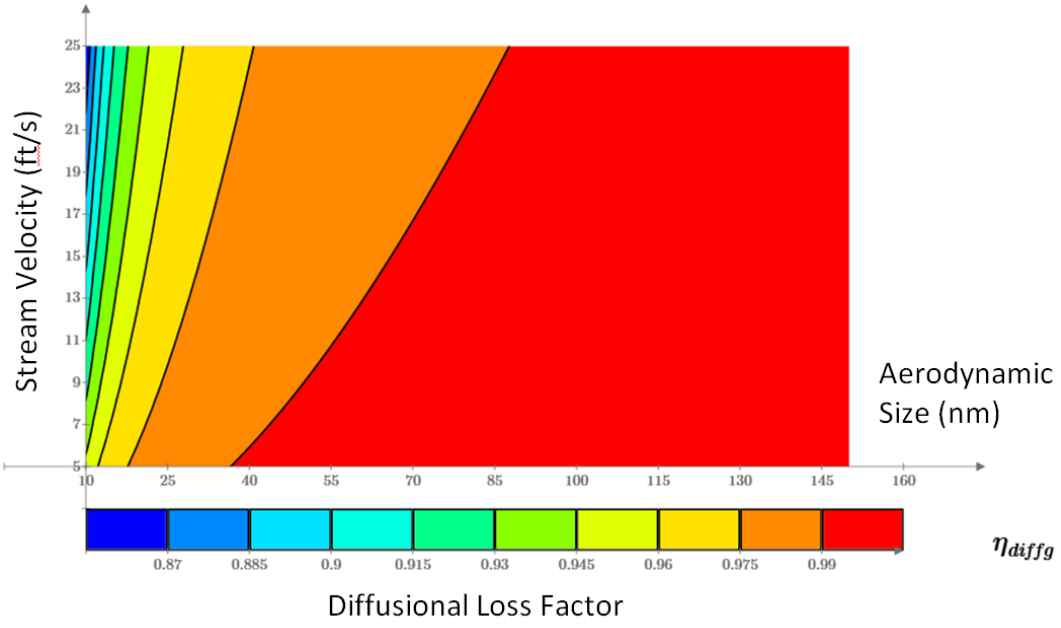

Figure 3-11 Diffusional Losses Plotted

In fact the losses of particles for the system sampling pickoff ports are rather low with the diffusional losses being the primary means of inefficiencies. These losses show up most on the ambient air measurement line as the length is much longer than it is for the bleed air sampling line. However, the losses are still low and the error of sampling from the 3in line is no more than about 5% nominally for all losses combined, including gravitational settling, curve bending efficiency, and various other corrections. The particles measured by the equipment are representative of the bleed air line. Recall that sensors utilized for the bleed air measurement will also be in a similar location to that of the bleed air line pickoff. The bleed air oil injection losses are also minimal and express efficiencies close to 98%.

The system was designed based on standard equations of heat transfer and pressure drop. From information gained from testing, the design flow rate was in error by 1% to 7% from the measured flow rates. The measured flow rates are calculated according to ASME orifice plate standards with values of coefficients provided on the data sheet given by Lambda Squared.

3.3 Results and Discussion

3.3.1 Notes on data naming

Refer to section 2.2.2.2.1 for the discussion of graph legends.

3.3.2 Notes on FTIR Data

The data taken by the FTIR during the engine testing were found to be very low in resolution compared to ambient conditions. The data were for all practical purposes indistinguishable from the ambient readings and thus no solid conclusions could be made. While there were some apparent CO2 peaks that occurred, nothing was definitive to a great degree. These low concentrations are most likely due to the large volume of air compared to the minor amount of oil injected. CO2 and CO peaks were able to be picked up on the bleed air simulator,

but only after the connecting directly to the injection system after the heater tube and before the airstream was diluted by the main airflow. This arrangement bypassed the dilution air of the bleed air simulator and enabled the FTIR to distinguish the gas compositions from the atmospheric baseline. Increasing CO levels were observed for increasing pressure and temperatures. CO measurements had a maximum at 42 ppm at 310°C and 690kPa (100psi) with concentrations being lower at lower temperature conditions. Since it is impossible to separate the dilution air from the oil injection air in a gas turbine setting, the FTIR measurements yielded nothing. The flow rate for the oil injection air at the BAS was approximately 75LPM (2.7cfm) while the C18 engine flow rates are up to 2500scfm, and thus the 42ppm CO measurement, taken at 310°C and 690kPa (100psi) on the BAS, will be diluted below the resolution of the FTIR. Detailed FTIR and aldehyde concentration data will be addressed by Dr. Shahin Nayyeri Amiri in a complementary project.

3.3.3 Ambient Separation

The first data set taken on the engine was intended to establish the ambient, background and air plenum box readings. This data set was intended to ensure that the concentrations measured during the injection of oil were due to the oil going through the engine and not an artifact of ambient particulates or exhaust gases. The background refers to measurements taken with no engine running with no oil injection. It is used to establish the baseline readings of a sample location. The ambient readings refer to data taken by the equipment not hooked up to a sample location but measuring from the ambient air next to the testing stand. These data were taken in sample sets of five runs back to back and the data shown below are the averaged values.

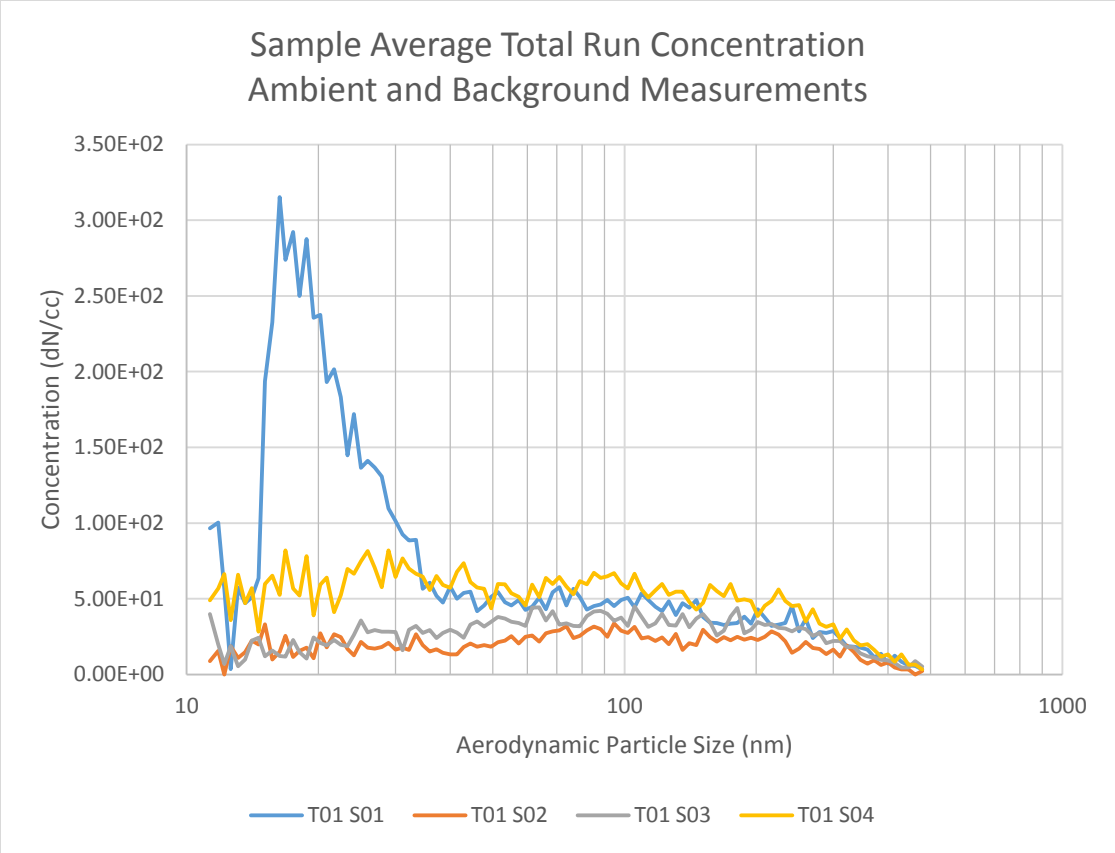

Figure 3-12 C18 Background Measurements

T01 S01 and T01 S04 are both ambient measurements. S02 and S03 are both measurements of the bleed air sample port and the air plenum box sample ports respectively. As can be seen, the information shown indicates that the ambient measurements are all relatively close in concentrations and are low in concentrations. The typical concentrations seen over a 120s run on the SMPS system indicate concentration levels around 1E3 dN/cc for ambient readings.

Data were then recorded while operating the engine at the following conditions: 84-82% N1, 80-78% N2, 200°C, 53 psia, and about 100hp in the same five sample increments. These sample runs add up to approximately 11 minute data sets that are shown as averaged.

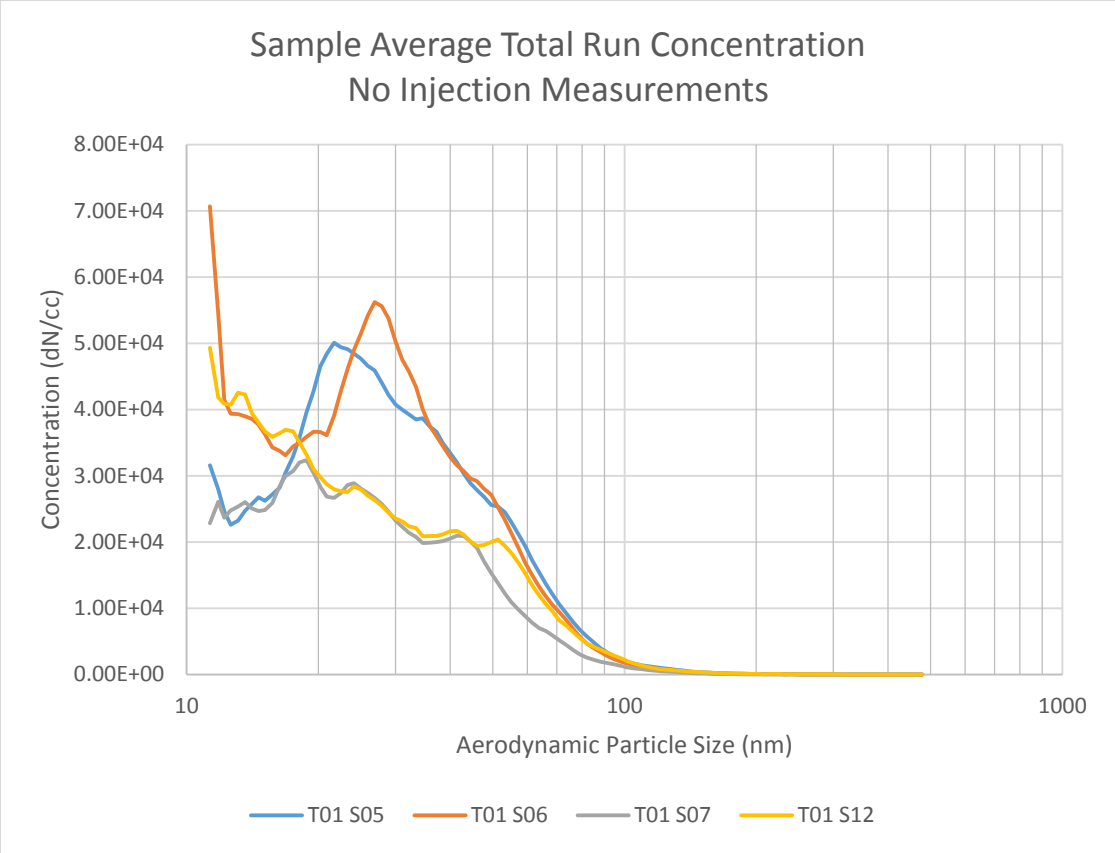

Figure 3-13 C18 No Injection

It may be seen from Figure 3-13 that there are particles picked up during the running of the engine. These particles are most likely then the particles associated with the combustion gases of the exhaust. The concentrations are also a magnitude higher than the background and ambient baseline concentrations. S05 and S12 are ambient while S06 and S07 are both bleed line measurements.

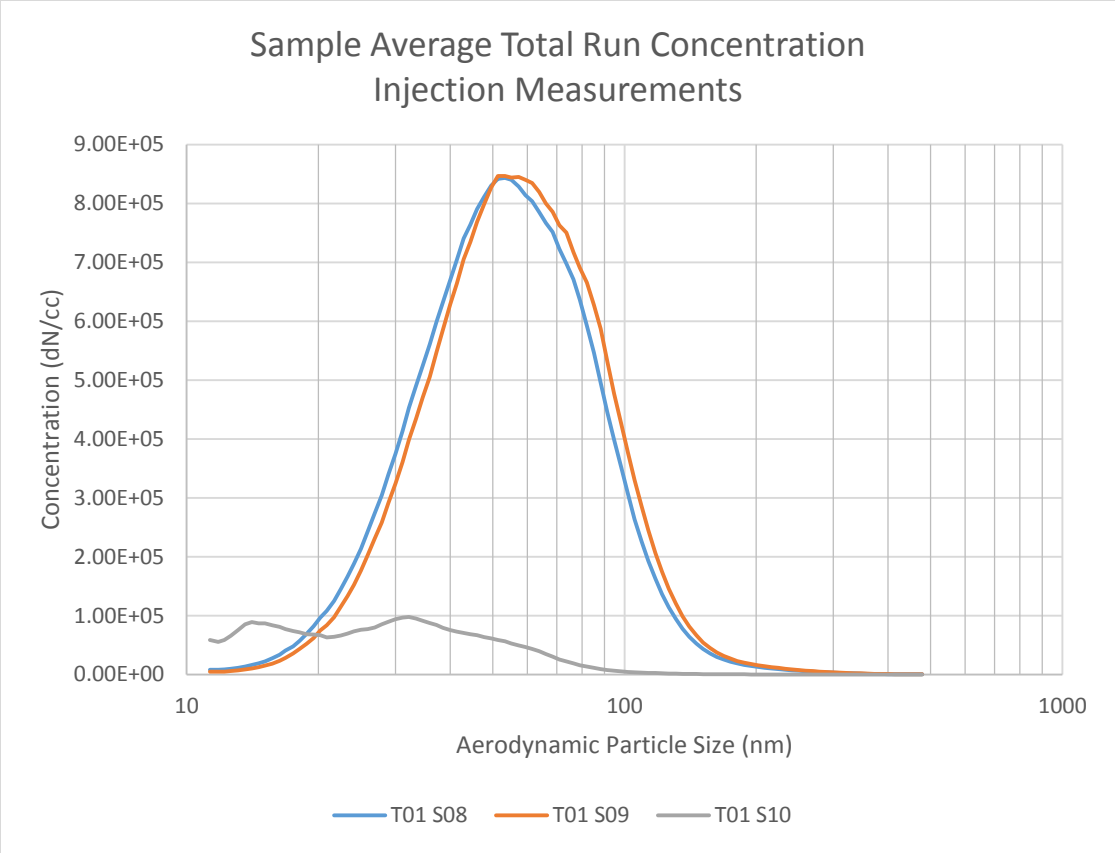

Figure 3-14 C18 Initial Injection

Figure 3-14 shows the data taken when oil was injected. S08 and S09 are both bleed air line measurements while the S10 is the air plenum box measurement. The air plenum box is indeed much lower as there should be no oil pickup from this measurement. A comparison of the air plenum box while the engine is running to the no injection measurements of the air plenum box is shown in Figure 3-15. This measurement indicates that while oil is being injected, the particulate matter may increase in the exhaust gases; the increase is marginal compared to the concentrations seen in Figure 3-14.

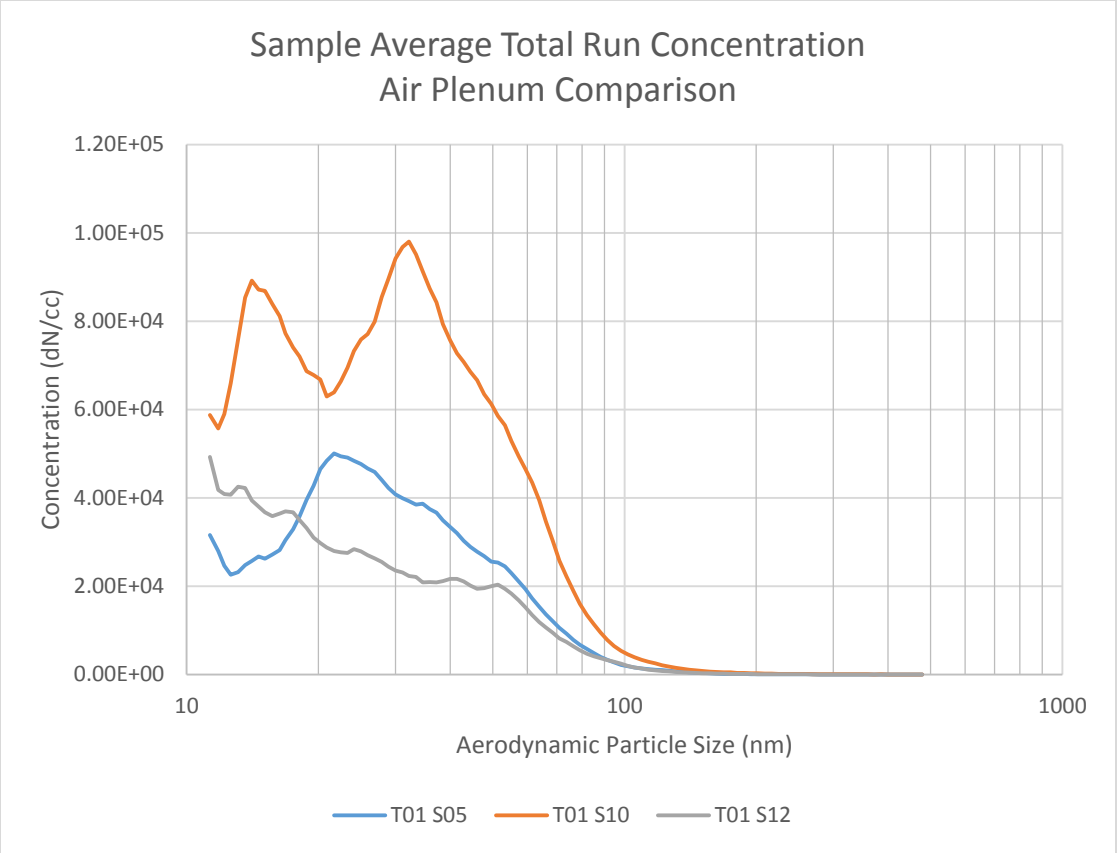

Figure 3-15 Air Plenum Comparison

However, it was observed that oil did build up on the system during the test and this effect is shown in the Figure 3-16. S08 and S09 are both the oil injection measurements while all S11 RXX data points are taken after the oil has been turned off. This figure clearly shows that oil residual will remain on the engine after the oil is turned off and that this oil deposition effect could potentially impact the results. It is further seen that the concentrations move to the smaller sizes as the test continues. This begs the question if the amount of oil injected will affect the concentration peaks and how long until the oil is removed after the injections take place. It is obvious that this process will be longer than 10 minutes as the mass decay may be seen in Figure 3-17. These figures seem to indicate a thin layer of oil film being deposited on surfaces in the

engine. The deposition of particles on the inlet intake transition is likely to be small as the main point of impact will obviously be the compressor blades.

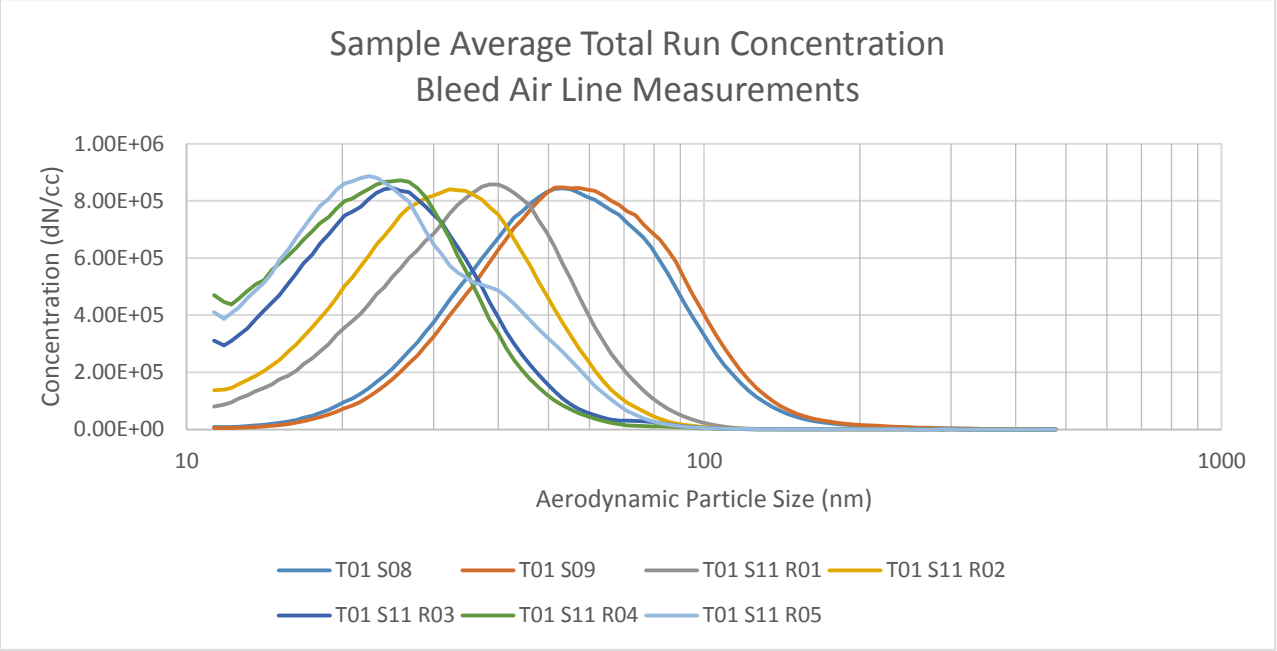

Figure 3-16 C18 Bleed Air Line Measurements

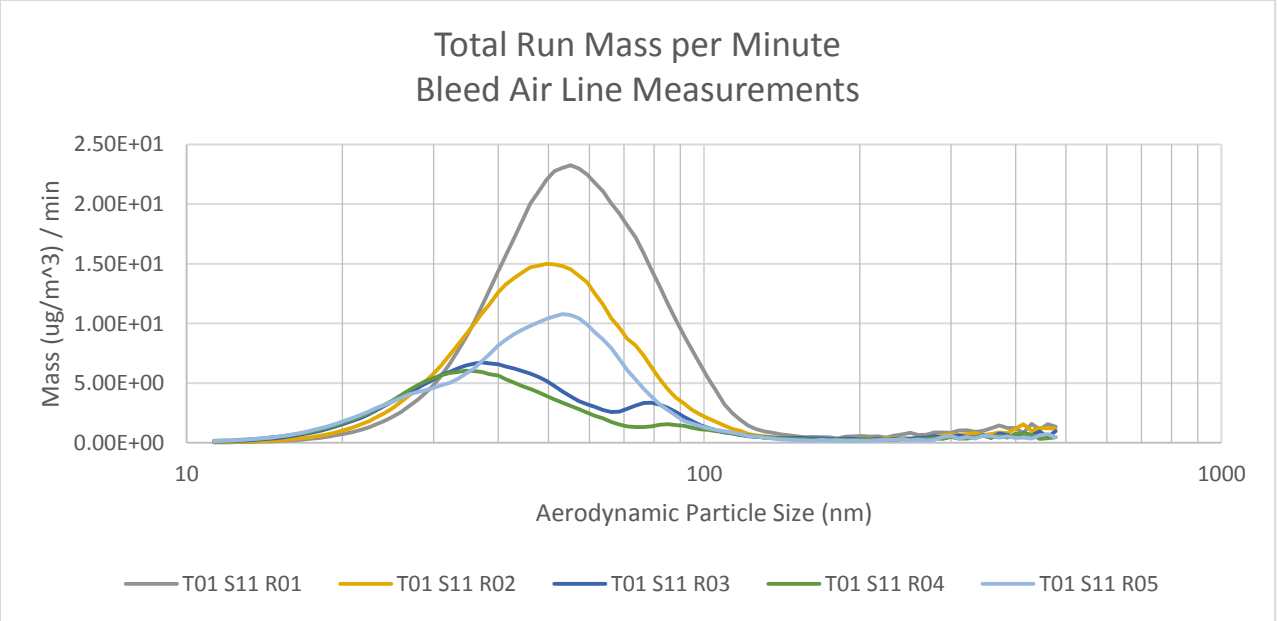

Figure 3-17 C18 Initial Mass Decay

3.3.4 Steady State Decay

The steady state decay measurements were taken at similar conditions to those in the T01 data set. The engine conditions were maintained at approximately 200°C and 60 psia – 57psia. These engine conditions gave an approximate power output of 126hp – 117hp as the ambient temperatures of the plenum varied from 70°F to 77°F. These variations took place over a three hour time period and illustrate the difficulties of maintaining a constant testing state of the engine. The test was done by first injecting oil with a single Laskin nozzle. The number of nozzles was increased incrementally up to three and immediately following the completion of the three nozzle test the aerosol generator was removed and the injection line sealed with a cork to prevent any further injection. Thus, with no more oil being injected and the source of oil injection removed the decay of the oil film on the engine was measured over a 1hour and 15minute period.

3.3.4.1 Nozzle Injection Variation of Particle Concentrations

In this test, T04 to T06 correspond to increasing number of nozzles for injection. From Figure 3-18 and Figure 3-19 it may be seen that the variation in particle size concentration varies with the amount of oil injected. Several theories may be developed from these data. This author puts forth the idea that as more oil is deposited, a thicker layer will form on blade surfaces and allows larger particles to develop and thus shift the size distribution to the right. The shift in the data from each nozzle is approximately 8 to 10nm for each additional nozzle. Figure 3-19 also indicates that the geometric mean diameter for the data is actually relatively stable considering the uncertainty on size is ±3.5%. This stability in geometric mean diameter indicates that the data were taken at a steady state operating condition and that the time of injection for the oil does not matter. If the time of injection were to influence the data, the trends would have a positive

slope. Additionally, each test was initiated no more than 30 seconds after the previous test indicating that the film build up is very quick as well. It is possible that the accumulation of the oil layer is responsible for the apparent increase in the first point of the single Laskin nozzle injection. What is also seen is that the concentration levels are very close in amount measured as well, providing further evidence that the Laskin nozzles have a repeatable injection rate for concentration and mass.

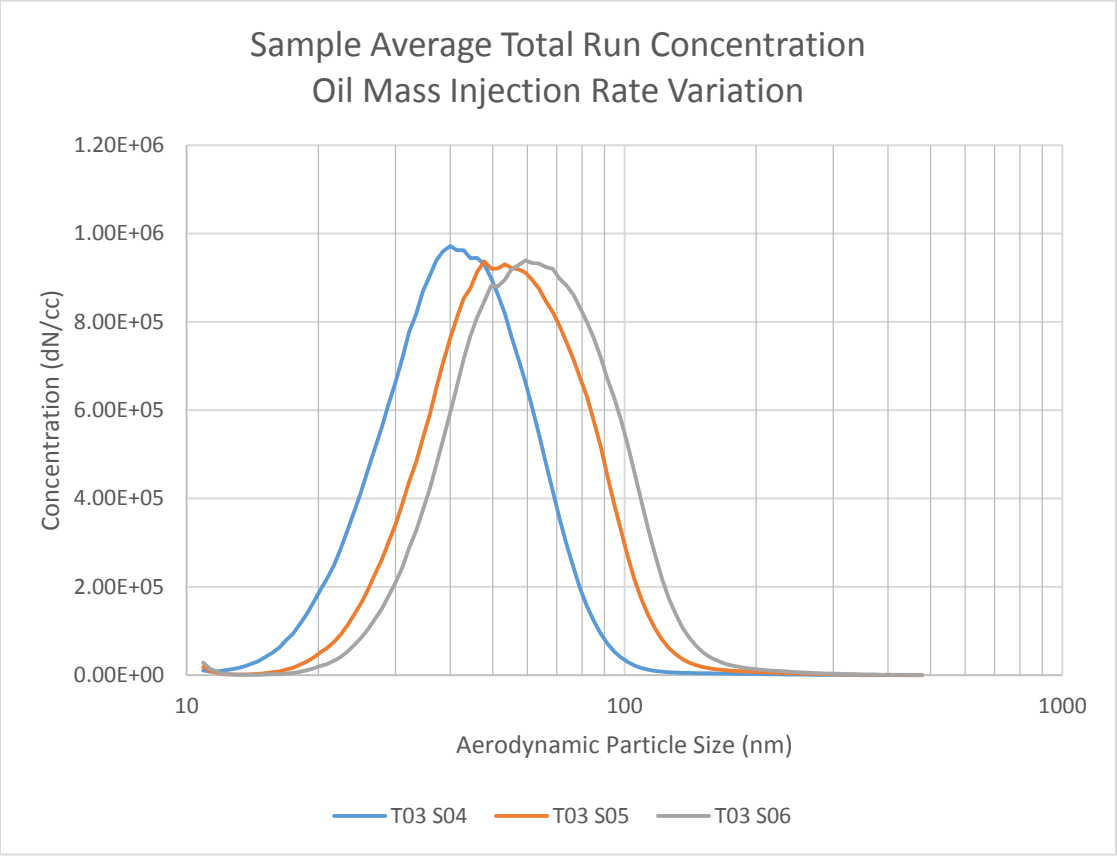

Figure 3-18 C18 Nozzle Concentration Variation

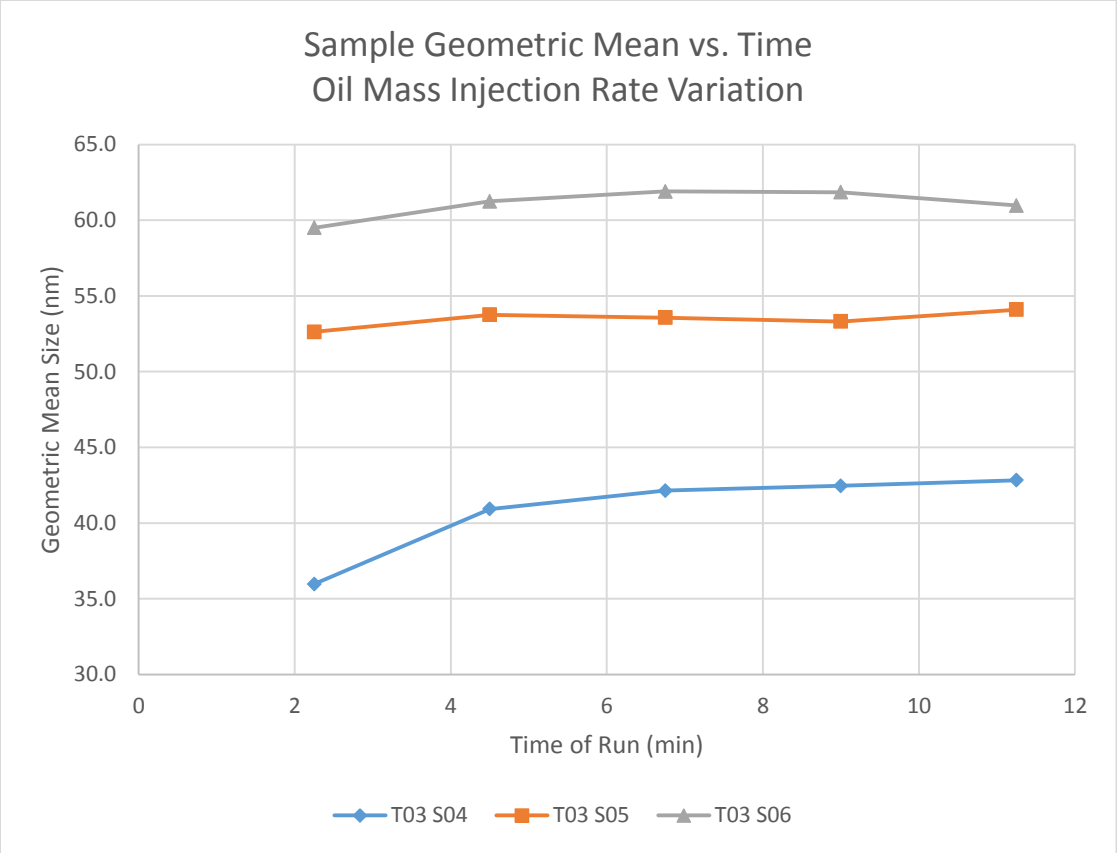

Figure 3-19 C18 Nozzle Geometric Mean Variation

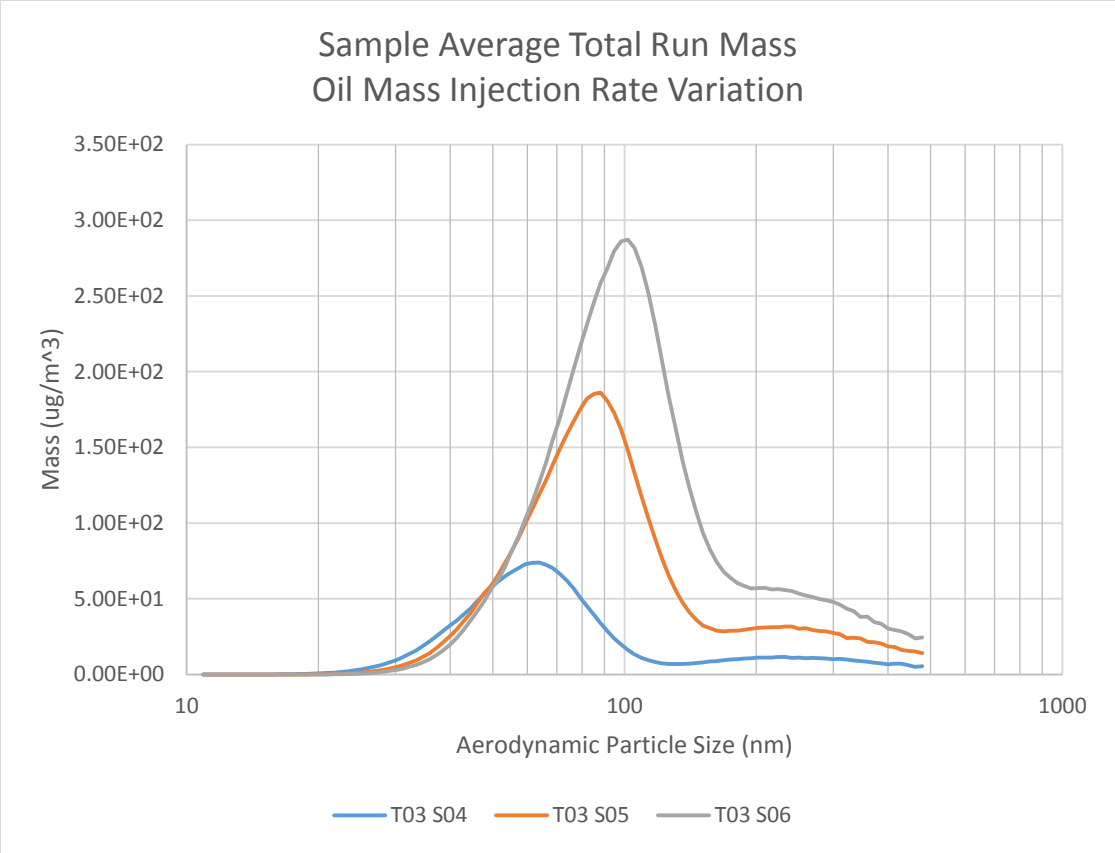

Figure 3-20 Nozzle Variation – Mass

Figure 3-20 shows that the mass also increases for more nozzles being activated as would be expected. Figure 3-21 provides the total calculated mass through time and indicates as well that the mass increase between each nozzle is clearly seen. The amount of mass increase is approximately the same between the number of nozzles activated and is estimated at 2835 $\mu g/m^3$ and 2700 $\mu g/m^3$ for one to two and two to three respectively.

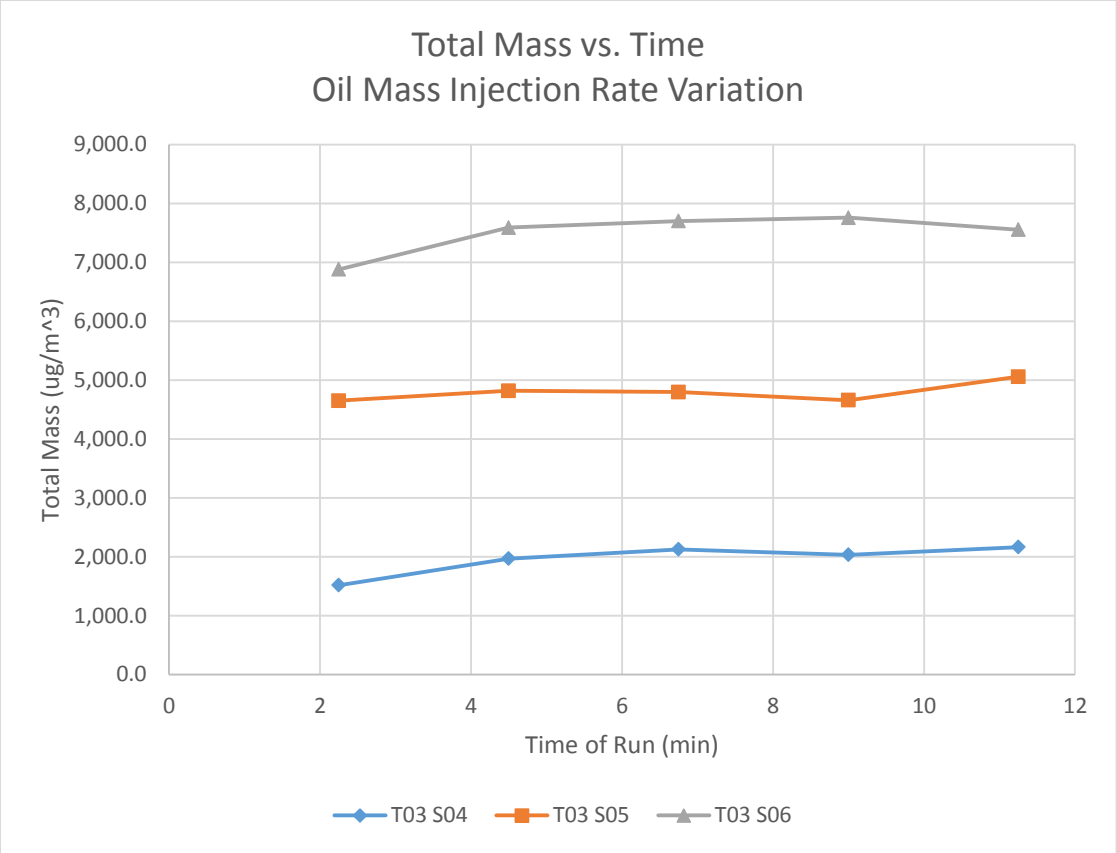

Figure 3-21 Nozzle Variation Total Mass

3.3.4.2 Decay of Oil Film

T02 and T03 both recorded the decay in concentration after the oil being injected into the engine test stand ceases. The main difference between the two tests is that T03 was recorded for a longer period of time and oil was reintroduced into the system for five minutes between T02 S08 and T02 S09. Figure A-22 and Figure 3-23 clearly illustrate the oil decay happening during the recorded measurements. The cumulative distribution is used to show that at test T02 S09, almost 90% of the recorded particle sizes are below the size of 20nm. T02 S09 was recorded an hour after the initial oil injection and 20 minutes after the reinjection. Likewise T02 S07 shows that about 80% of the particles are below 20nm. The oil mass recorded also decays at a fairly exponential rate as is seen in T02 S05 on the total oil mass graph. Oil mass being shed by the

system reaches approximately 79µg/m^3 after 35 minutes before oil is reintroduced into the system. After a five minute time period of oil injection into the system, the recorded mass reaches approximately 45µg/m^3 within 10 minutes of no oil injection. The relative concentrations stayed approximately the same in number as can be shown in Figure 3-24 thus indicating that there is an oil film buildup and that the oil film decays relatively slowly compared to the buildup times. The time of buildup seems to be faster than the 120s test time period as seen in Figure 3-19.

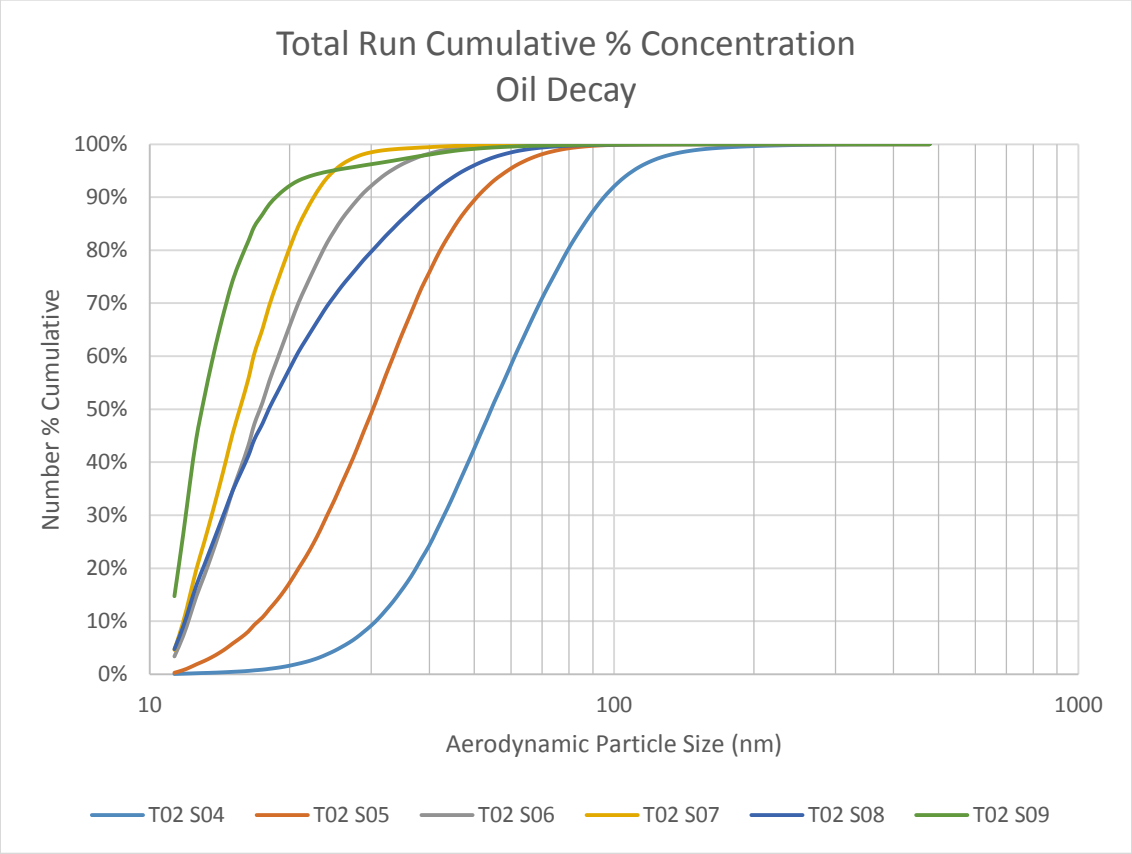

Figure A-22 T02 Oil Decay Total %

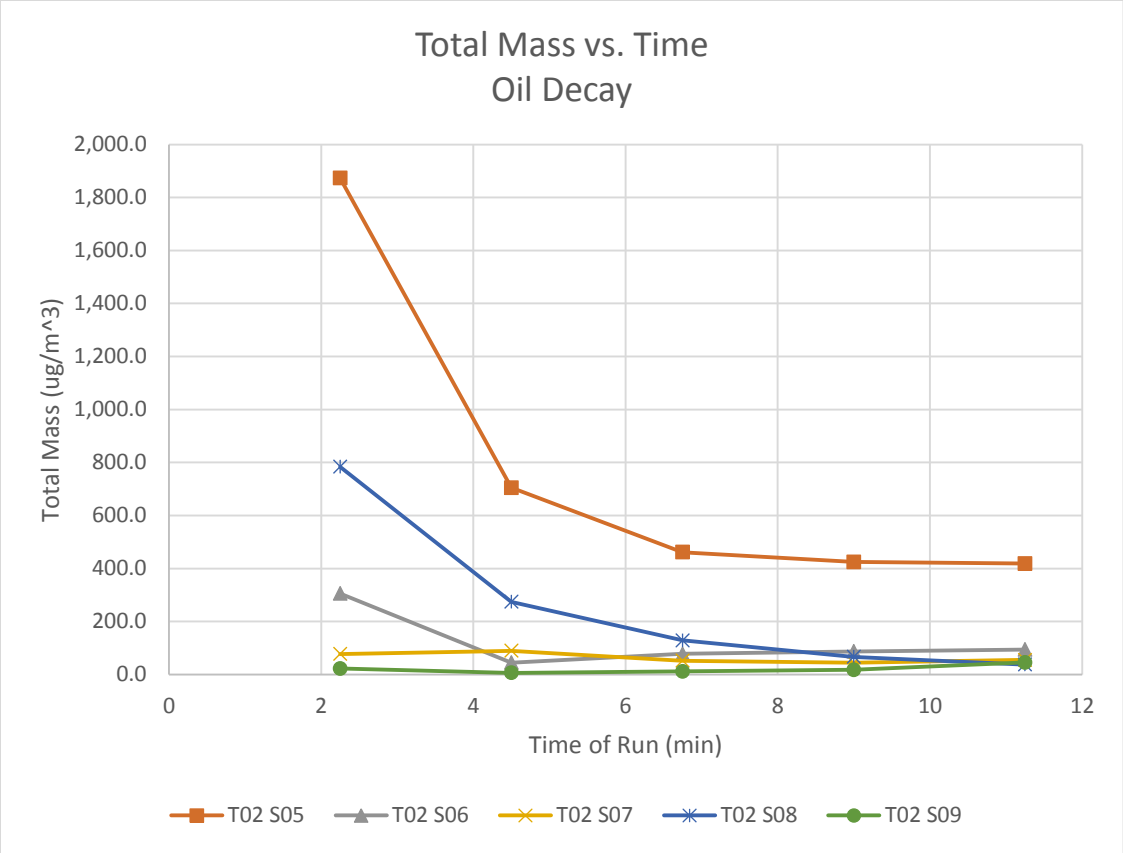

Figure 3-23 T02 Oil Decay Total Mass

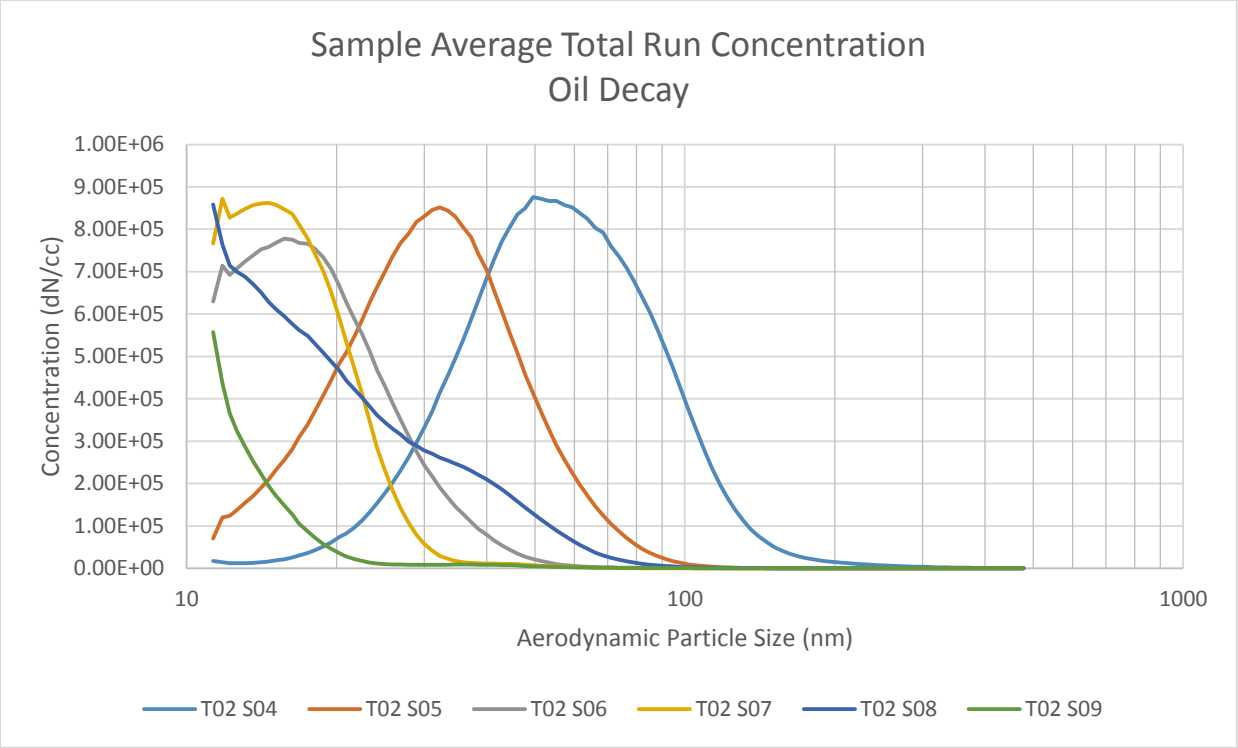

Figure 3-24 T02 Oil Decay Concentration 11min averages

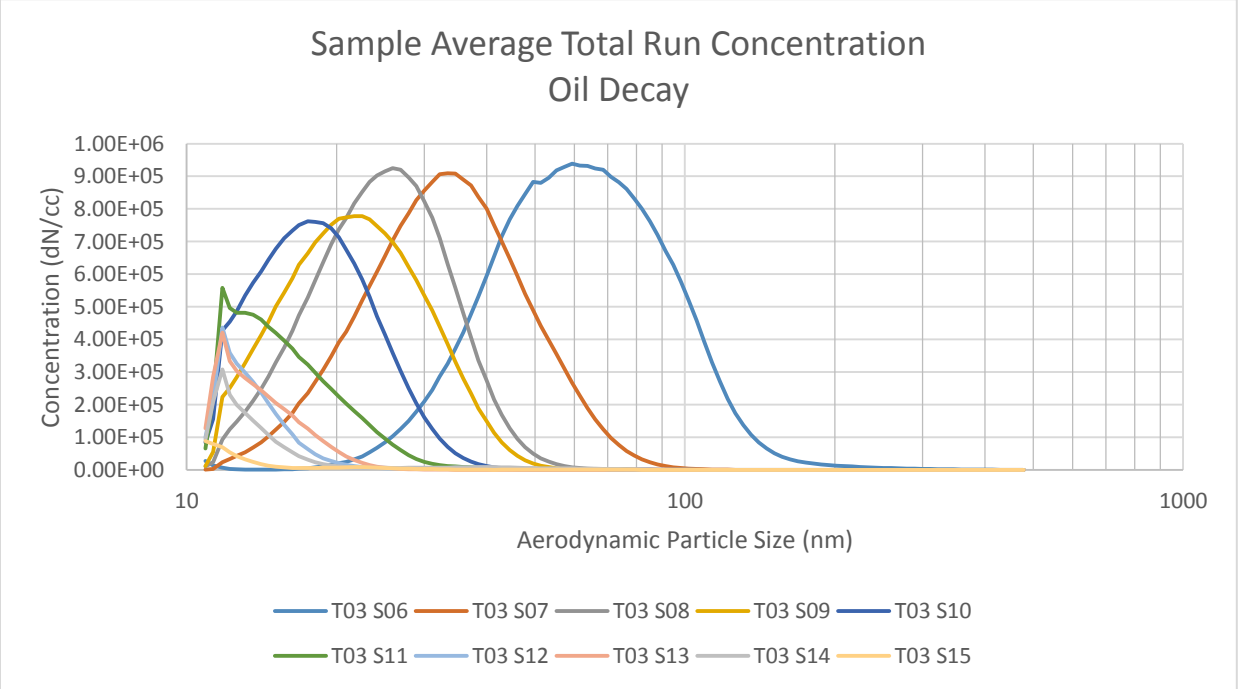

Figure 3-25 T03 Oil Decay Concentration 11min averages

The oil decay rate may be seen from Figure 3-25. S06 was taken with three nozzles injecting with the following data at the same approximate 11minute intervals. Thus S07 to S15 show the decay of the oil injection. The same trend may also be observed as in T02. The data also indicate that the particulate distribution shifts lower and lower until the equipment is no longer able to measure the nanoparticles. Figure 3-26 is also given for the T03 test data and indicates again the movement of the particle distribution to the smaller and smaller sizes as the oil is removed from the system. By S12 95% of the oil particle distribution is below 20nm. The mass is a cubic function of the concentrations, and thus will decay much faster as observed in earlier figures.

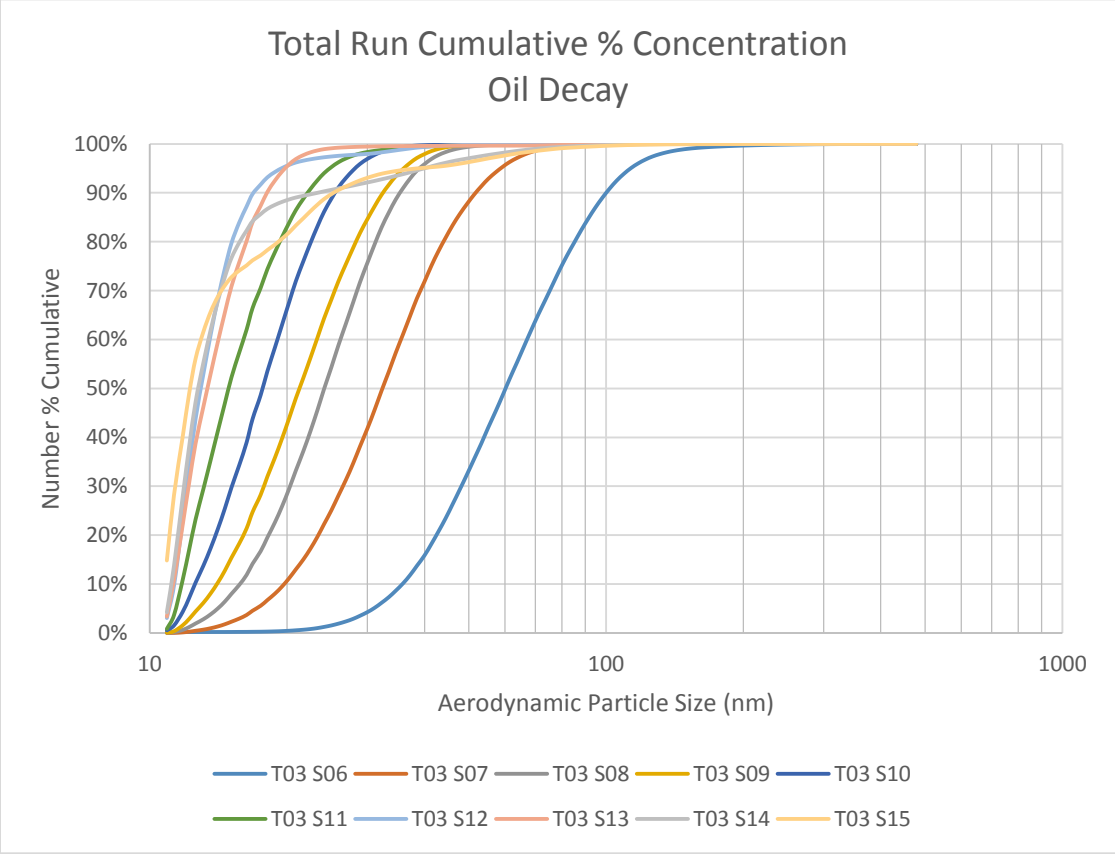

Figure 3-26 Oil Decay T03 Total %

The preceding data also establish the information needed in order to vary engine conditions. While these tests were recorded at approximately the same engine power throughout the test, we need to test other temperatures and pressures. Thus, with fuel supply limiting the testing run time, we will vary the engine conditions with knowledge that the buildup of any oil film will be quick and that while the oil is being injected the system will be at a constant state. Oil in the remaining tests was injected with three nozzles and left on during engine transitions.

3.3.5 Results & Trends

The following graphs will present the data for various temperatures and pressures. It is unknown why the concentrations varied so much between some runs and is thought to be attributed to the engine flow rate and power variations due to atmospheric temperature and pressure differences. It is unfortunate that the data are not consistently repeatable between days, but there are some trends evident. As the temperature increases a trend in the particle sizes may be seen. There is also evidence that the blades do impact the particles generated at lower temperatures.

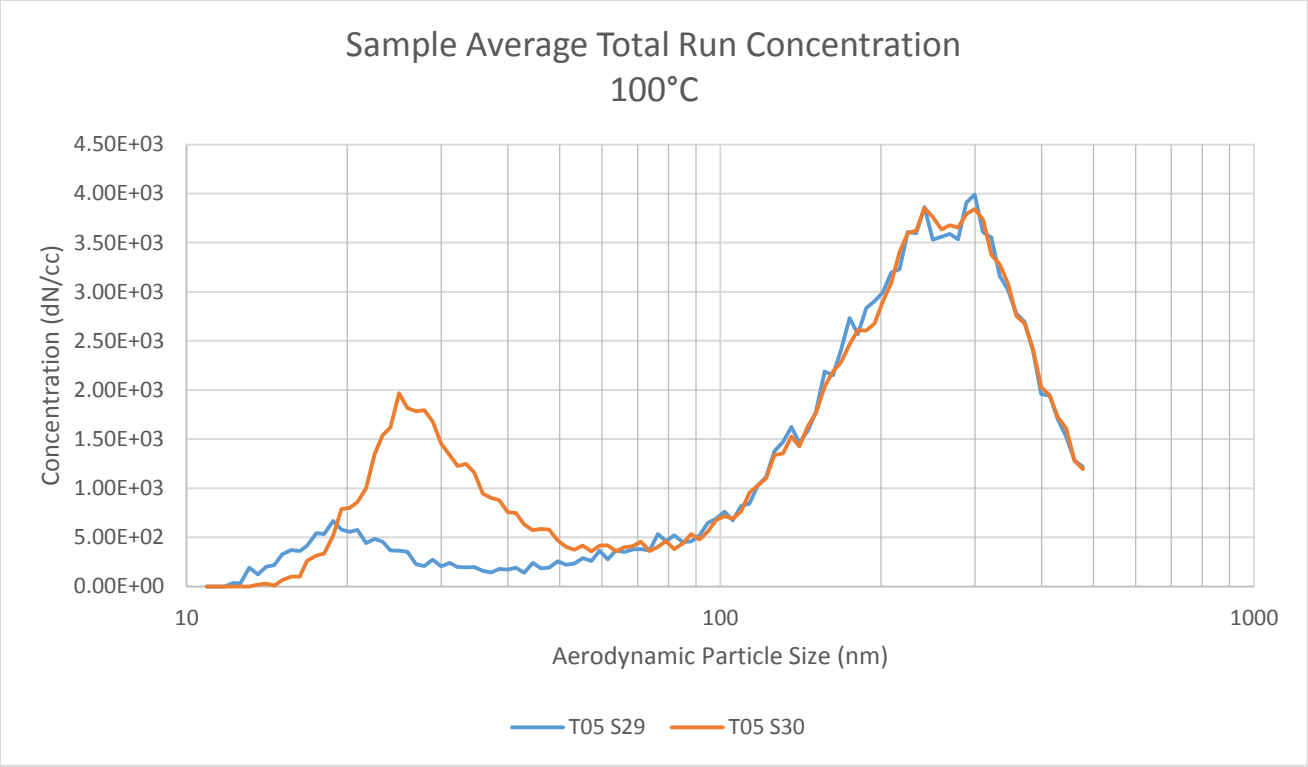

Figure 3-27 C18 100°C Compiled Concentration Data

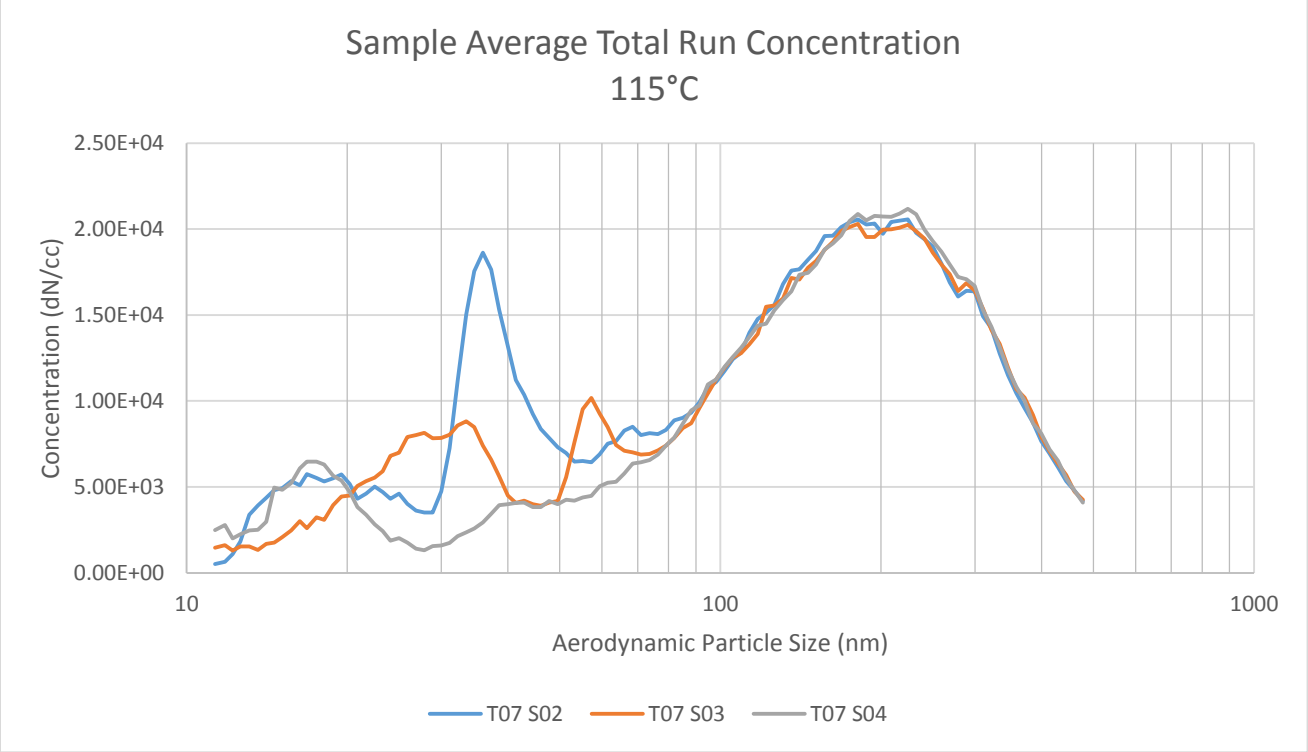

Figure 3-28 C18 115°C Compiled Concentration Data

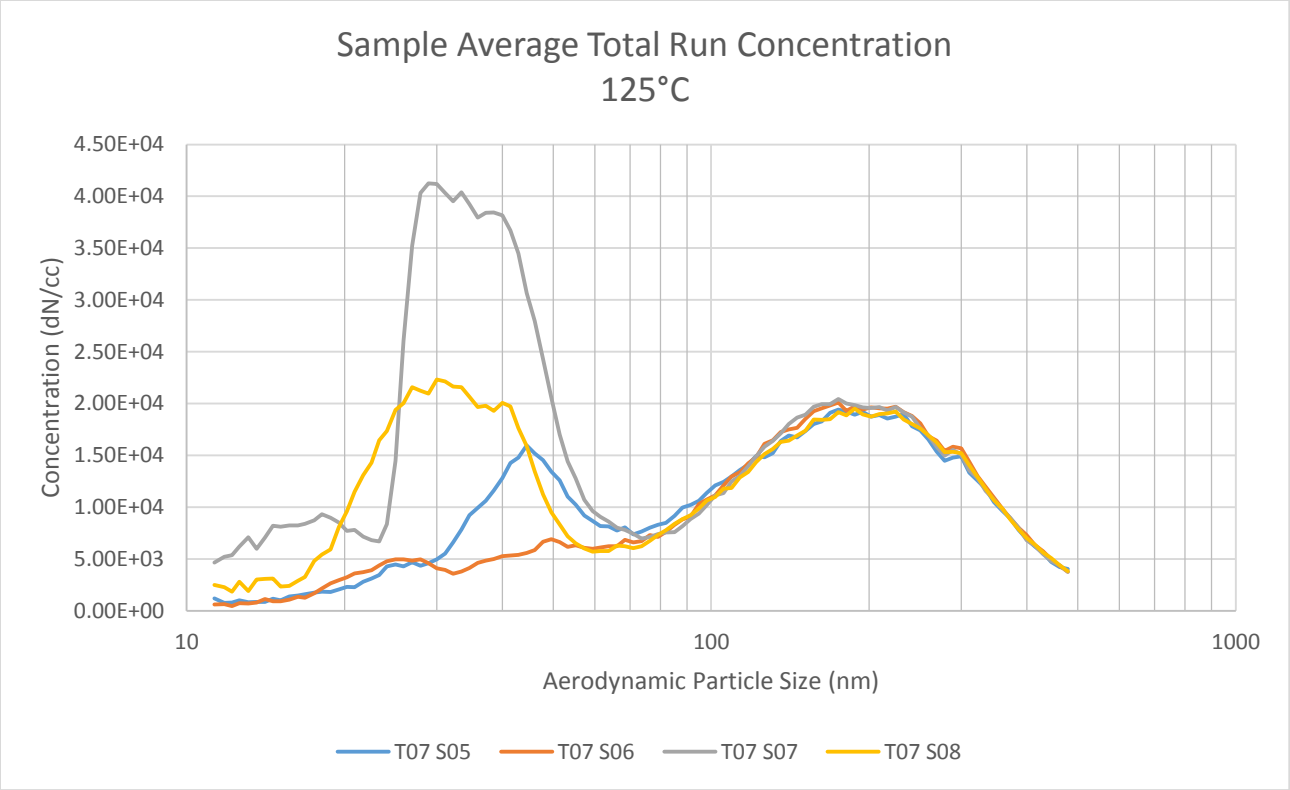

Figure 3-29 C18 125°C Compiled Concentration Data

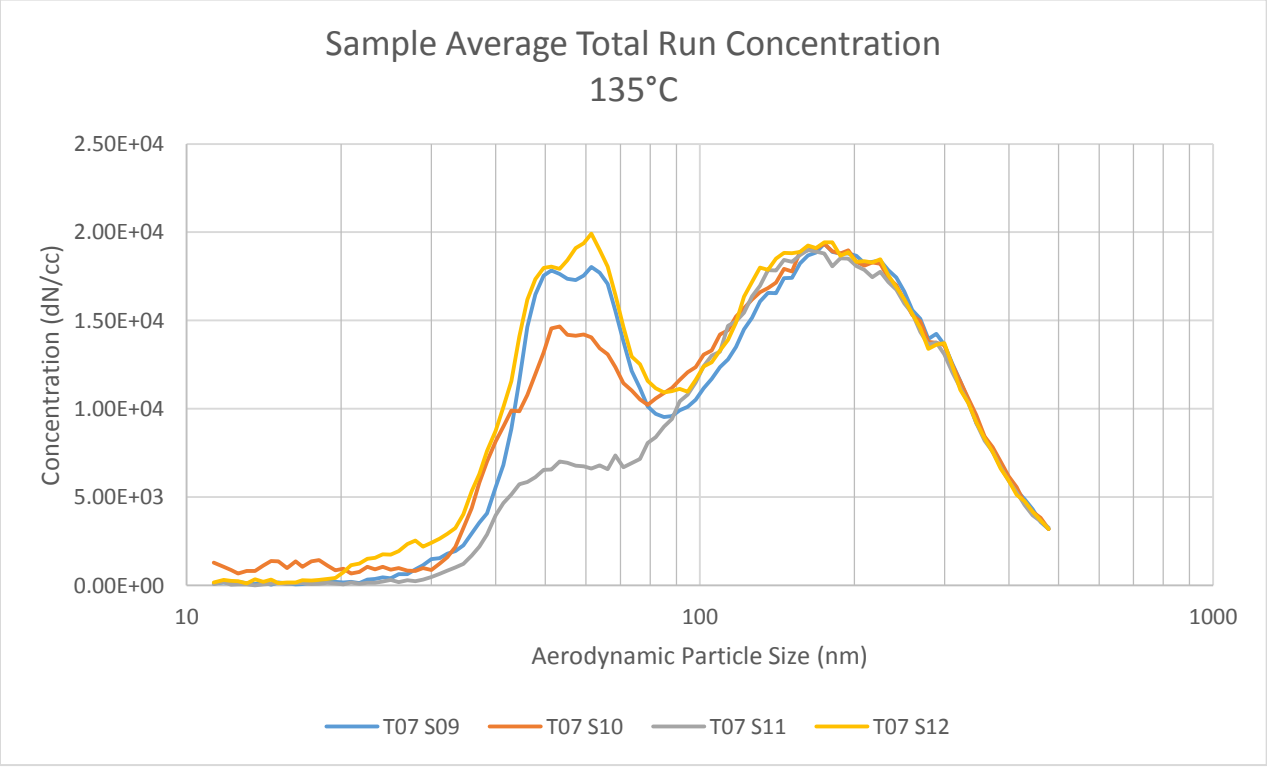

Figure 3-30 C18 135°C Compiled Concentration Data

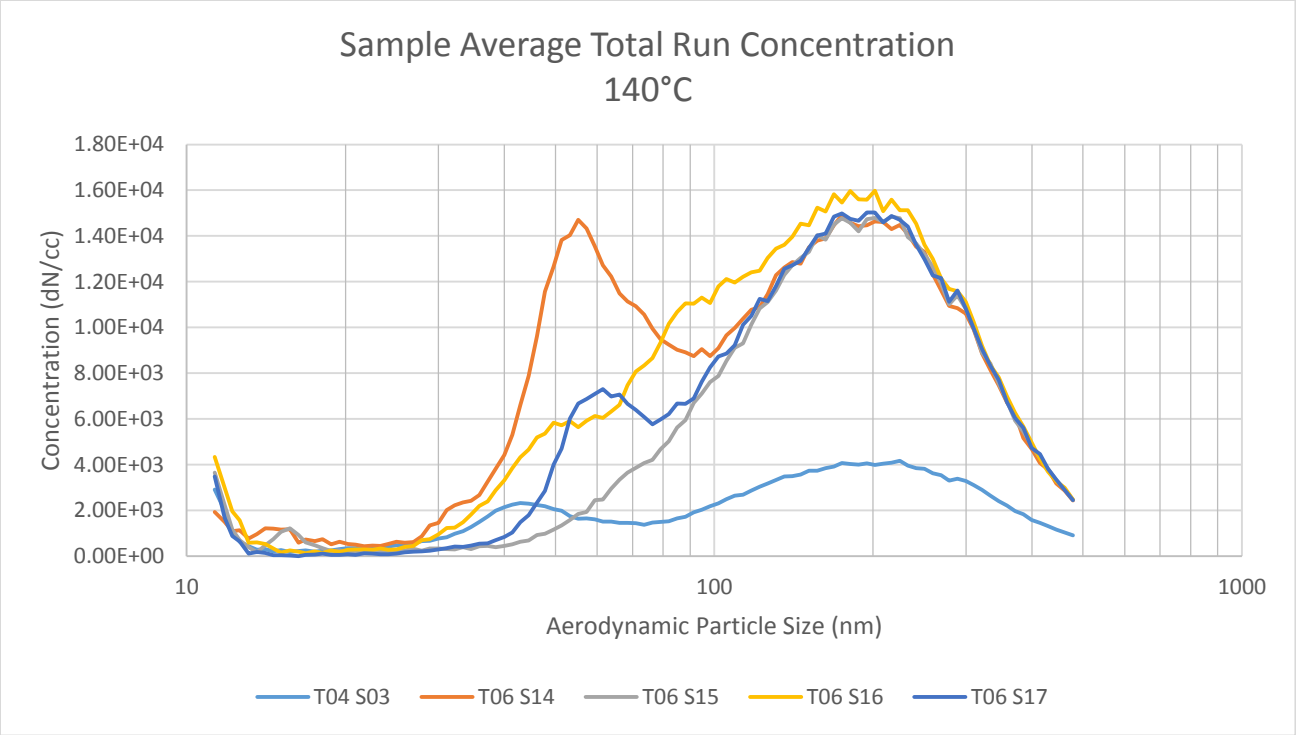

Figure 3-31 C18 140°C Compiled Concentration Data

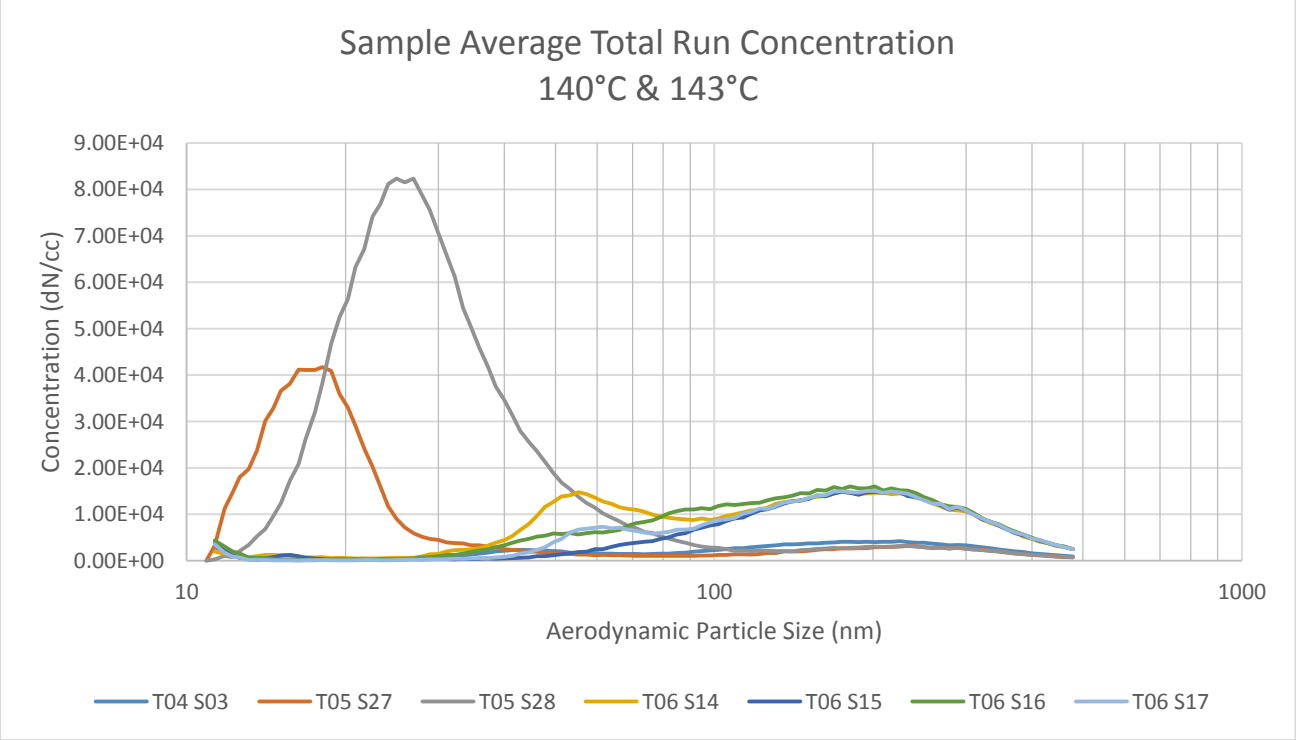

Figure 3-32 C18 140°C & 143°C Compiled Concentration Data

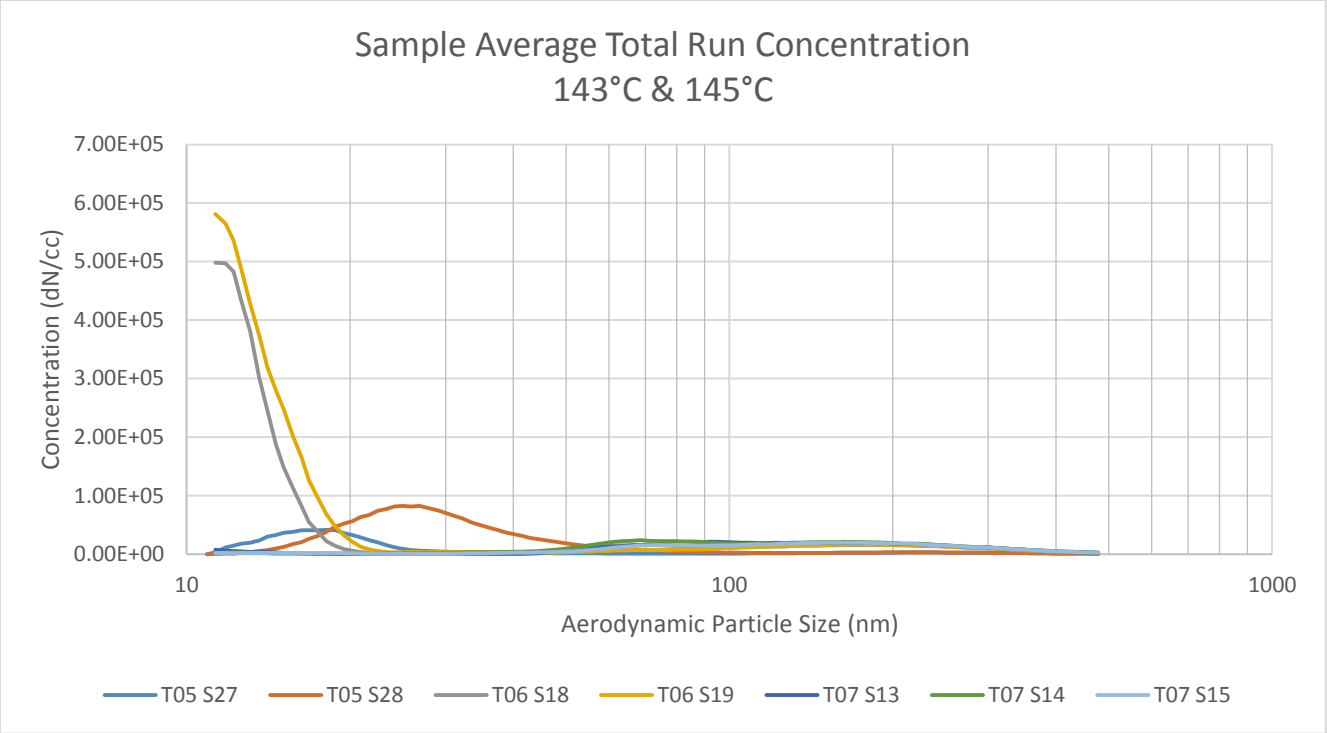

Figure 3-33 C18 143°C & 145°C Compiled Concentration Data

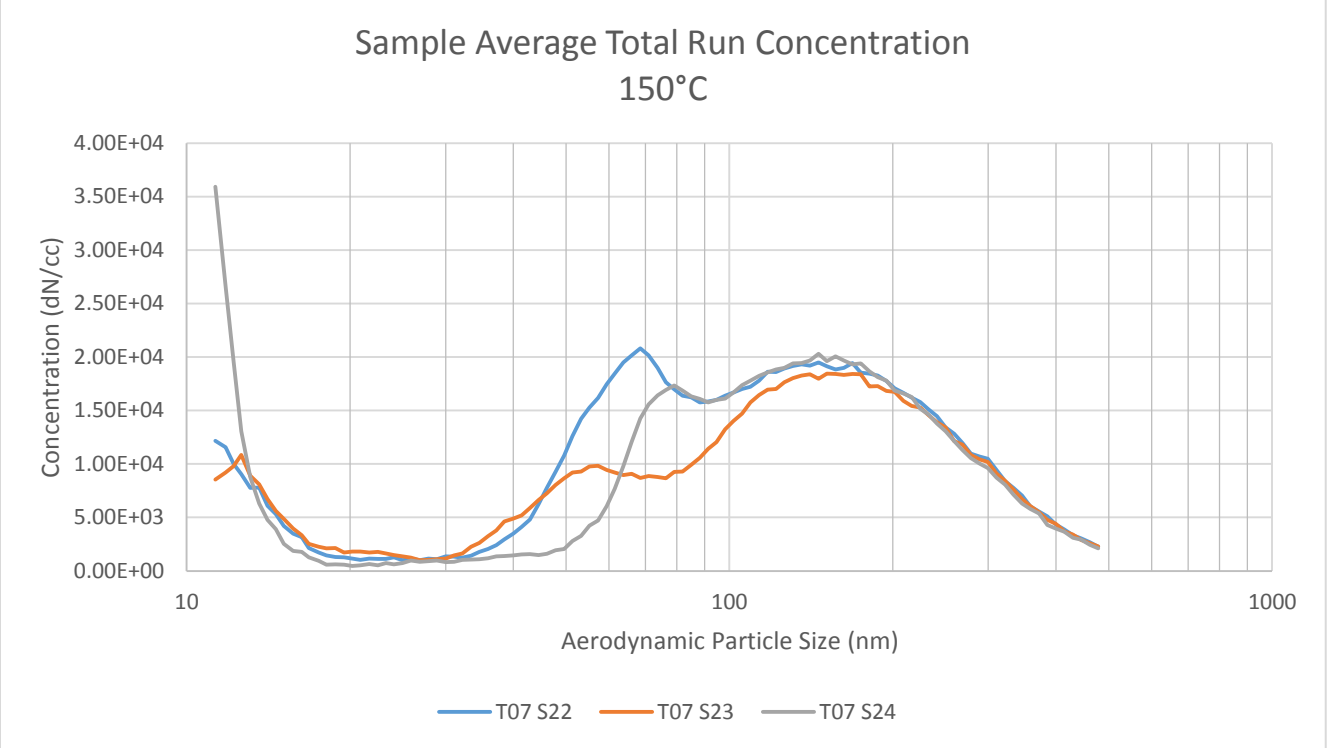

Figure 3-34 C18 150°C Compiled Concentration Data

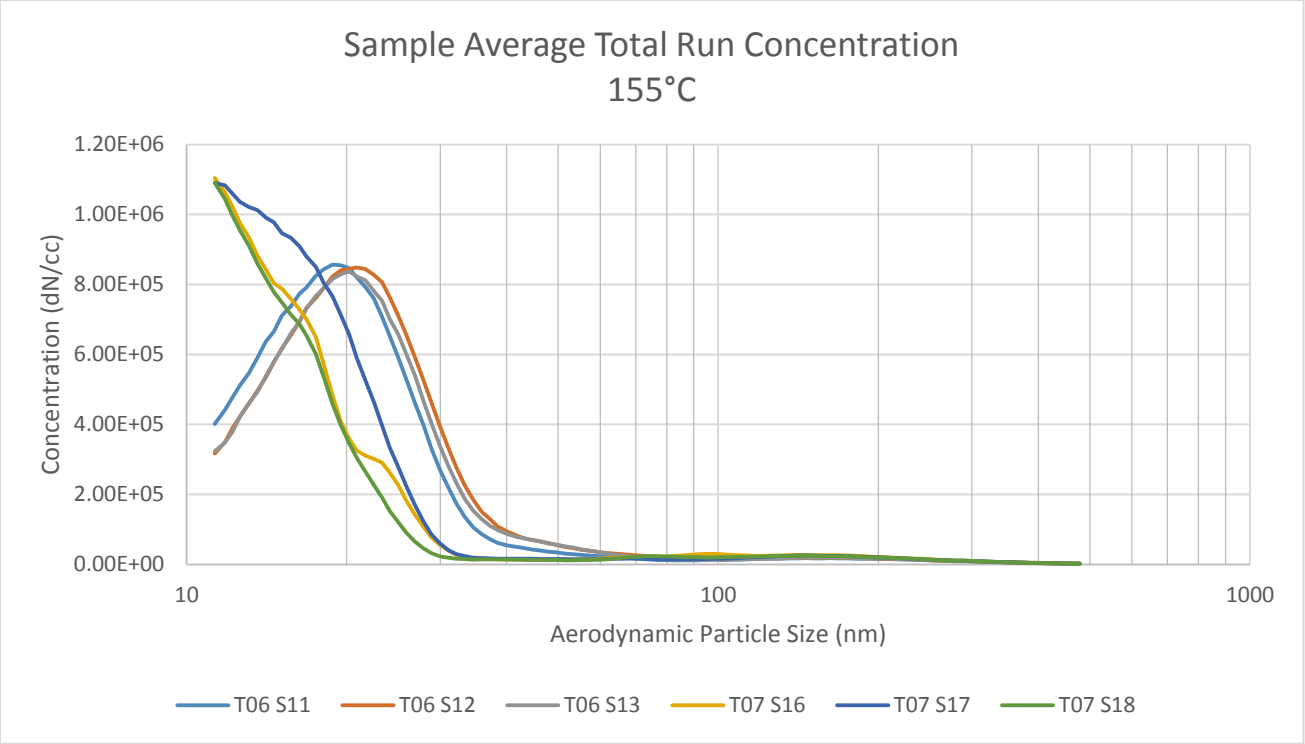

Figure 3-35 C18 155°C Compiled Concentration Data

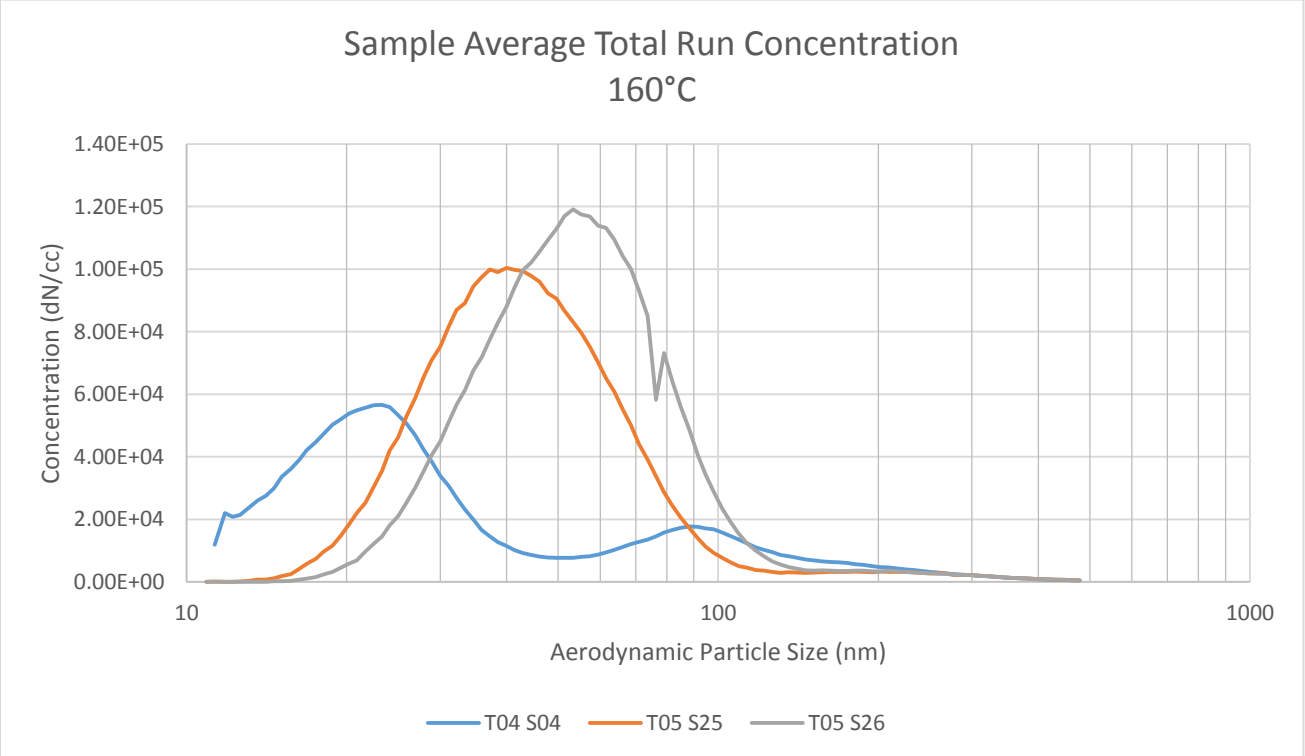

Figure 3-36 C18 160°C Compiled Concentration Data

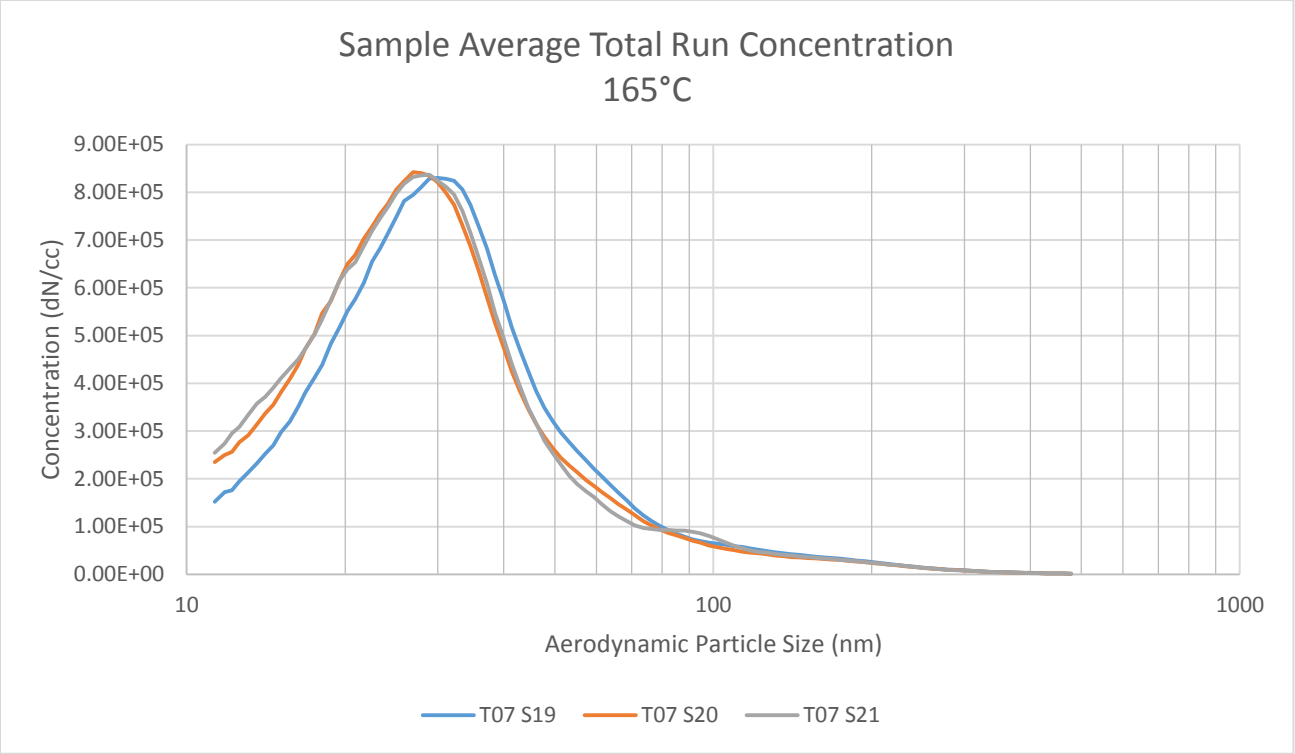

Figure 3-37 C18 165°C Compiled Concentration Data

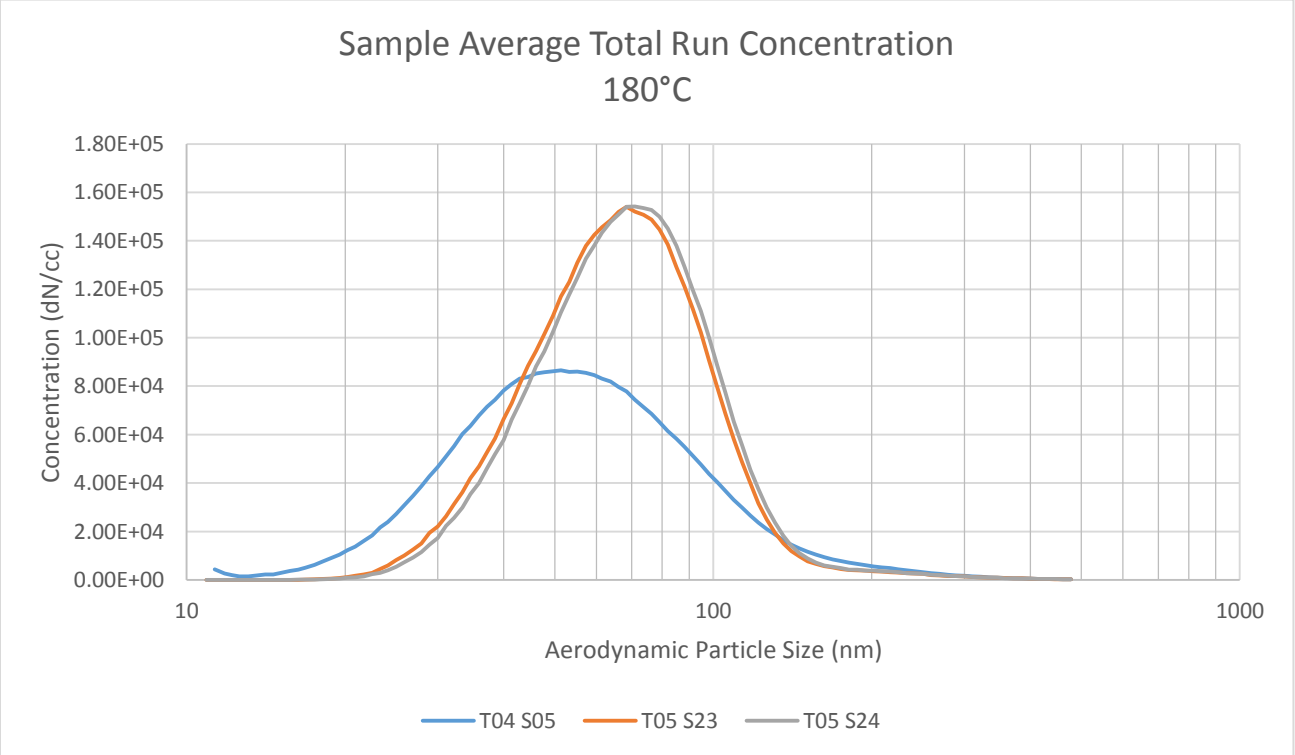

Figure 3-38 C18 180°C Compiled Concentration Data

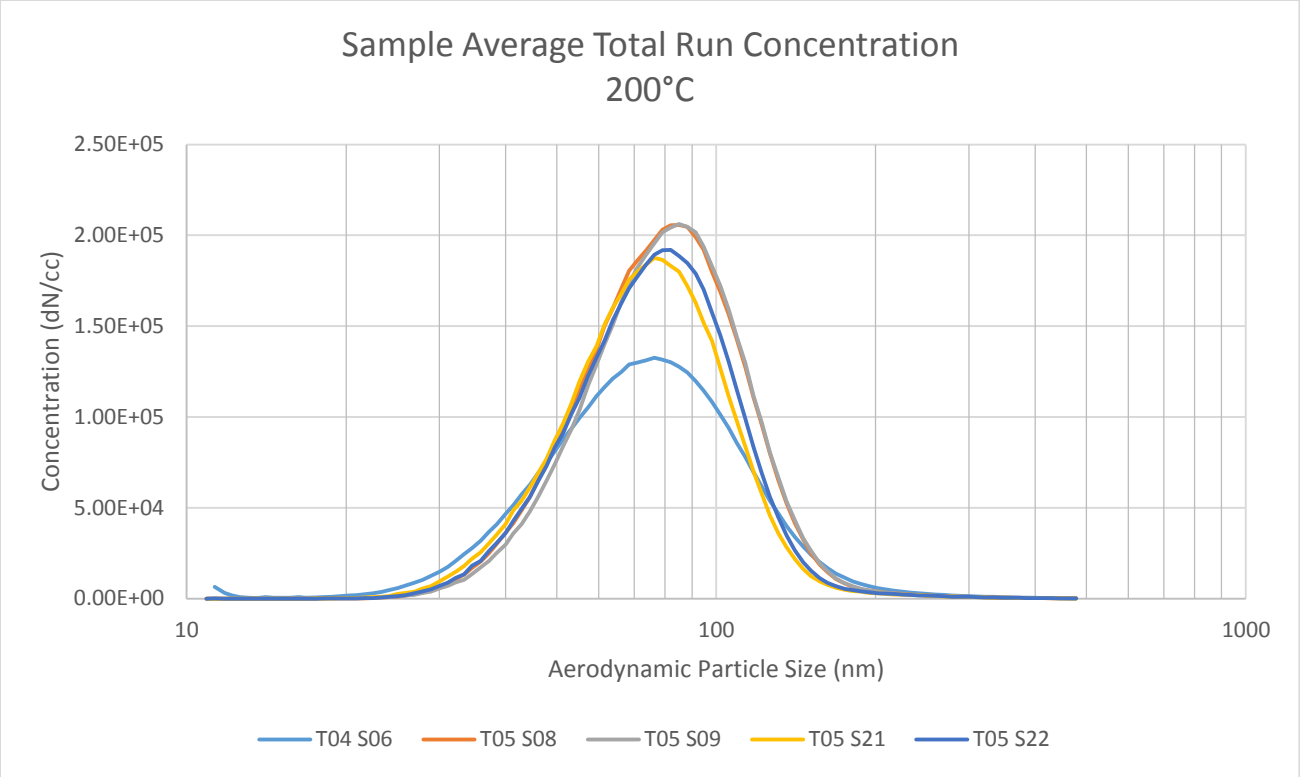

Figure 3-39 C18 200°C Compiled Concentration Data

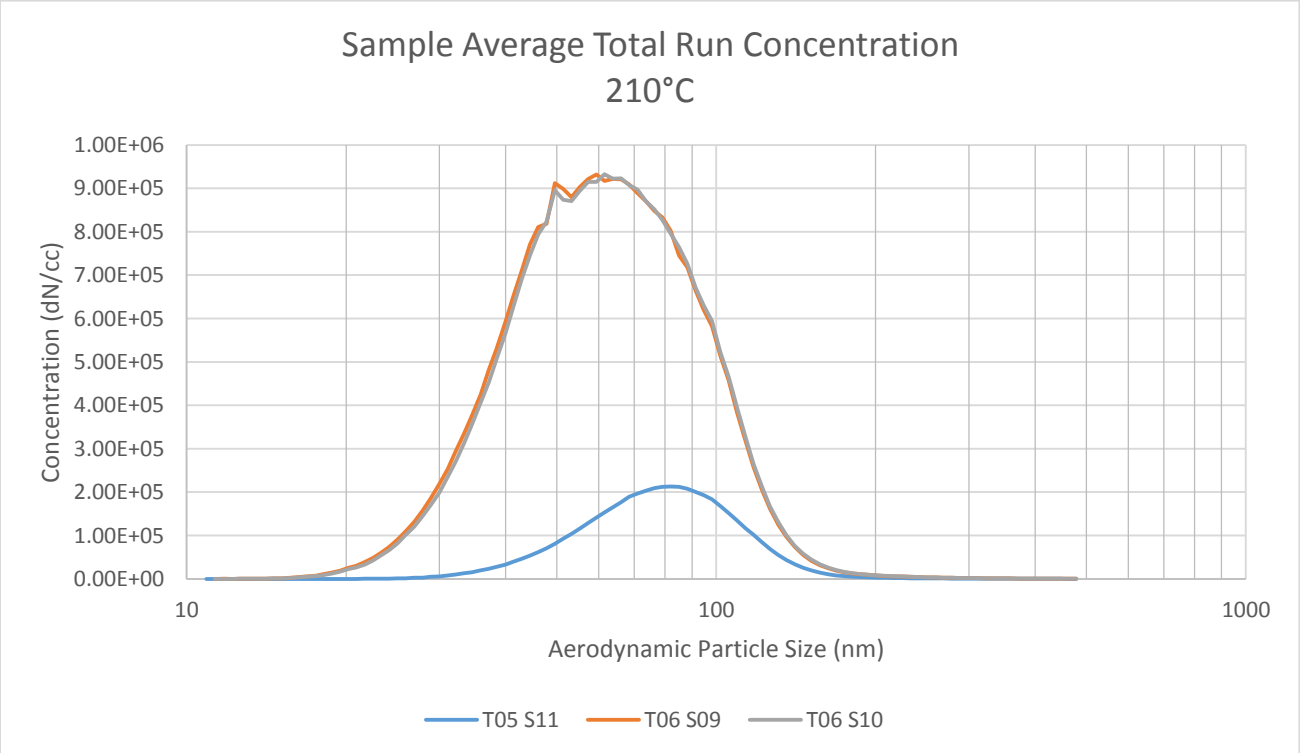

Figure 3-40 C18 210°C Compiled Concentration Data

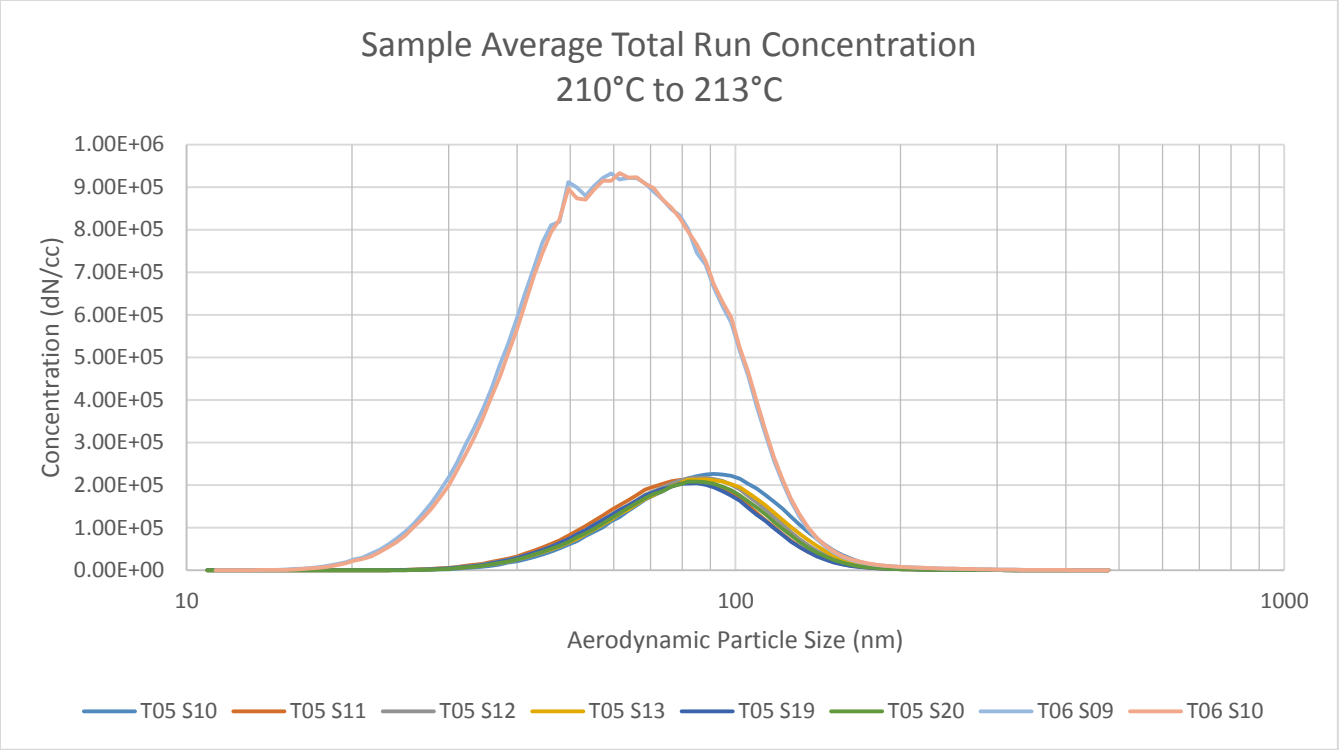

Figure 3-41 C18 210°C & 213°C Compiled Concentration Data

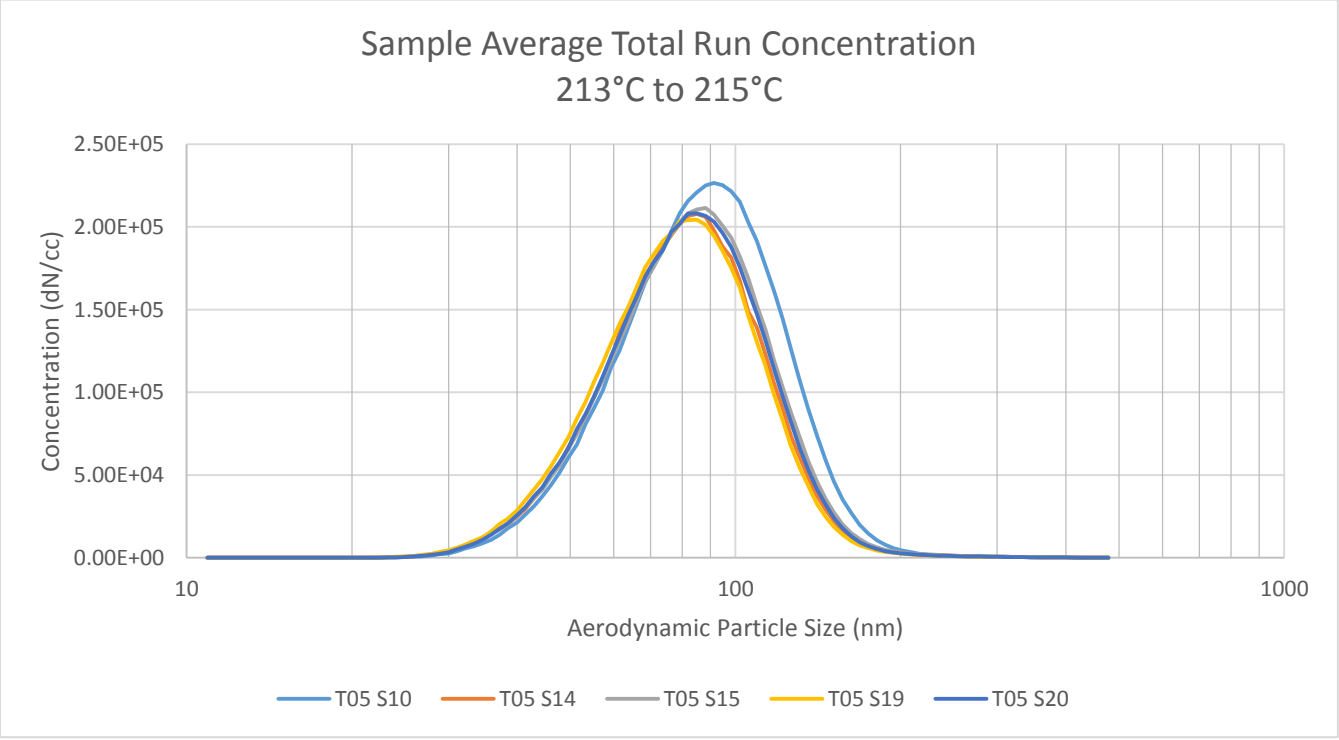

Figure 3-42 C18 213°C & 215°C Compiled Concentration Data

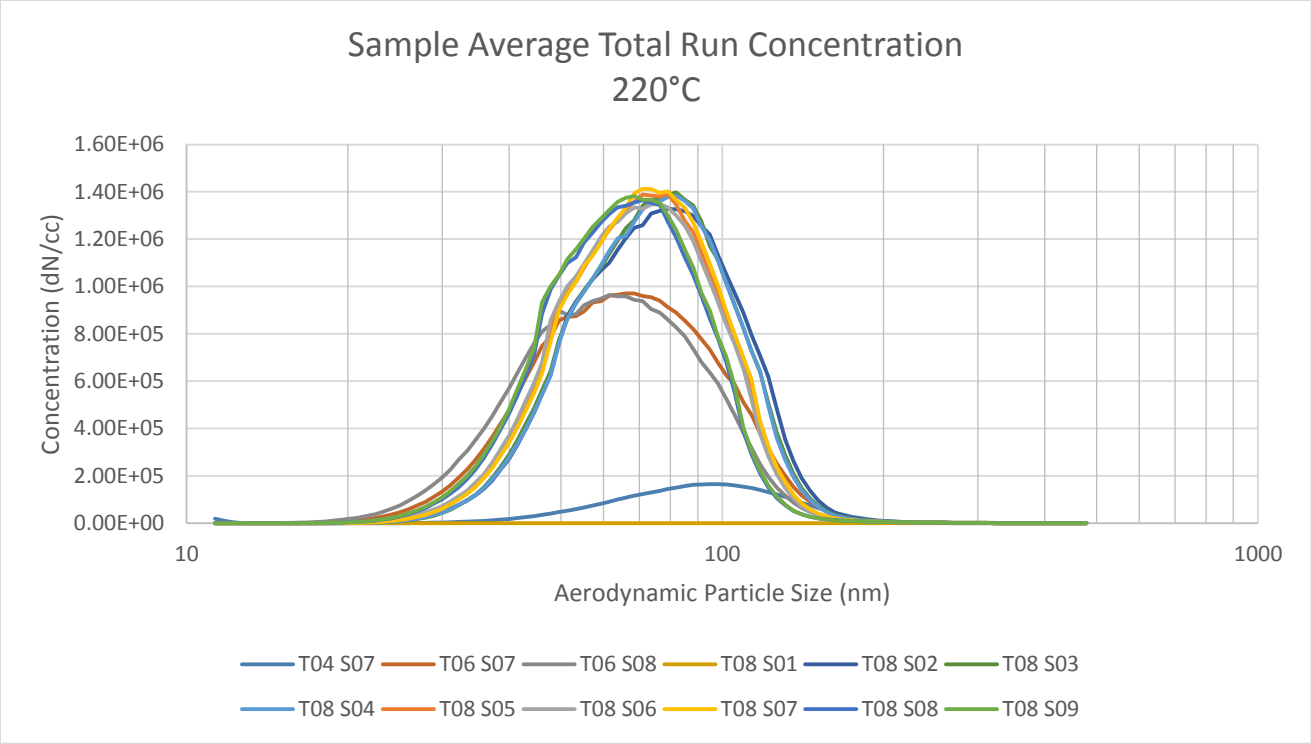

Figure 3-43 C18 220°C Compiled Concentration Data

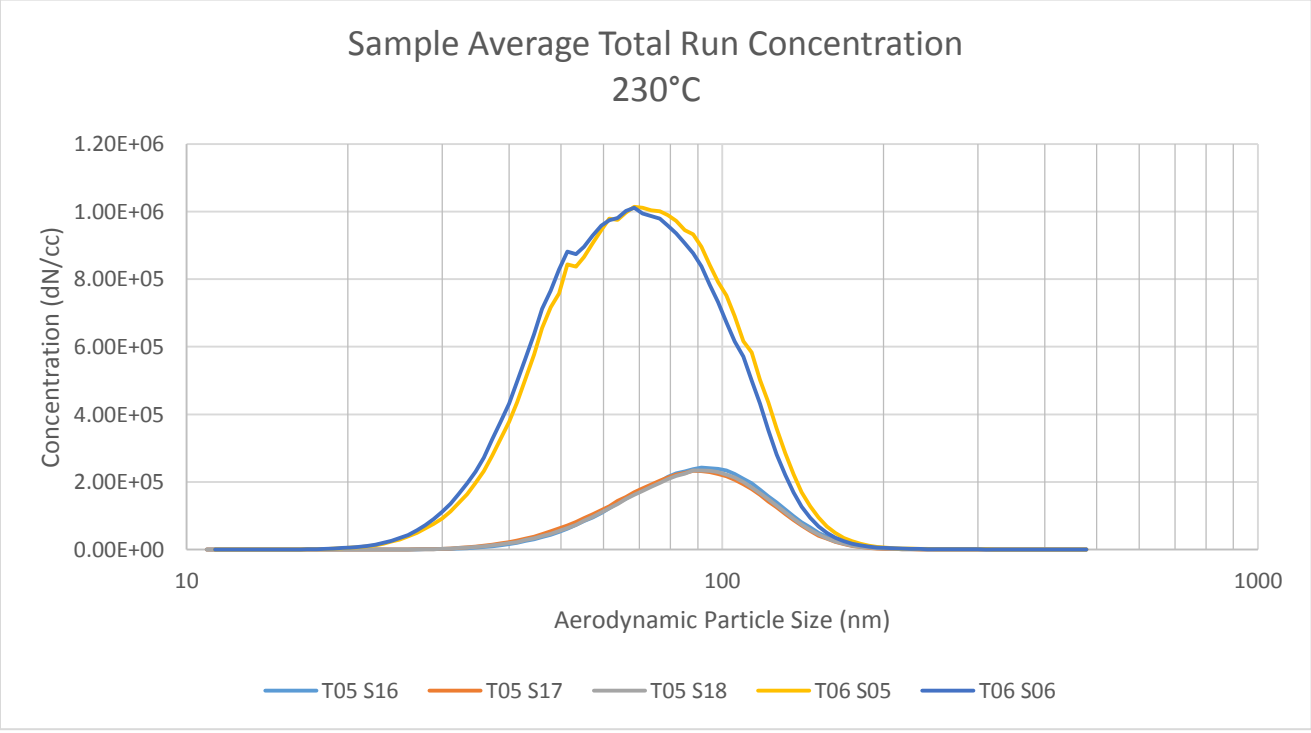

Figure 3-44 C18 230°C Compiled Concentration Data

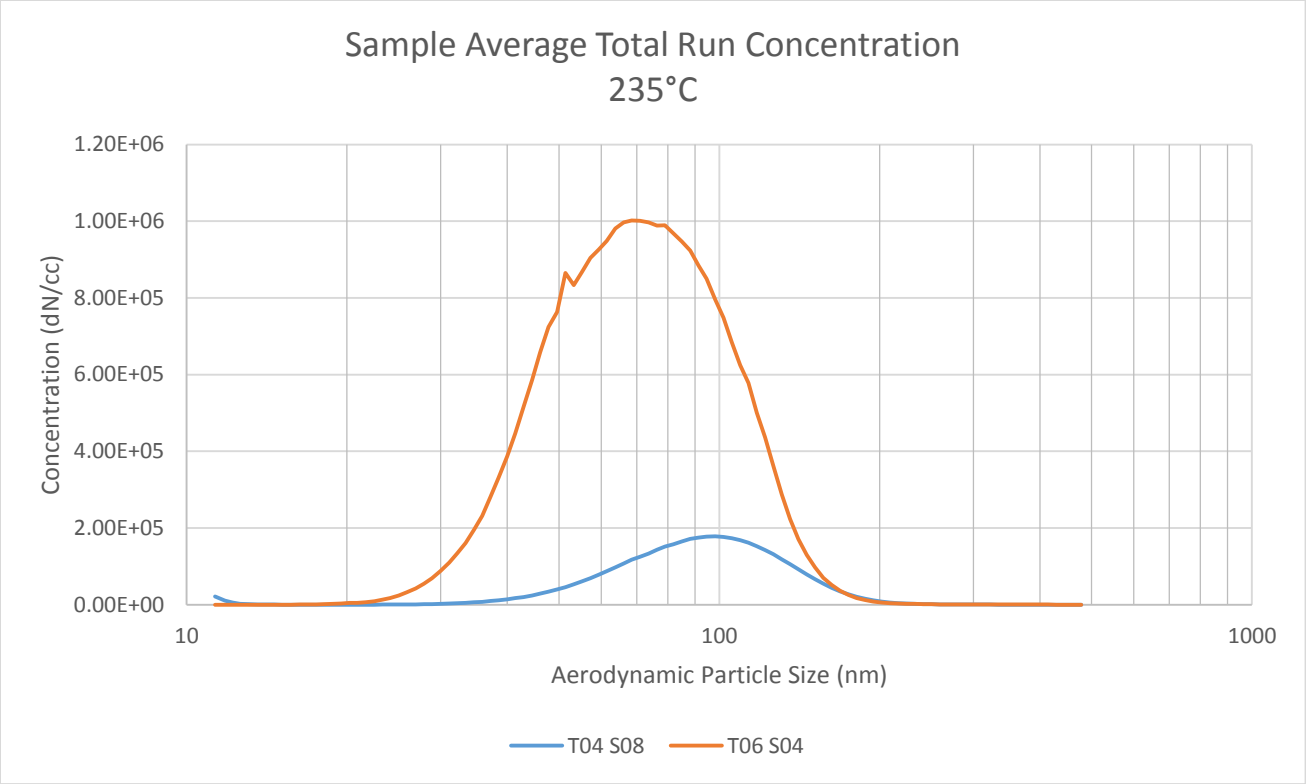

Figure 3-45 C18 235°C Compiled Concentration Data

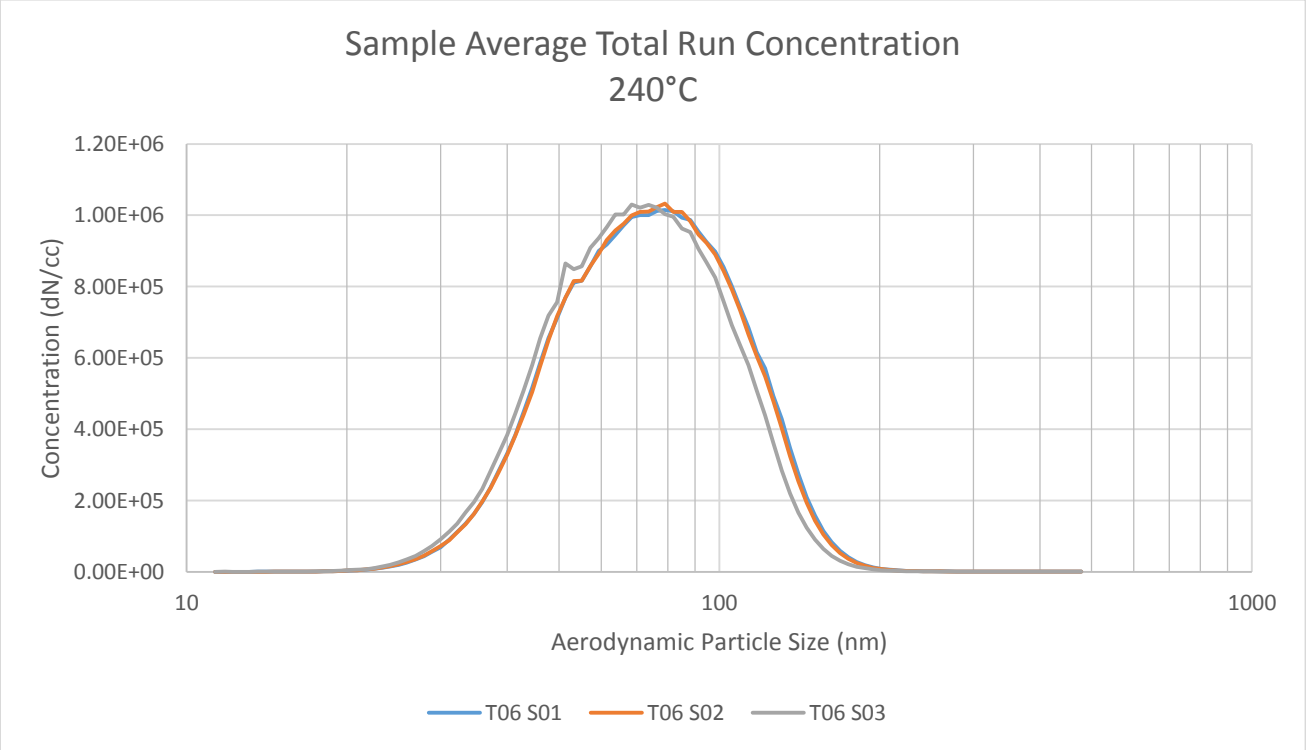

Figure 3-46 C18 240°C Compiled Concentration Data

3.3.6 Discussion

Further information is in the appendices including presentation of the cumulative percent distribution. The cumulative percent graphs and sample average concentration graphs provide the necessary information to also derive many of the graphs and other information needed.

The low temperature tests of 140°C and below show variations in the concentration during a run. These variations are likely due to the engine running close to idle and the fluctuations of the power turbine that result from such a low power setting. The power turbine will fluctuate slightly as very little torque load is applied at the conditions producing a temperature range of 100°C to 150°C. Additionally the aerosol may not be mixing adequately at such a low flow rate.. A gas turbine is not meant to be run close to idle and is very inefficient when running at such power settings. The 100°C graph shows the main aerosol peak distribution center at approximately 230nm. This information concurs with the information from the Laskin nozzle testing, though the peak may be slightly higher due to some coagulation of the particles. There is also the appearance of a smaller peak around the 20nm range. As the settings of the engine increase up to 140°C the smaller peaks start to shift towards the 200nm range peak. Additionally the 200nm peaks start to move to lower particle sizes slightly. Both peaks are about the same concentration magnitudes indicating the majority of mass is still at the aerosol size generated by the Laskin nozzles. It is evident that the temperatures are much lower than the temperatures required for thermal decomposition and the prime suspect causing the smaller peaks is blade shear. The blades at 140°C are rotating at approximately 35750rpm, which amounts to blade tip velocities in excess of 800ft/s. Thermal decomposition is estimated at 180°C to 230°C from the bleed air simulator and literature. The possibility that the particle sizes

are being influenced by blade shear indicates that the bleed air simulator results may not be accurate in modeling what happens in a gas turbine engine. The main difference is how compression is achieved. In the simulator a reciprocating compressor was used, while, in a gas turbine, axial and centrifugal compressor stages are used in order to compress the incoming air.

From 140°C to 150°C the smaller peak seems to move out of the measureable range while slightly increasing in concentration. It is very possible that an effect with the speed of sound and the particle shear is taking place as the blade velocities are approaching the speed of sound at these temperatures. It is also indicative that the particles are being sheared very readily when the peaks completely vanish as seen at 155°C and 145°C. The oil is being injected at this point, but the particles cannot be detected, and only the end of the size distribution seems to appear.

At 165°C the particle data appear to have stabilized and are under the influence of thermal factors. All of the data taken above 165°C are monomodal in nature and no secondary peaks occur as was observed on the bleed air simulator. The mode of the data appears to be at 30nm. The data at 165°C lines up very nicely, but were taken on a single day.

The measurements at 180°C however do not entirely line up as expected but the trend is observed in the shift in peak sizes. These data show that the peaks are shifting to the right and sit at approximately 50nm to 70nm. As the graphs clearly show, the peaks continue to shift to the right as the temperature increases and stop at approximately 60nm to 100nm with the data sets starting to line up better. While the inconsistency between the tests may be observed, the information about the trend remains clear. The particle size distribution collapses to a monomodal peak and is fairly consistent in the mode of size between 200°C and 240°C.

Chapter 4: Comparison Results & Discussion

The data generated by the bleed air simulator produced results that are somewhat representative of the gas turbine data. Figure 4-1 shows the bleed air simulator and the gas turbine data compared. The data from the 30 minute run on the BAS is lower in concentration due to the difference in flow rate and mass injections. During the BAS tests only one Laskin nozzle was used, which when run on the gas turbine was shown to have a smaller peak size distribution on the data by about 20nm when compared to the three nozzle injection rate. The difference in peaks are approximately 20nm in size and thus the information between the BAS and the gas turbine do indeed correlate when these factors are taken into account. Unfortunately no test of multiple nozzles were run on the simulator primarily due to the reason that the particles would overwhelm even the SMPS and APS systems and would produce inaccurate measurements. The fractional concentrations also show that the two test points correlate, although the bleed air simulator produced results more tightly clustered with a lower geometric deviation. Table 4-1 shows this information in a condensed form. The C18 data are represented by the T06 and T07 data sets while the BAS is represented by the others. As noted earlier, the C18 and Laskin nozzle data are uniquely named by the TXX & SXX system. The BAS data has no naming system.

Table 4-1 230°C 70psia Test Conditions

	BAS	BAS_Shifted	T06 S05	T06 S06
Geo. Mean	44.89	65.6	69.46	67.04
Geo. STD	1.376	1.242	1.454	1.453

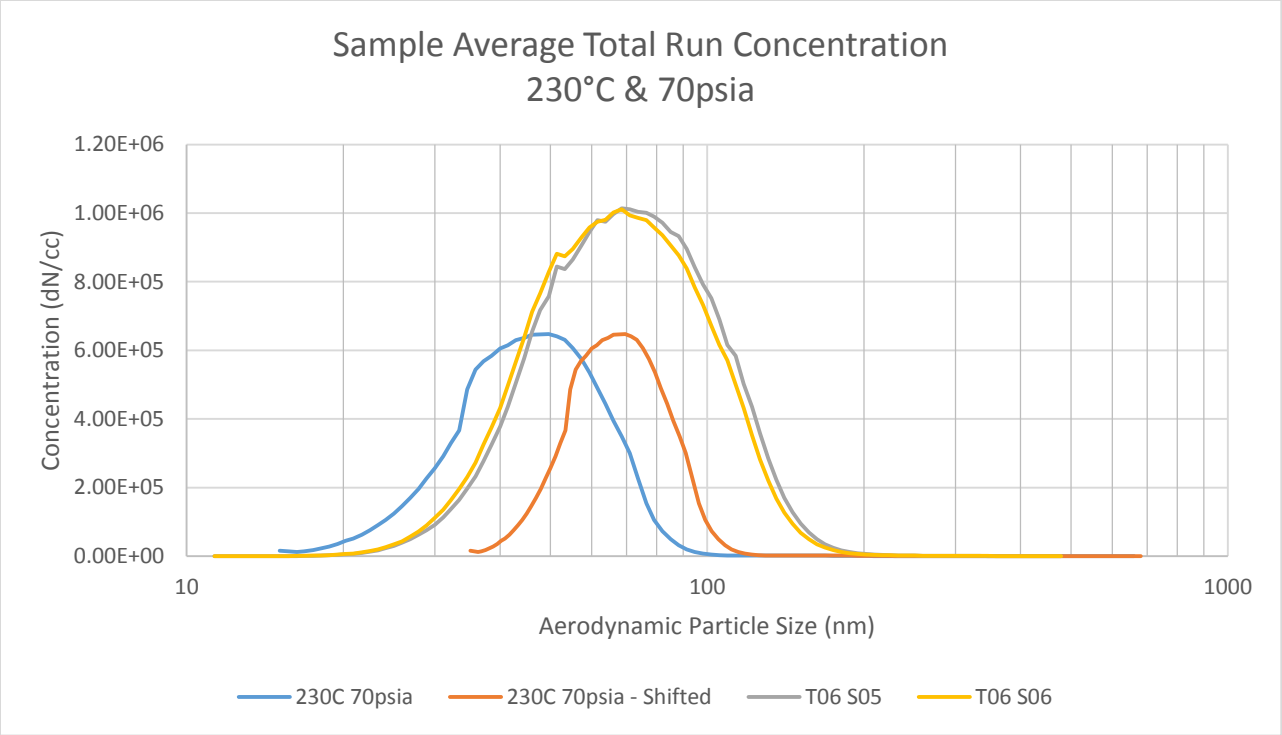

Figure 4-1 C18 & BAS Comparison

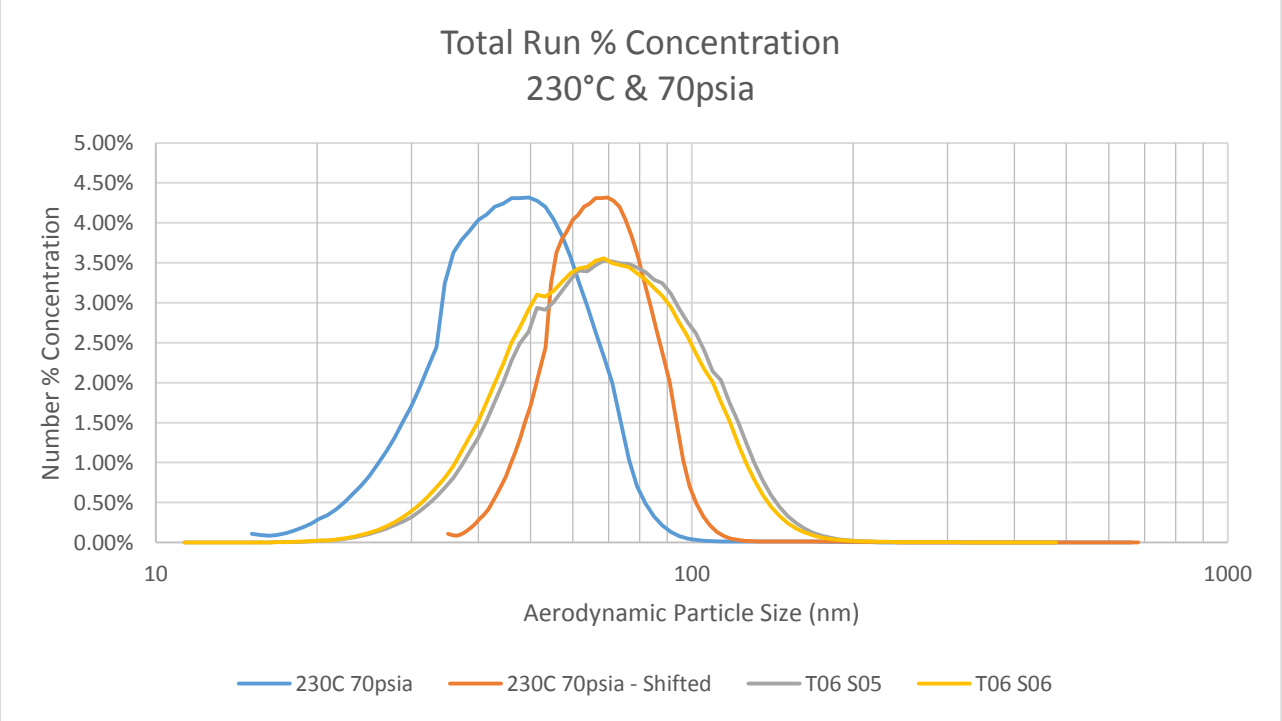

Figure 4-2 C18 & BAS Comparison Percent

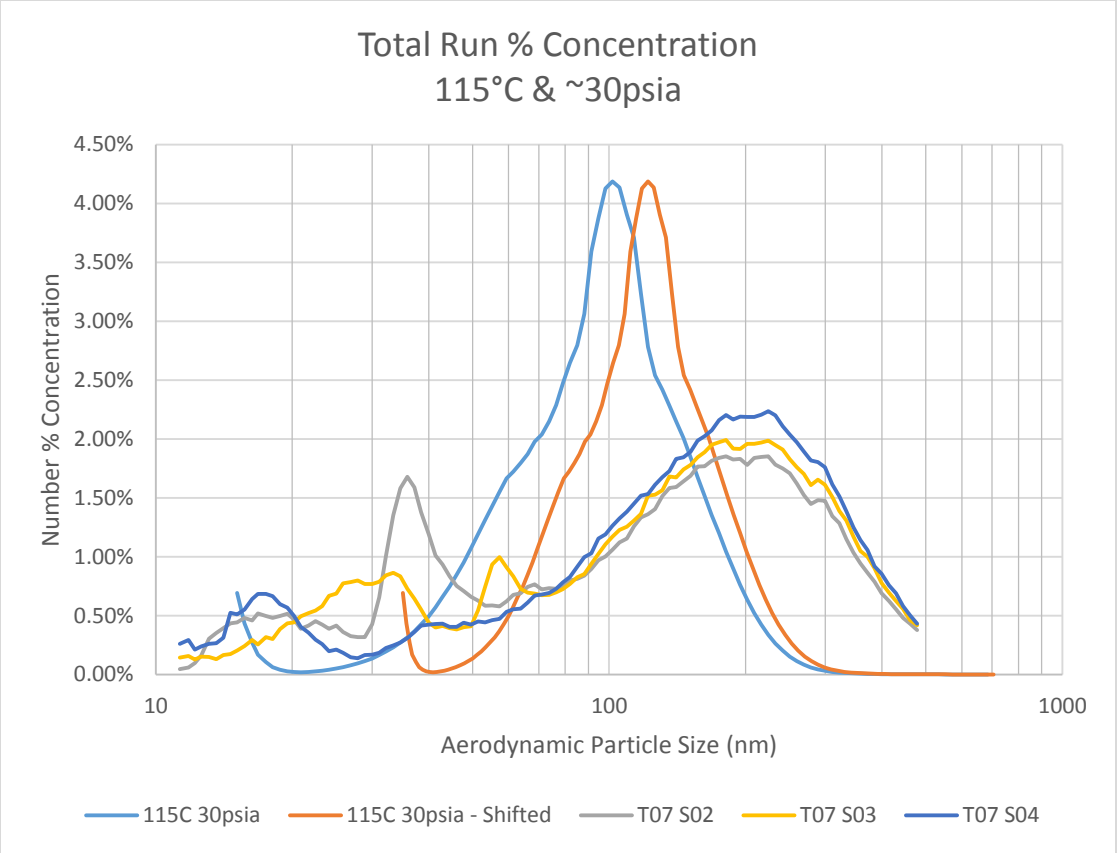

Figure 4-3 C18 & BAS Low Run Comparison

Figure 4-3 shows results from tests with temperature maintained at approximately 115°C where the conditions between the BAS and C18 are closest. This figure seems to indicate that the type of compression does influence the particle sizes. It is possible that the heater tube temperature may be affecting the distribution, but in the 115°F test, the reciprocating compressor produced a heat of compression approximately at 110°F and thus the heater tube's highest temperature was 115°F. The most likely reason for of the differences is the reciprocating compressor for the BAS

and the axial blade shearing for the gas turbine tests.

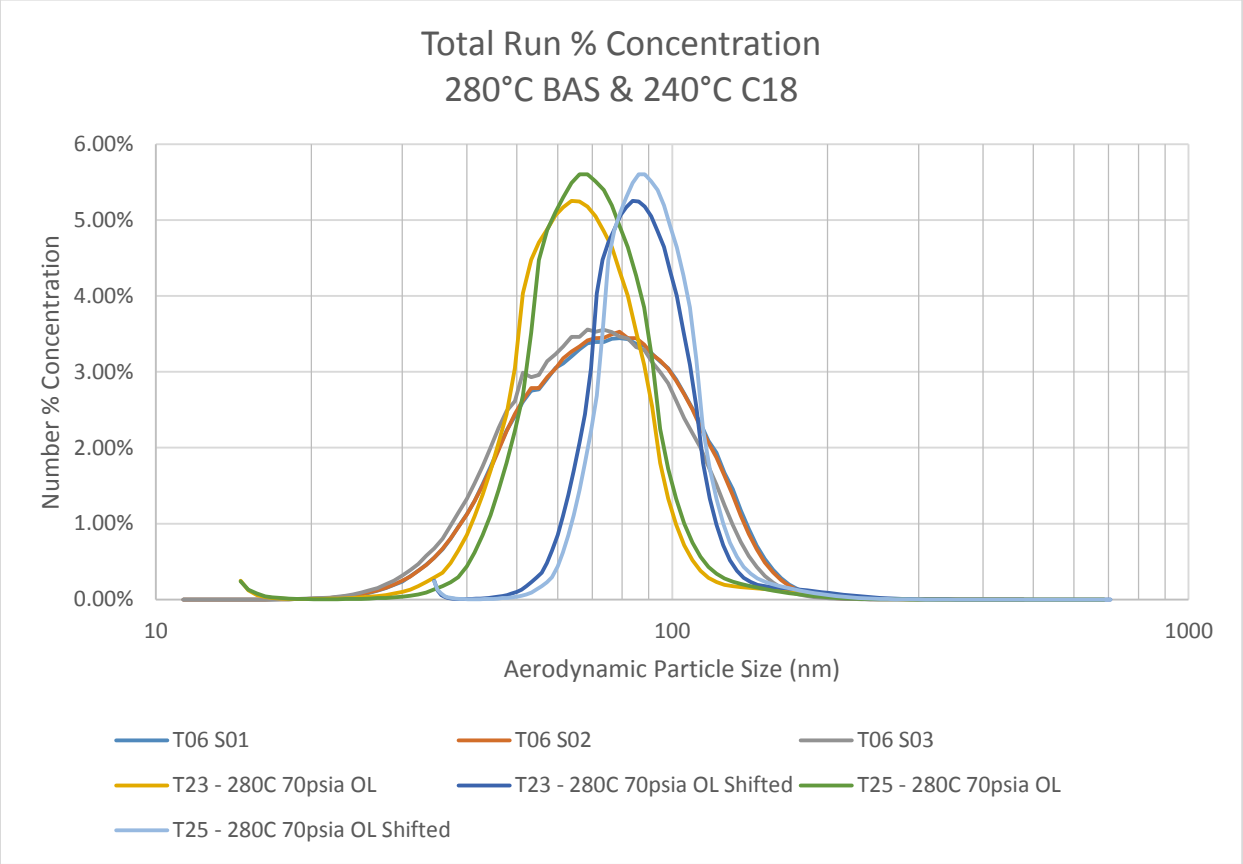

Figure 4-4 High Temperature Test Comparison

Figure 4-4 shows the data for 280°C on the BAS and at 240°C for the C18 engine. T23 & T25 are both from the BAS while the T06 samples are from the C18. The concentration mode for the C18 at 240°C is at approximately 80nm. This is a 10nm offset from the data at 230°C shown in Figure 4-1. If comparing the geometric means, the offset between C18 at 240°C and 230°C is only 3nm. However, the data from 280°C is the next closest point to compare and they do not line up as well, although the data do show the trend discussed earlier. The BAS has a smaller geometric standard deviation than the C18 data with T23 and T25 having a 1.25 and 1.24 respectively. T06 S01, T06 S02, and T06 S03 have geometric standard deviations of 1.46, 1.41 and 1.415 respectively. As a reminder the geometric standard deviation is a dimensionless quality with a value equal to or greater than 1.0.

Chapter 5: Conclusions

Overall the information presented in this paper gives the reader insight into the aerosol distributions of oil by a bleed air simulator and a gas turbine engine. The data produced by the bleed air simulator was shown to be approximately similar to the gas turbine generated data when corrections for various factors were considered at the elevated temperatures. The information produced by the BAS did not correlate well at the lower temperature settings and the type of compression is thought to affect the aerosol distribution. However, in a very general sense there is consistency in that the majority of the particles measured in all cases are well into the submicron range.

The particle size distributions are seen to be affected by the compressor type at low speeds; however at higher speeds the temperature appears to be the controlling factor. Additionally, above approximately 200°C the aerosol seems to be between 60-100nm depending slightly on the conditions. This trend is observed on both the gas turbine and BAS when comparable conditions are considered. Increasing the BAS to 310°C showed this same trend while increasing pressures in a similar manner to those seen on the gas turbine. However, when pressure was lowered at conditions such as 310°C secondary peaks started to appear in the 20-30nm range.

While it is not possible to know the exact physical processes that lead to aerosol generation in the engine compressor, blade shear in the gas turbine is likely to have an effect on the particle size distribution as the particles disappear below the smallest size measureable by the SMPS equipment, but then reappear as the temperature and pressure increase.

It was also observed that the amount of oil injected into the system would influence the particle sizes with a peak shift up to 20nm with a change of approximately a factor of three in the

injection mass rate. It was decided to run the engine tests with all three nozzles injecting oil into the system to maintain consistency and to allow rapid data collection. The latter consideration is important due to fuel consumption. The data produced by the engine indicates that repeatability is very unlikely. While the gas turbine will produce consistent data during an operation or test, the results will vary from day to day. Variations in atmospheric conditions may influence the mass flow and power settings of the engine, and is thought to be the primary contributor for these discrepancies.

While the above discussion focuses on the differences between the BAS and C18 results and on variations in the results, there is one overriding and consistent result. Regardless of whether the BAS or C18 is used and regardless of the test conditions at temperatures representative of engine operation, there are large numbers of submicron particles at concentrations well above background levels. Thus, there is every reason to believe that an appropriate submicron particle detector would be a reliable indicator of oil contamination of bleed air. The chemical gas analysis data collected thus far indicates that exceedingly low detection levels may be required for reliable oil contamination detection by gaseous chemical detection means.

5.1 Future Work

Future work should ultimately include the investigation of testing sensors designs on aerosols similar in nature to those presented in the data in this report. The reason is so that an actual low cost sensor capable of detecting air quality incidents may be developed and deployed on commercial aircraft.

Further additional work for the future is to repeat the testing of oil injection into an aircraft engine with a higher pressure ratio. Current work is being done to ready an Allison 250

C28B engine on the test stand at NGML at KSU. This newer engine has a pressure ratio of approximately 7.0. This pressure ratio should allow the engine compressor to achieve the higher temperatures that are necessary to produce thermal decomposition of Mobile Jet II. Overlapping conditions such as the temperature range of 160°C to 200°C may also be tested to analyze the effect of how the gas is compressed. The C28B engine has only a single centrifugal stage for compression, which is in contrast to the 5 axial stages and one centrifugal stage on the C18 engine. The compression may very well alter the particle sizes.

A possible option to gain better understand the effects of temperature, pressure and engine speed would be to repeat the work in an altitude chamber. This would allow for the control of ambient pressure and temperature which would allow the operator some control over the parameters. A major drawback to this option is the extraordinary costs that would be unavoidable. Very few facilities have this capability and the engine test stand must include a rigid metallic bleed air extraction line.

In addition, work should also be undertaken on a commercial aircraft engine such as the F117-PW-100 power plant used in C17 airframes. Kansas State University is currently involved in a large scale project that will utilize the aforementioned engine for various research goals. Industry partners such as Boeing, Honeywell, and NASA are heavily involved in the investment of the research project code named VIPR taking place at Edwards Air Force Base (EAFB). Kansas State University paired with Auburn University working under the Aircraft Cabin Environmental Research (ACER) Lab are working on measuring particles and gas constituents from oil injected after the 6^{th} stage of compression. This research will be taking place in the summer of 2015 and should provide more information about the process of thermal decomposition of oil.

Bleed air contamination with hydraulic fluids should be tested as these fluids can be the cause of bleed air incidents. Hydraulic fluids were not tested on the current system and as such, may show an entirely different aerosol distribution peak. Thermal decomposition of hydraulic fluids occurs at different but similar temperature conditions as Mobile Jet II oil. The thermal decompositions may affect the aerosol output just as the different viscosity may affect the particles generated due to blade shear.

Another consideration is to model an oil leak in a gas turbine engine. It could very well be that smaller oil leaks occur throughout the flight, but due to flow patterns the contamination would not reach a bleed air tap. Modeling an engine and evaluating the probability of heated oil entering the bleed air flow stream may be a significant factor. Oil leaks in a larger gas turbine may not be well distributed as assumed in this project. An oil leak occurring on the compressor may or may not reach the bleed air extraction port.

References

Air Techniques International. (2014). Laskin Nozzle Generators TDA-4B and TDA-4Blite. Operation and Maintenance Manual.

Andrews, L., McDiarmid, T., Vijayakumar, R., & Mills, O. (2003). Characterization of particle size distributions of atomizers and condensation generators used for testing high efficiency filters BT - ESTECH 2003: 49th Annual Technical Meeting and Exposition of the Institute of Environmental Science and Technology. Pro (pp. 67–76). Air Techniques International, Owings Mills, MD: Institute of Environmental Sciences and Technology.

ASHRAE. (2013). *Handbook Fundementals* (SI). ASHRAE.

Baron, P. A., & Willeke, K. (2001). *Aerosol Measurement* (Second).

Bartl, P., Völkl, C., & Kaiser, M. (2008). Chemical characterization of polyol ester aviation lubricant residues. *Journal of Synthetic Lubrication*, (January), 1–16. http://doi.org/10.1002/jsl

Crane, C. R., Sanders, D. C., Endecott, B. R., & Abbott, J. K. (1983). *Inhalation Toxicology: III. Evaluation of thermal degradation products from aircraft and automobile engine oils*.

Currie, K. (1995). *Oil Mist Assessment. BAe 146 Aircraft Rear Flight Attendant Seat*. Sydney.

Eckels, S. J., Jones, B. W., Mann, G. W., Mohan, K. R., & Weisel, C. P. (2014). Aircraft Recirculation Filter for Air-Quality and Incident Assessment. *Journal of Aircraft*, *51*(1), 320–326. http://doi.org/10.2514/1.C032458

Friedlander, S. (2000). *Smoke, Dust, and Haze. Fundementals of Aerosol Dynamics* (Second). Oxford University Press, Inc.

Ghose, H. M., Ferrante, J., & Honecy, F. C. (1987). The effect of Tricresyl-Phosphate (TCP) as an additive on wear of Iron (Fe), (August 1987). Retrieved from http://hdl.handle.net/2060/19870017597

Gormley, P. G., & Kennedy, M. (1949). Diffusion from a Stream Flowing through a Cylindrical Tube. *Proceedings of the Royal Irish Academy. Section A: Mathematical and Physical Sciences*.

Guan, J., Wang, C., Gao, K., Yang, X., Lin, C.-H. H., & Lu, C. (2014). Measurements of volatile organic compounds in aircraft cabins. Part II: Target list, concentration levels and possible

influencing factors. *Building and Environment*, *75*, 170–175. http://doi.org/10.1016/j.buildenv.2014.01.023

Hinds, W. C. (1999). *Aerosol Technology* (Second).

Hood, E., Environmental, S., Perspectives, H., & Apr, N. (2001). Indoor Air Quality. OPs Cause Bad Trips? *Environmental Health Perspectives*, *109*(4), A156 CR – Copyright © 2001 The National Inst. http://doi.org/10.2307/3454873

Hunt, E. H., Reid, D. H., Space, D. R., & Tilton, F. E. (1995). Commercial Airliner Environmental Control System Engineering Aspects of Cabin Air Quality. *Aerospace Medical Association Annual Meeting*, 1–8.

Incorporated, T. (2014). Aerosol Statistics Lognormal Distributions and dN / dlogD p.

Jian-Wen, C., & Jin-chun, S. (2009). Measurement of the size of oil mist droplets. *… , 2009. ICIEA 2009. …*, 373–376. http://doi.org/10.1109/ICIEA.2009.5138231

Kostic, M. (2003). Particle-Size Distribution Data Presentation : Why NOT to use Log-Density Distribution.

Lemmon, E. W., Jacobsen, R. T., Penoncello, S. G., & Firend, D. G. (2000). Thermodynamic properties of air and mixtures of nitrogen, argon, and oxygen from 60 to 2000 K at pressures to 2000 MPa. *Journal of Physical and Chemical Reference Data*. http://doi.org/10.1063/1.1285884

Lighty, J., Veranth, J., & Sarofim, A. (2000). Combustion aerosols: factors governing their size and composition and implications to human health. *Journal of the Air & Waste …*, *50*(9), 1565–1618. http://doi.org/10.1080/10473289.2000.10464197

Magoha, P. (2012). *Incident-response monitoring technologies for aircraft cabin air quality*. Kansas State University. Retrieved from http://adsabs.harvard.edu/abs/2012PhDT.....166M

Mann, G. W., Eckels, S. J., & W. Jones, B. (2014). Analysis of particulate size distribution and concentrations from simulated jet engine bleed air incidents. *HVAC&R Research*, *20*(7), 1–18. http://doi.org/10.1080/10789669.2014.950922

Matthews, K. (2013). Bleed Air Cooling Time C17 Discussion.

Nagda, N., & Rector, H. (2003). A critical review of reported air concentrations of organic compounds in aircraft cabins. *Indoor Air*, *13*, 292–301. Retrieved from http://onlinelibrary.wiley.com/doi/10.1034/j.1600-0668.2003.00202.x/full

National Research Council. Committee on Air Quality in Passenger Cabins of Commercial Aircraft, B. on E. S. and T. (2002). *The Airliner Cabin Environment and the Health of Passengers and Crew*. Washington, D.C.: Washington, D.C. : National Academy Press.

Overfelt, R. A., Jones, B. W., Loo, S. M., Haney, R. L., & Neer, A. J. (2012). *Sensors and Prognostics to Mitigate Bleed Air Contamination Events 2012 Progress Report*.

Overfelt, R. A., Neer, A. J., Andress, J. R., Haney, R. L., Fergus, J. W., & Mathison, L. C. (2011). Preliminary Investigation into Thermal Degradation Behavior of Mobil Jet Oil II. In *Carbon41st International Conference on Environmental Systems* (pp. 1–7). Portland, Oregon.

Payet, S., Boulaud, D., Madelaine, G., & Renoux, a. (1992). Penetration and pressure drop of a HEPA filter during loading with submicron liquid particles. *Journal of Aerosol Science*, *23*(7), 723–735. http://doi.org/10.1016/0021-8502(92)90039-X

Rural, S., Affairs, R., & Committee, T. R. (2000). *Air Safety and Cabin Air Quality in the BAe 146 Aircraft*.

Saravanamuttoo, H., Rogers, G., Cohen, H., & Straznicky, P. (2009). *Gas Turbine Theory* (6th ed.). Pearson Education Limited.

Shehadi, M., Hosni, M., & Jones, B. W. (n.d.). Characterization of the Frequency and Nature of Bleed Air Contamination Events in Commercial Aircraft. *Indoor Air*.

Sommer, K. (2001). 40 Years of Presentation Particle Size Distributions–Yet Still Incorrect? *Particle & Particle Systems Characterization*, *18*(1), 22–25. http://doi.org/10.1002/1521-4117(200102)18:1<22::AID-PPSC22>3.0.CO;2-2

Starik, a. M., Savel'ev, a. M., Titova, N. S., Loukhovitskaya, E. E., & Schumann, U. (2004). Effect of aerosol precursors from gas turbine engines on the volatile sulfate aerosols and ion clusters formation in aircraft plumes. *Physical Chemistry Chemical Physics*, *6*(13), 3426. http://doi.org/10.1039/b314038e

Van Netten, C. (1999). Multi-elemental analysis of jet engine lubricating oils and hydraulic uids and thier implication in aircraft air quality incidents. *The Science of the Total Environment*.

Van Netten, C. (2005). Aircraft air quality incidents, symptoms, exposures and possible solutions. *Air Quality in Airplane Cabins and Similar Enclosed …*, *4*(August), 193–210. Retrieved from http://link.springer.com/chapter/10.1007/b107244

Van Netten, C., & Leung, V. (2000). Comparison of the constituents of two jet engine lubricating oils and their volatile pyrolytic degradation products. *Applied Occupational and Environmental Hygiene*. http://doi.org/10.1080/104732200301593

Van Netten, C., & Leung, V. (2001). Hydraulic Fluids and Jet Engine Oil: Pyrolysis and Aircraft Air Quality. *Environmental Health: An International Journal*, *56*(2), 277–283.

Vasak, V. (1992). *Cabin Air Contamination in BAe 146 in East West Airlines*. St. Ives.

Wilson, C. W., Petzold, A., Nyeki, S., Schumann, U., & Zellner, R. (2004). Measurement and prediction of emissions of aerosols and gaseous precursors from gas turbine engines (PartEmis): an overview. *Aerospace Science and Technology*, *8*(2), 131–143. http://doi.org/10.1016/j.ast.2003.10.006

Winder, C., & Balouet, J.-C. (2000). AEROTOXIC SYDROME : ADVERSE HEALTH EFFECTS FOLLOWING EXPOSURE TO JET OIL MIST DURING COMMERCIAL FLIGHTS. In *Towards a safe and Civil Society. Proceedings of the International Congress on Occupational Health Conference* (pp. 4–6).

Winder, C., & Balouet, J.-C. (2001). Aircrew exposure to chemicals in aircraft symptoms of irritation and toxicity. *Journal of Occupational Health Safety*.

Winder, C., & Balouet, J.-C. (2002). The toxicity of commercial jet oils. *Environmental Research*, *89*(2), 146–164. http://doi.org/10.1006/enrs.2002.4346

Appendix A: Bleed Air Simulator Data

Data for the mass distributions are shown first for the 10 minute and 30 minute data. They are later followed by the data sets of cumulative percent concentration for both the 10 minute and 30 minute data sets.

A.1 30 Minute Data Summary

The data table below shows the information of the tests conducted on a 30 minute time period. The graphs following are given for various temperature and pressures.

Table A-1 30 Minute Data Summary

	Actual		Std. Deviation		Reactor Tube Temp				
	C	psi	C	psi	C	C	C	C	C
Designated Name	Temp	Pressure	Temp	Pressure	TS1	TS2	TS3	TS4	TS5
115C 30psia	115	29	0.72	0.46	106	113	116	116	115
185C 30psia	187	28	2.96	0.41	157	192	208	215	225
230C 30psia	230	29	2.95	0.46	186	232	255	281	291
230C 50psia	230	54	0.51	1.01	181	217	239	262	271
230C 50psia T2	N/A	N/A	N/A	N/A	N/A	N/A	N/A	N/A	N/A
230C 50psia T3	N/A	N/A	N/A	N/A	N/A	N/A	N/A	N/A	N/A
230C 70psia	236	69	1.43	1.77	185	219	241	263	273
250C 30psia	248	30	3.14	0.50	195	247	272	301	313
280C 30psia	281	31	4.00	0.53	217	279	309	344	357
280C 50psia	285	51	1.74	1.01	210	263	295	331	344
280C 50psia T2	274	50	1.16	0.78	233	282	307	331	340
280C 70psia	281	69	1.69	1.33	202	250	282	317	332
305C 67psia	305	66	2.89	1.78	220	274	312	352	368

A.2 Mass Data 30Minute Simulator

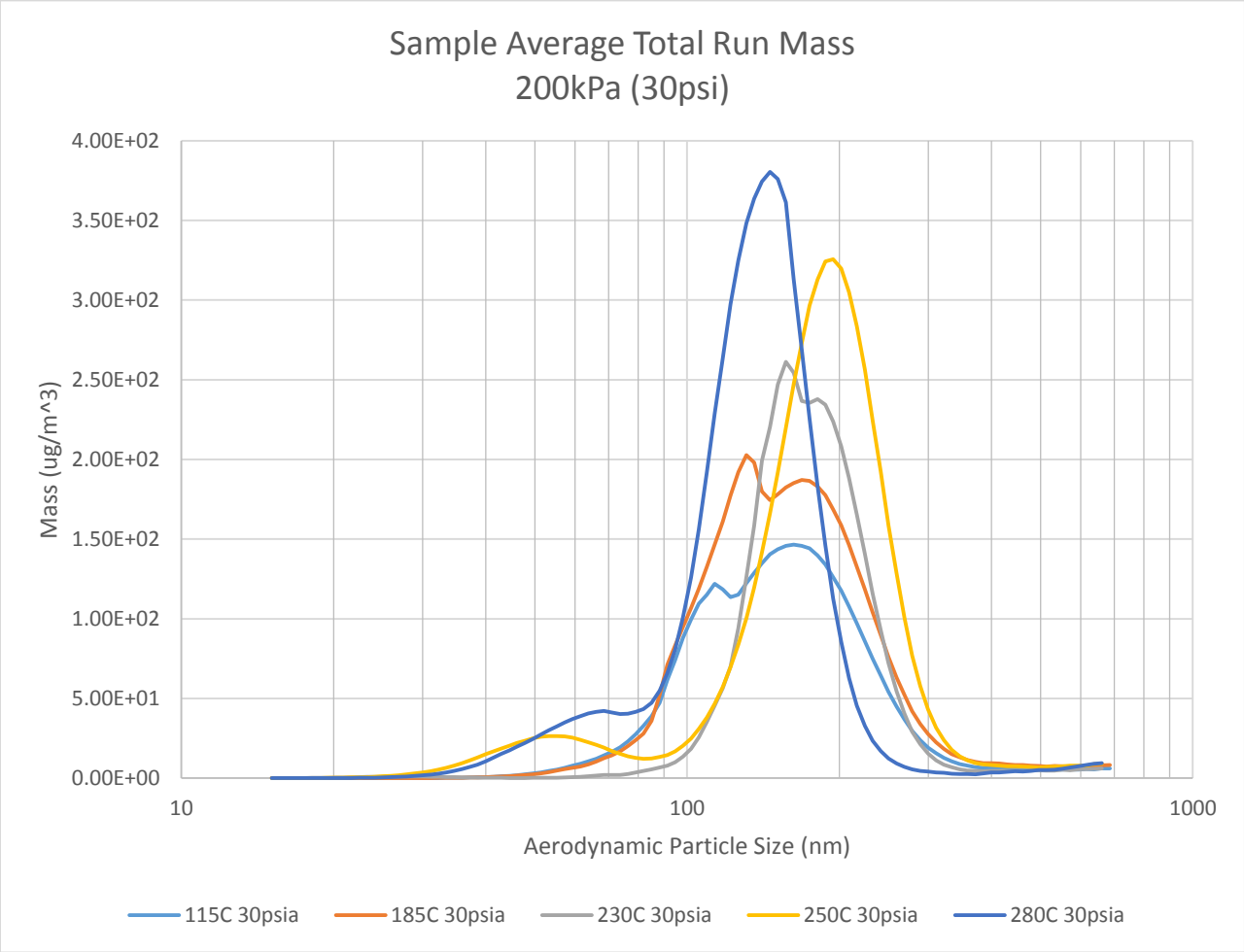

Figure A-1 BAS 30Min Mass - 200kPa (30psi)

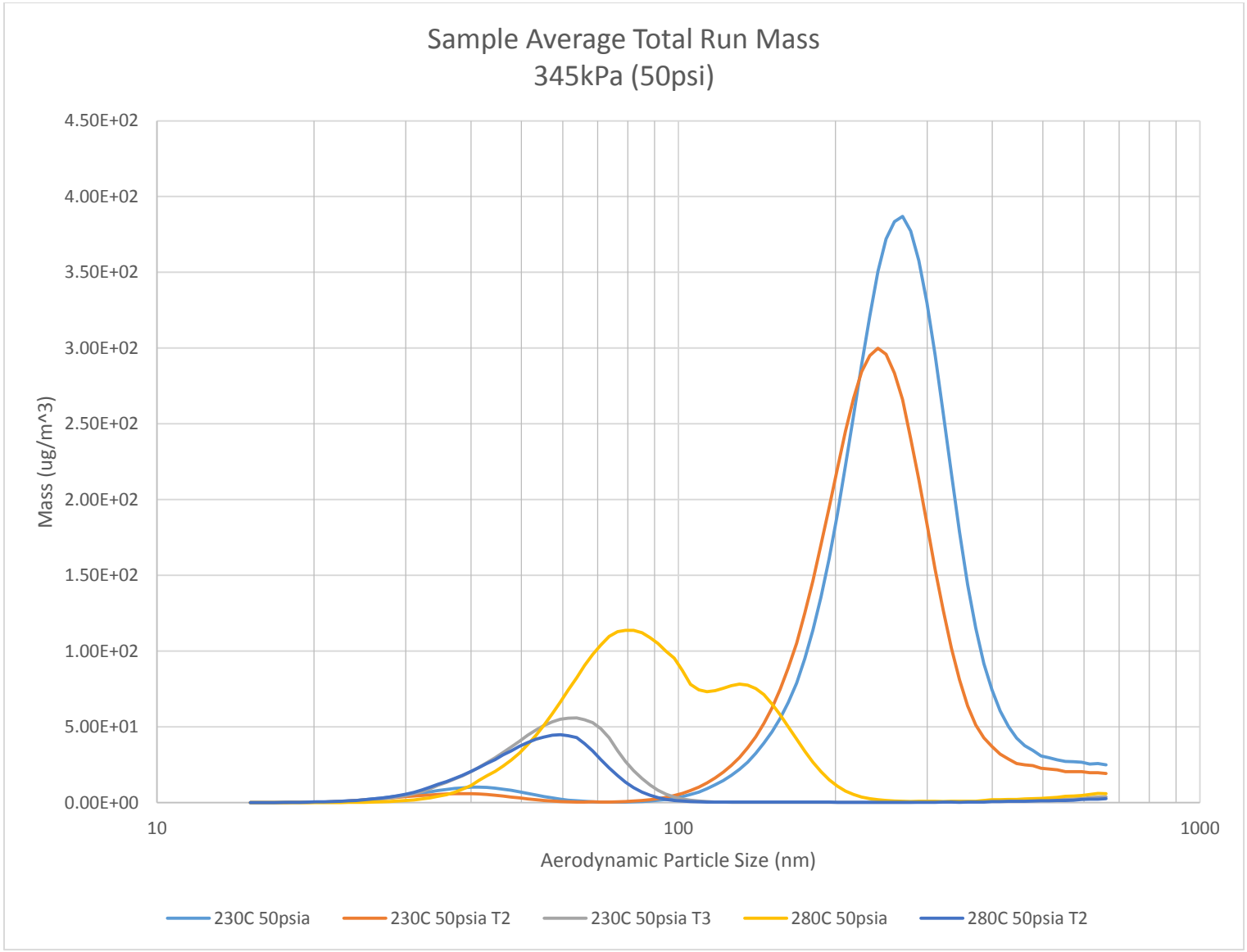

Figure A-2 BAS 30Min Mass - 345kPa (50psi)

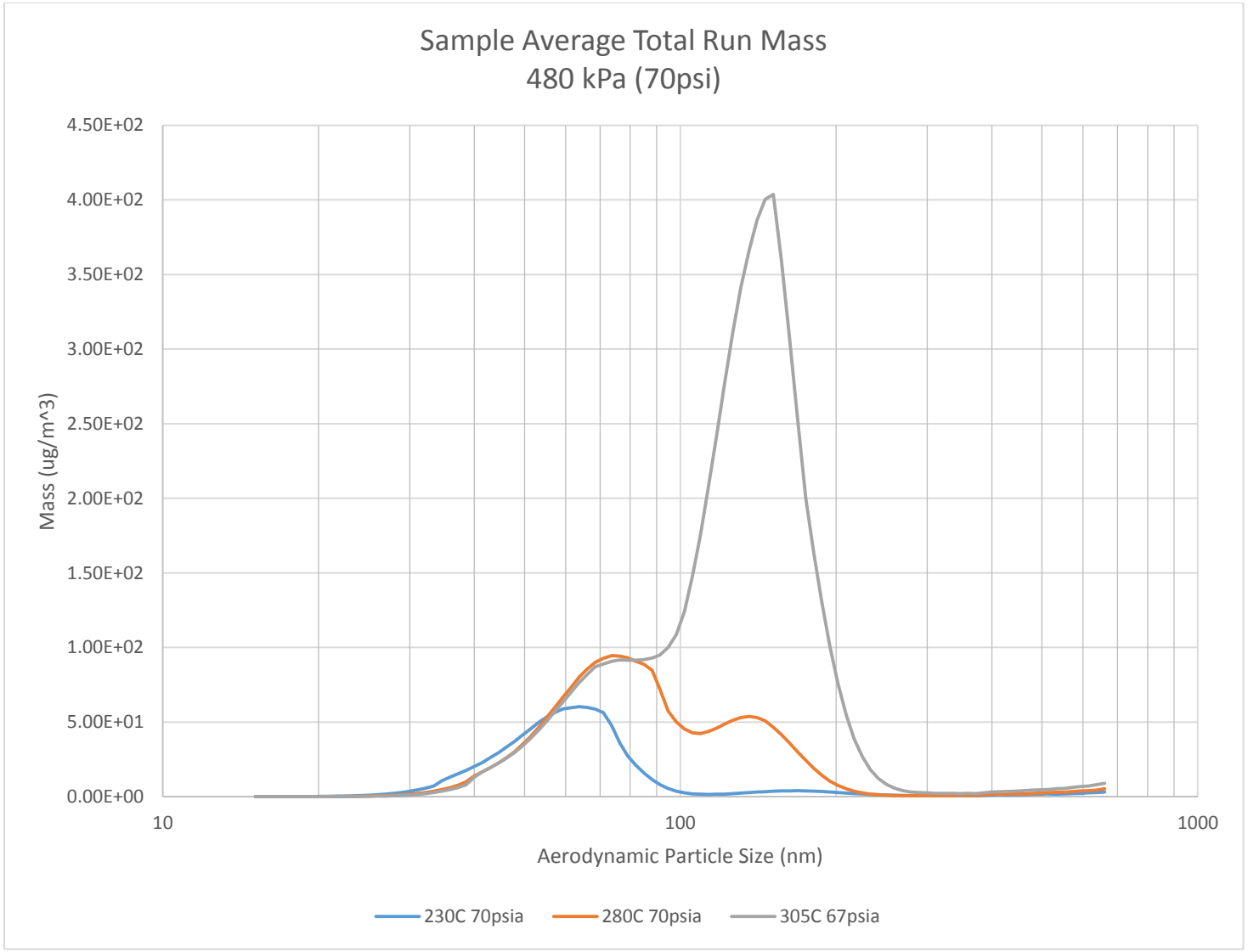

Figure A-3 BAS 30Min Mass - 480kPa (70psi)

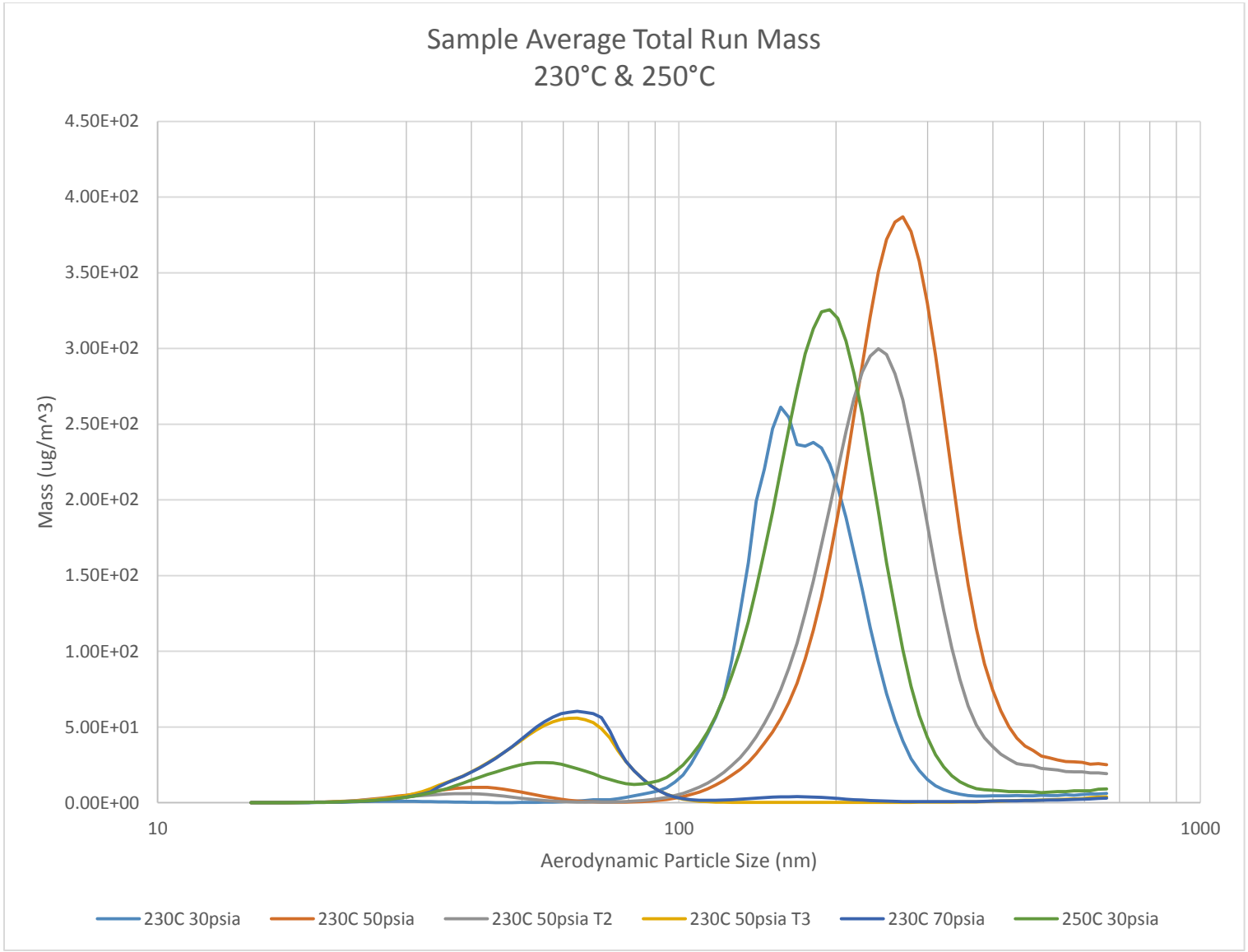

Figure A-4 BAS 30Min Mass - 230°C & 250°C

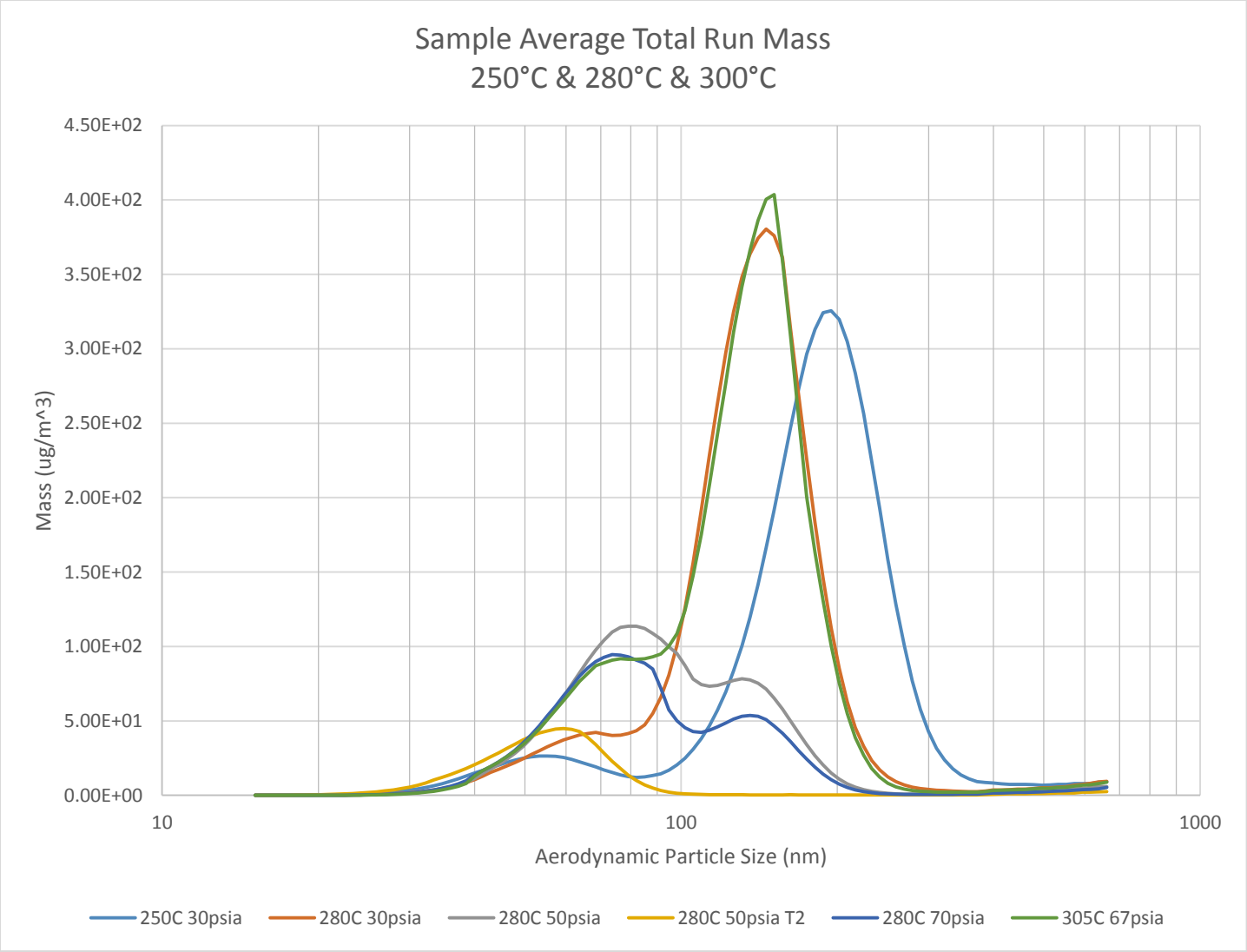

Figure A-5 BAS 30Min Mass - 250°C to 300°C

A.3 10 Minute Data Summary

The 10 minute data are summarized in the table below. The conditions are listed along with the naming convention used. TXX is used as the primary unique identifier with the temperature and pressure following. Suffix of OL indicates that oil injection was done while a suffix of A indicates that the tests were done with no oil injection. Only one nozzle was used during the 10 minute testing.

Standard deviations are given from the average measured temperature and pressures. Highlighted values in red are given for tests that had a standard deviation above 2. The enthalpy and Gibbs plots earlier used the average measured temperatures for calculating the graphs.

Table A-2 10 Minute Data Summary

Test #	Targets Pressure psia	Temp Deg C	Pavg psia	P sig psia	Tavg Deg C	T sig Deg C
1	30	220	30.62	0.461	215.40	6.861
2	30	250	31.08	0.375	254.71	1.185
3	30	280	31.07	0.484	280.11	0.902
4	30	310	31.64	0.507	310.68	6.206
5	30	185	30.29	0.419	183.57	3.457
6	30	220	31.61	0.462	217.30	2.406
7	30	250	32.56	0.384	245.83	1.600
8	30	280	34.15	0.588	279.22	0.987
9	30	310	34.79	0.448	304.10	3.966
10	50	185	48.41	1.413	180.33	1.41
11	50	185	49.76	0.460	187.24	0.474
12	50	220	49.62	0.438	220.49	0.590
13	50	250	49.12	0.441	249.29	0.677
14	50	280	49.20	0.485	278.14	0.542
15	50	310	49.21	0.482	309.87	0.398
16	70	310	75.72	1.391	309.25	0.984
17	100	310	124.06	17.237	313.77	1.001
18	70	310	66.08	3.005	309.20	1.108
19	50	310	52.04	0.361	306.69	0.36
20	70	185	70.75	0.730	178.49	2.150
21	70	220	69.67	1.079	221.25	1.957
22	70	250	69.36	0.694	253.73	1.007
23	70	280	70.86	0.662	289.63	1.113
24	70	310	70.96	0.977	310.47	1.138
25	70	280	72.56	0.802	284.74	0.588
26	70	250	72.35	0.923	256.15	0.752
27	70	220	70.75	0.982	221.95	4.702
28	70	185	67.88	11.248	185.09	3.648
29	100	185	-	-	-	-
30	100	220	-	-	-	-
31	100	250	-	-	-	-
32	100	280	-	-	-	-
33	100	310	100.09	0.831	308.96	1.883
34	100	280	101.67	0.821	281.56	1.199
35	100	250	103.47	0.787	247.53	0.972
36	100	220	103.31	0.801	219.62	3.068
37	100	185	103.40	0.685	191.64	2.644

A.4 Mass Data 10 Minute Simulator

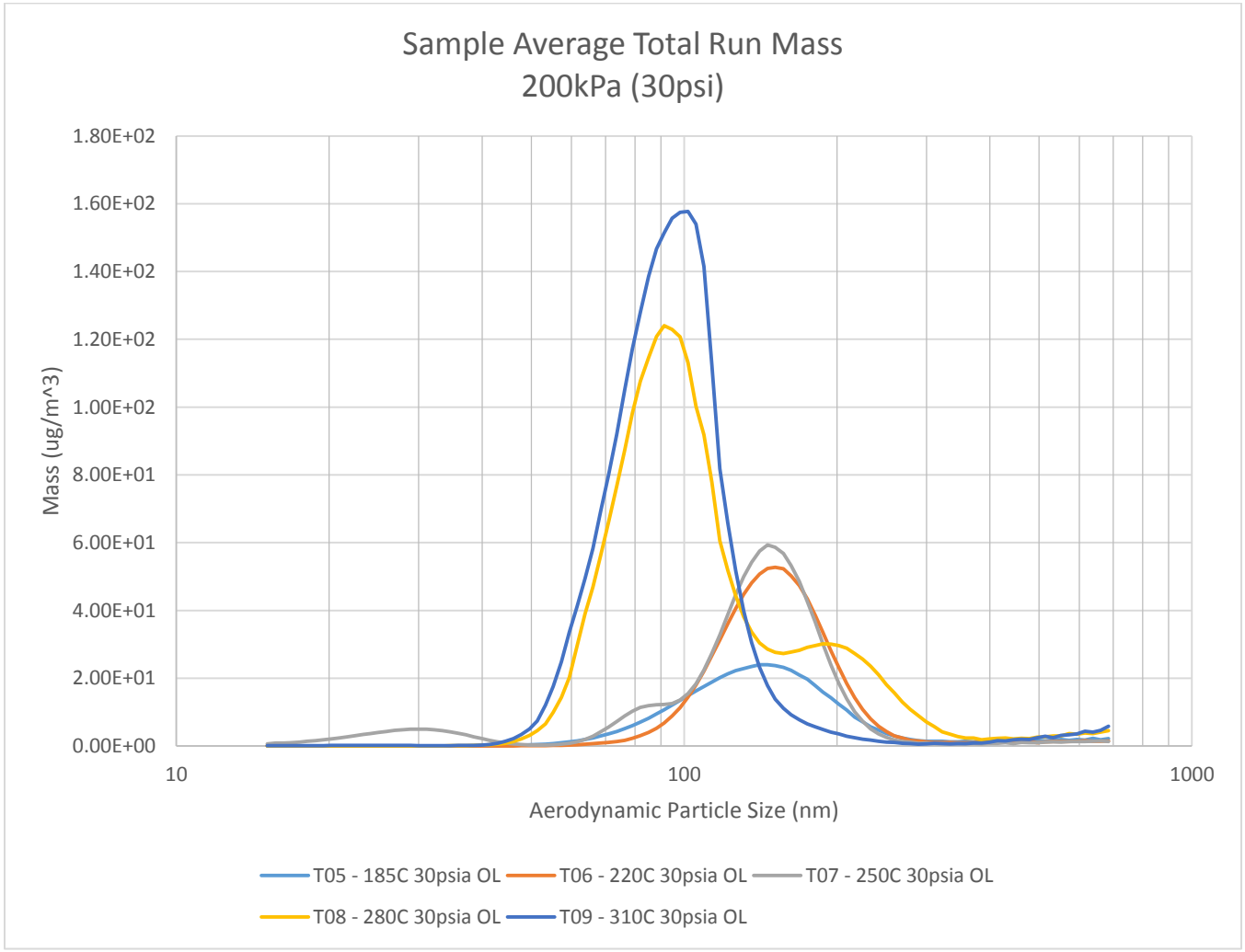

Figure A-6 BAS 10Min Mass - 200kPa (30psi)

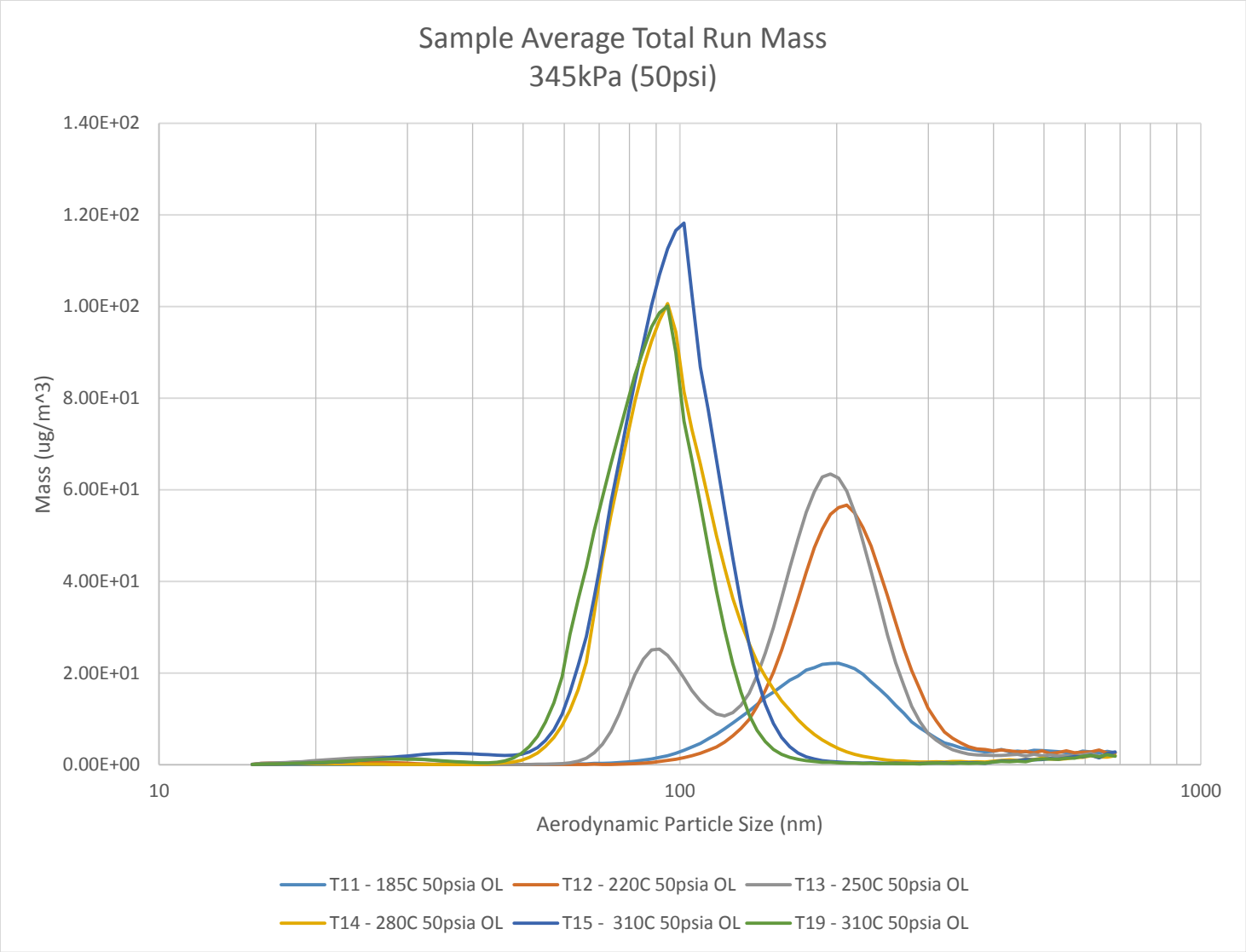

Figure A-7 BAS 10Min Mass - 345kPa (50psi)

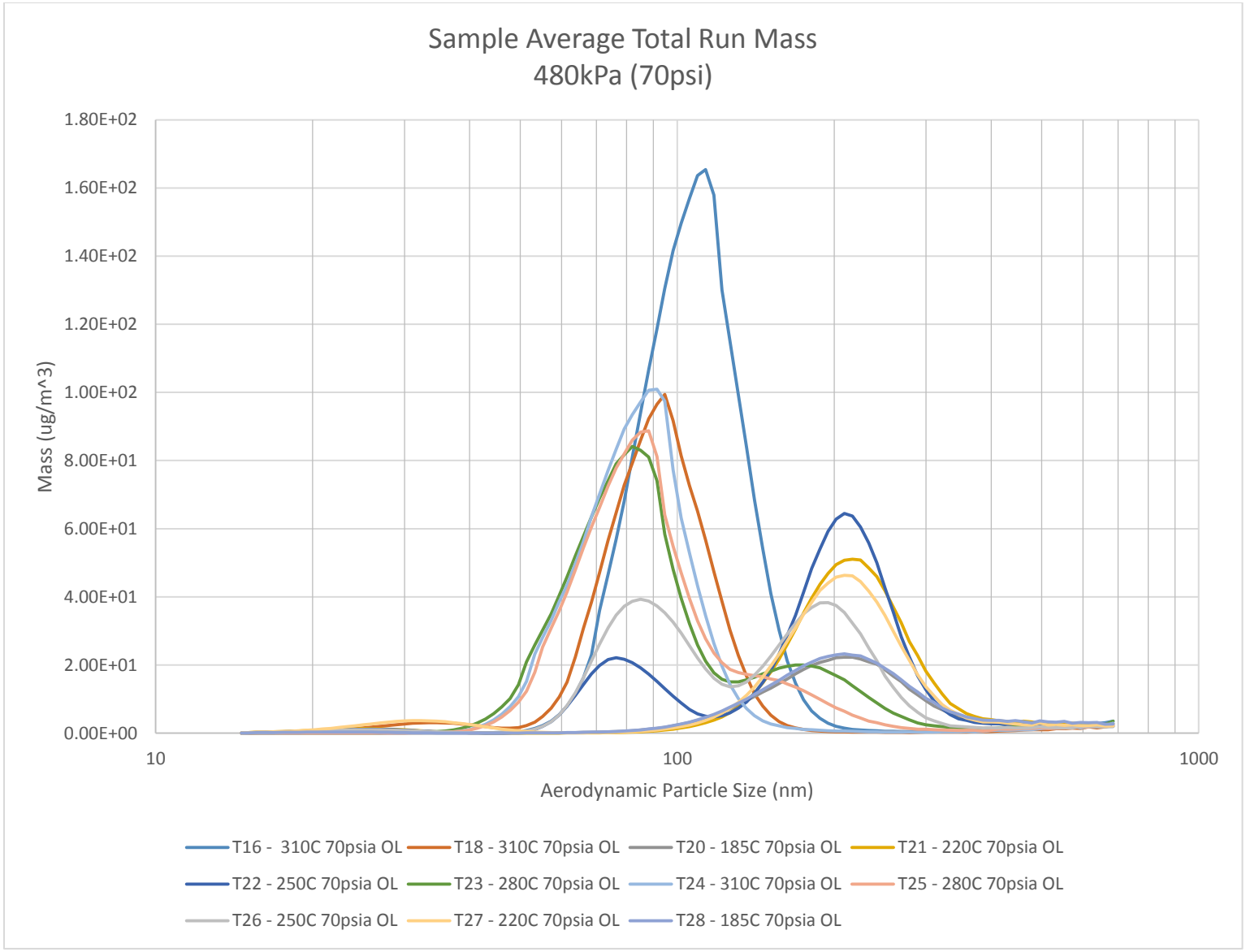

Figure A-8 BAS 10Min Mass - 480kPa (70psi)

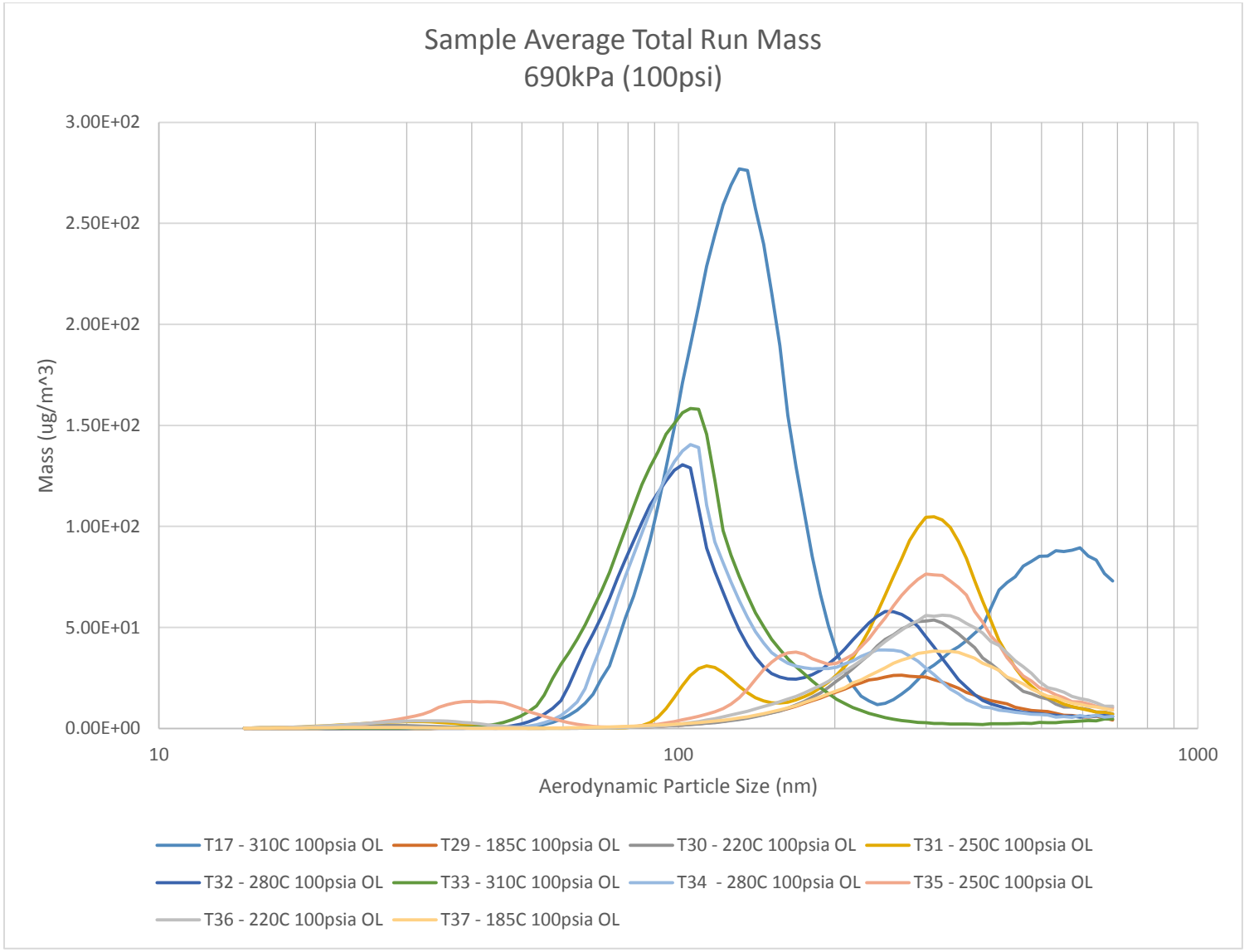

Figure A-9 BAS 10Min Mass - 690kPa (100psi)

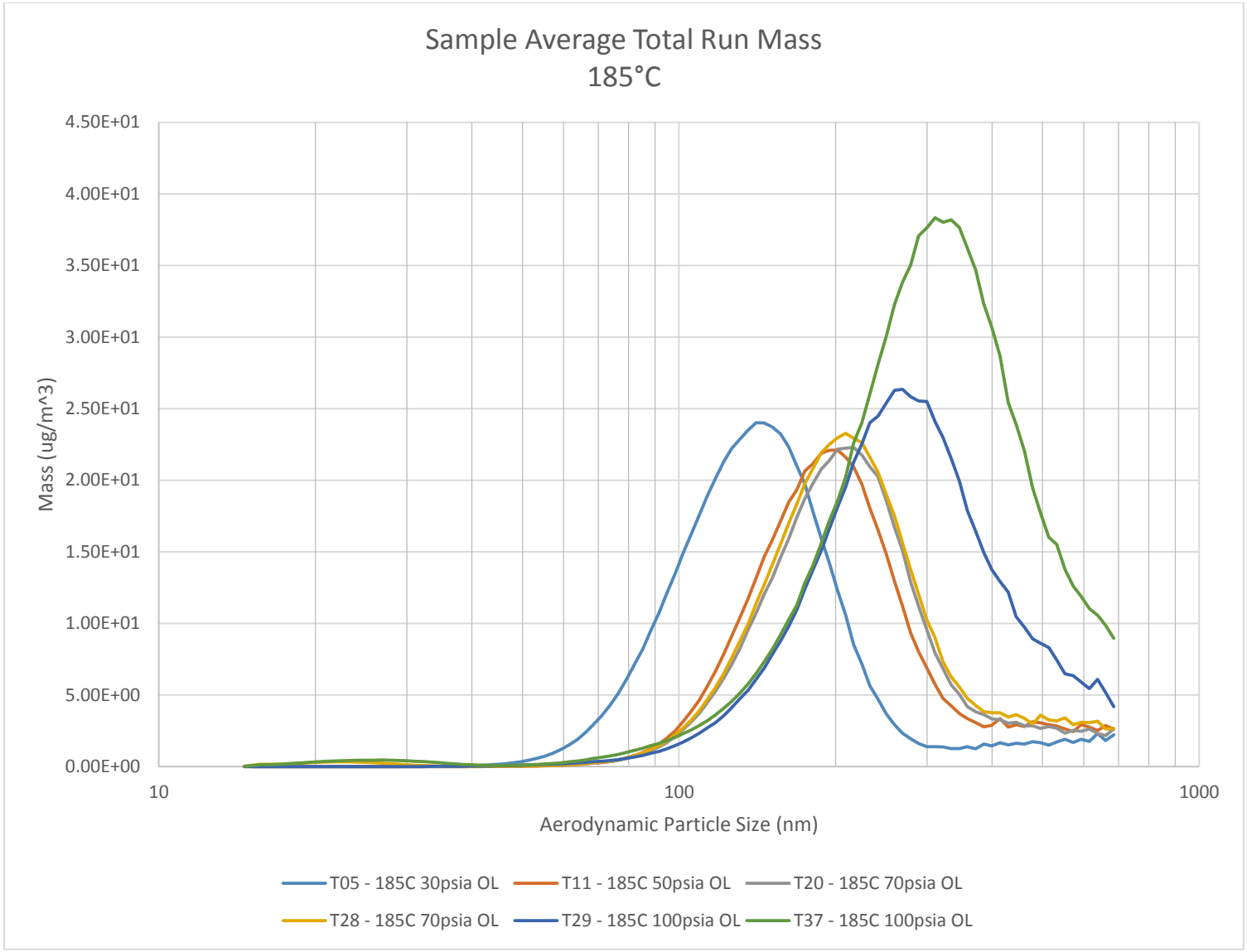

Figure A-10 BAS 10Min Mass - 185°C

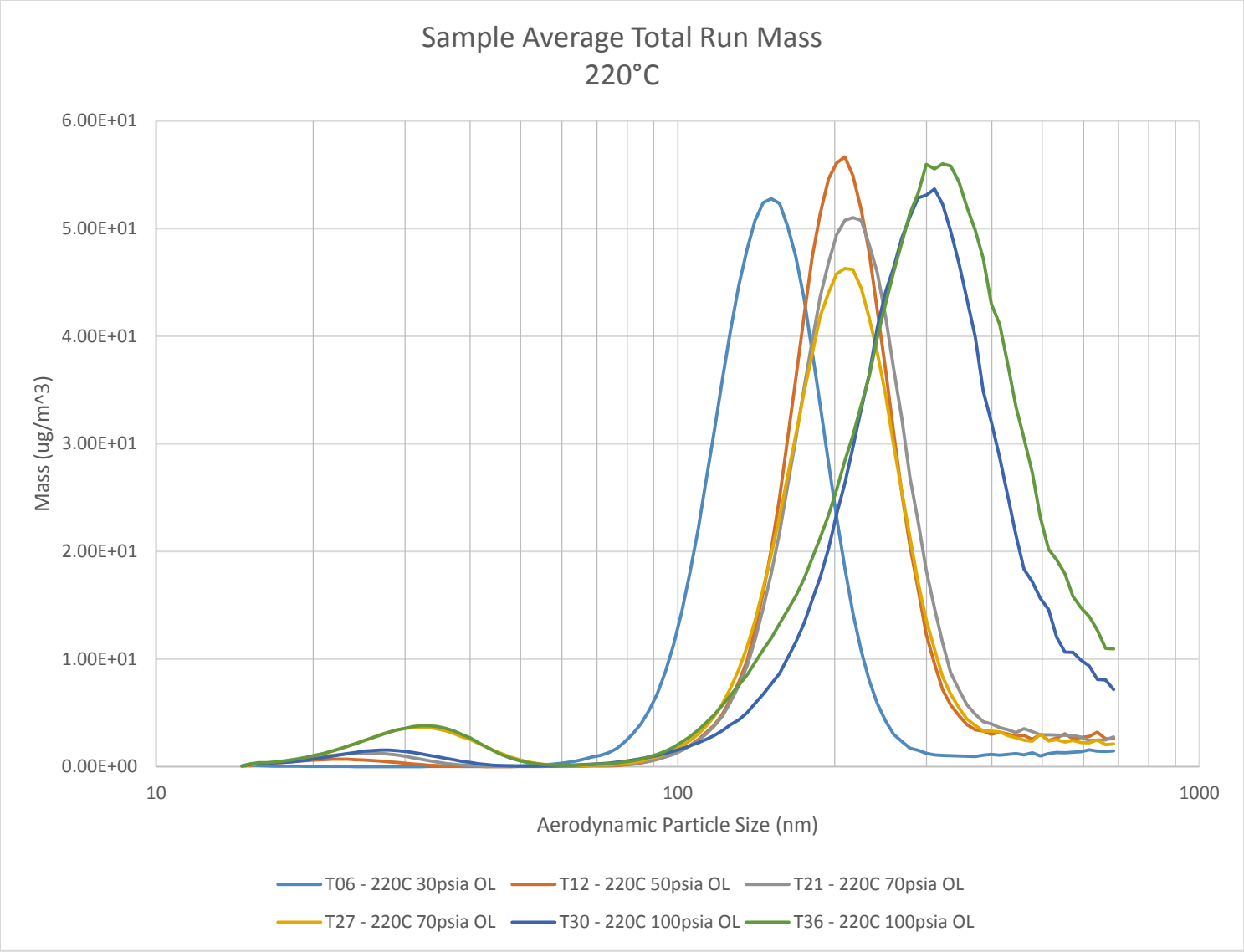

Figure A-11 BAS 10Min Mass - 220°C

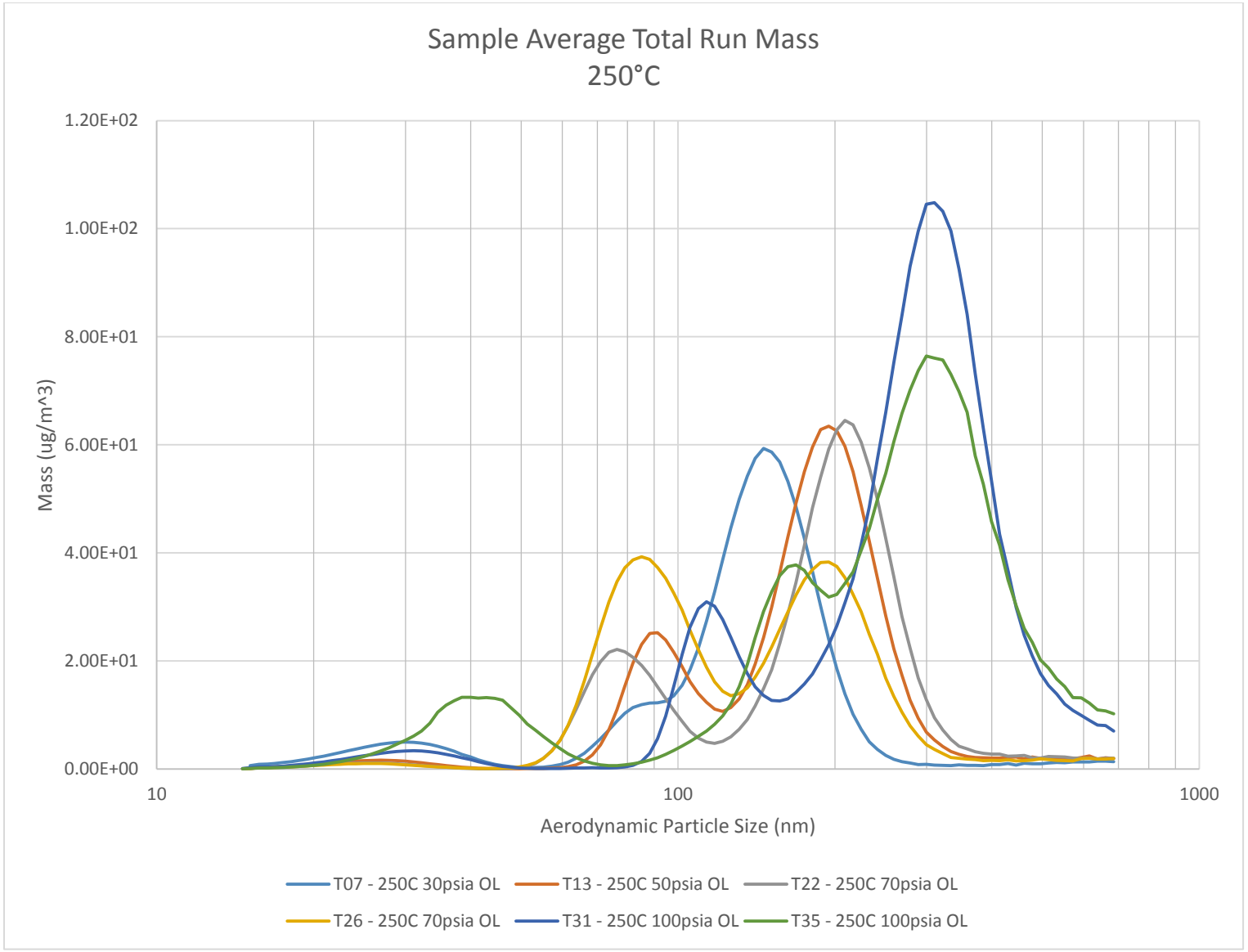

Figure A-12 BAS 10Min Mass - 250°C

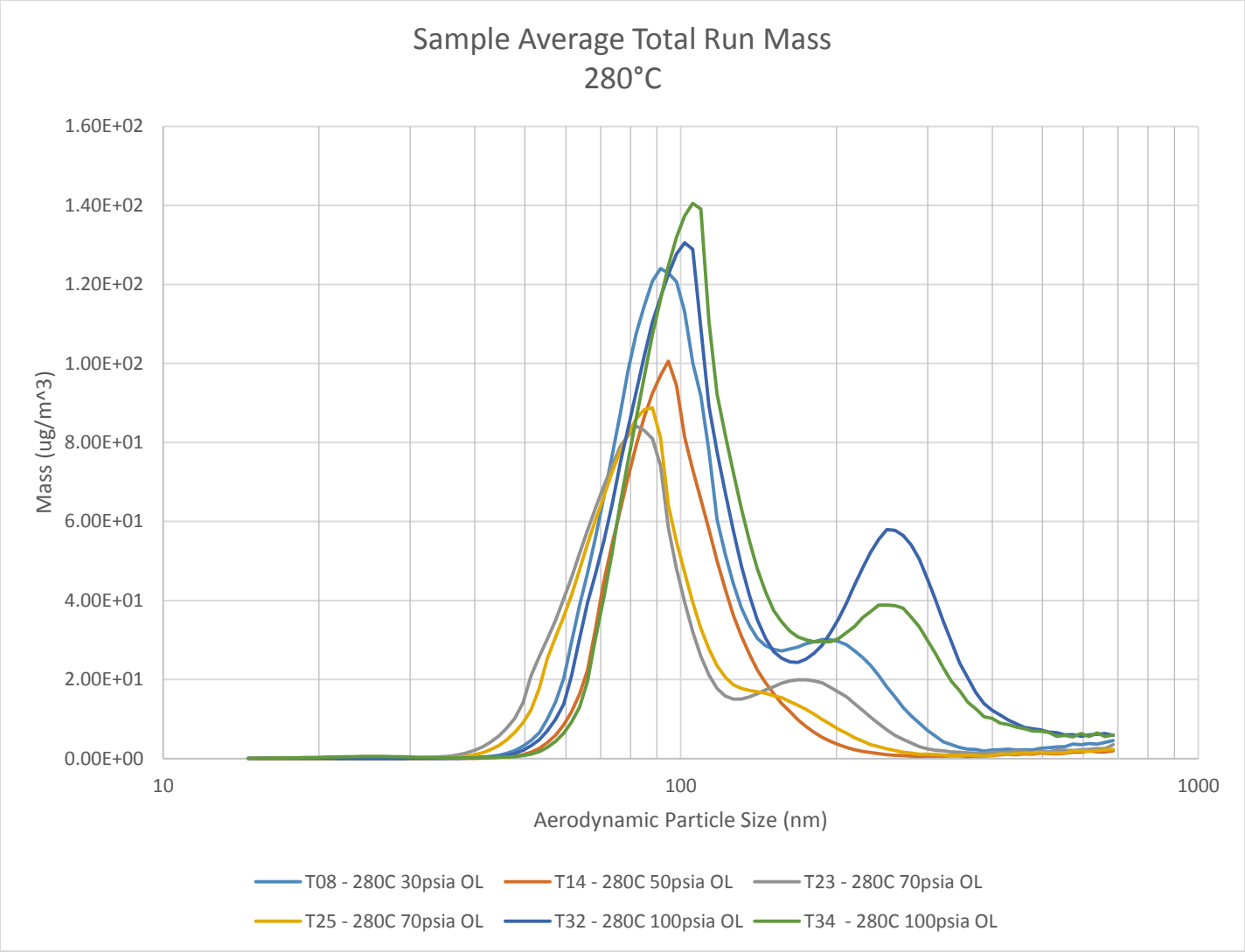

Figure A-13 BAS 10Min Mass - 280°C

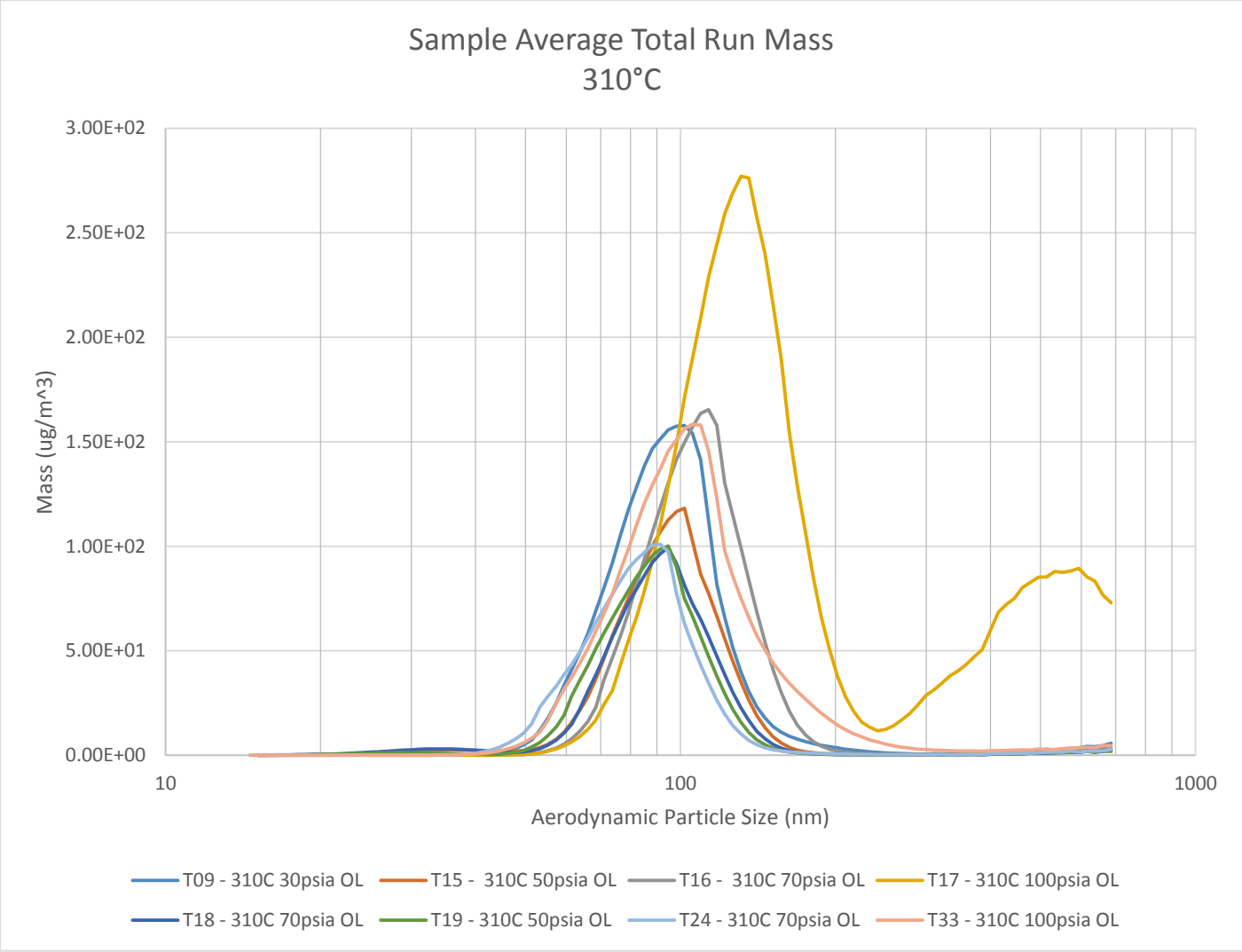

Figure A-14 BAS 10Min Mass - 310°C

A.5 Cumulative Percent 30 Minute Simulator

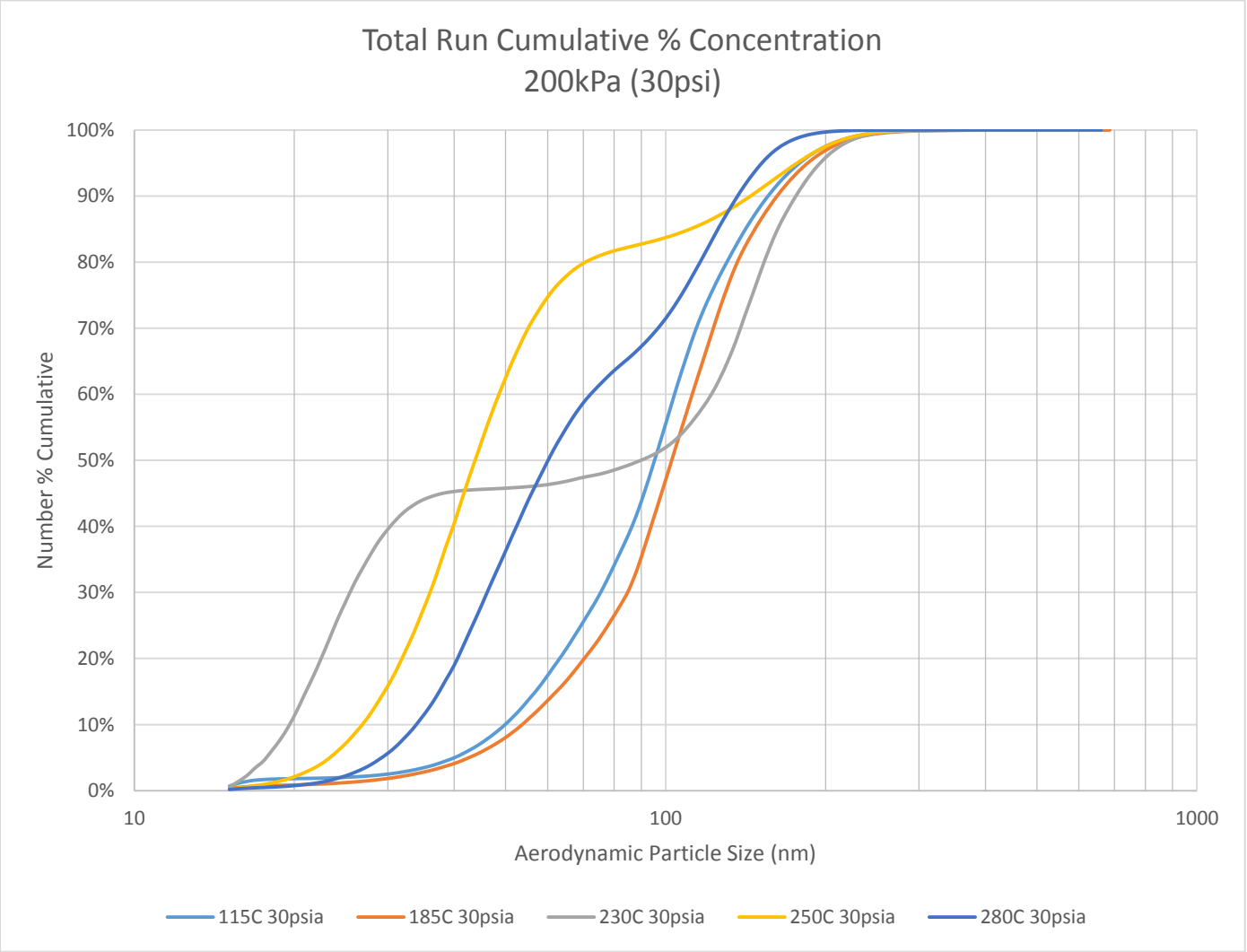

Figure A-15 BAS 30Min Cumulative - 200kPa (30psi)

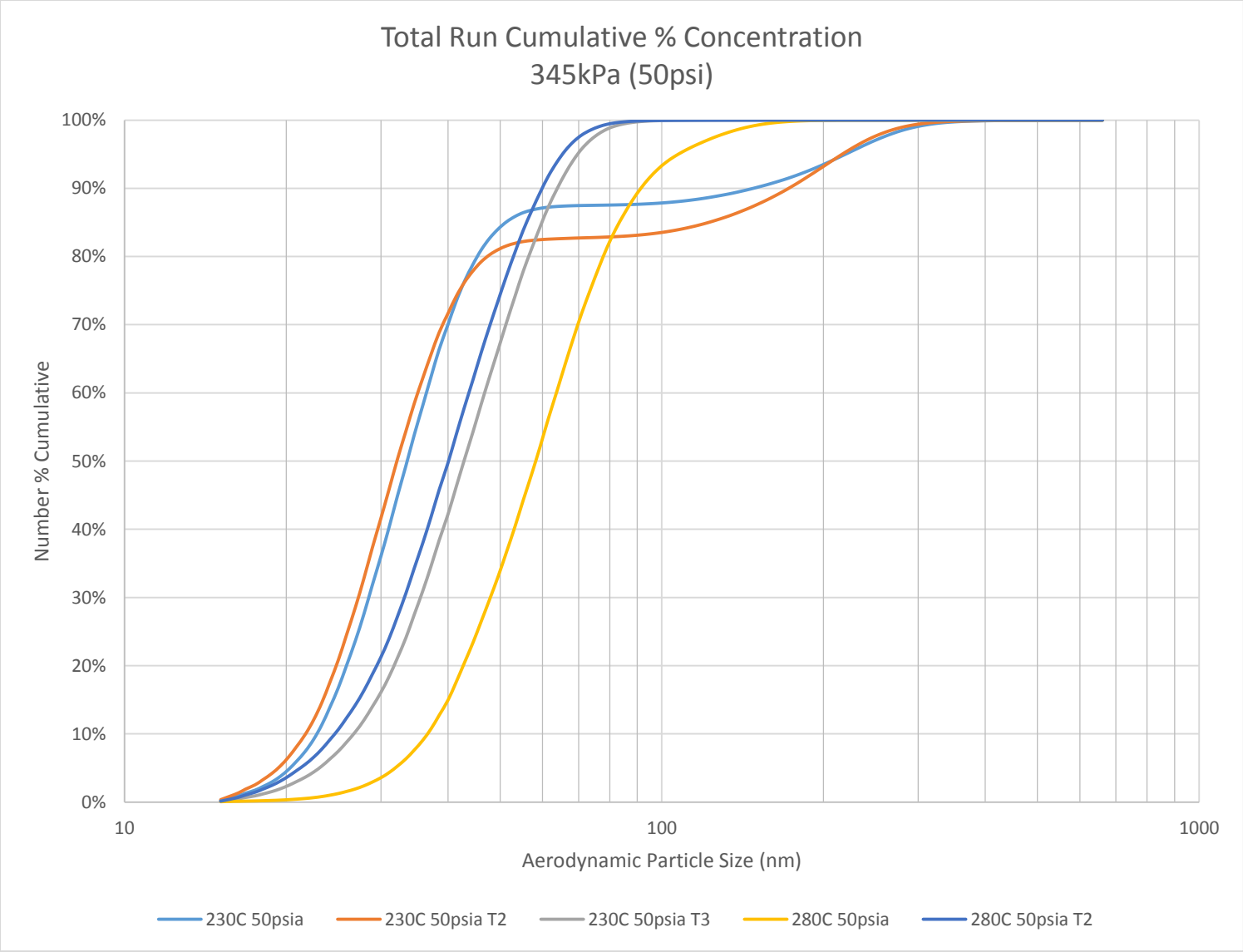

Figure A-16 BAS 30Min Cumulative - 345kPa (50psi)

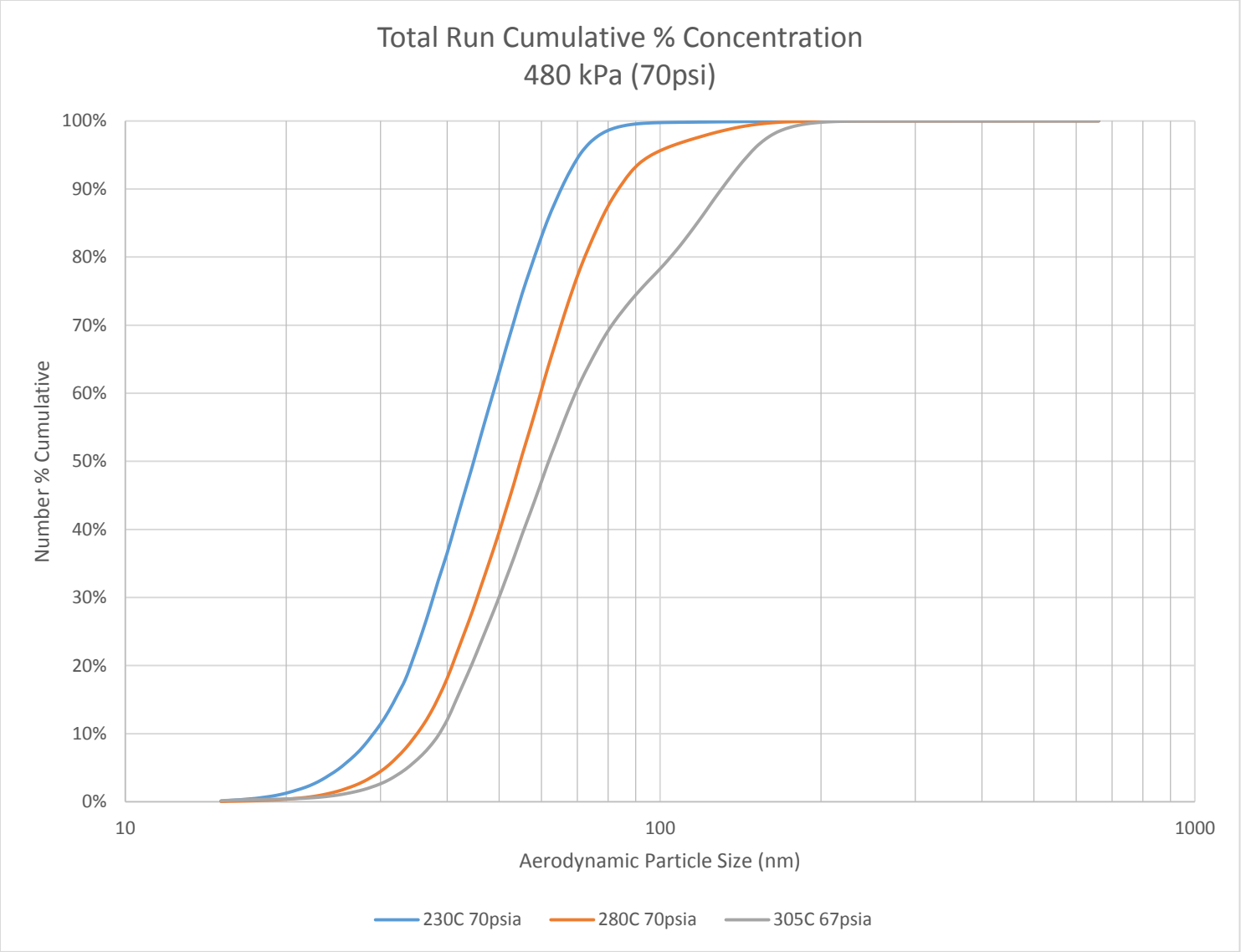

Figure A-17 BAS 30Min Cumulative - 480kPa (70psi)

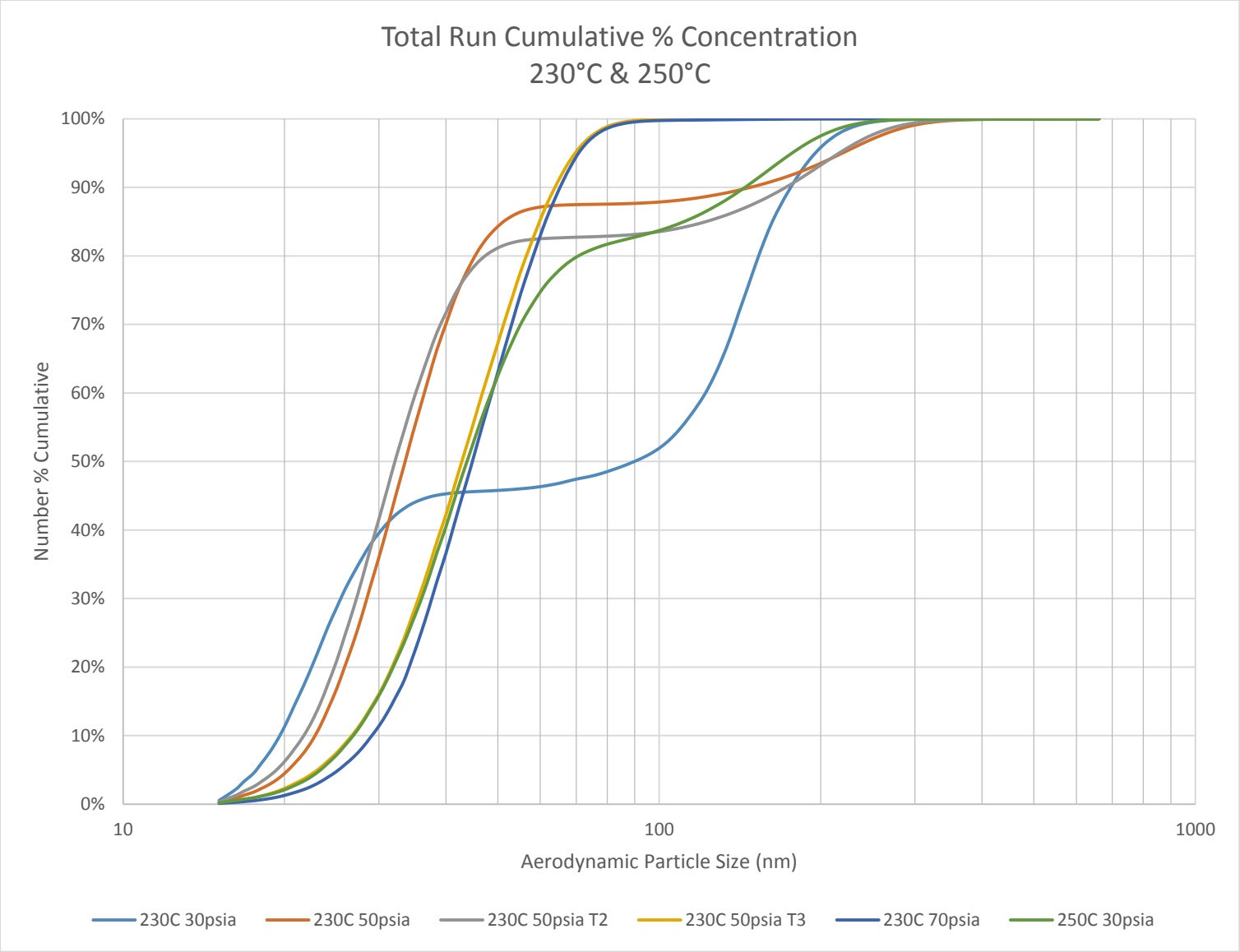

Figure A-18 BAS 30Min Cumulative - 230°C to 250°C

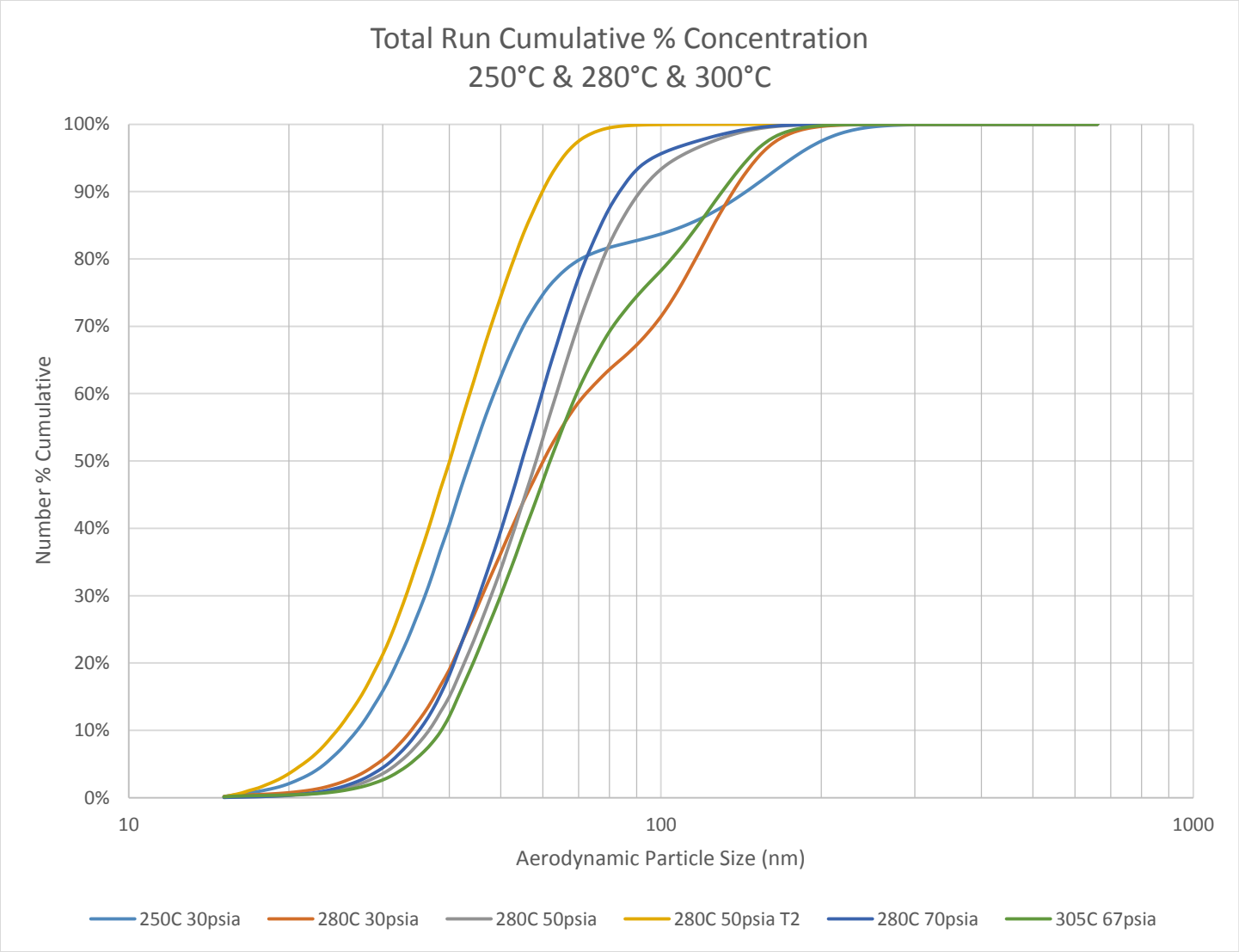

Figure A-19 BAS 30Min Cumulative - 250°C to 300°C

A.6 Cumulative Percent 10 Minute Simulator

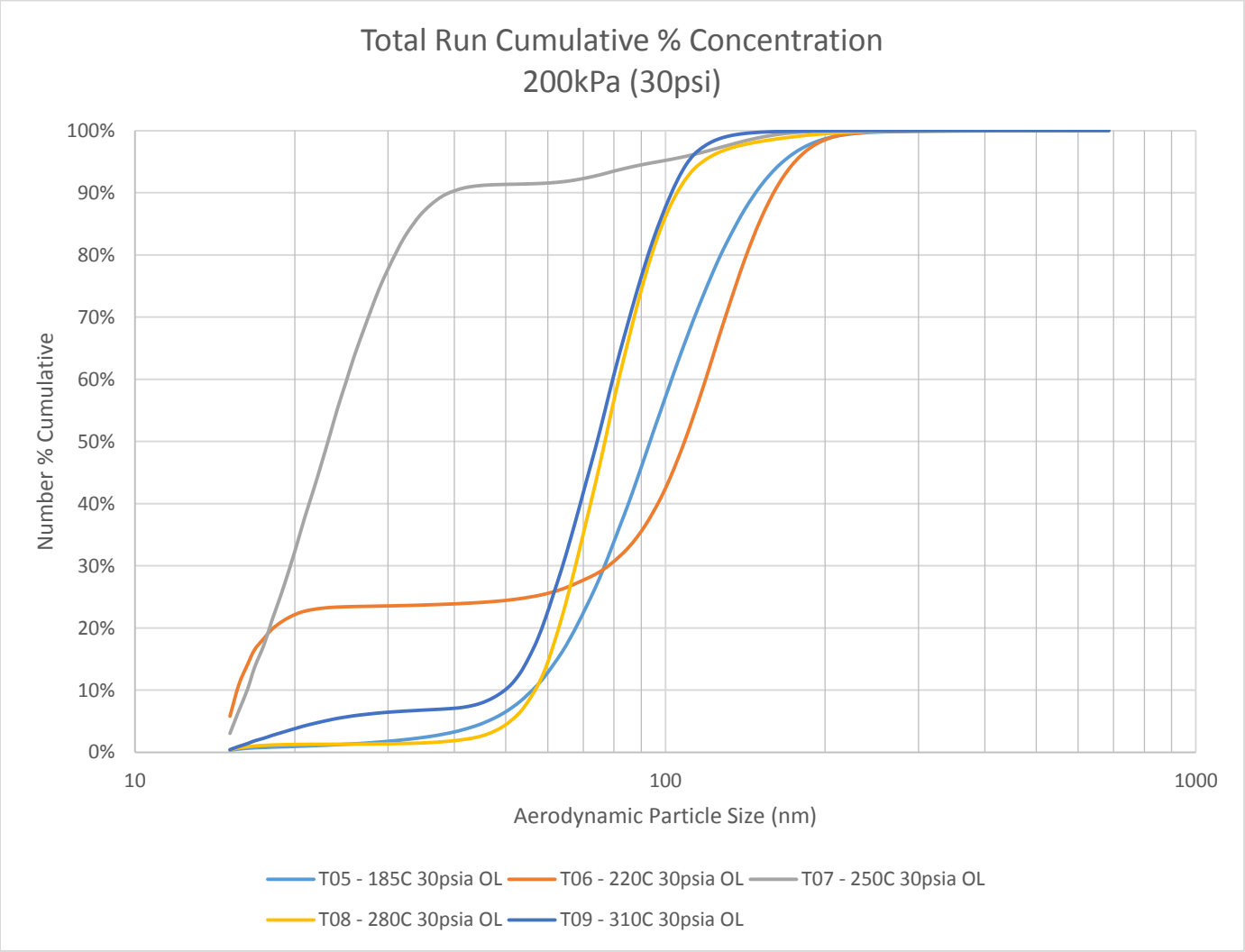

Figure A-20 BAS 10Min Cumulative - 200kPa (30psi)

Figure A-21 BAS 10Min Cumulative - 345kPa (50psi)

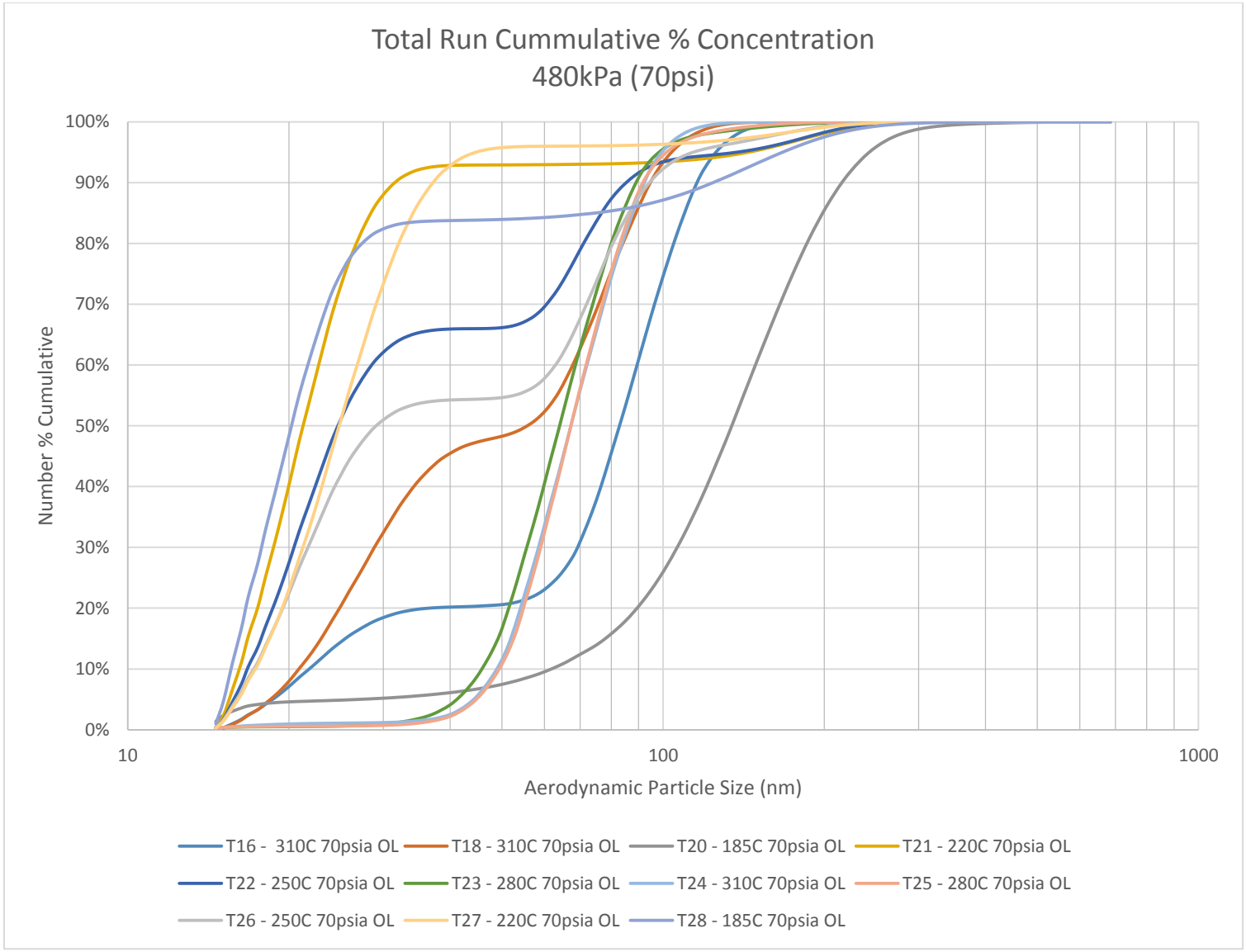

Figure A-22 BAS 10Min Cumulative - 480kPa (70psi)

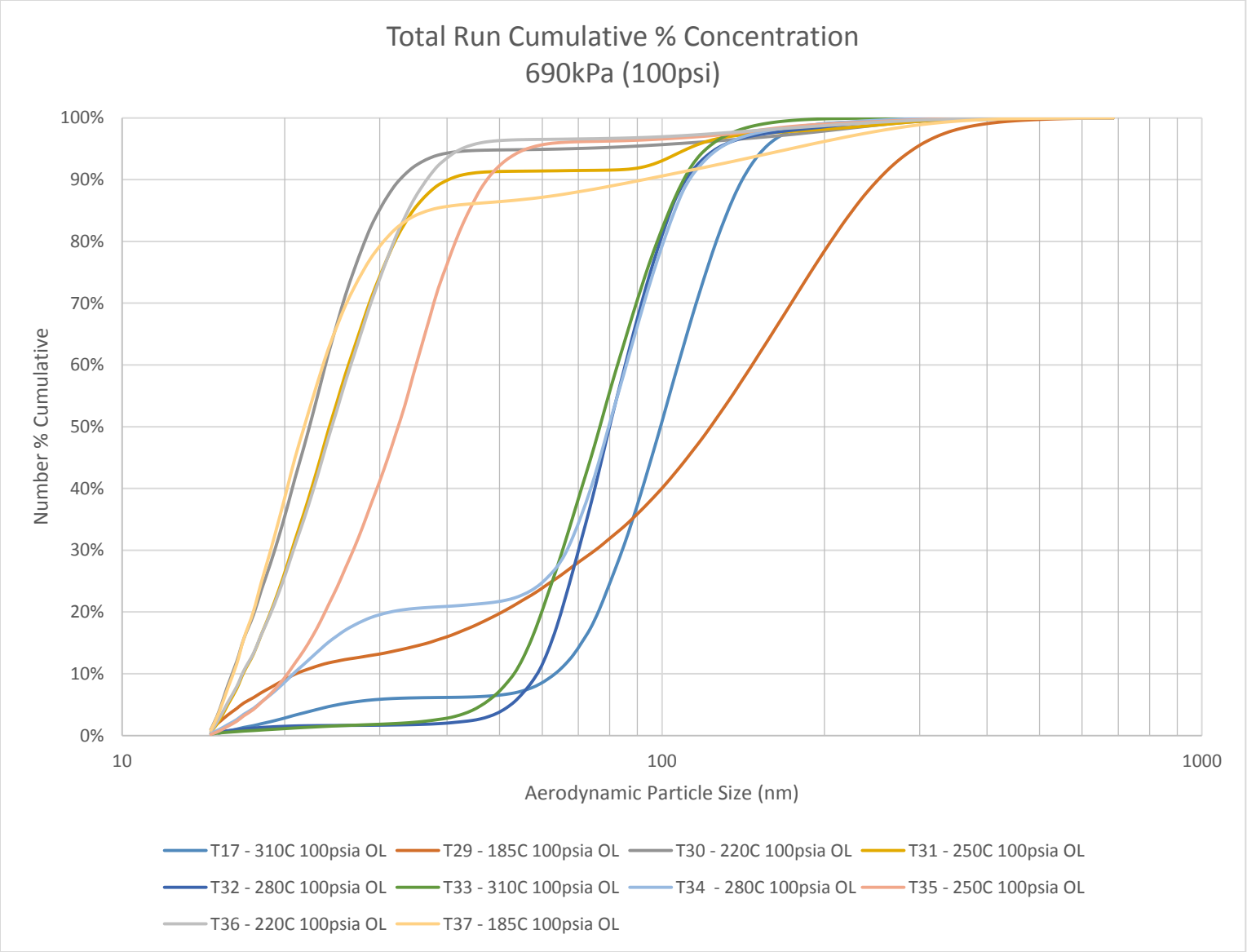

Figure A-23 BAS 10Min Cumulative - 690kPa (100psi)

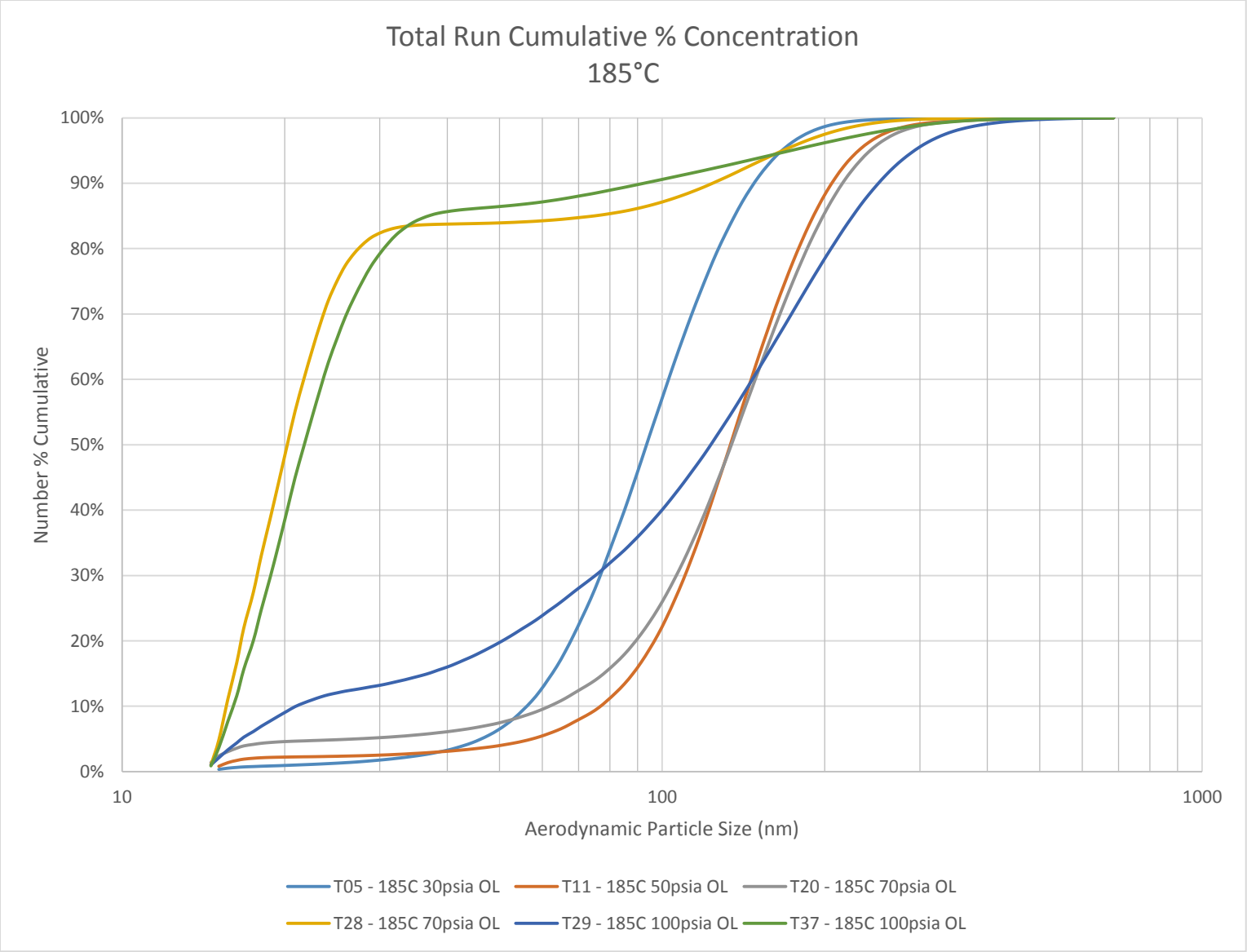

Figure A-24 BAS 10Min Cumulative - 185°C

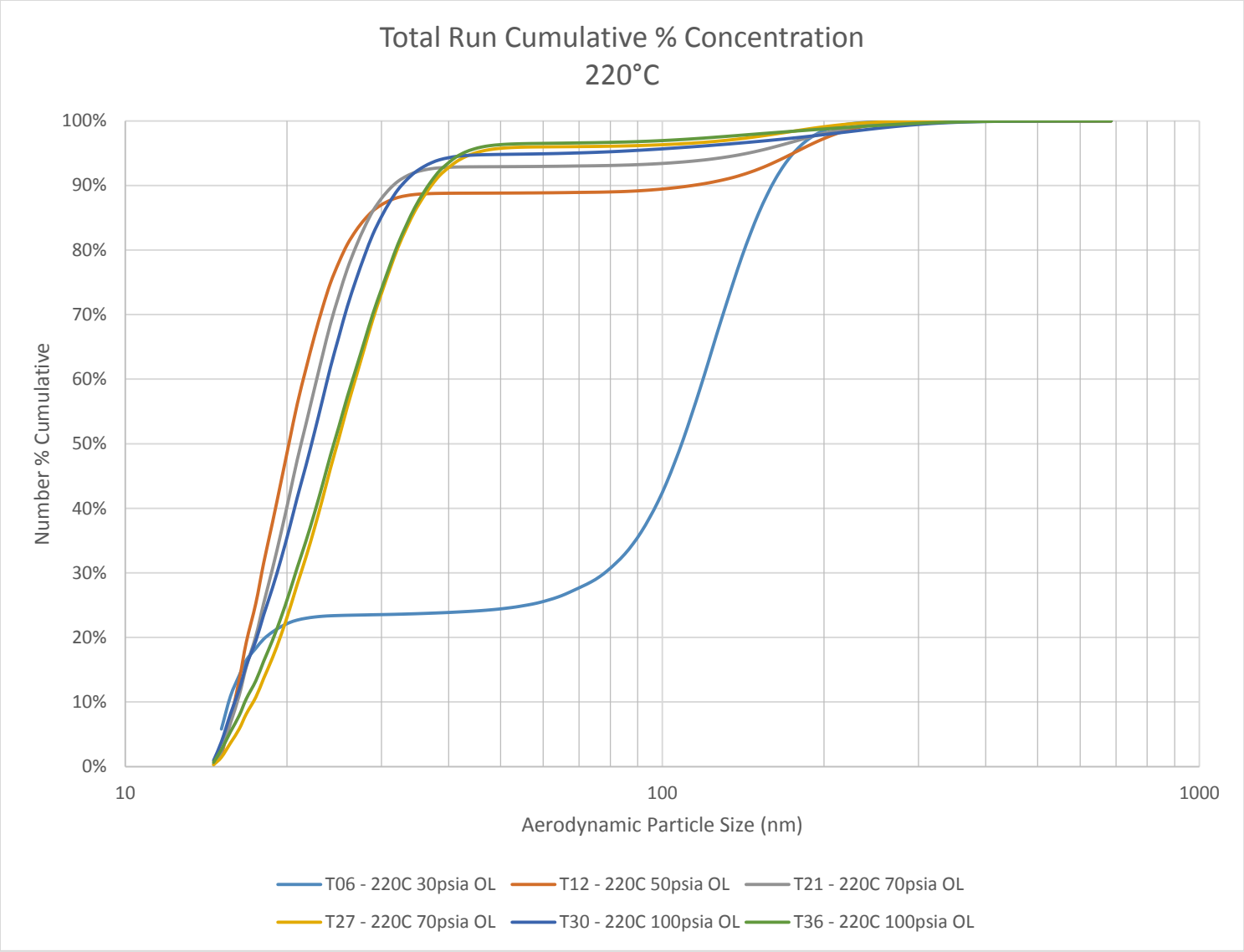

Figure A-25 BAS 10Min Cumulative - 220°C

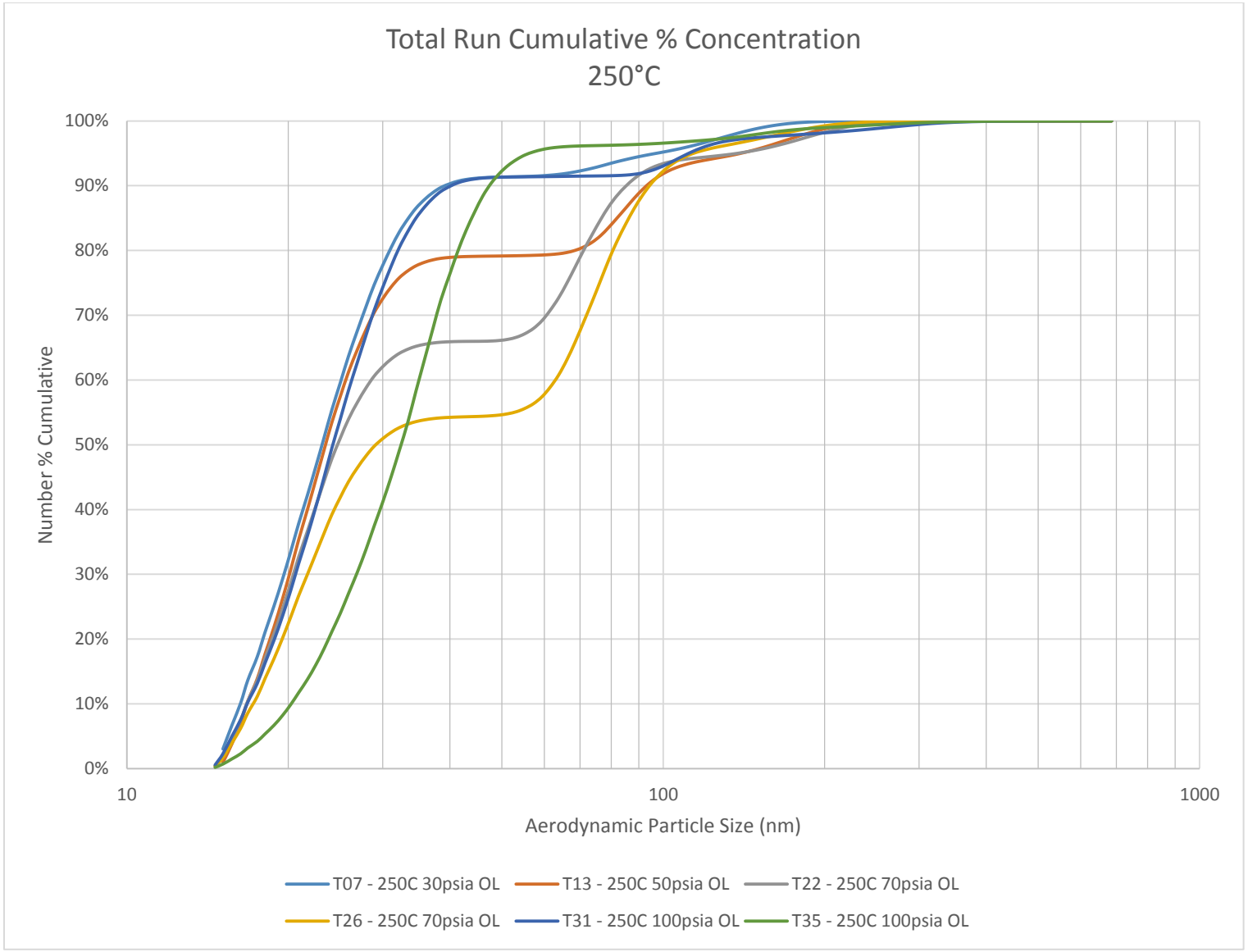

Figure A-26 BAS 10Min Cumulative - 250°C

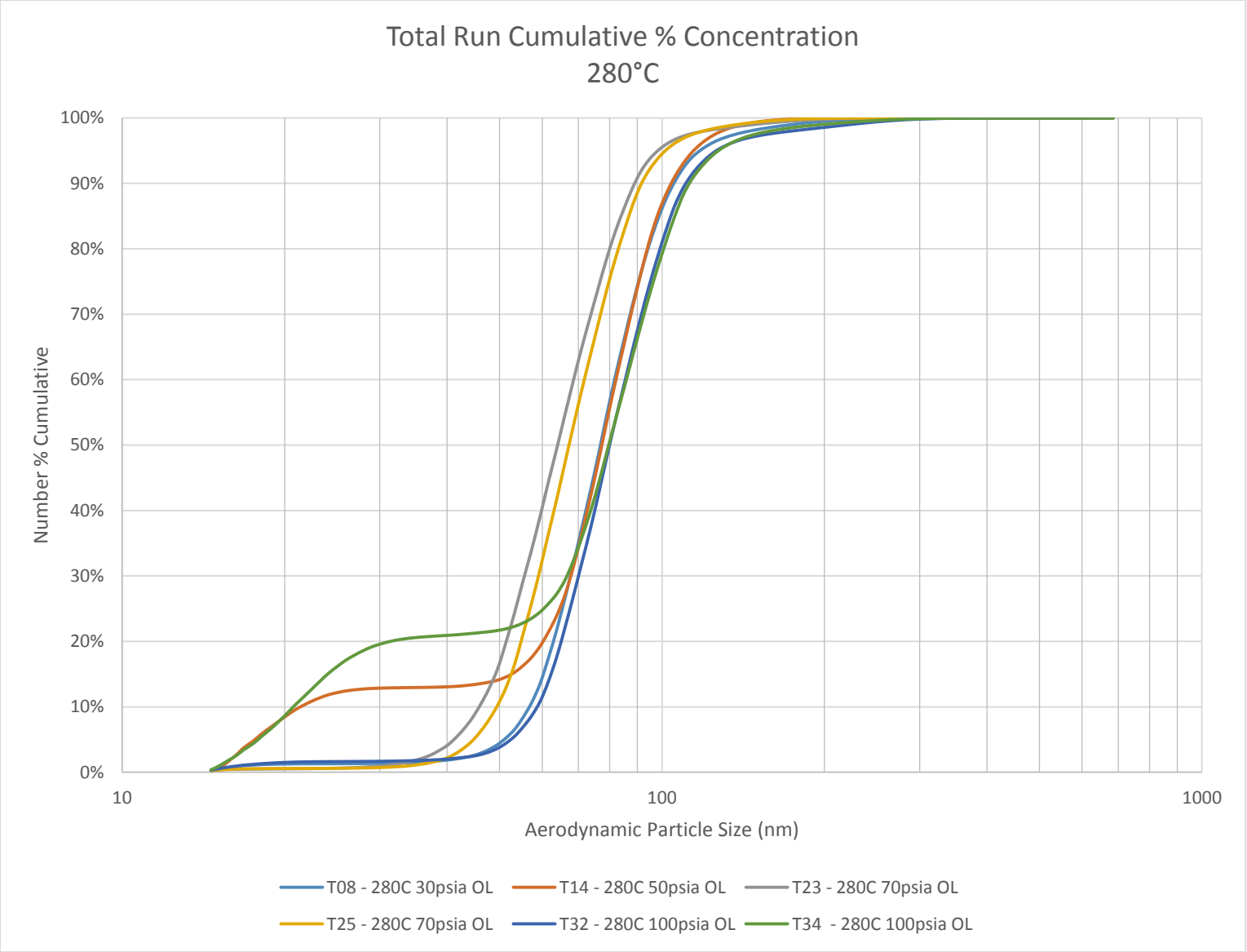

Figure A-27 BAS 10Min Cumulative - 280°C

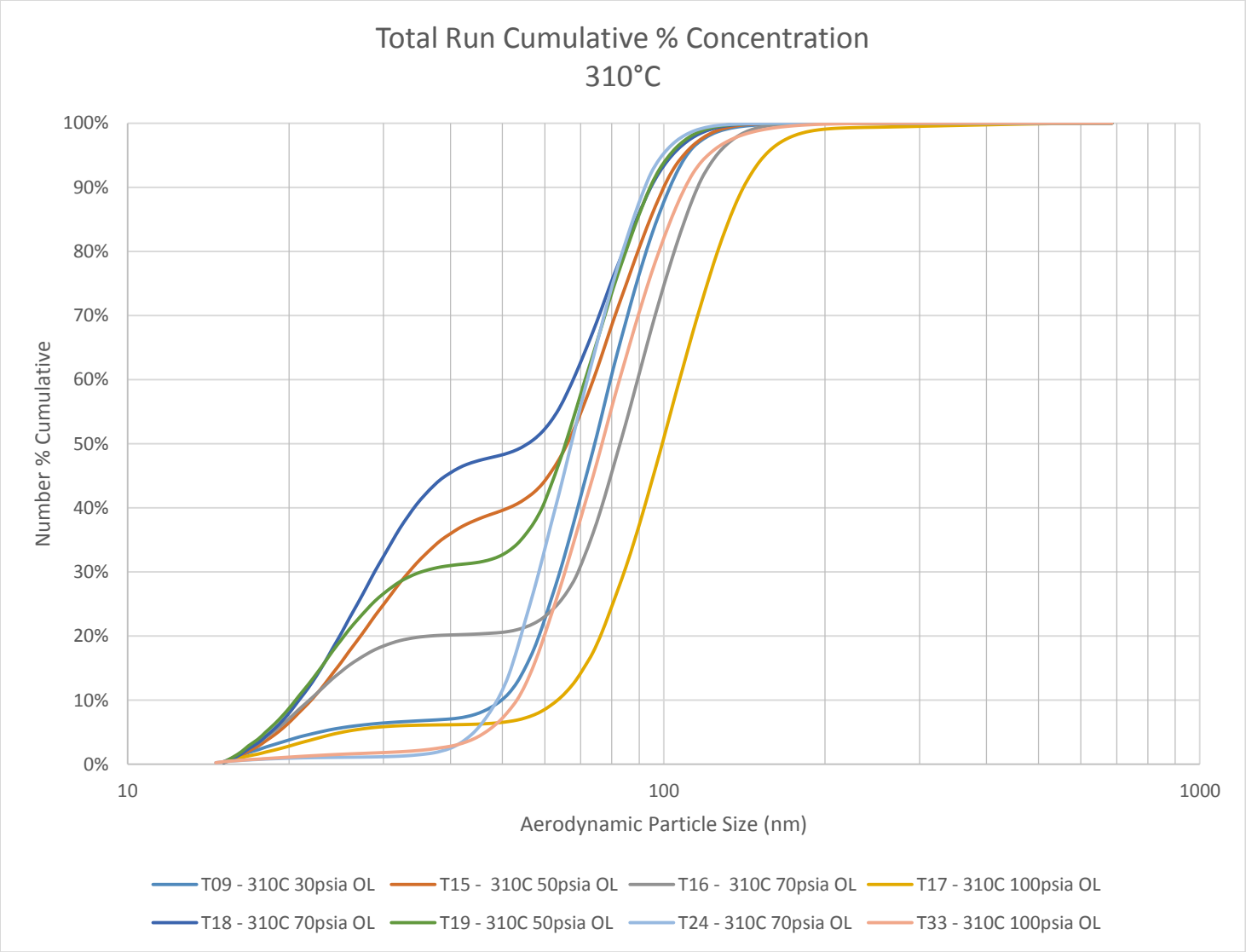

Figure A-28 BAS 10Min Cumulative - 310°C

Appendix B: C18 Engine Data

Similar to Appendix A, the following section has the data table summarizing the test conditions along with the naming convention shown for each test. The sample numbers are given as shown in the AIM software and as mentioned during the initial introduction in section 2.2.2.2.1. Samples taken back to back are listed as a run with the naming convention of RXX. The MMP number corresponds to the engine data output file which has the various engine parameters such as temperatures, pressures, and flow rates. The heading labeled location shows the type of measurement taken. Ambient refers to the ambient air measured while Bkgnd refers to a measurement taken inside the lines. BL indicates the measurement taken from the bleed air extraction line while AP refers to the air plenum box measurement. Following the word 'Inject' is a number that symbolizes the number of aerosolizing nozzles used during the test. No Inject refers to a measurement taken where no oil was injected during the test but the engine was running. These conditions are more prevalent during the steady state decay measurements.

Following the data table are the cumulative percent concentration graphs for the same data sets as shown in section 3.3.5. Hundreds of graphs were generated during the analysis of the data, but only the most important ones are shown in this report. This information allows the reader the ability to derive any set of data as seen below. [It should be noted that printing in color is the best way to observe the graphs as over 100 data points are used for each line, thus making geometric symbols an unwieldy way of showing the data].

A.1 C18 Data Test Point Targets

Table B-1 C18 Data Summary

Name	Sample #	End	MMP#	T	P	Location
T01 S01	1	5	-	200	53	Ambient
T01 S02	6	10	-	200	53	BL Bkgnd
T01 S03	11	15	-	200	53	AP Bkgnd
T01 S04	16	20	-	200	53	Ambient
T01 S05	21	25	-	200	53	AP No Inject
T01 S06	26	30	-	200	53	BL No Inject
T01 S07	31	35	-	200	53	BL No Inject
T01 S08	36	40	-	200	53	BL Inject 3
T01 S09	41	45	-	200	53	BL Inject 3
T01 S10	46	50	-	200	53	AP Inject 3
T01 S11	51	55	-	200	53	BL No Inject
T01 S12	56	60	-	200	53	AP No Inject
T02 S01	1	5	-	200	53	Ambient
T02 S02	6	10	-	200	53	BL Bkgnd
T02 S03	11	15	-	200	53	BL No Inject
T02 S04	16	20	1	200	53	BL Inject 3
T02 S05	21	25	2	200	53	BL NO Inject
T02 S06	26	30	3	200	53	BL No Inject
T02 S07	31	35	4	200	53	BL No Inject
T02 S08	36	40	5	200	53	BL No Inject
T02 S09	41	45	6	200	53	BL No Inject
T03 S01	1	5	-	200	57	Ambient
T03 S02	6	10	-	200	57	BL Bkgnd
T03 S03	11	15	1	200	57	BL No Inject
T03 S04	16	20	2	200	57	BL Inject 1
T03 S05	21	25	3	200	57	BL Inject 2
T03 S06	26	30	4	200	57	BL Inject 3
T03 S07	31	35	5	200	57	BL No Inject
T03 S08	36	40	6	200	57	BL No Inject
T03 S09	41	45	7	200	57	BL No Inject
T03 S10	46	50	8	200	57	BL No Inject
T03 S11	51	55	9	200	57	BL No Inject
T03 S12	56	60	10	200	57	BL No Inject
T03 S13	61	65	11	200	57	BL No Inject
T03 S14	66	70	12	200	57	BL No Inject
T03 S15	71	75	13	200	57	BL No Inject
T04 S01	1	5	-	-	-	Ambient
T04 S02	6	10	1	138	38	BL Bkgnd

T04 S03	11	15	2	140	38	BL Inject 3
T04 S04	16	20	3	160	45	BL Inject 3
T04 S05	21	25	4	180	50	BL Inject 3
T04 S06	26	30	5	200	53	BL Inject 3
T04 S07	31	35	6	220	60	BL Inject 3
T04 S08	36	40	7	235	63	BL Inject 3
T05 S01	1		-	-	-	Ambient
T05 S02	2		1	160	54	BL Inject 3
T05 S03	3		2	160	52	BL Inject 3
T05 S04	4		3	160	52	BL Inject 3
T05 S05	5		4	160	53	BL Inject 3
T05 S06	6		5	200	65	BL Inject 3
T05 S07	7		6	200	65	BL Inject 3
T05 S08	8		7	200	65	BL Inject 3
T05 S09	9		8	200	65	BL Inject 3
T05 S10	10		9	213	70	BL Inject 3
T05 S11	11		10	210	70	BL Inject 3
T05 S12	12		11	211	70	BL Inject 3
T05 S13	13		12	211	70	BL Inject 3
T05 S14	14		13	215	70	BL Inject 3
T05 S15	15		14	214	70	BL Inject 3
T05 S16	16		15	230	77	BL Inject 3
T05 S17	17		16	230	77	BL Inject 3
T05 S18	18		17	230	77	BL Inject 3
T05 S19	19		18	213	70	BL Inject 3
T05 S20	20		19	213	70	BL Inject 3
T05 S21	21		20	200	65	BL Inject 3
T05 S22	22		21	200	66	BL Inject 3
T05 S23	23		22	180	58	BL Inject 3
T05 S24	24		23	180	58	BL Inject 3
T05 S25	25		24	160	53	BL Inject 3
T05 S26	26		25	160	53	BL Inject 3
T05 S27	27		26	143	49	BL Inject 3
T05 S28	28		27	143	50	BL Inject 3
T05 S29	29		28	103	36	BL Inject 3
T05 S30	30		29	100	36	BL Inject 3
T06 S01	1		1	240	70	BL Inject 3
T06 S02	2		2	240	70	BL Inject 3
T06 S03	3		3	240	72	BL Inject 3
T06 S04	4		4	235	69	BL Inject 3
T06 S05	5		5	230	68	BL Inject 3
T06 S06	6		6	230	68	BL Inject 3
T06 S07	7		7	220	63	BL Inject 3

T06 S08	8	8	220	66	BL Inject 3
T06 S09	9	9	210	62	BL Inject 3
T06 S10	10	10	210	62	BL Inject 3
T06 S11	11	11	155	48	BL Inject 3
T06 S12	12	12	155	48	BL Inject 3
T06 S13	13	13	155	48	BL Inject 3
T06 S14	14	14	140	42	BL Inject 3
T06 S15	15	15	140	42	BL Inject 3
T06 S16	16	16	140	42	BL Inject 3
T06 S17	17	17	140	42	BL Inject 3
T06 S18	18	18	146	44	BL Inject 3
T06 S19	19	19	145	45	BL Inject 3
T07 S01	1		-	-	BL Background / Ambient
T07 S02	2	1	115	32	BL Inject 3
T07 S03	3	2	115	32	BL Inject 3
T07 S04	4	3	115	32	BL Inject 3
T07 S05	5	4	124	35	BL Inject 3
T07 S06	6	5	125	35	BL Inject 3
T07 S07	7	6	125	35	BL Inject 3
T07 S08	8	7	125	35	BL Inject 3
T07 S09	9	8	135	38	BL Inject 3
T07 S10	10	9	135	38	BL Inject 3
T07 S11	11	10	135	38	BL Inject 3
T07 S12	12	11	135	38	BL Inject 3
T07 S13	13	12	145	40	BL Inject 3
T07 S14	14	13	145	40	BL Inject 3
T07 S15	15	14	145	40	BL Inject 3
T07 S16	16	15	155	44	BL Inject 3
T07 S17	17	16	155	45	BL Inject 3
T07 S18	18	17	155	45	BL Inject 3
T07 S19	19	18	165	48	BL Inject 3
T07 S20	20	19	165	48	BL Inject 3
T07 S21	21	20	165	48	BL Inject 3
T07 S22	22	21	150	41	BL Inject 3
T07 S23	23	22	150	42	BL Inject 3
T07 S24	24	23	150	43	BL Inject 3
T08 S01	1		-	-	BL Background / Ambient
T08 S02	2	1	220	61	BL Inject 3
T08 S03	3	2	220	61	BL Inject 3
T08 S04	4	3	220	61	BL Inject 3
T08 S05	5	4	220	61	BL Inject 3

T08 S06	6	5	220	61	BL Inject 3
T08 S07	7	6	220	61	BL Inject 3
T08 S08	8	7	220	61	BL Inject 3
T08 S09	9	8	220	61	BL Inject 3

A.2 C18 Percent Cumulative Data

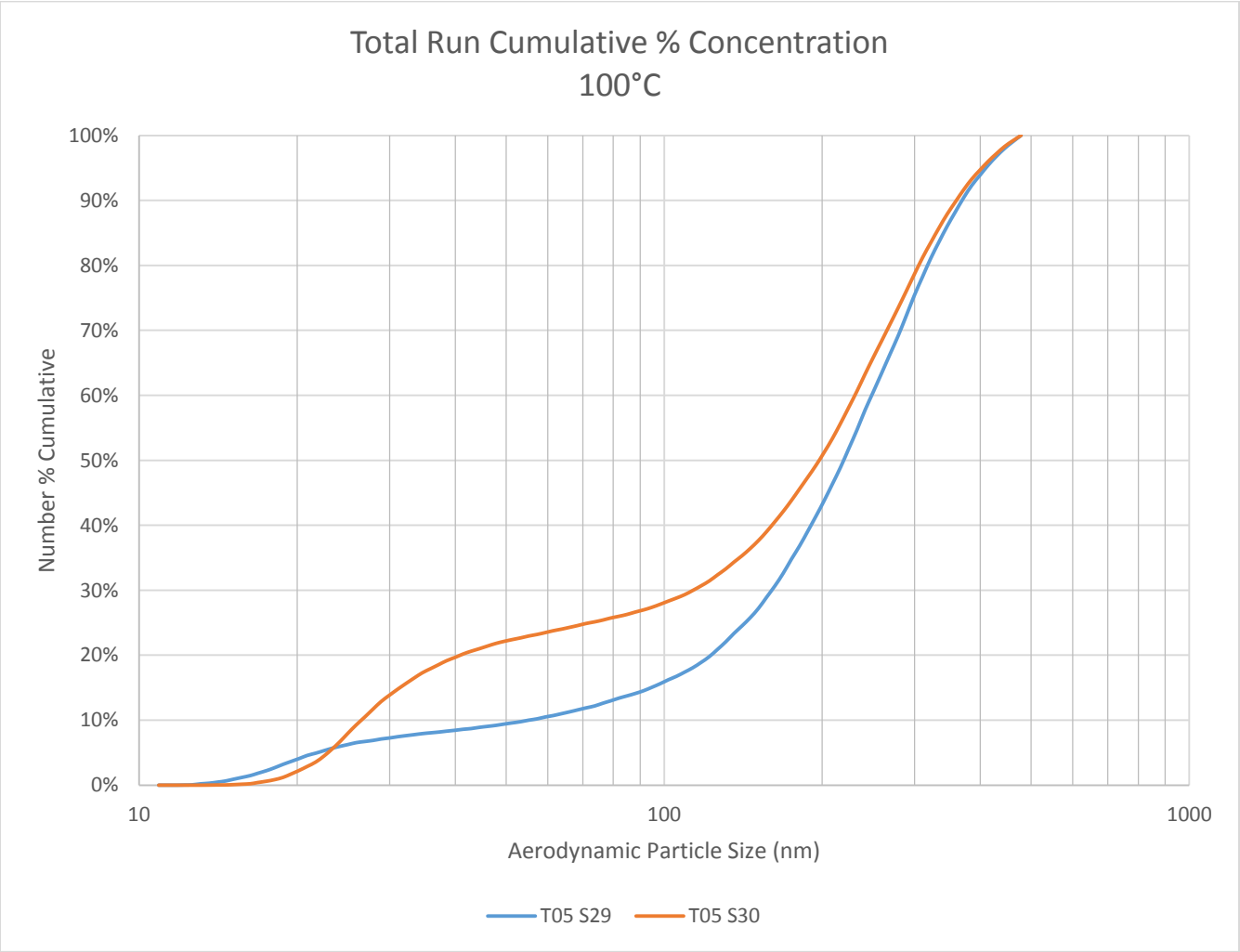

Figure B-1 C18 Cumulative - 100°C

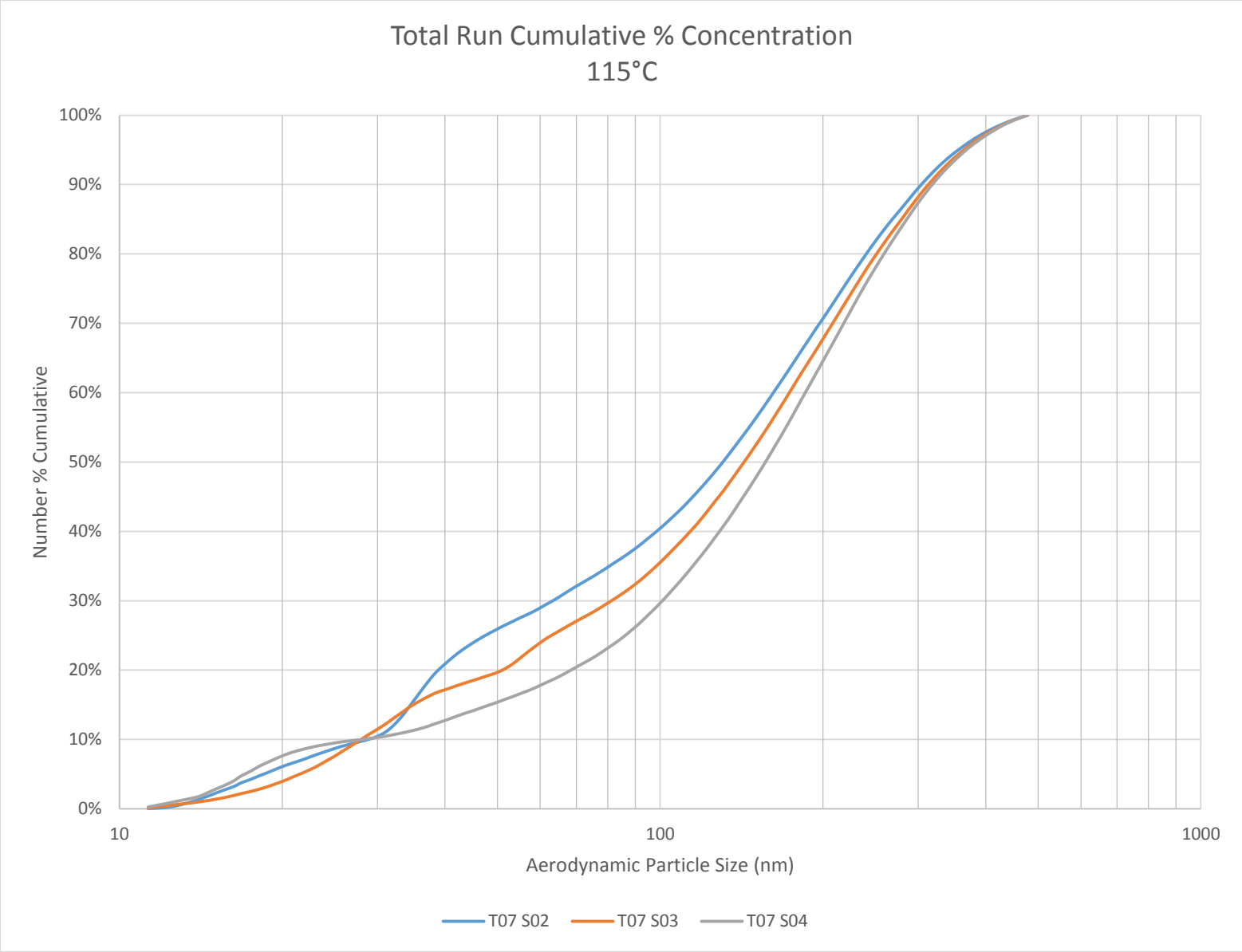

Figure B-2 C18 Cumulative - 115°C

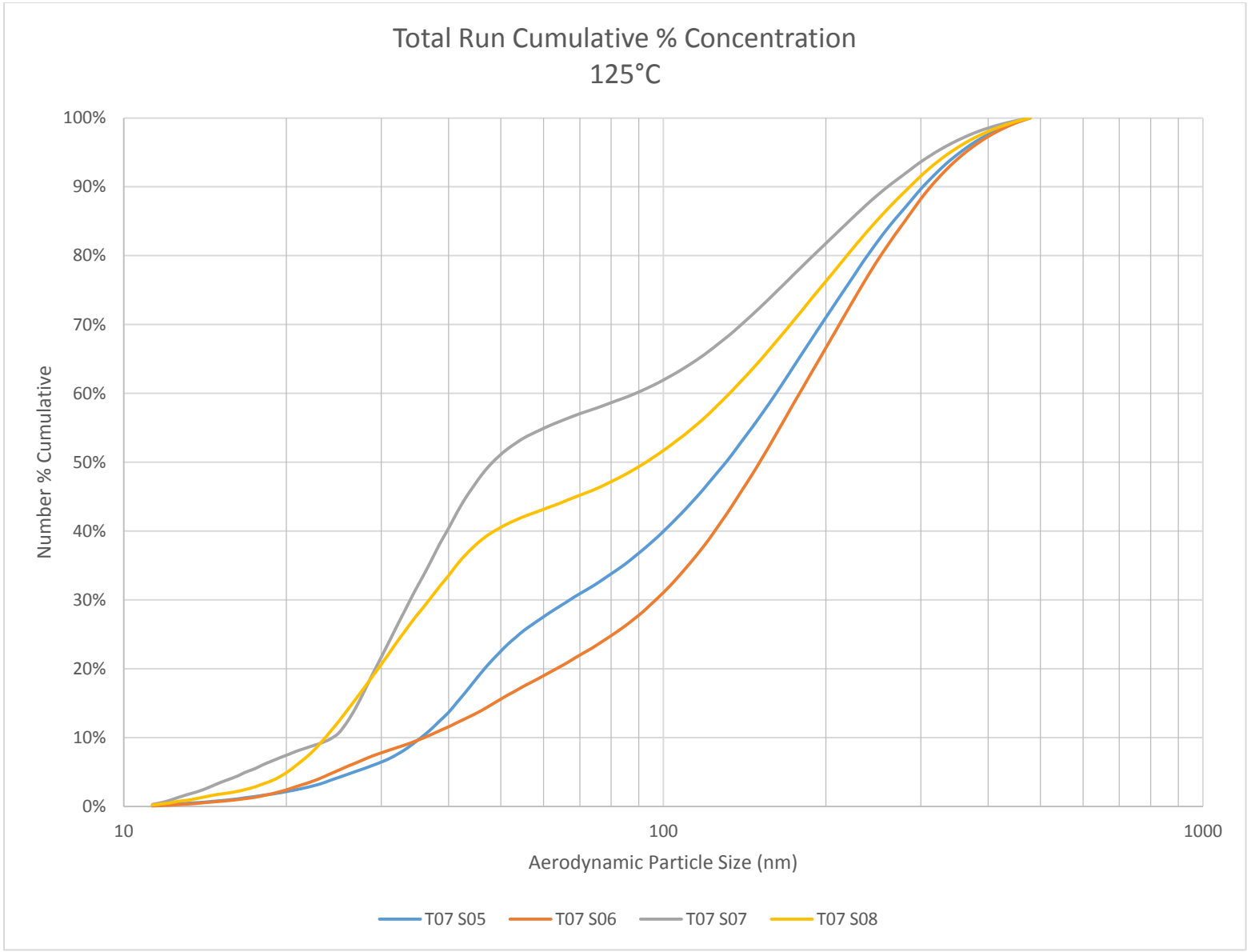

Figure B-3 C18 Cumulative - 125°C

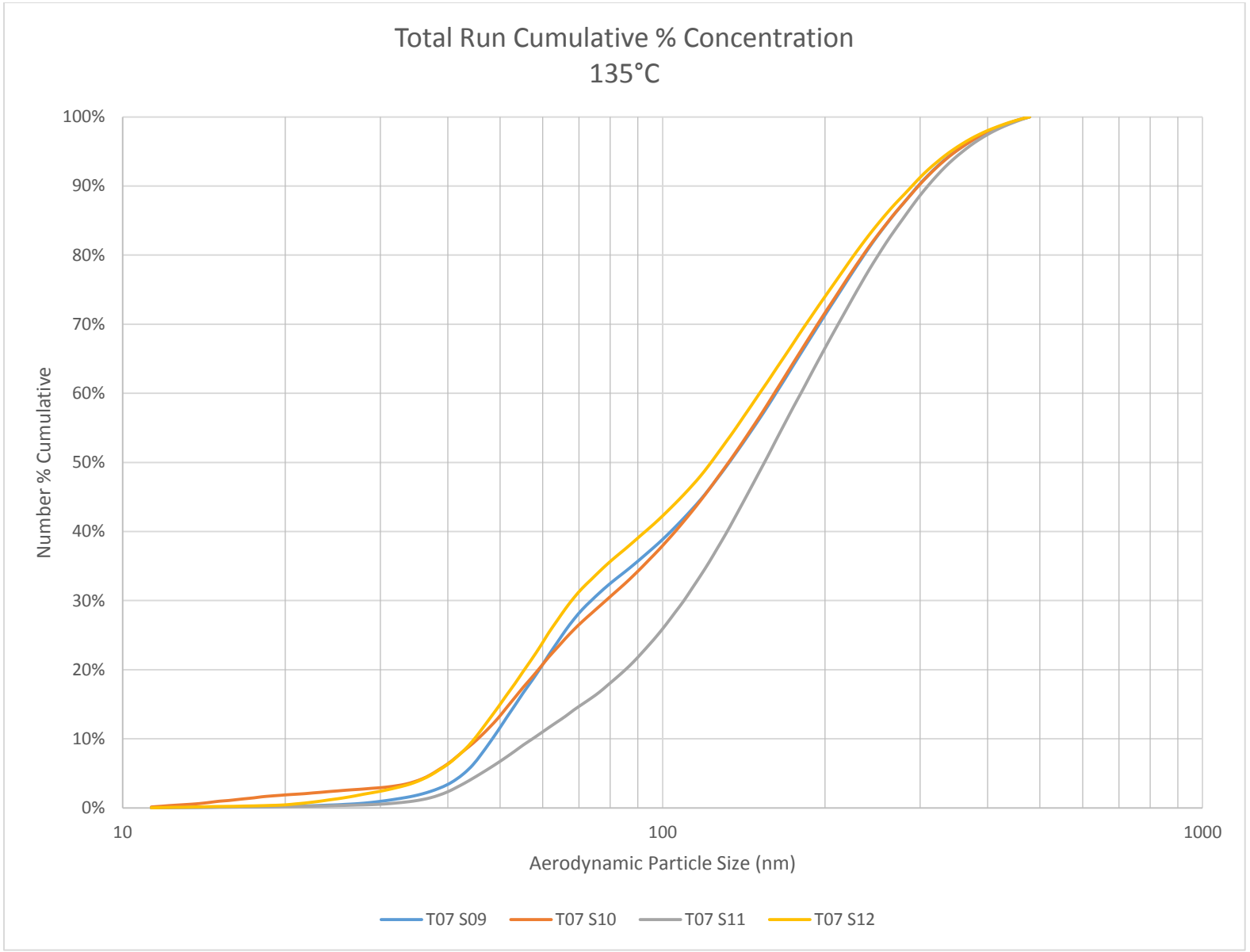

Figure B-4 C18 Cumulative - 135°C

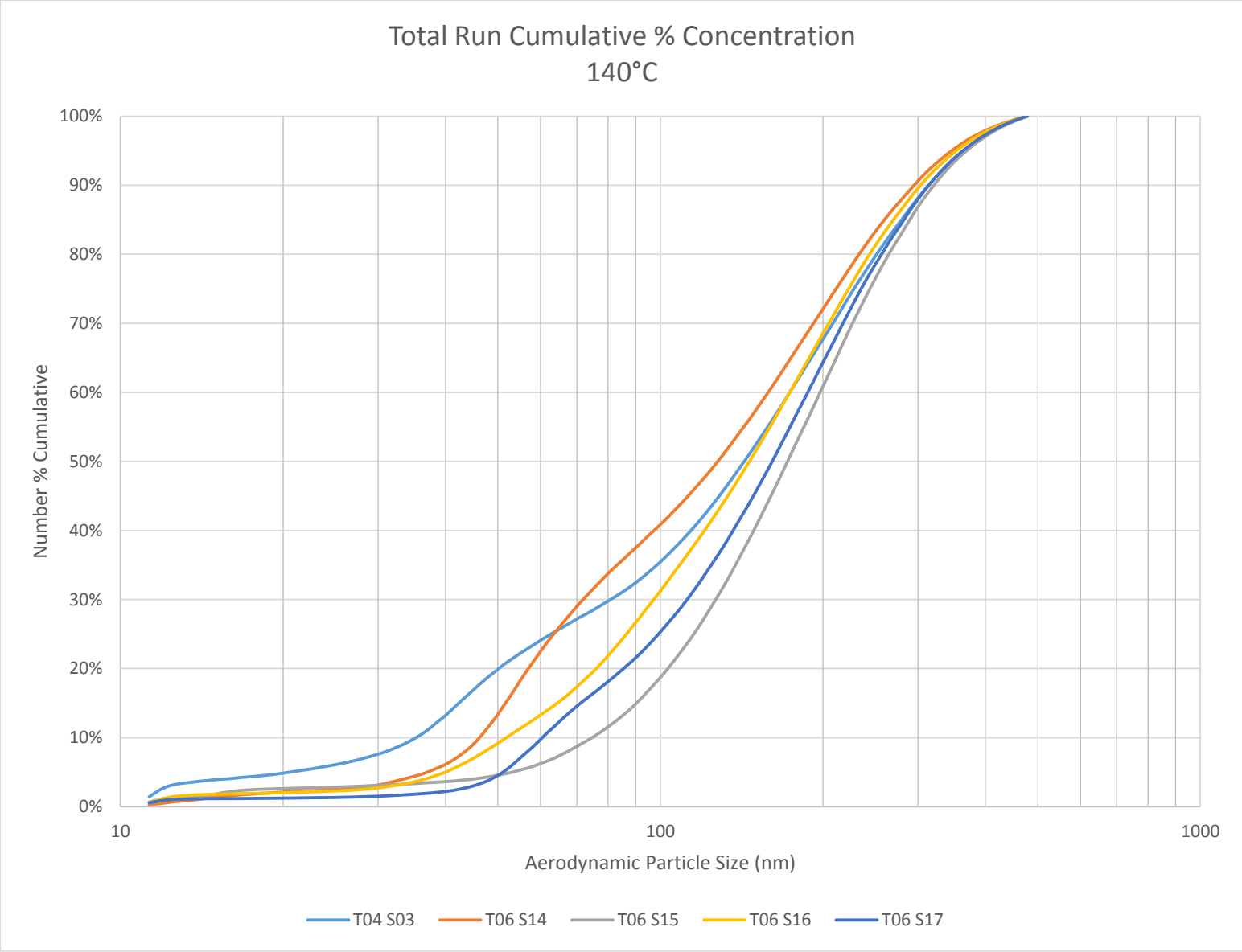

Figure B-5 C18 Cumulative - 140°C

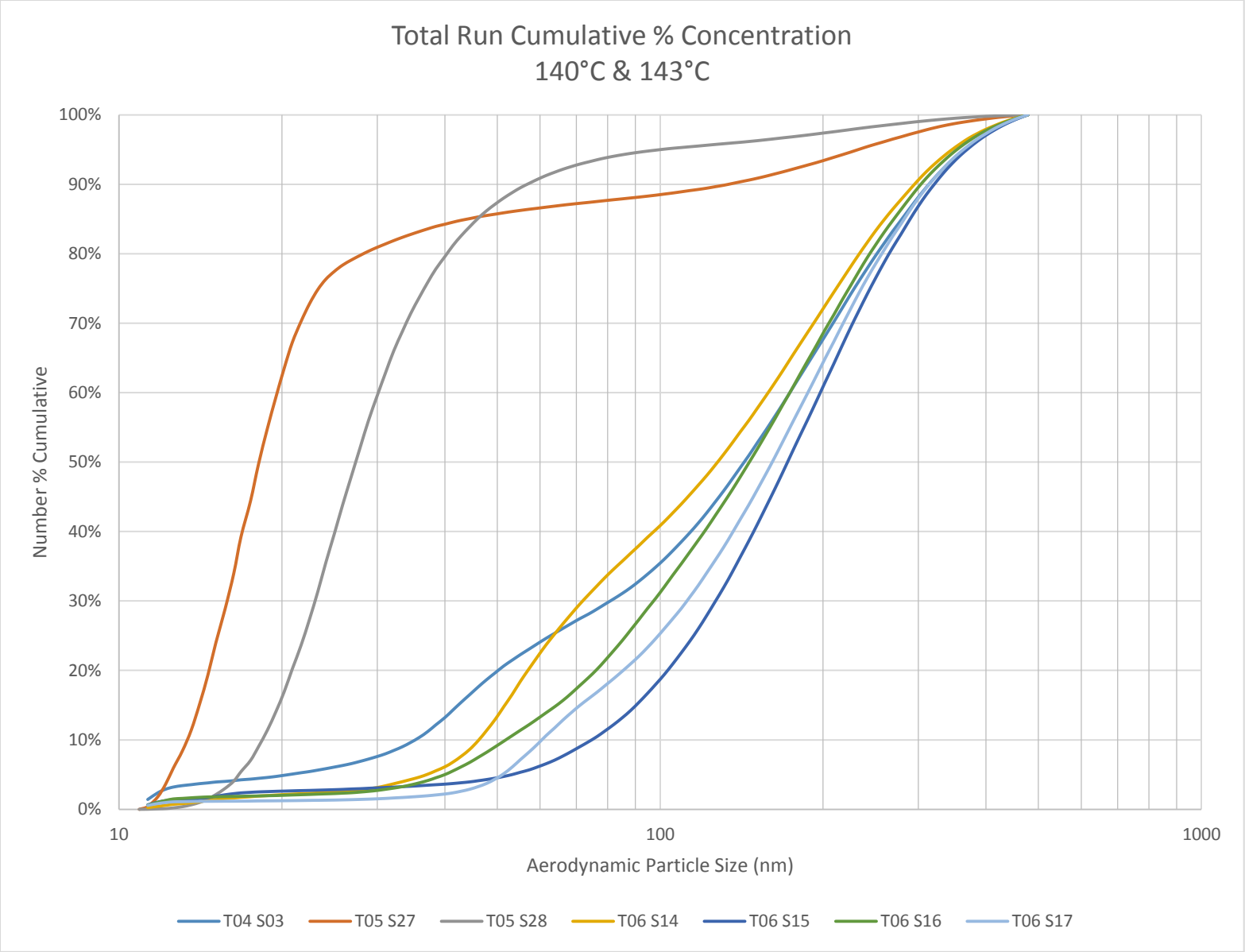

Figure B-6 C18 Cumulative - 140°C to 143°C

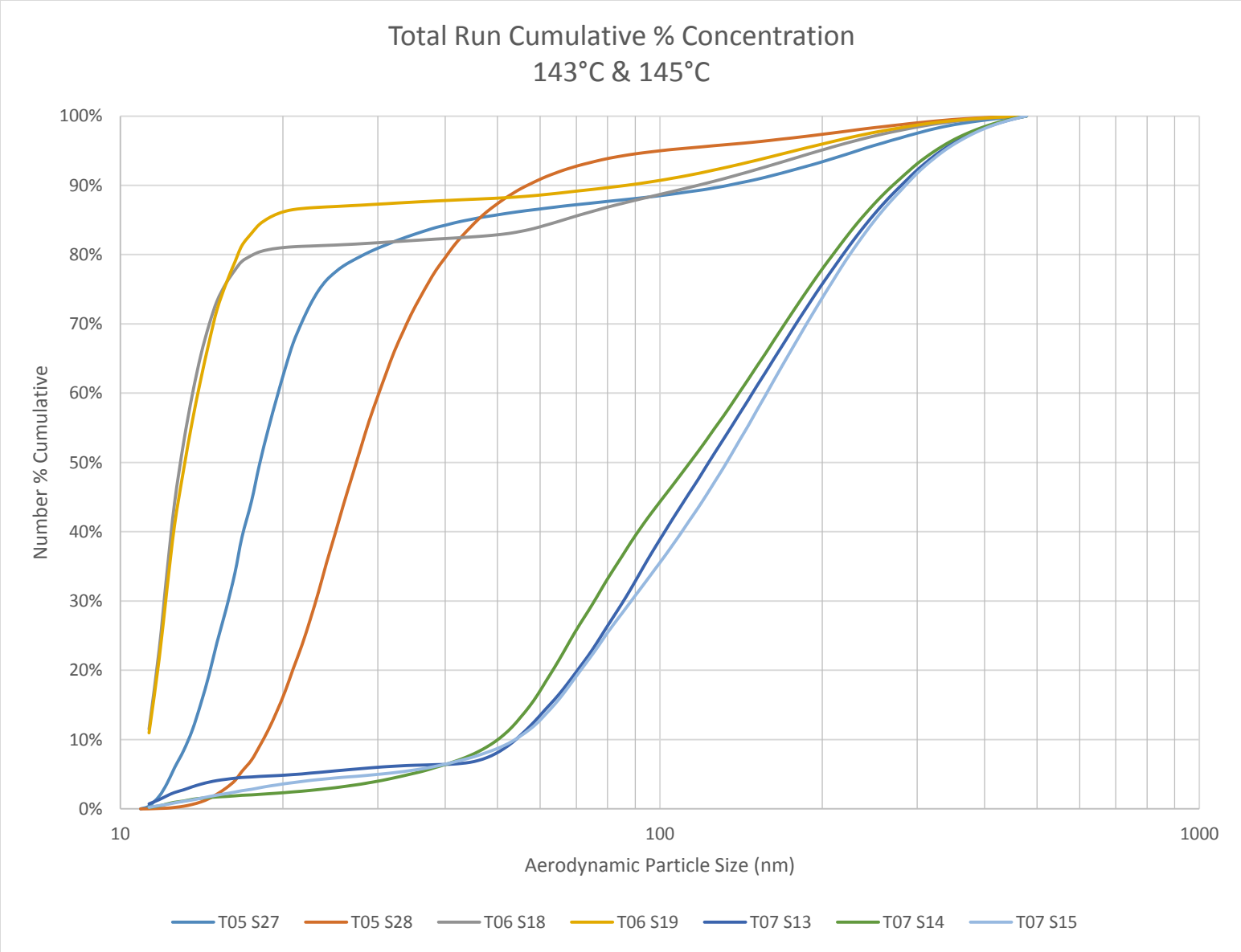

Figure B-7 C18 Cumulative - 143°C to 145°C

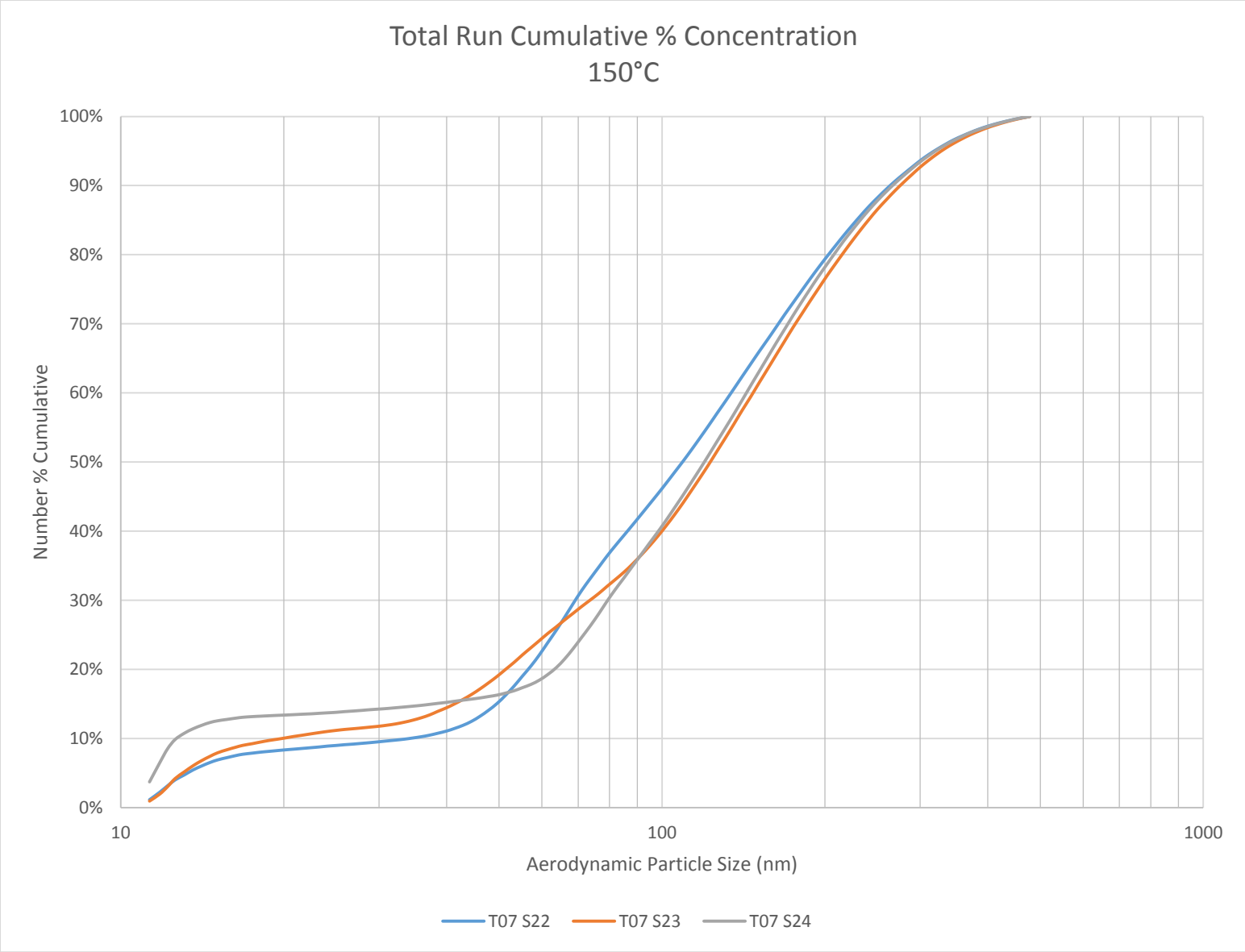

Figure B-8 C18 Cumulative - 150°C

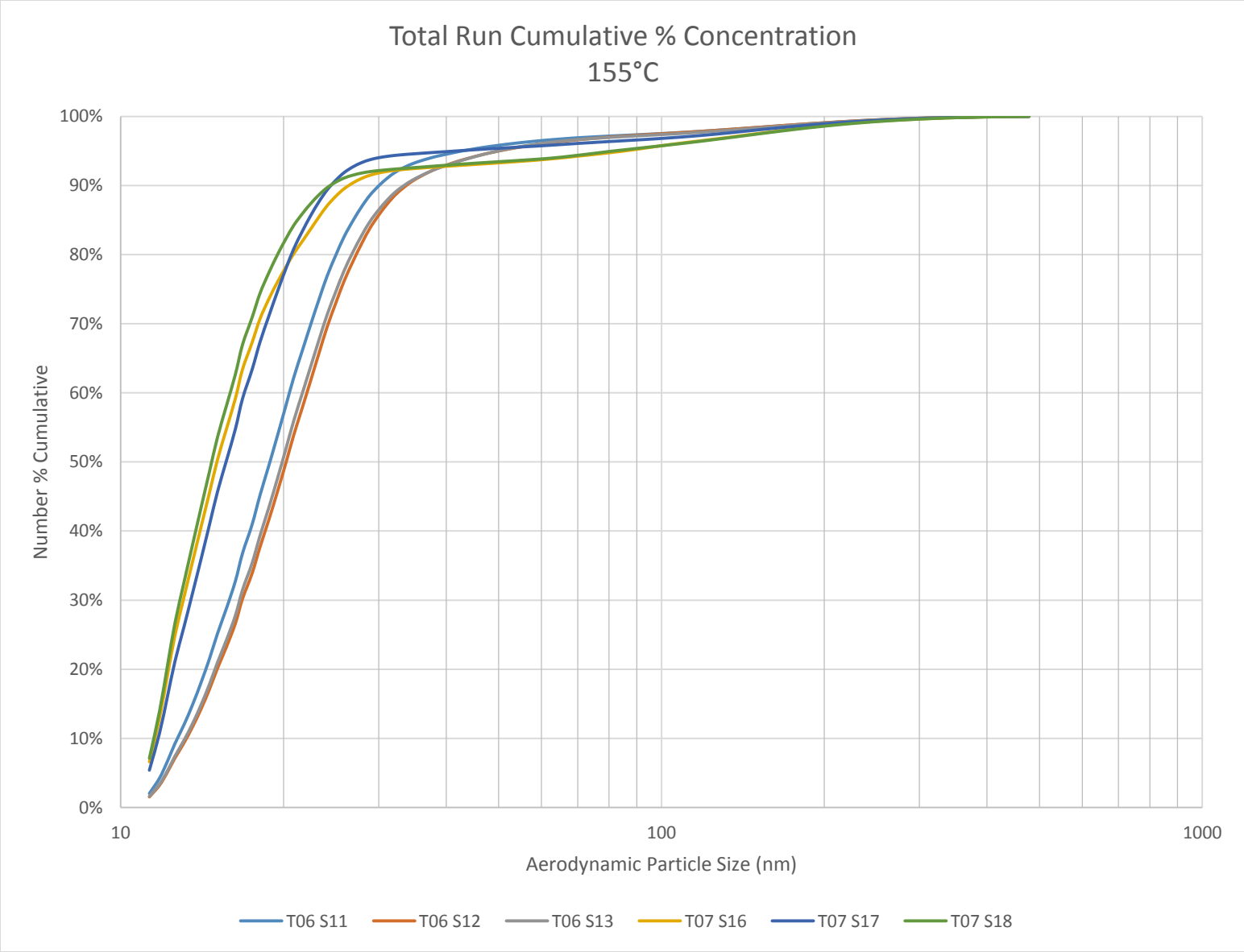

Figure B-9 C18 Cumulative - 155°C

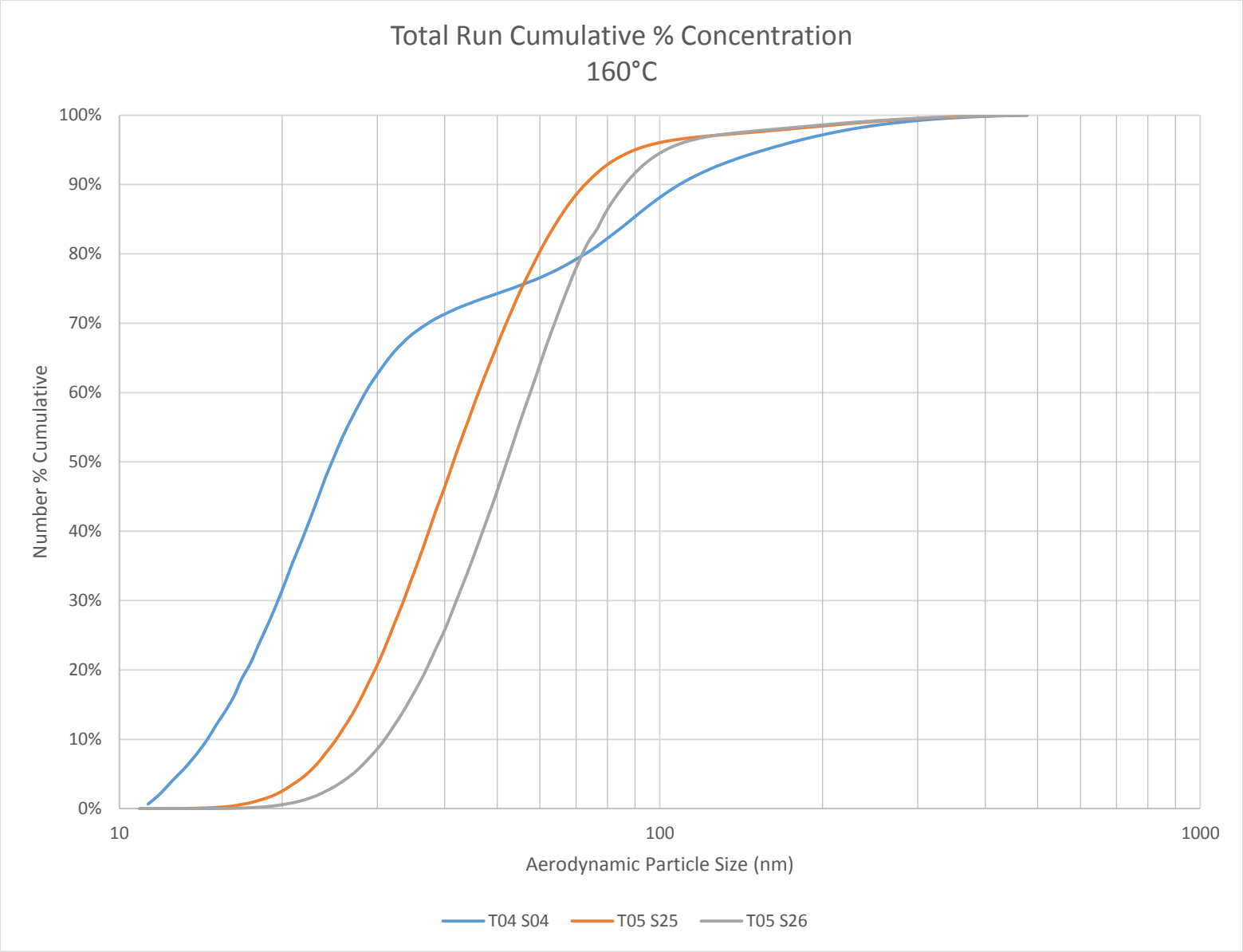

Figure B-10 C18 Cumulative - 160°C

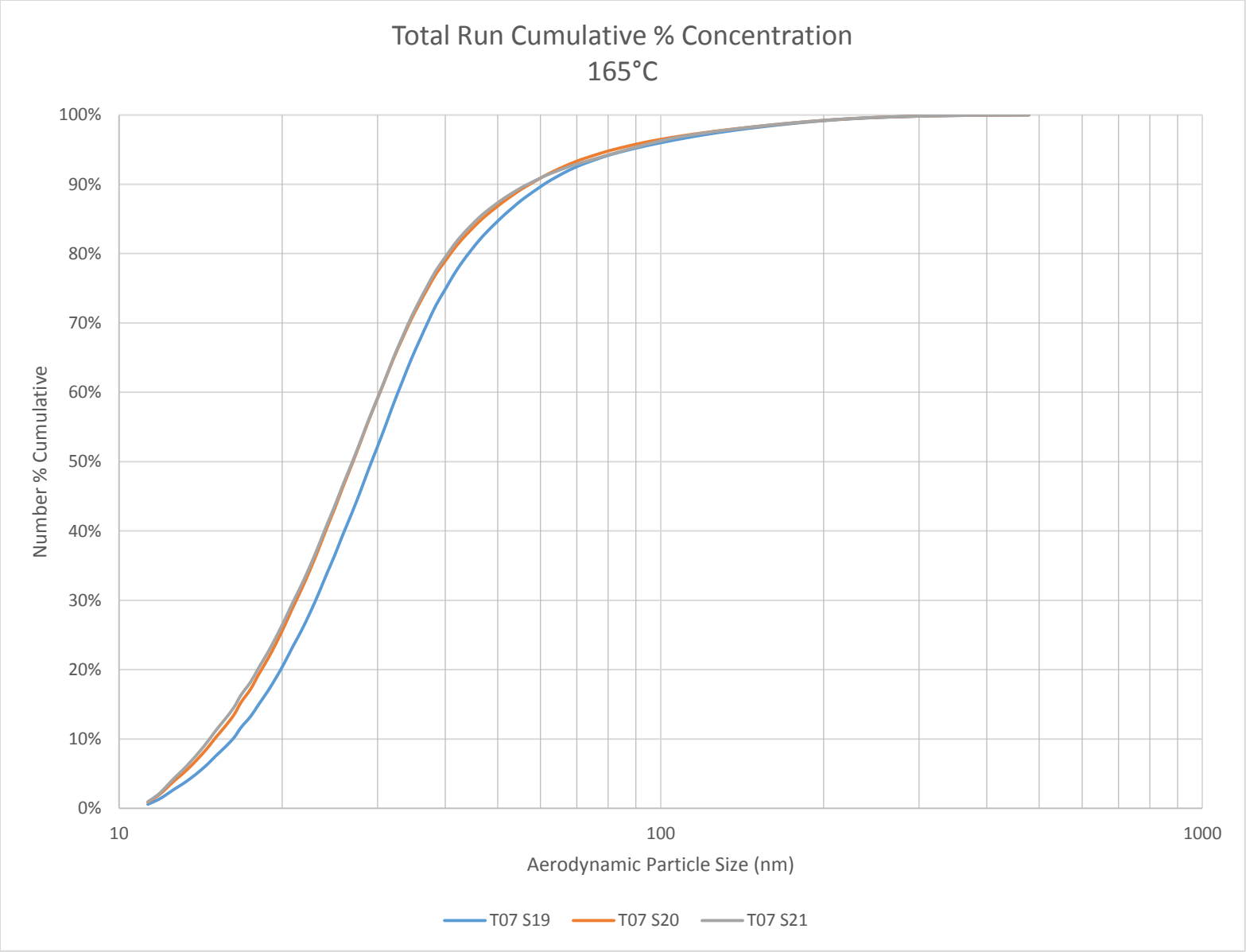

Figure B-11 C18 Cumulative - 165°C

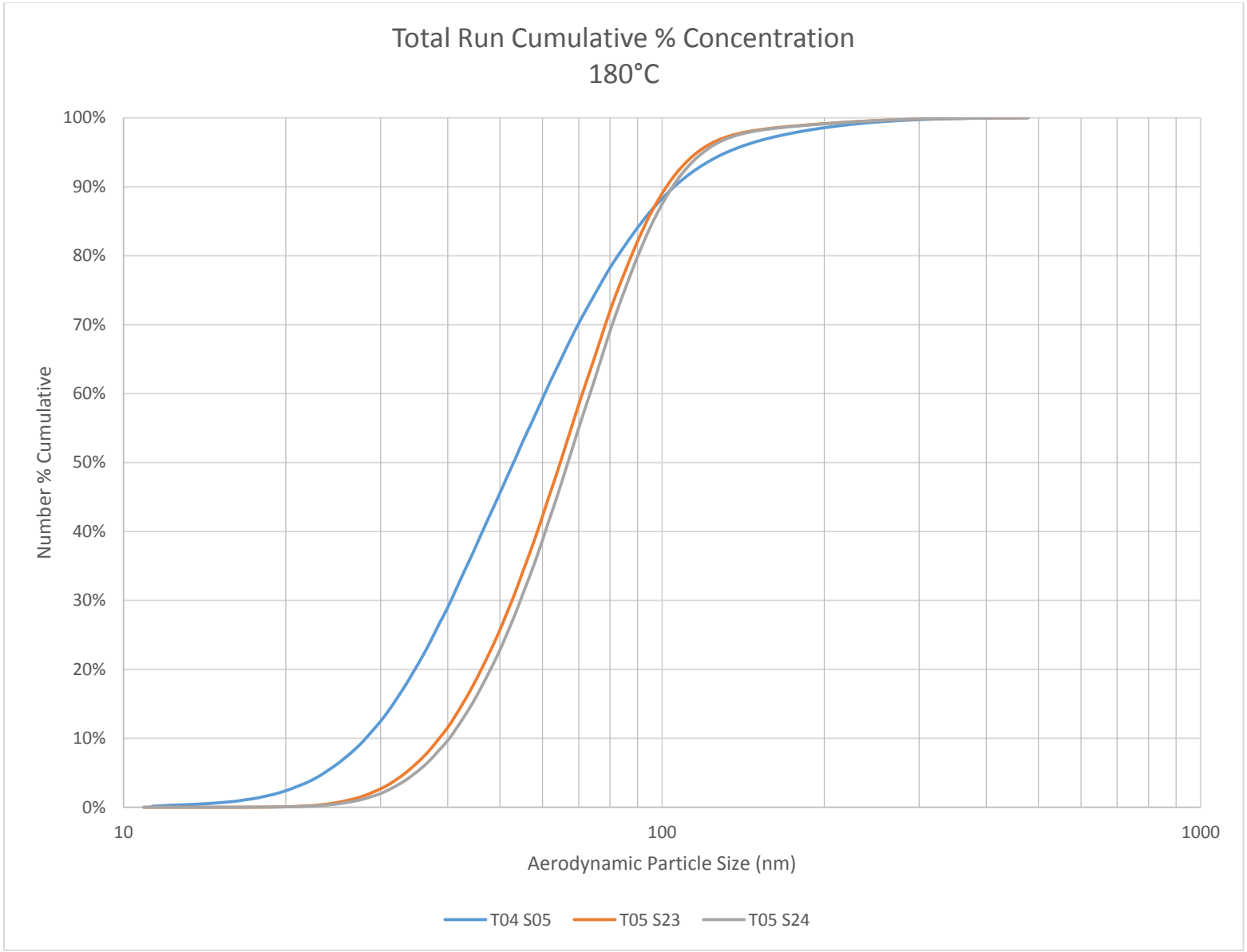

Figure B-12 C18 Cumulative - 180°C

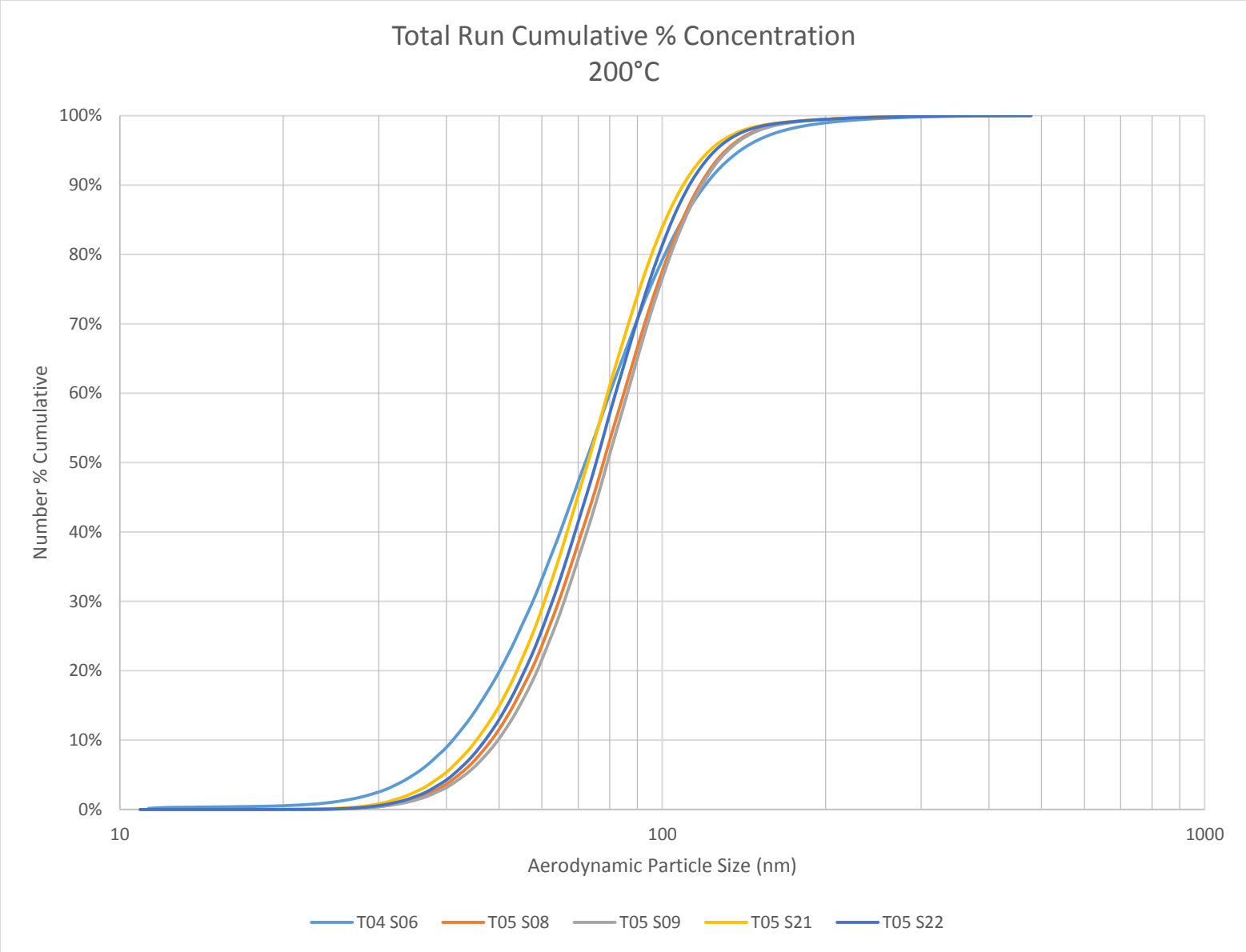

Figure B-13 C18 Cumulative - 200°C

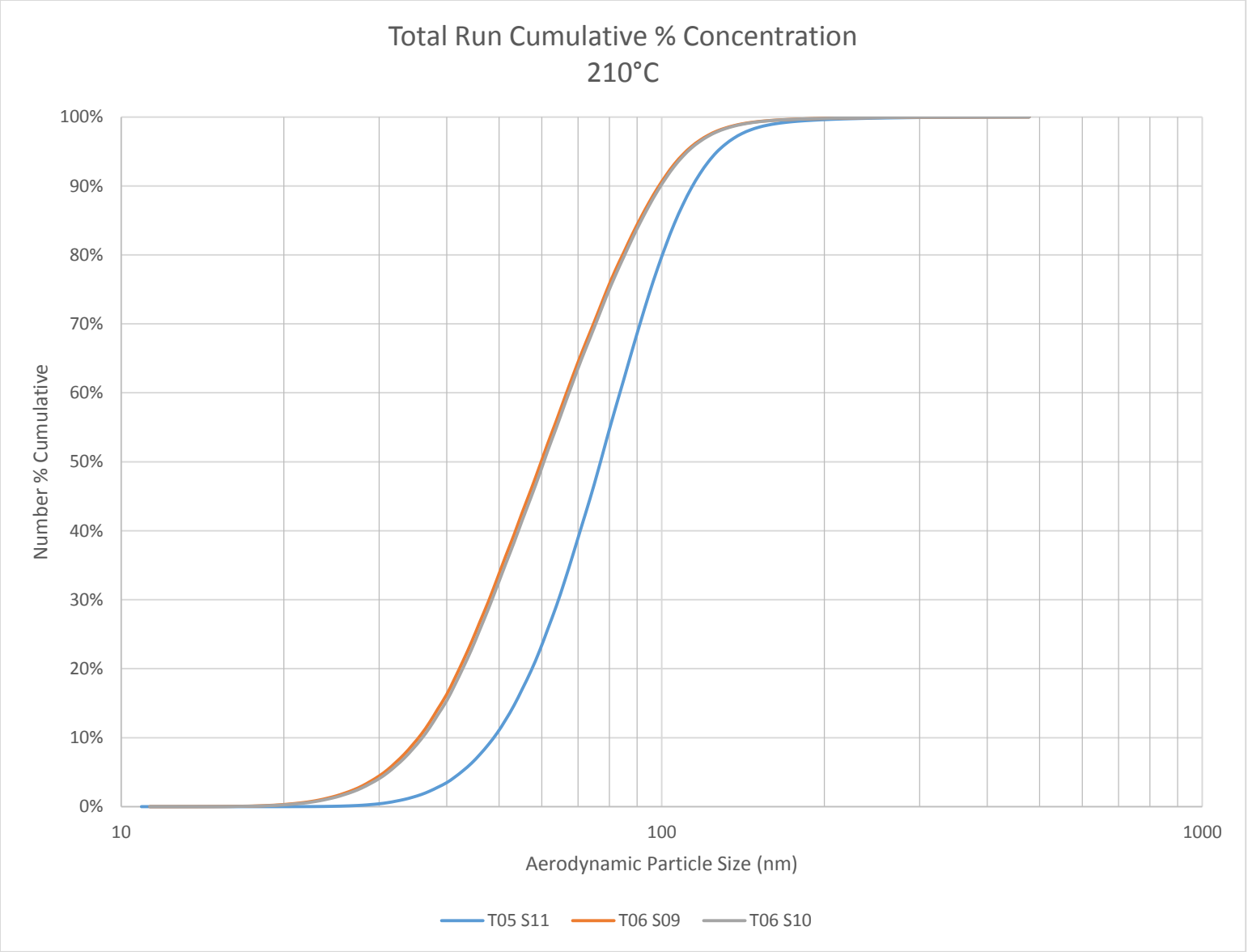

Figure B-14 C18 Cumulative - 210°C

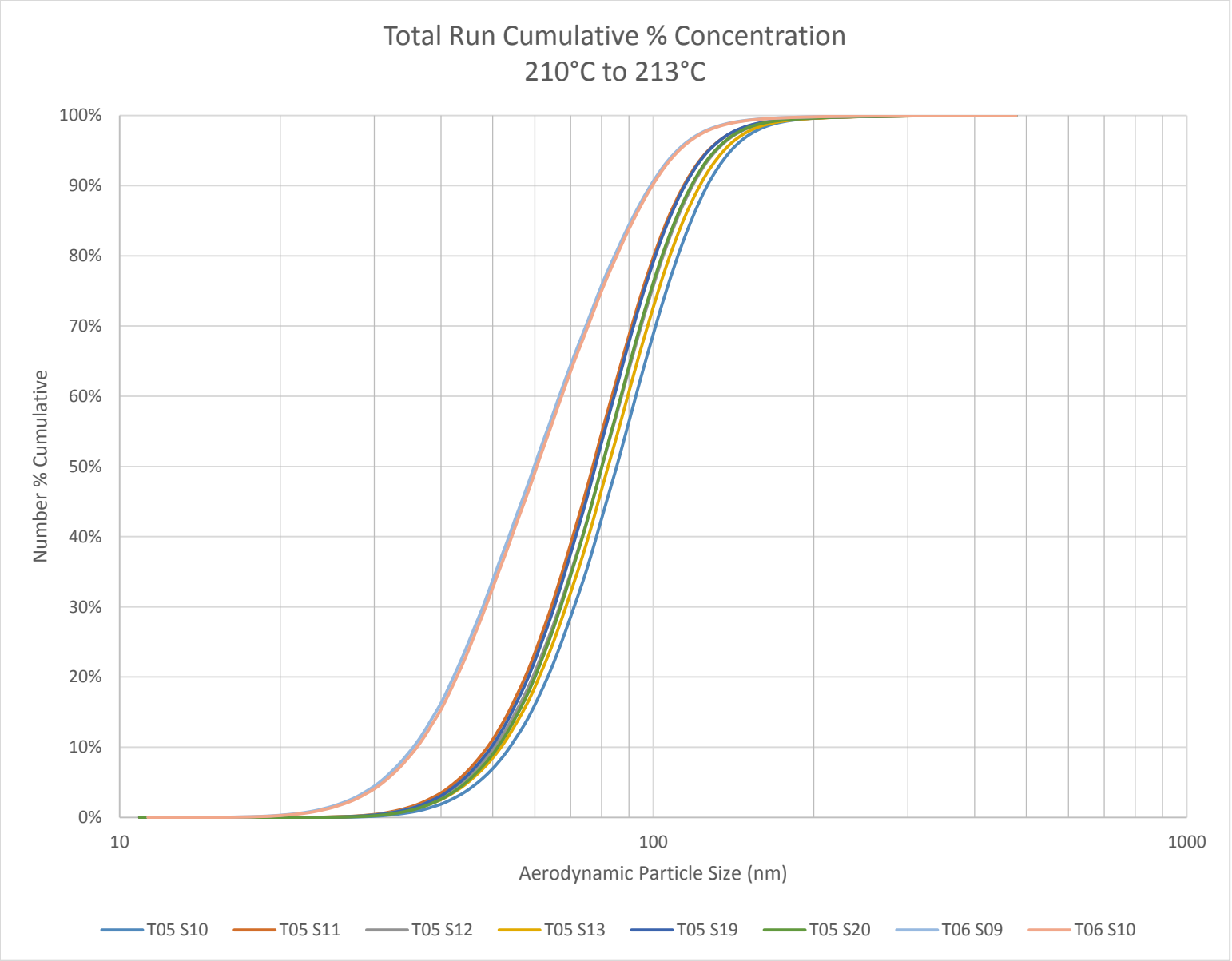

Figure B-15 C18 Cumulative - 210°C to 213°C

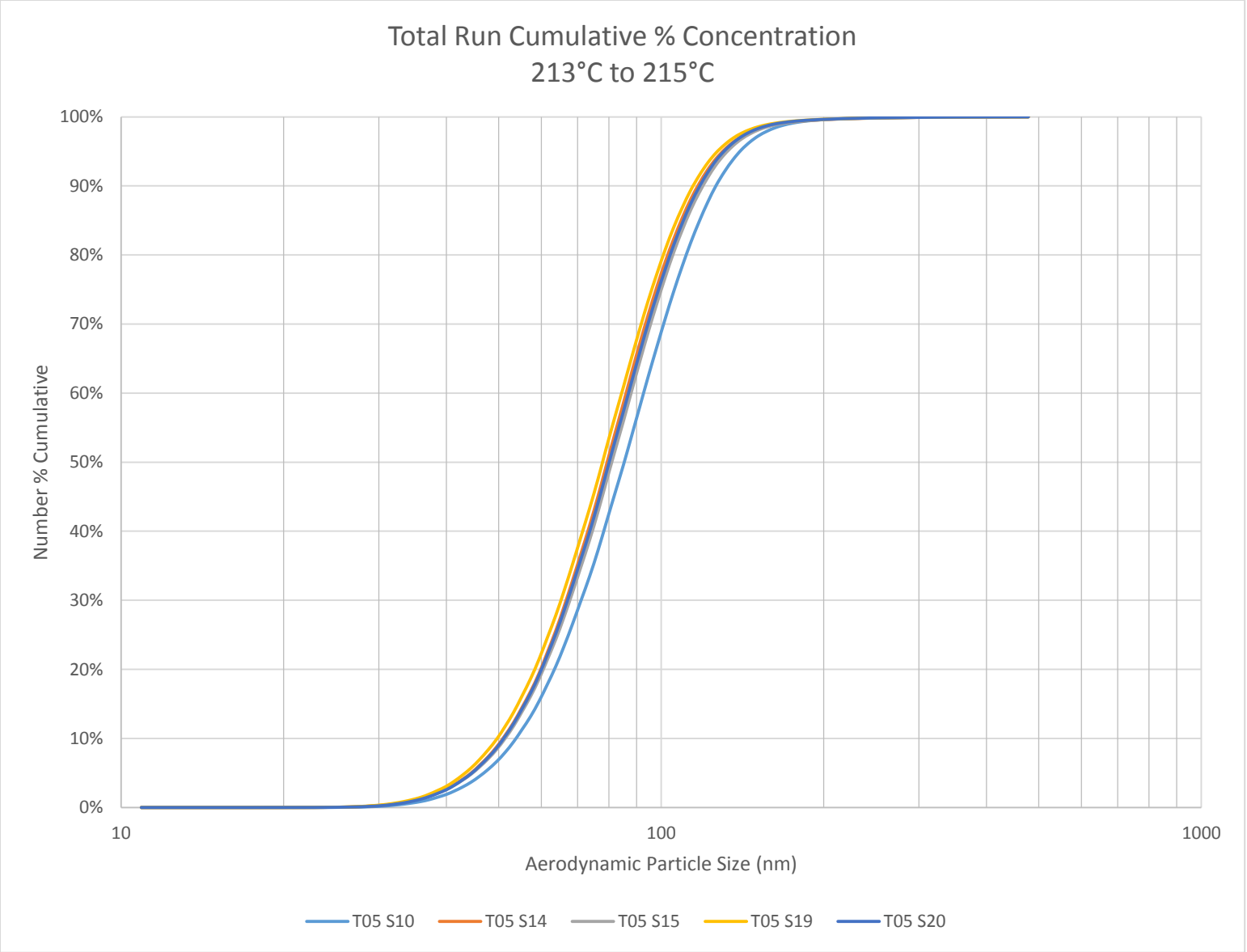

Figure B-16 C18 Cumulative - 213°C to 215°C

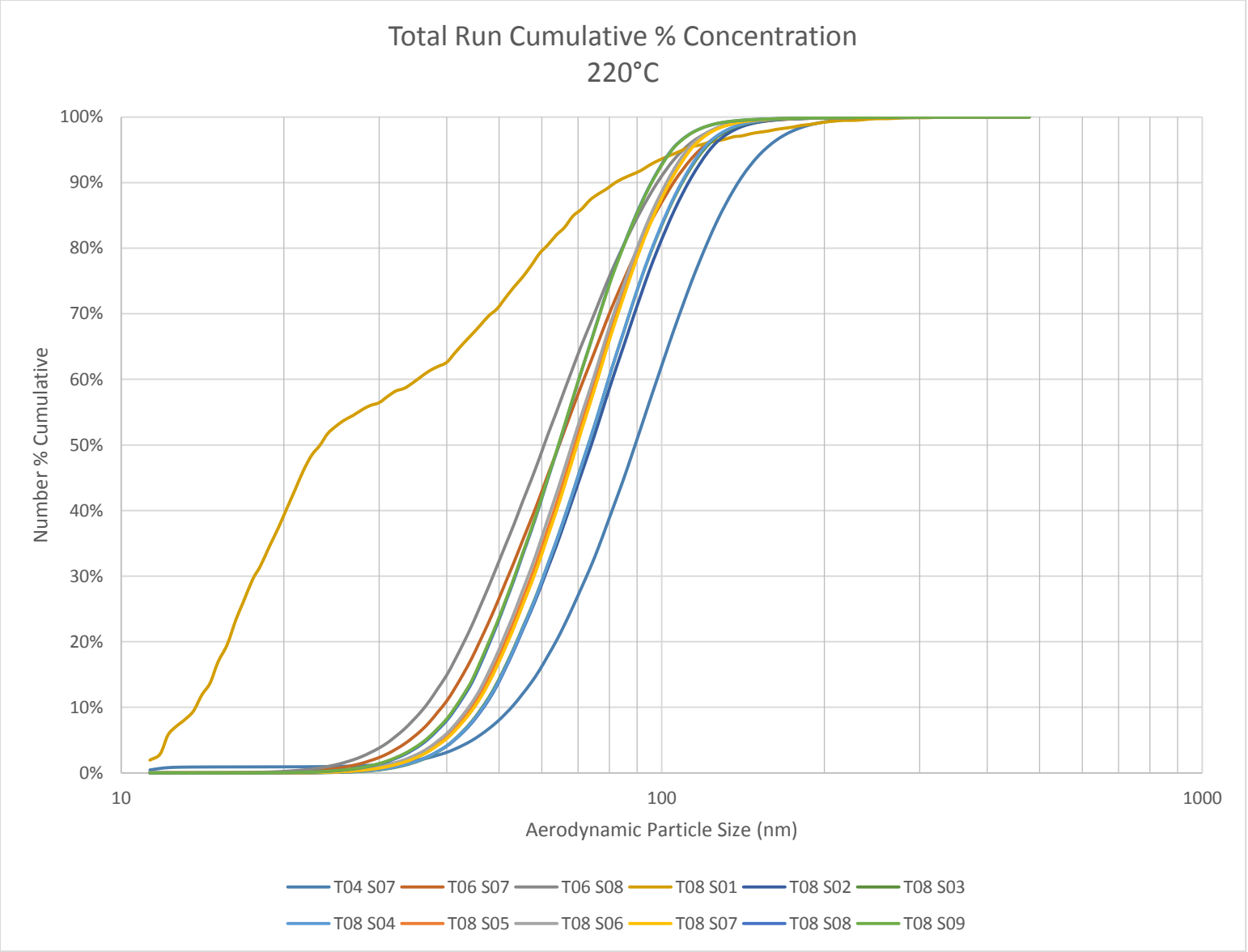

Figure B-17 C18 Cumulative - 220°C

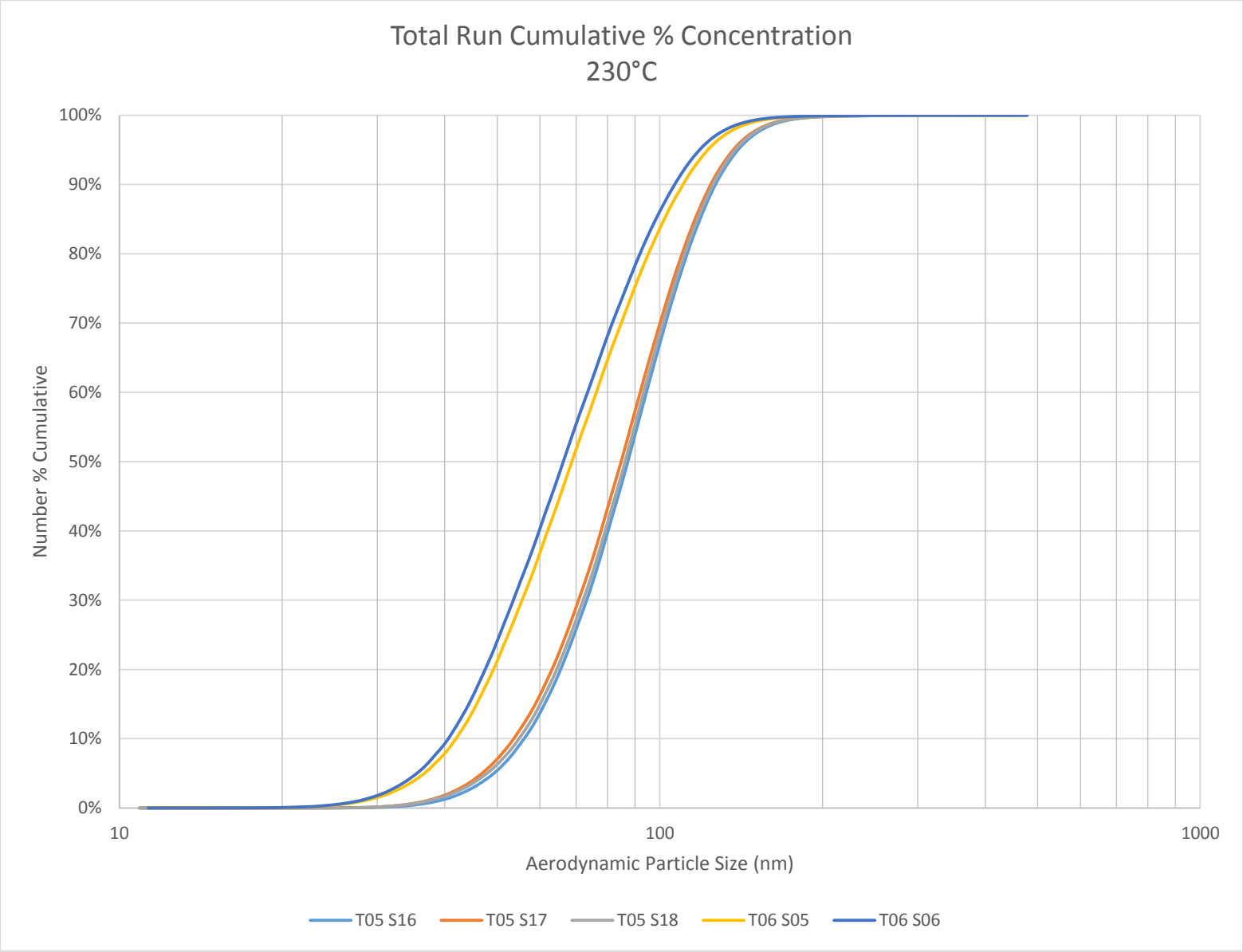

Figure B-18 C18 Cumulative - 230°C

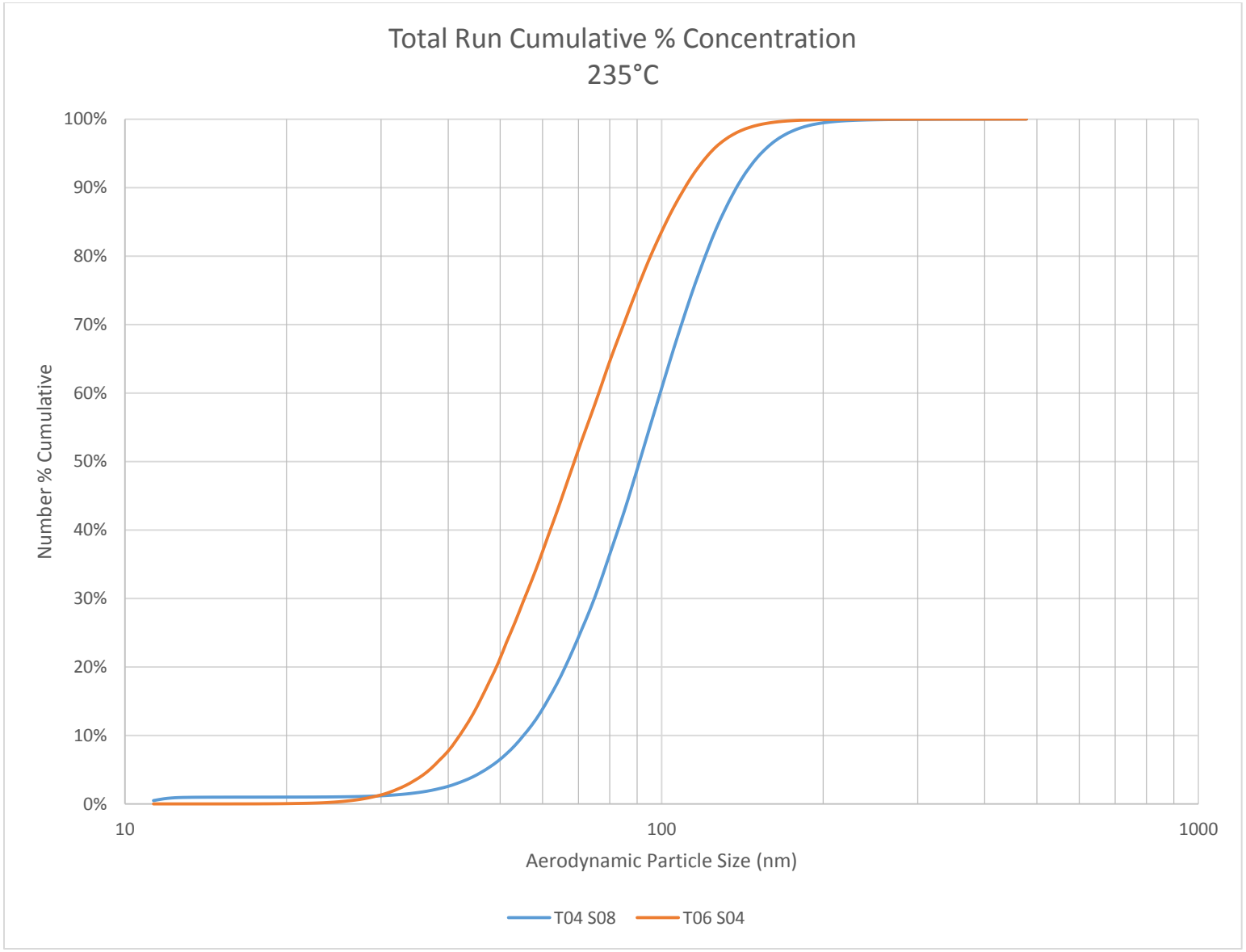

Figure B-19 C18 Cumulative - 235°C

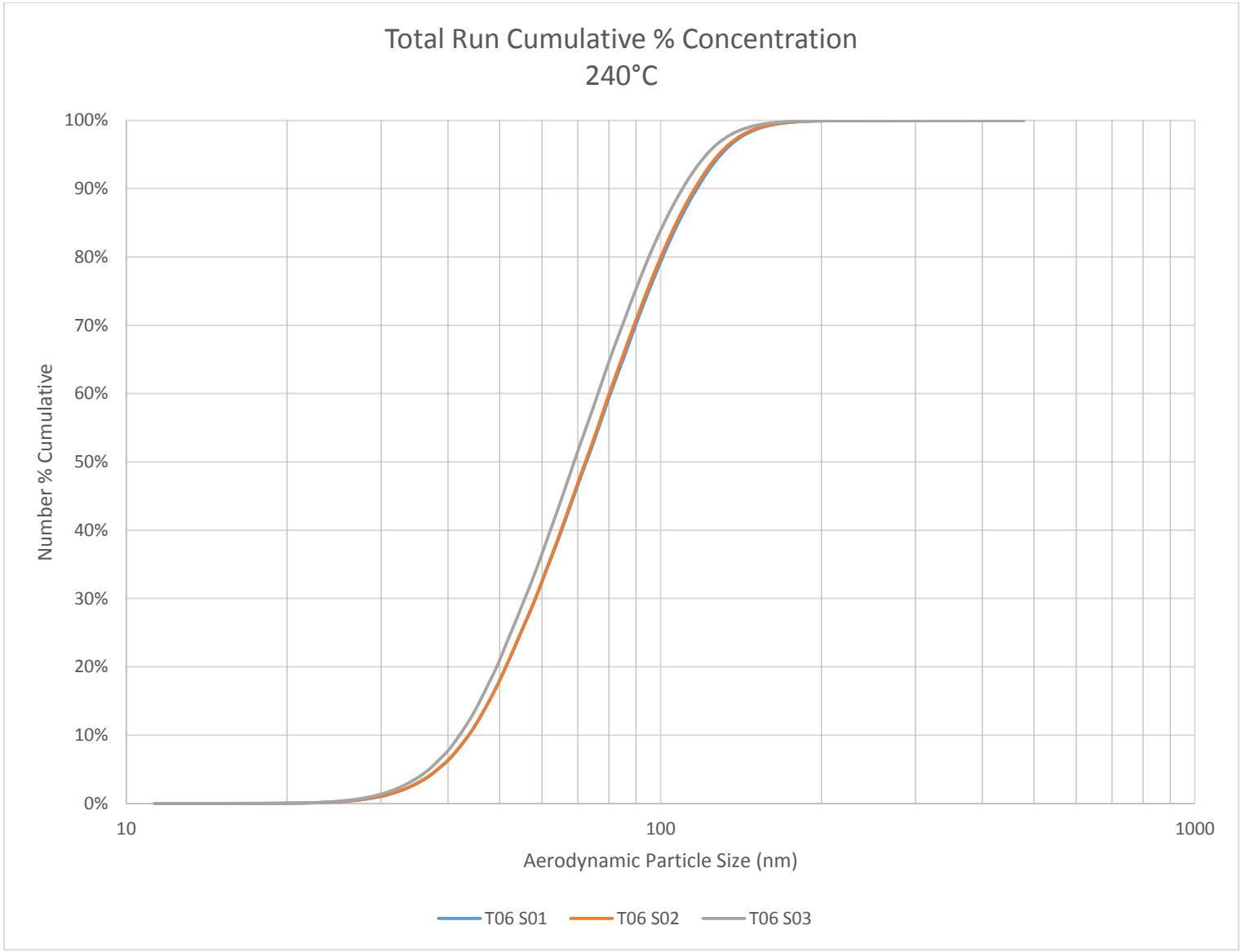

Figure B-20 C18 Cumulative - 240°C

Appendix C: C28B Engine Information & Data

Figure C-1 C28B Test Engine

A.1 Notes about testing

Unfortunately due to various issues including a driveshaft vibration issue the data was not obtained before this thesis was written. This appendix is here for documentation purposes.

A.2 Experimental Setup

The experimental setup of the C28 is almost identical to that of the C18 engine. The main difference is how the bleed air controls work on this particular engine. The bleed air must be vented properly to prevent the centrifugal compressor from surging. Unfortunately this engine did not come with a large portion of the controls that are supposed to be installed by default. Modifications were made to the bleed air line and a sample was only able to be drawn

from on port. However, the residence time is nearly identical and varies by no more than 2ms from the previous engine. The velocities are higher for a longer period, but the lines are kept straighter with fewer bends or turns compared to the sample lines on the C18.

C.2.1 Bleed Air Extraction Line

A single bleed air extraction line was used on the C28B. The other line on the C28B is used for the internal fuel control of the engine. Pressure from the compressor is generally relayed to the fuel governors and the system automatically controls the fuel. Additionally the C28B has only a single centrifugal compressor stage and no axial stages.

C.2.2 Design and Error Estimations

The design error estimations are the same for the C28B engine. No large changes were made and the 0.25in orifice plate was used for testing in order to minimize the bleed air extraction flow rate while still meeting the residence time of approximately 60ms for the bleed air to be cooled.

C.2.3 Process Control and Monitoring

The C28B engine uses the same method of process and control as the C18 used. There is a minor difference in the systems using relays and other electronics. However, none of these systems will influence the particle data being generated.

A.3 Data Analysis

The data for the C28B engine was processed in the same manner as the C18 engine. The custom software written was updated along the way and the information imported into the newer version if errors or useful information updates were found.

Appendix D: Bleed Air C17 Data Information

Record of Discussion

Log Number: PWMSE-VIPR-2013-001

Date: November 13, 2013

Boeing Author: Kurt Matthews

Kansas State Recipient: Jake Roth

Subject: Time to cool

References:

1. Email, Bleed Air – Time to cool, Jake Roth to Kurt Matthews, dated Oct 1, 2013
2. MDC J9135, Rev E, C-17 ECS Description, Operation and Controls, dated Apr 30, 1997
3. MDC J9591, Rev D, Volume 1, C-17 Environmental Control System Design Analyses Report, dated May 30, 1997
4. SAE ARP699, Rev E, High Temperature Pneumatic Duct Systems for Aircraft, dated Dec 1997
5. 17N8N0880, 17N7N0735, 17N6N0680, 17N2N0250 & 17N2N0251, C-17 Pneumatic Ducting Installation Drawings, Engine Compartment to Air Conditioning Packs

Summary: Reference (1) states the following:

I am currently working on a turboprop engine to replicate the bleed air systems that are typical in an aircraft for the oil injection experiment. As such, one of the critical parameters I am looking at is the time it takes for the bleed air discharge from the compressors to the bleed air coolers. Would you know the typical time for this process to take, and or the time that it takes to cool? If you do, is there a large difference between the C17, a typical passenger airliner, and a

smaller plane? If you do not know off hand, would you be able to direct me to literature or somebody that know.

The operating conditions I'm looking at are as follows:

1. Initial Descent from Cruise
2. End of Descent
3. High Pressure to Low Pressure
4. Cruise
5. Top of Climb

The C-17 is a four engine turbojet aircraft. Just considering the inboard engine, the pneumatic duct installation is similar to that of all passenger jet aircraft with an on-wing engine. The air is routed from the engine compressor to a close coupled heat exchanger (precooler) in order to drop the compressed air temperature to safe levels as quickly as possible. The engine compressor temperature can reach values up to 1000F, while the exit temperature of the precooler is modulated to 300F. The distance between the two is roughly 6 ft. The air is then ducted down the wing, into the fuselage and down the the air cycle machine located in the wheel pods. Many commercial passenger planes locate their air cycle machines in the belly under the cargo floor, but at the same general fuselage station as the C-17 machines in the pods. Therefore, the distances of duct run would be similar. The travelled distance from the engine compressor (including precooler) to the air cycle machines is roughly 68 ft. The duct diameter is 5.0 inches for the entire run.

The referenced reports were reviewed to see if there were any specific analyses or flight test measurements conducted to determine the air velocities within the pneumatic distribution

ducting. There were none found. Reference (4) stipulates a maximum design velocity of 0.20Mach (217 fps) inside any pneumatic duct. This standard is meant to avoid resonance issues with bellows and noise in the system. Since this standard is routinely met, it can be stated that at no point in the system the velocity will be higher. A senior engineer involved in the original analyses and flight test was contacted to confirm this was the case.

Five operating conditions are of interest, but for the C-17, these actually reduce to (3) sets of flow rates. Operating conditions 1), 4) & 5) have a flow rate on the order of 34 lbm/min, condition 2) is 45 lbm/min and condition 3) is 74 lbm/min. The regulated system pressure for all cases is 34 psig.

Two very rough calculations were performed looking at the 74 lbm/min and 34 lbm/min flow rates. Please note that friction, bend and other loss affects such as butterfly valves and the like were not considered. The purpose was only to get a rough idea of internal duct air velocity and compare that to the SAE requirement. The calculated velocity for the 74 lbm/min flow was 196 fps and the 34 lbm/min flow was 98 fps. That falls within the requirement, so it's a good starting point.

Utilizing those velocities and just looking at overall length (no other losses from walls, bends, tees, valves, etc) the time for the air to transit from the engine to the precooler is less than a second. The time for it to transit from the engine to the air cycle machine is less than 2 seconds.

Considering the losses, it can be safely said that the time it takes the air to go from the engine compressor to the precooler outlet would not exceed 1.0 seconds. The time to go from the engine to the engine compressor to the air cycle machine would not exceed 5.0 seconds. The time for the air to pass through the air cycle machine itself (compressor, intercooler, turbine) is not published, but I guess would be another 2-3 seconds.

The C-17 values should compare well to other passenger aircraft in its class with underwing engines. Since the velocities are relatively high, only a few seconds would separate a 737 from say a much larger 777. Turboprop aircraft may be somewhat slower due to the lower bleed flow rates and pressures, but that would be offset by the shorter distances. If there is a written comparison between different classes of aircraft, the author is not aware of it.

In summary, a good estimate would be in the 5-8 second range. If any experiments are conducted, perhaps a wider band to determine sensitivity is in order.

Appendix E: Fractional Concentrations Calculation Routine

This document details some of the calculations of the items below:

5/29/2013 15:19:50	5/29/2013 15:22:05	5/29/2013 15:24:20	5/29/2013 15:26:35	5/29/2013 15:28:50

Outputs

$D_p := excel_{\text{“A23:A128”}}$ $N_c := excel_{\text{“U23:U128”}}$

$N_{per} := excel_{\text{“T23:T128”}}$

Percent of Particles per Dp

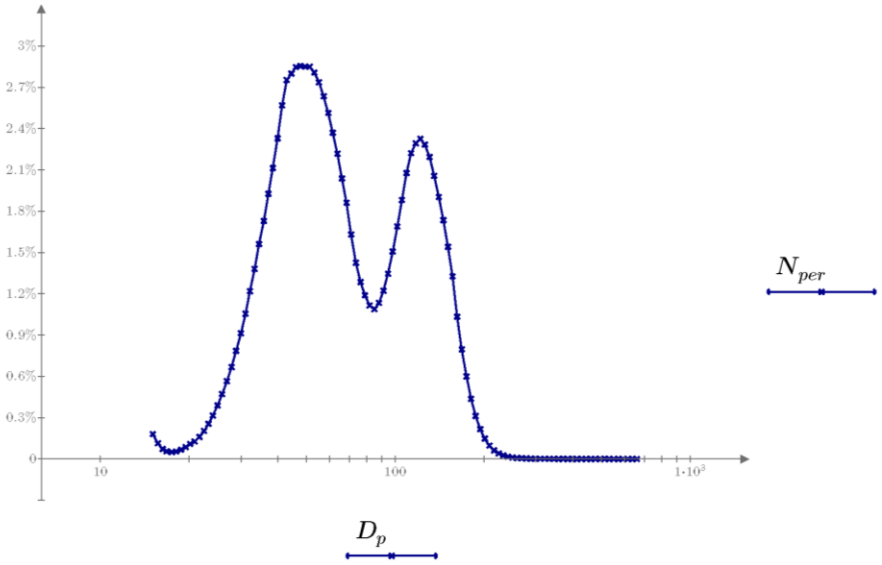

Cummulative Percent of Particles

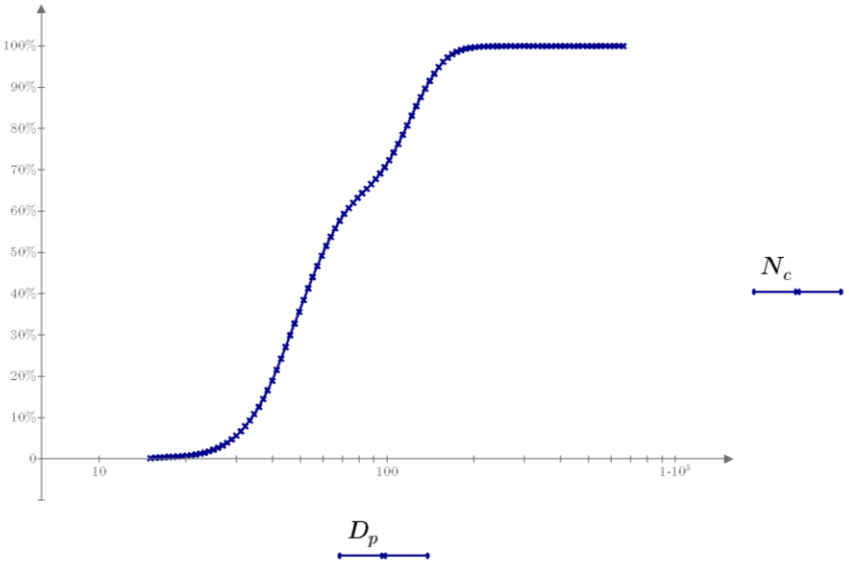

$$range(D_p) := \left\| \begin{array}{l} Vec \leftarrow \dfrac{0 \cdot (\max(D_p) - min(D_p))}{\text{length}(D_p)} + min(D_p) \\ \text{for } i \in 1 .. \text{length}(D_p) \\ \quad V \leftarrow \dfrac{i \cdot (\max(D_p) - min(D_p))}{\text{length}(D_p)} + min(D_p) \\ \quad Vec \leftarrow \text{stack}(Vec, V) \end{array} \right.$$

Defining the B-Spline:

One using the Midpoint Diameter

Other using a linear range

$b := \text{Spline2}(D_p, N_c, 3)$ $\quad \text{DWS}(b) = 2.271$

$sp := \text{Binterp}(D_p, b)^{\text{T}}$ $\quad sp_{rng} := \text{Binterp}(range(D_p), b)^{\text{T}}$

Defining a cubic spline fit as below:

$c := \text{cspline}(D_p, N_c)$

$fitc(x) := \text{interp}(c, D_p, N_c, x)$ x is the independant variable of evaluation

$$dfitc(r) := \frac{\overrightarrow{\text{d}}}{\text{d}r} fitc(r)$$

Defining the Cubic Spline Fit for the percentage vs particle size

$nper := \text{cspline}(D_p, N_{per})$

$fit_{nper}(x) := \text{interp}(nper, D_p, N_{per}, x)$

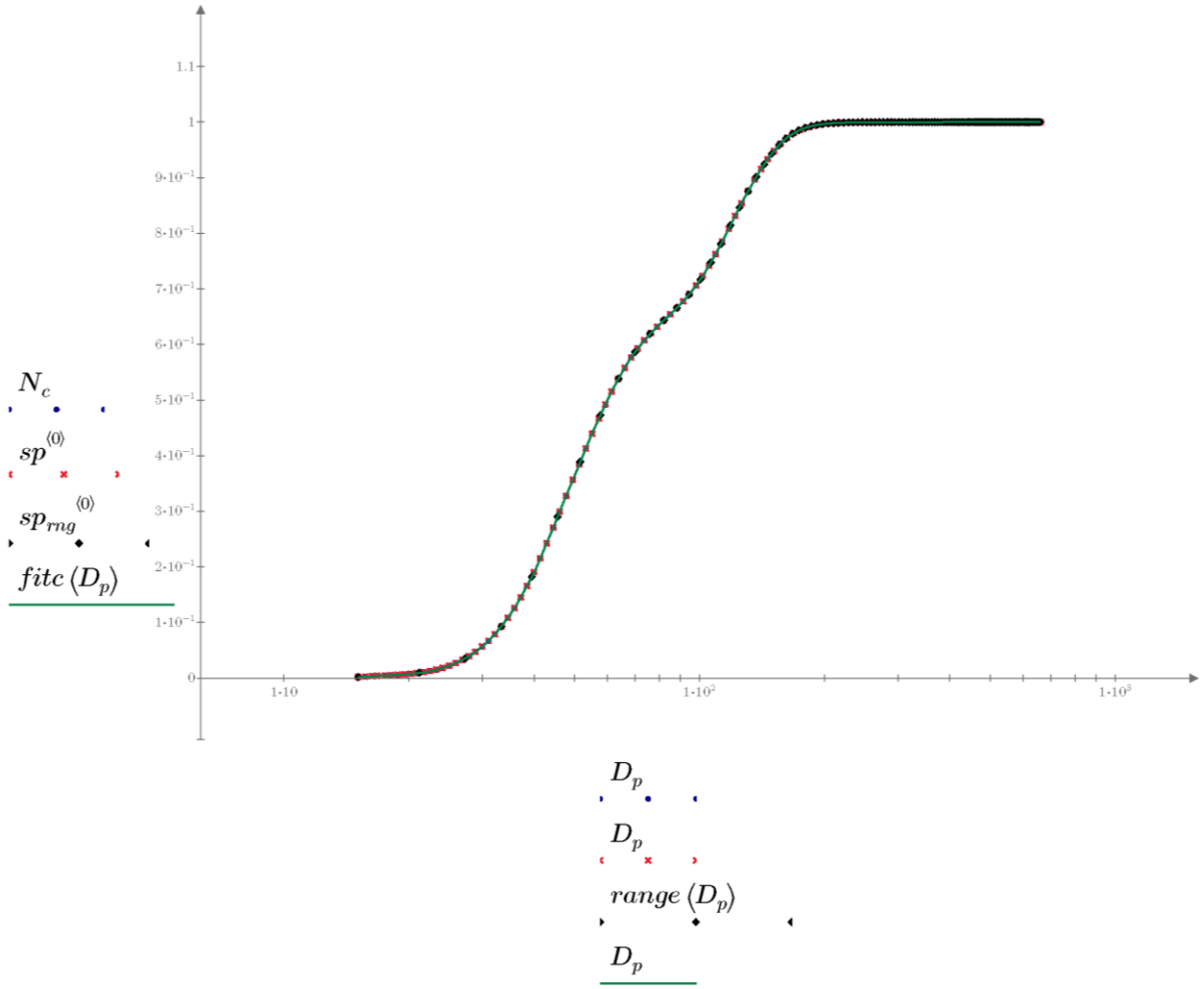

As we can see, our 3 curves fit the data very nicely. The sp line has the logrithmic spacing, as given by the diameter midpoint vector of TSI's equipment. The sp_{rng} line has the linear spacing which has divisions equal to the number of elements given. The last line is a cubic line fit.

The entire reason for expressing the data this way is due to the fact that the bins are spaced logrithmically. The is due to the observed data that most of the particles occur as smaller ranges and aerosols generally tend to have a logrithmic distribution. As such however, when looking at the data, it can be misrepresented due to this bin spacing. The example is if we had a constant distribution of particles, the bins with larger bounds will pick up more particles and respresent that we have more at the higher range, when infact this is not correct. It is also not a benificial to express the values as a logrithm, as that would also skew the data as $ln(x)$ is not a constant. As such, we are normalizing the data by removing the bin bounds by taking the derivative.

The area under the derivative curve should be equal to one, as the cummulative concentration is equal to 1.

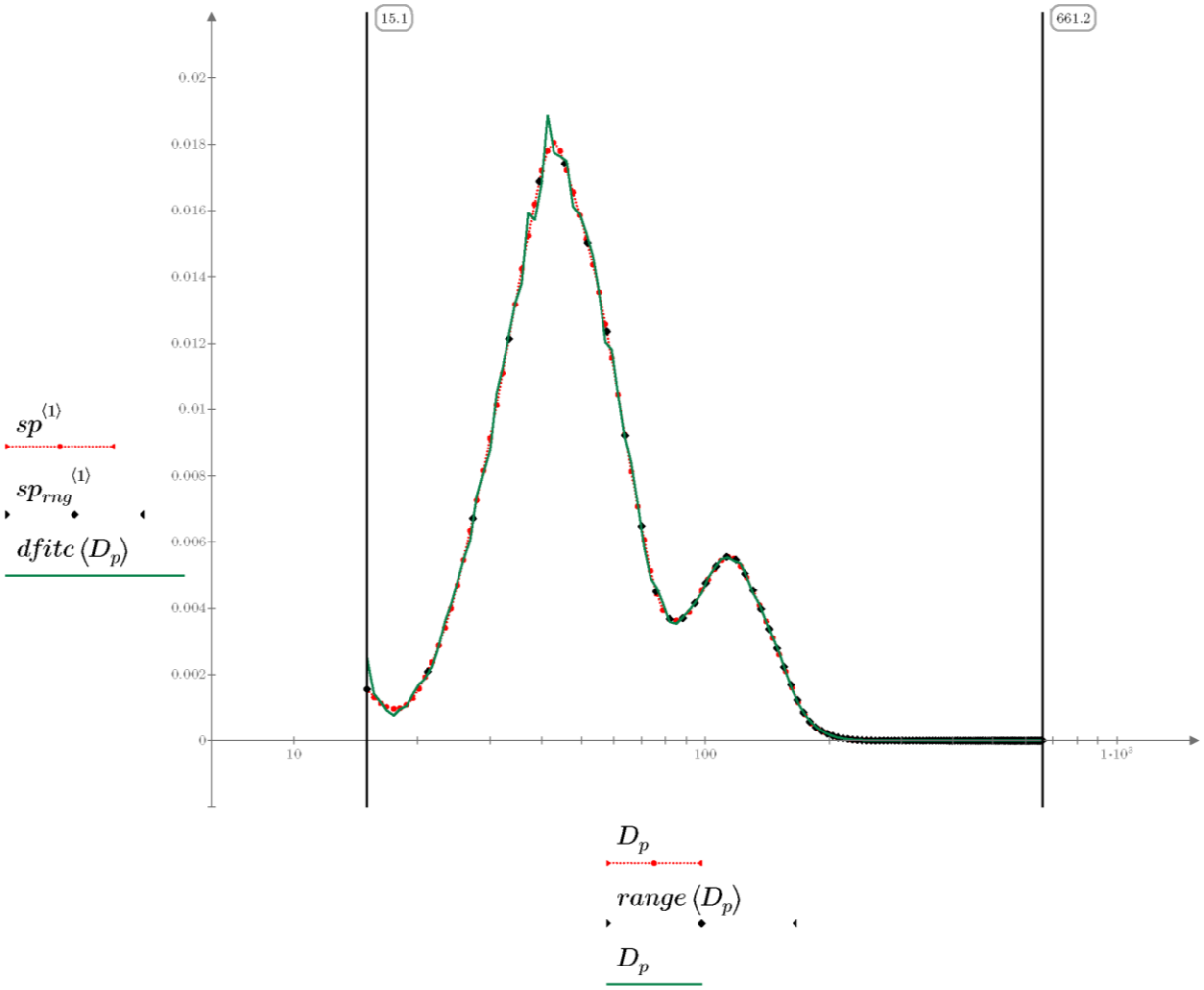

As we can see, the B-Spline derivative is continuous through our entire range, where as the Cubic Spline is not. The B-Spline was developed to be continuous, and as such, is our best way to represent the data in a normalized manner.

A question the reader might ask is why not use the precent values for the distribution representation? The answer is that the area under the representation curve is not equal to 1 as it is under the fractional representation. There is the added 'increase' to the height of the curve from the spacing and this fractional representation will normalize each curve.

$$\int_{D_{P_0}}^{D_{P_{\text{last}}\langle D_p\rangle}} dfitc\left(D_p\right)\,\mathrm{d}D_p = 0.998 \qquad \int_{D_{P_0}}^{D_{P_{\text{last}}\langle D_p\rangle}} fit_{nper}\left(D_p\right)\,\mathrm{d}D_p = 2.759$$

The cubic fit lines are not perfect and thus they fall short on the exact values of integration. However, the point being made is clear; the fractional representation is a normalized set of data that accurately portraies the information regardless of bin spacing.

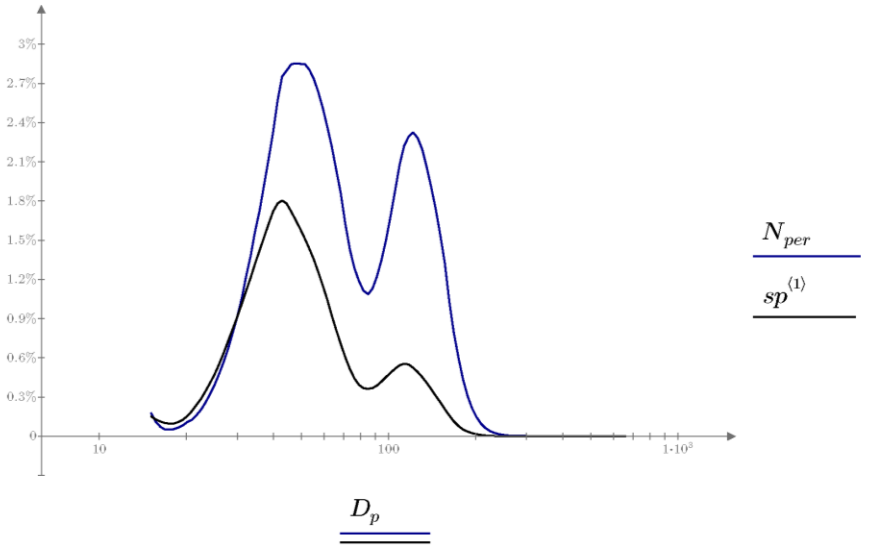

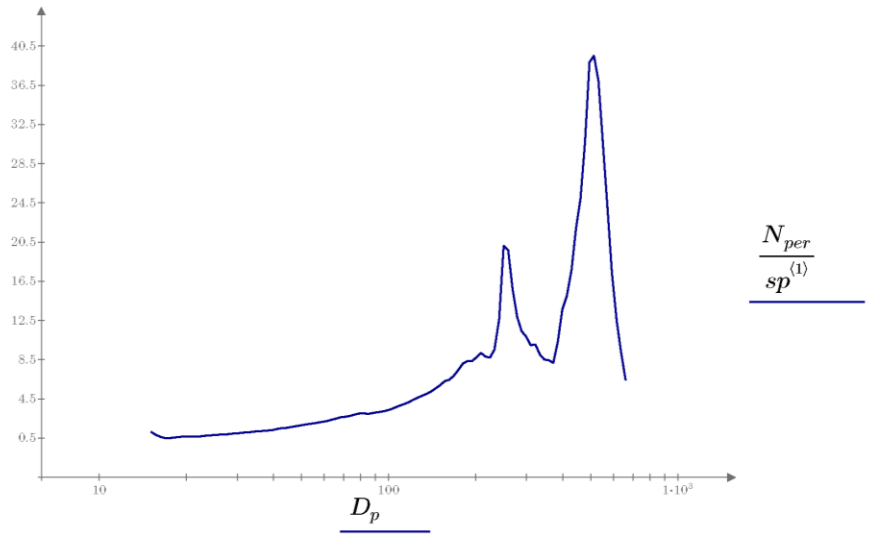

Appendix F: Additional Photos of Project

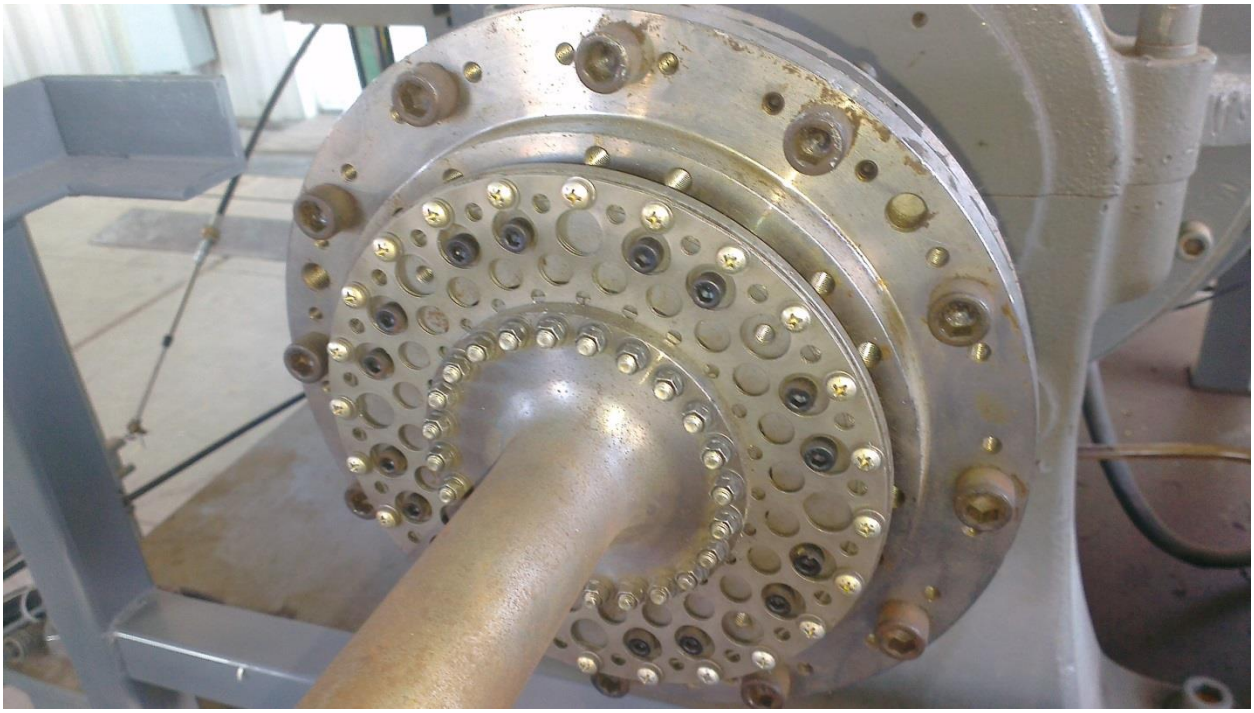

Figure F-1 Driveshaft required to run engine

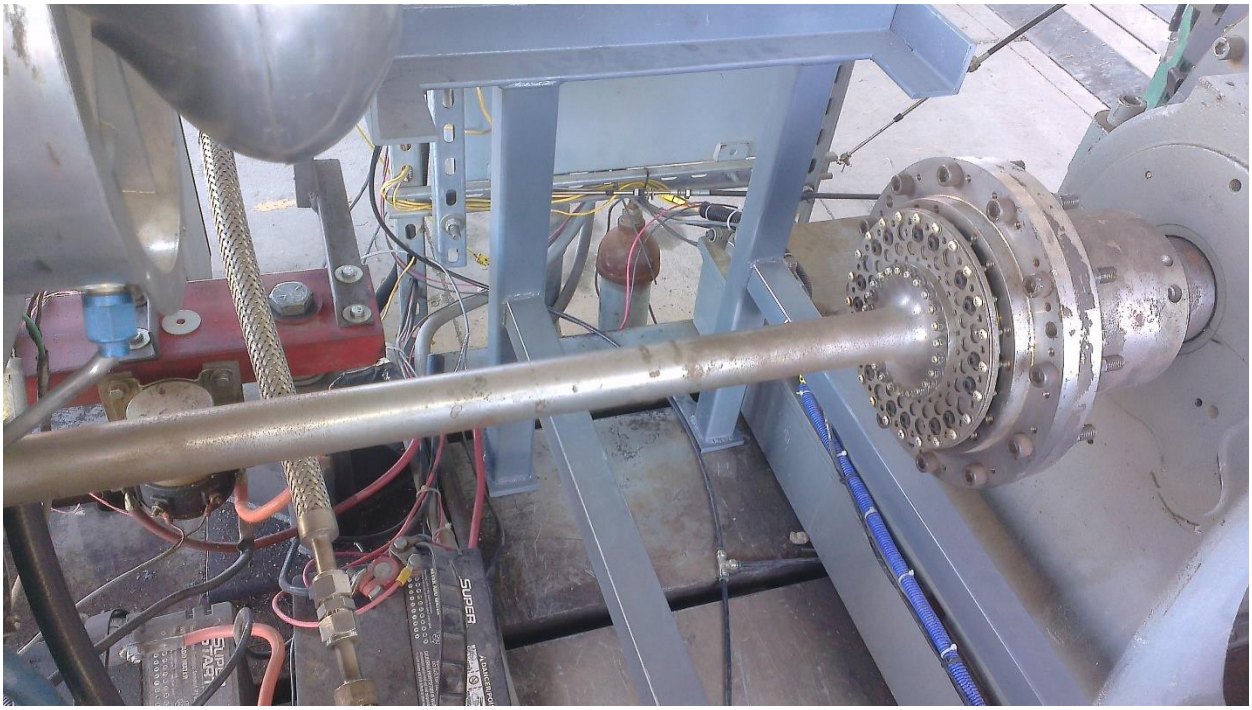

Figure F-2 C8 Driveshaft 2

Figure F-3 Engine Inspection after Hot Start

Figure F-4 Close-up of Engine Turbines during Inspection

Figure F-5 C18 Bleed Ports Illustrated

Figure F-6 C18 Setup 2

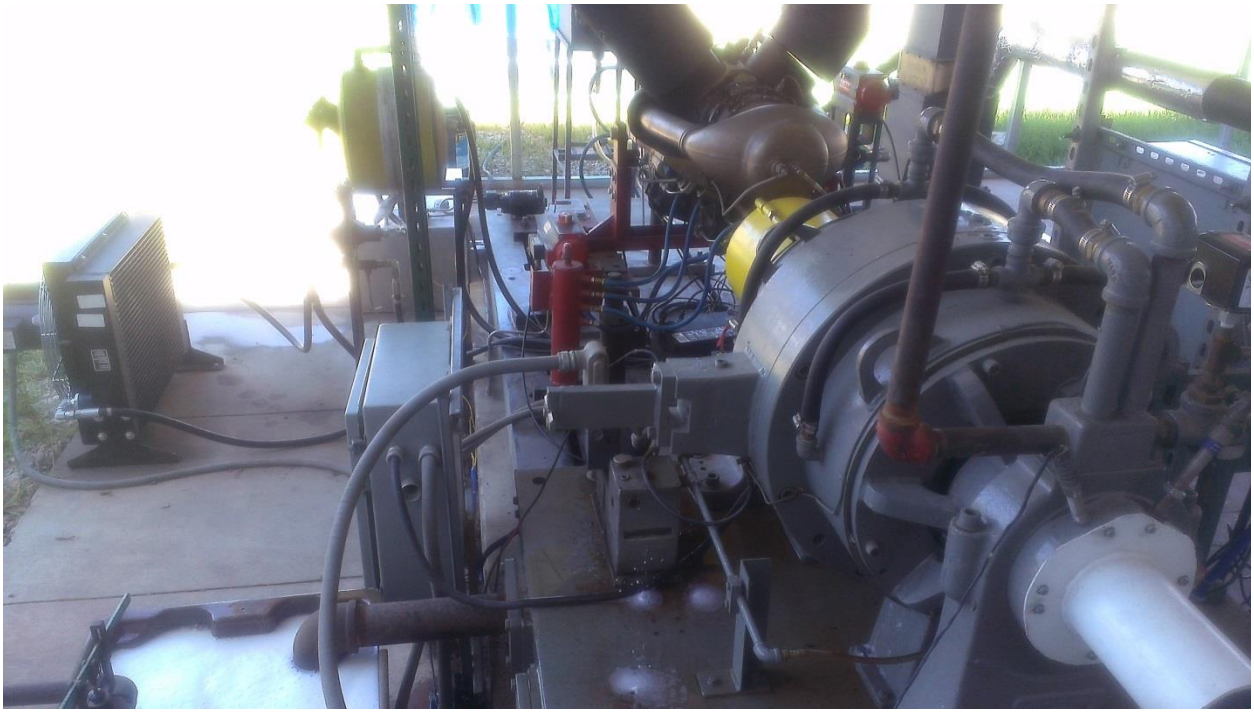

Figure F-7 C18 During test run

Figure F-8 C28B Engine Setup

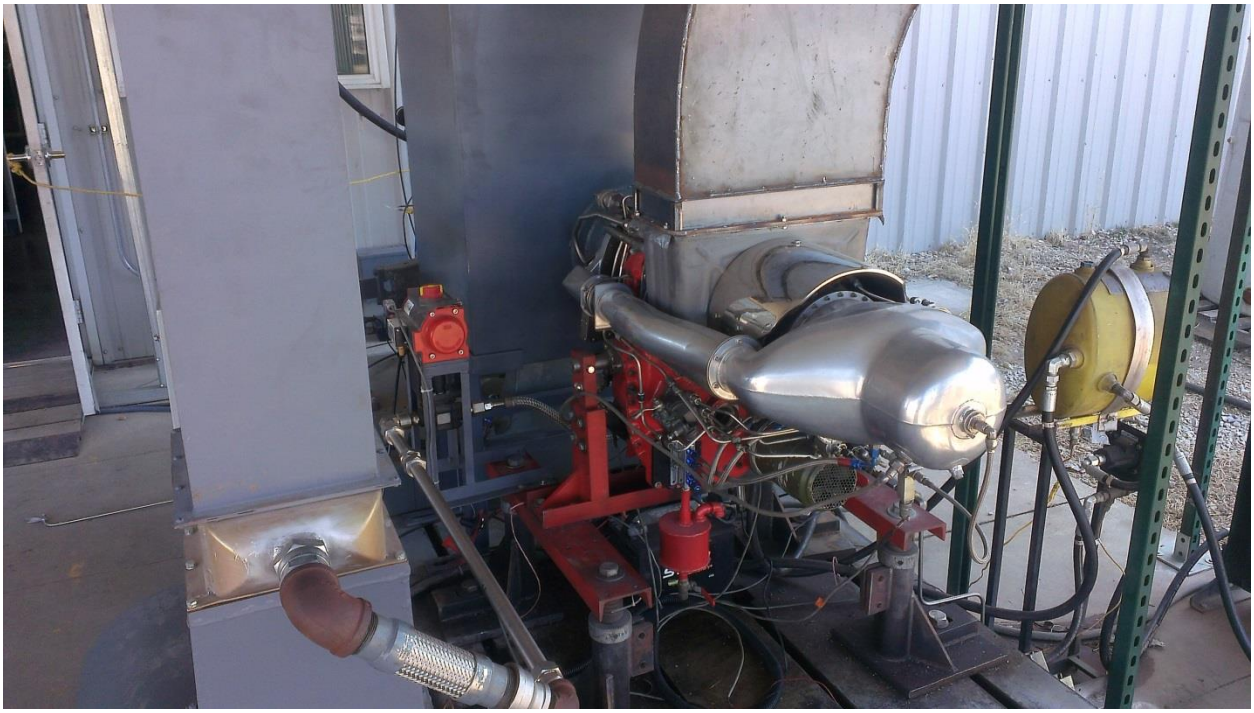

Figure F-9 C28B Engine Setup_2

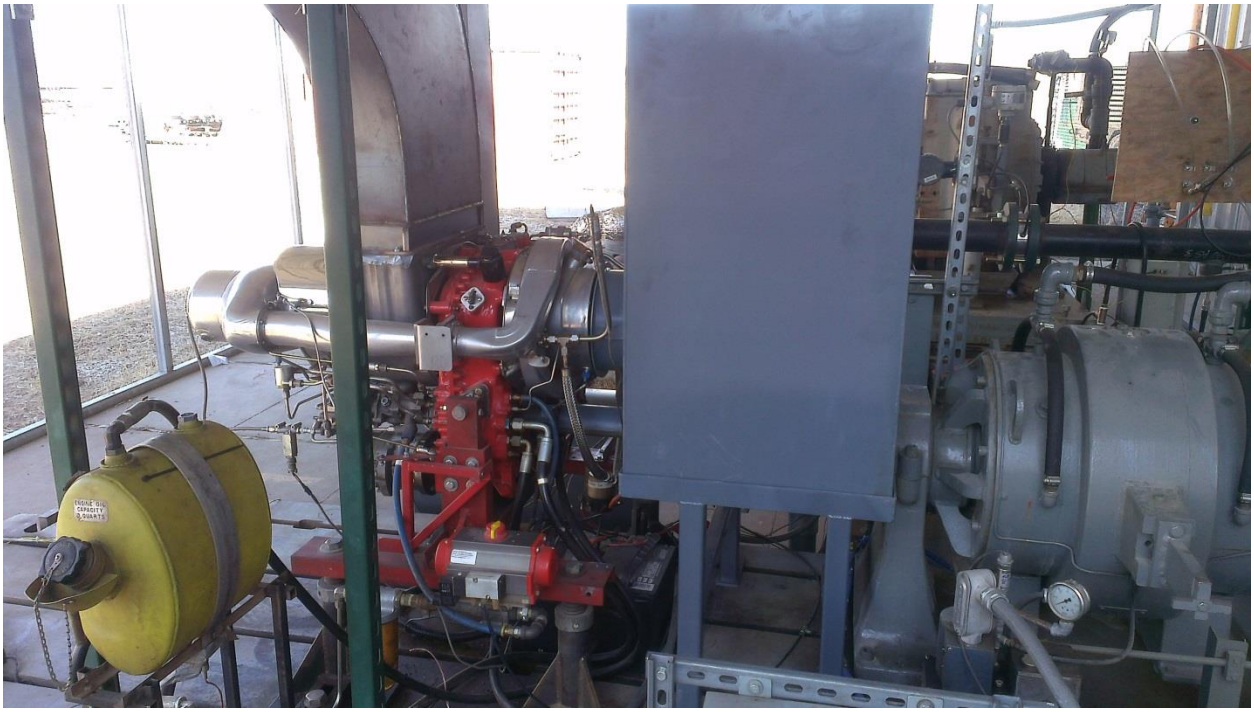

Figure F-10 C28B Engine Setup_3